Physicochemical Behaviour of Complexants in Actinide Separation Processes

A thesis submitted to The University of Manchester for the degree of Doctor of Philosophy in the Faculty of Engineering Sciences and Physical Sciences

2021

Richard J L Blundell

School of Chemical Engineering and Analytical Science

1 Table of Contents

1.1.1 ***List of Figures***

1.1.2 ***List of Tables***

1.2 Abstract

With the implementation of future recycling concepts and their associated contacting techniques, processes must be robustly evaluated to ensure the design and operation of safe and efficient liquid-liquid extraction processes. This relies on the characterisation of both the extraction performance and physicochemical behaviour between the organic and aqueous phases. This was achieved in this project through small-volume extractions and physicochemical studies performed using identified techniques (both commercially procured and developed in-house).

This work has implemented a thorough evaluation of the first Group Actinide Extraction (GANEX-1) cycle through high concentration uranium extraction studies and the resulting impact of acid and metal extraction on the physicochemical behaviour and has tied mass transfer and separation fundamentals to these exhibited physical properties. The work undertook an assessment of experimental techniques and equipment for the purpose of physicochemical measurements of radioactive liquids and provided a recommendation for techniques within a laboratory environment. An empirical expression was derived to allow for the density and viscosity of any molar composition of DEHiBA or TBP in *n*-dodecane between 278 – 333 K for the use in modelling strategies. Proposed process conditions of the 1st GANEX cycle involving the bulk extraction of uranium from 2 -6 M nitric acid by 1 M DEHiBA in *n*-dodecane between 293 – 333 K. Obtained uranium distribution ratios showed that at acidic aqueous concentrations between 4 – 6 M HNO_3 provided the most favourable extraction conditions for the DEHiBA containing solvent. However, at 6 M HNO_3 and high uranium concentrations, 1 M DEHiBA in *n*-dodecane formed third phase at 293 K, highlighting an unfavourable operating regime. The studied properties of this third phase have shown that the density of the organic phase can be used to detect and avoid maloperation regimes.

Radiolytic degradation of the GANEX and EURO-GANEX extractant systems with ^{60}Co γ-radiation up to 750 kGy showed relatively minor changes to the density and viscosity of the systems. However, the negative trend between interfacial tension and total dose illustrated the requirement for a solvent regeneration technique to remove surface-active degradation products that could impair the effective separation of the aqueous and organic phases after mixing.

1.3 Declaration

No portion of the work referred to in the thesis has been submitted in support of an application for another degree or qualification of this or any other university or other institute of learning.

1.4 Copyright

1.5 Acknowledgements

Sometimes I wondered and doubted that I would ever make it this far. That I have is only down to ME….eting some unbelievably supportive, generous and helpful people both inside and outside of university life.

Firstly, thank you to those who have helped make my internment in HMP 'The Mill', M1 3AL, an, on the whole, enjoyable experience. Personally, and professionally I extend my thanks to Clint, for his ability to deliver me to this moment, having the patience to support some unique interests for a PhD student and their encompassing issues as well as just generally sorting me out! Enormous thanks must go to Hugues, who continues to motivate me and provide guidance to this day - and was partly to blame for embarking on this journey an adult lifetime ago. Thank you, Kathryn who has kept a tight ship in running E50 and your countless moments of assistance, Tom J for introducing me to the power of ImageJ (lifesaver!), Tim for always being up for a summer beer or office whiskey, Dan for making me seem like an upbeat person by comparison and Tatiana for being so unbelievably organised and hardworking (it is a shame it never rubbed off despite sharing an office!). I also am grateful to Andrew Masters who has also been a source of knowledge and has provided continued development of this project and without whom I am sure I would not have made it this far!

Thank you to all those both in Manchester (especially the analytical department of Chemistry) and in other walks of academia and industry, from Sheffield to Sellafield who have given their time and effort in supporting my development.

Outside of university there are too many to acknowledge but thanks to Mark for everything you've done since I started this PhD, I could not have got here without the support (and meals) you offered. Thank you to all the friends I made along the way, in alphabetical order, Drej, Elliot, Emily, Jason, Luke, Rory, Sam and the many others from sport and social clubs. Thank you to those I've worked with pursuing interests in the British Army, it has provided a continued avenue of personal development and challenge.

Lastly thank you to Layla, for the many fantastic memories we made in Manchester and for always picking me up when things became stressful, it meant more than I will ever be able to express. Thank you to my parents, Hilary and Rob, and to my brother and sister-in-law. I am profoundly grateful to years of the support, emotional and more, you all offered, without prompting and always in abundance. It is with certainty that I say I could not have completed this project without you all!

Next stop… *the real world*!

1.6 Abbreviations

AGR	AGR
An	Actinides
BWR	Boiling Water Reactor
CEA	Commissariat à L'Energie Atomique (French Atomic Energy Commission)
CFC	Consolidated Flow Concept
CHON	Carbon, Hydrogen, Oxygen and Nitrogen
CyMe4-BTPhen	2,9-bis(5,5,8,8-tetramethyl-5,6,7,8-tetrahydro-1,2,4-benzotriazin-3-yl)-2,2'-bypyridine
DEHA	Diethylhexylamine
DEHiBA	*Di*-2-ethyl-hexyl-isobutyamide
DIAMEX	Diamide Extraction process
D_m	Distribution ratio of metal, m
DMDOHEMA	Dimethyl-dioctyl-hexylethoxy-malonamide
DOA	Dioctylamine
DOAA	*N*,*N*-dioctylacetamide
DOFA	*N*,*N*-dioctylformamide
DOGA	*N*,*N*-dioctylglycoamide
EHiBA	Monoethylhexylisobutyramide
FP	Fission Products
GANEX	Group ActNide EXtraction
GC-MS	Gas Chromatography – Mass Spectrometry
Gen IV	Generation IV Nuclear Reactor Technologies
HAR	Highly Active Raffinate
HLW	High Level Waste
ICP-OES	Inductively Coupled Plasma – Optical Emission Spectroscopy
IFT	Interfacial Tension
LLE	Liquid-Liquid Extraction
Ln	Lanthanides
LWR	Light Water Reactor
LWR	Light Water Reactor
MA	Minor Actinides
MOX	Mixed Oxide
NFC	Nuclear Fuel Cycle

OK	Odourless Kerosene
P&T	Partitioning and Transmutation
PHWR	Pressurised Heavy Water Reactor
PST	Phase Separation Time
PUREX	Plutonium Uranium Reduction EXtraction
PWR	Pressurised Water Reactor
RPM	Revolutions Per Minute
SANEX	Selective Actinide Extraction
S_f	Separation Factor
SFT	Surface Tension
SI	Système international (The International System of Units)
SNF	Spent Nuclear Fuel
SO_3-Ph-BTP	2,6-bis(5,6,-di(sulfophenyl)-1,2,4-triazin-3-yl)pyridine
TBP	Tri-butyl phosphate
TODGA	*N,N,N',N'*-tetraoctyl-3-oxapentanediamide
TPF	Third Phase Formation
TPH	Tetrapropylene hydrogenated
TRU	Transuranic
UREX	Uranium Extraction Process
XRF	X-Ray Florescence

2 Introduction

2.1 Overview

Since its inception, the nuclear fuel cycle has been perceived as a sector with enormous energy potential and a pathway to reduce global carbon emissions.[1] However, the technology has never been overwhelmingly embraced as an acceptable method for energy transition from traditional fossil fuels.[2] The primary reasons for this are the associated environmental and safety concerns of all fuel cycle operations, especially with regards to the management of waste streams which can polarise the general public when combined with a lack of understanding and awareness of the industry.[3]

One of the most heavily criticised areas of the fuel cycle is the waste stage.[3] The purpose for the recycling of spent fuel has shifted over the decades from the proliferation concept that reprocessing was founded. This designed selective extraction of plutonium for military purposes now restricts nuclear energy from being exported to less developed countries.[4] Recycling aims to extract any uranium not utilised in the reactor burn form the waste stream for further energy production as well as any other viable fission products.

Globally there is a lack of cohesion on reprocessing strategy and there is no longer an obligation for countries to reprocess their waste and it can be stored, a cheaper alternative.[5] As a result, countries such as the United States are no longer operating civil reprocessing sites.[6] This lack of cohesion has led to the design and research into multiple fuel cycle strategies, both aqueous and pyrochemical, many being independently pursued by individual nations determined by underlying geopolitical requirements.[7]

Should a new generation of reactors and fuel cycles be commissioned, there is likely to be a demand for a new reprocessing cycle to be implemented alongside. What type of advanced recycling operations should be used to support next generation fuel cycles is still debated as research continues to advance scientific understanding to aid the eventual decision.[8]

Ultimately, as with any geological resource, uranium is finite and should be managed efficiently. Current estimates allow for many decades of supply[9], although it is difficult to say with certainty, due to hypothesised advances in reactor design and uranium mining and extraction methods, how long

supplies will last, it will be in the magnitude of several thousands of years[10]. Therefore, this should not be the primary motivation for implementation of an effective recycling operation and future recycling methods must seek optimise the use of energy and resources during the recycling operation and to minimise waste volumes produced. This should be achieved through improvements in extraction chemicals, equipment, and technology. This project looks to develop the physicochemical knowledge of future liquid-liquid extraction systems to be used in spent fuel recycling step. The understanding of an aqueous recycling cycle's physicochemical properties can allow for accurate prediction and insight to the safe and efficient behaviour of engineering processes associated with future Generation IV systems.

2.2 The Nuclear Fuel Cycle

2.2.1 Front End

The first stage of the NFC (Nuclear Fuel Cycle) focusses on the extraction and fabrication of nuclear fuel using a uranium fuel cycle. Natural uranium contains approximately 99.3% ^{238}U, 0.7% ^{235}U as well as negligible amounts of ^{234}U. Natural uranium is not desirable for the majority of modern nuclear reactors as ^{238}U is not fissile with thermal neutrons (capable of sustaining a nuclear fission chain reaction), therefore mined uranium is enriched to between 3-5% fissile ^{235}U in order to sustain a nuclear reaction in the majority of currently operational nuclear reactors worldwide.[11] The steps of the front end of the NFC are given below:

1. Uranium ore is excavated or mined from the ground using *in situ* leaching techniques or through underground or open pit mining methods, determined by the conditions (uranium ore content, ore contaminants) in which the uranium ore is found.[12]
2. Uranium milling is the beneficiation stage and is used to recover the uranium from the ore. This phase entails crushing or grounding the ore into fine slurry, which is then leached in either a concentrated acid or alkali solution. This separates the uranium from various impurities in the ore and is precipitated and primarily recovered as, uranium oxide (U_3O_8), also known as "yellowcake". This then dry roasted.
3. Conversion of U_3O_8 to uranium hexafluoride, UF_6, if enrichment is required.
4. The enrichment stage is physical process, designed to increase the content of fissile ^{235}U in the fuel. This is undertaken by utilising the mass difference in the isotopes, most commonly through centrifuges. Gaseous UF_6 is separated into two streams consisting of the heavier, 'tails', depleted uranium stream and the lighter, slightly enriched, 'product' stream.
5. Fuel fabrication is the conversion of the enriched UF_6 to UO_2, which is then pressed and sintered into a suitable form (pellets). These pellets are arranged in a cylindrical form and encased in a cladding to form fuel rods ready for use in the reactor.[11]

2.2.2 Reactor Operations

Once in the reactor the uranium-235 undergoes fission, splitting the atom to create heat to produce, usually, steam (either directly or indirectly) for the generation of energy. This fission process burns the fissile uranium-235, fragmenting into other certain elements.[13] The amount of electricity produced for a given unit of fuel is defined as the burn-up, given as megawatt days per tonne (MWd/t).[14] There are many variations of reactor design, provided in Table 1, providing the unique characteristics of each one.

Table 1. Current Design of the Primary Nuclear Reactors[14]

Reactor	Fuel/ Form	Steam generation	Coolant	Moderator
PWR – Pressurised Water Reactor	UO_2, / Enriched	Indirect	H_2O	H_2O
BWR – Boiling Water Reactor	UO_2, / Enriched	Direct	H_2O	H_2O
PHWR – Pressurised Heavy Water Reactor	UO_2, / Natural	Indirect	D_2O	D_2O
LWR – Light Water Reactor	UO_2, / Enriched	Direct	H_2O	Graphite
AGR – Advanced Gas-Cooled Reactor	UO_2, / Enriched	Indirect	CO_2	Graphite

The transmutation of elements within fission reactors leads to the presence of neutron poisons which, in conjunction with the consumption of some of the fissile ^{235}U, results in a reduction in reactor efficiency. Fuel rod assemblies in oxide fuelled reactors are therefore typically changed every 18-36 months in order to maintain efficient reactor performance.[11]

2.2.3 Spent Nuclear Fuel

The spent fuel rods are removed and sent to storage ponds to cool. Depending on the type of fuel cycle being implemented, this SNF (Spent Nuclear Fuel) is then sent to be reprocessed (closed fuel cycle) or into interim storage followed by final disposal in a likely geological disposal facility (open fuel cycle). An approximate breakdown of the elemental constituents in SNF after burn up in a LWR are given in Table 2.

Table 2 Approximate composition of LWR spent nuclear fuel with a burnup of 50 GWd/tHM [15]

Constituent	% Composition in spent fuel
Uranium (Less than 1% U-235)	93.4
Plutonium	1.2
Fission Products	5.2
Minor Actinides	0.20

2.2.4 The Plutonium Uranium Reduction Extraction Process

The commercial method used currently is the PUREX (Plutonium Uranium Reduction EXtraction) process, or a modern variation of it[16] The PUREX method has been the primary industrial reprocessing technique used over the last 60 years since its inception in 1949 and its first industrial scale use at the U.S Atomic Energy Commission Savannah River site.[17,18] Adaptations of the process are now seen across the world. The liquid-liquid extraction method uses tri-*n*-butyl phosphate (TBP) as the extractant (industrial processes use 20-30% by volume) in an organic hydrocarbon diluent such as odourless kerosene (OK).[19] The spent fuel is removed from the reactor, conditioned and then dissolved in relatively concentrated nitric acid. It is then contacted with the organic solvent system in a counter-current extraction mechanism. Due to over 60 years of operational use and understanding of the process, it has produced an established and reliable extraction process.

2.2.4.1 The TBP Extractant

Tributyl phosphate (Figure 1) was used as a metal extractant at the advent of nuclear technology and has been comprehensively studied since its first use as an extractant for U(VI) and Pu(IV) in the early days of World War Two.[20] Its successful application as the solvent of choice in the nuclear reprocessing comes from both its extraction ability in addition to its physical properties and ability to have a little relative change to density and viscosity with the heavy loading of metals.[19] The physicochemical properties of TBP in various diluents are well understood and have been heavily investigated over the last 20 years in multiple studies and reviews.[21–23]

The high affinity of the phosphoryl group of TBP for actinides in the +6 and +4 oxidation states makes it selective for the extraction of U(VI) and Pu(IV) cations from 2-6 M nitric acid. The extraction reaction is shown in the following equations:

$$UO_2^{+2} + 2NO_3^- + 2TBP \leftrightharpoons [UO_2(NO_3)_2 \cdot 2TBP]$$

$$Pu^{+4} + 4NO_3^- + 2TBP \leftrightharpoons [Pu(NO_3)_4 \cdot 2TBP]$$

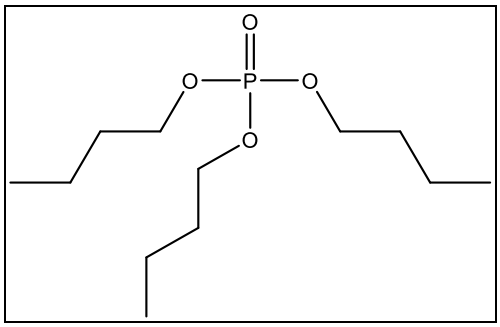

Figure 1. Skeletal diagram of tri-n-butyl phosphate

2.2.4.2 PUREX Flowsheet

A flow sheet of the PUREX process is shown in Figure 2. The process operates in a counter-current configuration to provide the greatest concentration gradient between the two phases. The first step of the reprocessing operation involves the conditioning of the spent fuel (dissolution in hot nitric acid). The aqueous phase is then contacted with an organic phase of TBP in a kerosene diluent. The phases are mixed in a contactor, facilitating the coextraction of the U(VI) and Pu(IV) by TBP into the organic phase, leaving the other fission products in the aqueous stream. To separate the plutonium from the uranium, the oxidation state of Pu(IV) must be reduced to Pu(III) through the addition of a reductant such as hydrazine (N_2H_4) or Fe(III) in the Magnox process, and the Pu(III) is then stripped from the organic into a clean aqueous phase. A similar step is repeated to remove the U(VI) by the addition of clean dilute acid in the U strip step, before the solvent is washed and regenerated for further use using a carbonate or hydroxide solution. Traditionally, the aqueous feeds, with their desired isolated uranium and plutonium metals, are then concentrated by evaporation, converted to a solid oxide form and fabricated into fuel.[24] There have been changes to the PUREX process to address issues such as the

isolation of Pu providing the ability to co-extract and produce mixed oxide fuels (MOX) as well advances to contactor equipment to increase plant efficiency.

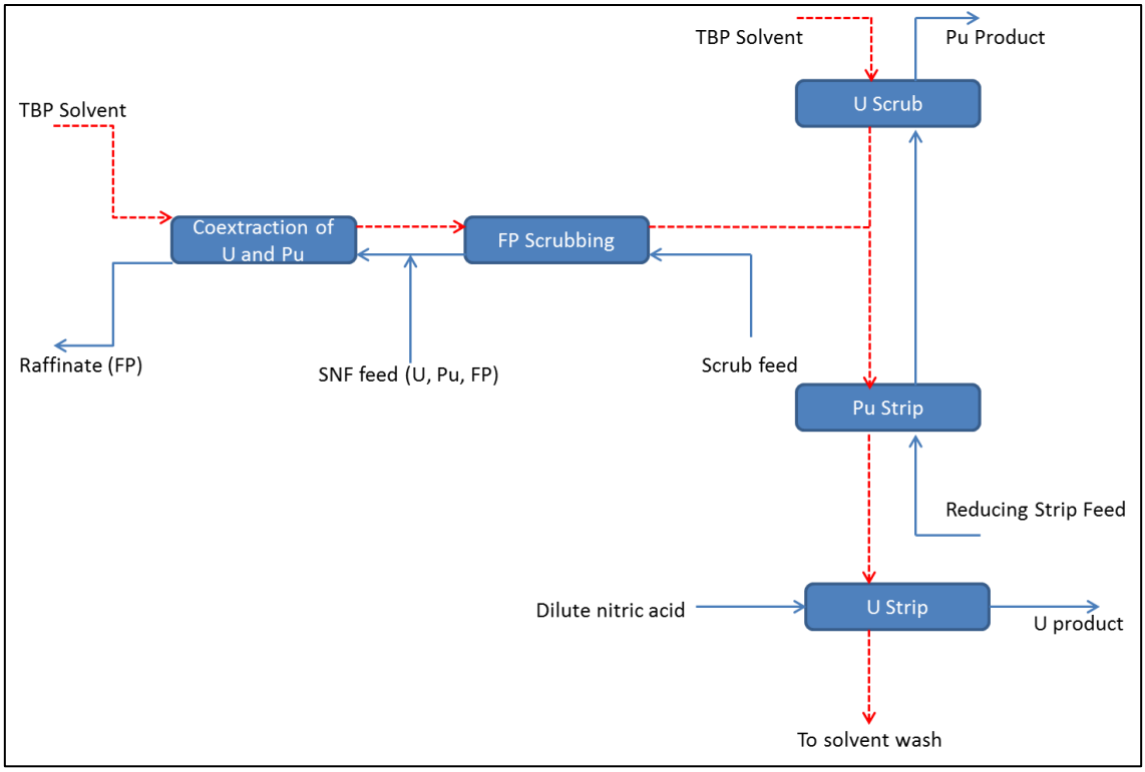

Figure 2. Adapted flowsheet of the PUREX process with a late U/Pu split [25]

2.2.4.3 Challenges with the PUREX Process

Since its inception the PUREX process has shown reliable operation and an ability to allow refinement to improve with evolving requirements. However, future advanced reactors would work with higher burnups resulting in the production of greater quantities of fission products such as plutonium and problematic neptunium (IV) and thermal decay heat.[26,27] Modern processes will require high uranium and plutonium loading capacities as well as the ability to extract the trivalent actinides. These aqueous systems will likely be integrated with centrifugal extractors that will require fast chemical and mass transfer kinetics.[28] This has made it necessary to look beyond TBP and the current PUREX process. The extraction chemistry involved in efficiently separating over 400 species[24] and is complex requiring the addition of additives to control the process, these can increase the waste volumes[29] as well as impacting the physical properties of the system either directly or indirectly through later degradation.

The increased quantity of plutonium and subsequent extraction can cause concern with the formation of a third phase as the Pu-TBP complex has relatively limited solubility.[30] Third phase formation (TPF) in liquid-liquid extraction systems occurs when the organic phase splits into two phases. This split can occur either due to excessive loading of metal or mineral acid in the organic phase. The organic phase is split into a light diluent rich phase, and a heavy extractant and metal rich phase. In general, for liquid-liquid, it is an extremely problematic phenomenon, as the extraction process is only designed to operate with two phases and can result in unwanted carry on of material into other unit processes. The formation of a dense, viscous, and metal rich third phase present a variety of maloperation and safety challenges. This "third phase" typically sits between the aqueous and organic layers although it can be denser than the aqueous, causing phase inversion and entrainment with the aqueous phase after separation. The resulting hydrodynamic issues with the process operation are increased viscosity due to the believed aggregation within the third phase[31], this increase can deviate the fluid's properties beyond the designed operating parameters. The result is a reduction in mixing, desired mass transfer and distribution coefficients and increased phase disengagement time. Lastly, and most crucially it can pose a criticality risk if fissile material such as Pu forms in this layer.[32] The factors known to influence third phase formation are:

- Temperature
- Acid concentration and pH
- Heavy metal concentration
- Diluent and type
- Extractant concentration

The reprocessing environment exposes the both the aqueous and organic phases of the PUREX process solvent system to harsh acidic and radiological conditions. This can lead to degradation of the organic and aqueous solvents, compromising the ability of the system to work efficiently and TBP can only be recycled a limited amount in the PUREX process before it loses its function as an extractant. This accumulative degradation causes a reduction in process efficiency due to both chemical and physical factors and can result in poor phase separation as surfactants are formed, reduced mass-transfer coefficients and decreased FP/actinide separation factors[33,34] and there is a gradual decrease of

extractant. The degradation of TBP due to hydrolysis is much less than compared to radiolysis TBP and when undergoing radiolytic degradation it has three major products, hydrogen, methane and dibutyl phosphate (DBP and MBP), which forms dibutyl phosphoric acid (also the main hydrolysis product of TBP). This can result in difficulties when trying to strip the Pu from the organic phase as well as increasing the susceptibility to TPF.[2424,35,36]

The final element of consideration relates to the social impact of the PUREX process and the susceptibility for it to be used for proliferation purposes. The well-known chemical route for co-extraction or U and Pu and subsequent isolation of both elements is no longer desirable and is a limitation for the globalisation of nuclear energy.

2.3 Principles of Solvent Extraction in the Nuclear Fuel Cycle

There are two potential avenues for recycling of SNF, aqueous (hydrometallurgical) and dry (pyrochemical). The work presented in this thesis will explore the aqueous route only. Solvent extraction (SX), also known as liquid-liquid extraction (LLE), is the method of separating desired components through the transfer of elements between two immiscible liquid phases, aqueous and organic or heavy and light based on density (in almost all systems the aqueous will be the heavy phase, and the organic the light).[37] This separation is achieved by the affinity for the desired extractable component to exist in one of the two phases. There are various types of process designs using different types of contacting and separating equipment, solvent and diluent mixes and general operating conditions, which are discussed in detail in Section 2.4.

The principles which dictate the efficiency of solvent extraction are complex but can be viewed as dependent on both chemical reaction kinetics and the physical conditions that determine the overall rate of mass transfer (across the phase boundary from one phase to another). The contactors are designed to vigorously mix the two phases and form an unstable emulsion, thus creating the conditions for enhanced mass transfer of a desired component between the two phases. One of these phases is the feed which carries the solute, and the other is the solvent. Once the mass transfer of the desired component has

occurred, there is a separation step to return the emulsion to its two individual phases and complete the selective extraction.

At set physical conditions (temperature, pressure and interfacial area) there will be an optimum mass transfer across the phase boundary of an organic and aqueous phase. This can be determined through techniques such as rotating diffusion cell or moving drops experiments.[38] A key challenge in developing any novel SX process is to optimise extractions under process conditions when scaling up to an industrial level. The rate of mass transfer is crucial in determining the most efficient contacting technique with respect to process times, plant footprint and ultimately cost. This optimisation involves the manipulation of the physical process conditions. As a result, the physical properties of the solvents and solutes are of high importance in solvent extraction due to the nature of this partitioning approach. Understanding the fundamental fluid properties of density, viscosity and interfacial tension play an important role in the optimisation and safe operation of a solvent extraction process.[39]

2.3.1 Mass transfer between phases

Two mechanisms describe the transfer of molecules within a single phase itself and between two immiscible phases. The first is diffusion theory, which explains the movement of mass (molecules of a solute) within a single phase and is governed by the principle of reaching equilibrium through the destruction of the concentration gradient within a mixture. The second is interphase transfer through film theory, which details the movement of the molecules from one phase to another phase of medium (liquid-liquid, gas-liquid *etc*.).

Diffusion Theory

Within a single phase at steady state (constant temperature, pressure, chemical composition *etc*.) and no external mixing, mass will move within the phase through molecular diffusion which is driven by the basics of diffusion and the movement of molecules from a high concentration to a low concentration. The mass transfer is described by Fick's first law, given below:

$$J_A = -D\frac{dC_A}{dz}$$

Equation 1. Fick's Law of Diffusivity

J_A – mass flux of solute A, kg m^{-2} s^{-1}
C_A – concentration of solute A, mol
Z – distance in the direction of the transport, m
D – diffusivity coefficient of solute, m^2 s^{-1}. This is negative as it indicates the movement from a high concentration to a low concentration.

The diffusion of the molecular species is dependent on many factors such as the fluid it is dissolved in, the temperature of the environment and the size of the molecule. There are many expressions used to calculate the diffusion coefficient, the first being the Stokes-Einstein equation.

$$D = \frac{k_{BT}T}{6\pi\mu R}$$

Equation 2. Stokes-Einstein Equation for Molecular Diffusion

k_{BT} – Boltzmann constant, $J.K^{-1}$
T – Absolute temperature, K
μ – Viscosity, $mPa.s^{-1}$
R – Radius of the particle, m

This expression introduces a new parameter, the mass transfer coefficient and seeks to quantify the effects of the particle size, the viscosity of the medium and the influence of temperature on the diffusion This association for the diffusivity with molecule, fluid and environmental parameters is useful for a generalisation but has since been developed and refined into sever further expressions such as the Wilke-Chang which is useful for aqueous or highly associated solvents and the Hay-duk et al. expression for chemicals in liquids.[40] As is evident from the Stokes-Einstein equation, temperature and viscosity are influential parameters, with the temperature influencing the viscosity as well. It can be expected that the viscosity of a solution will increase with increasing mass within the phase, reducing the diffusivity through the fluid.

However, typically there is more than just diffusive mass transport occurring and there will be a bulk fluid motion, known as convective diffusion, which will contribute to the overall mass transfer of a

solute within a solvent. This is either internal convection that can be caused through density differences, or through forced convection such as an impellor stirring a fluid. The mass transfer between two fluids is defined by a dimensionless value called the Sherwood number, Sh. There are many variations of this number and a plethora of equations used to define it which depend on the process conditions and the phase in question (dispersed or continuous). This number gives the ratio of the mass transfer by convection to mass transfer by diffusion over a length, indicated by the diameter of the droplet below.[41]

$$Sh = \frac{kd_{32}}{D}$$

Equation 3. Sherwood number

- d_{32} – Sauter mean diameter of droplet, m
- k – Partial mass transfer coefficient for the phase, g mol s^{-1} m^{-2}
- D – Molecular diffusion coefficient of the phase, m^2 s^{-1}

2.3.1.1 Mass transfer across the interface

Where mass transfer occurs between two different phases, as is in liquid-liquid extraction, two film stationary theory yields practical results for determining the mass transfer coefficients in liquid-liquid extraction, an illustration of this given below. This theory assumes a boundary film, thickness *Z*, on each side of the phase interface and within this film is where all mass transfer occurs, explained by the molecular diffusion coefficient discussed earlier, with the bulk of the fluid phase having a uniform concentration. The concentration of solute in phase 1 decreases as it reaches the interface between the two phases. It then crosses to phase 2 where it the interface has the greatest concentration of the solute and the bulk phase has the lowest concentration of the two phases. The rate of solute transfer is dictated by the rate of diffusion on both sides of the interphase and therefore effective mass transfer is maintained by ensuring this gradient in the favourable direction is maintained.

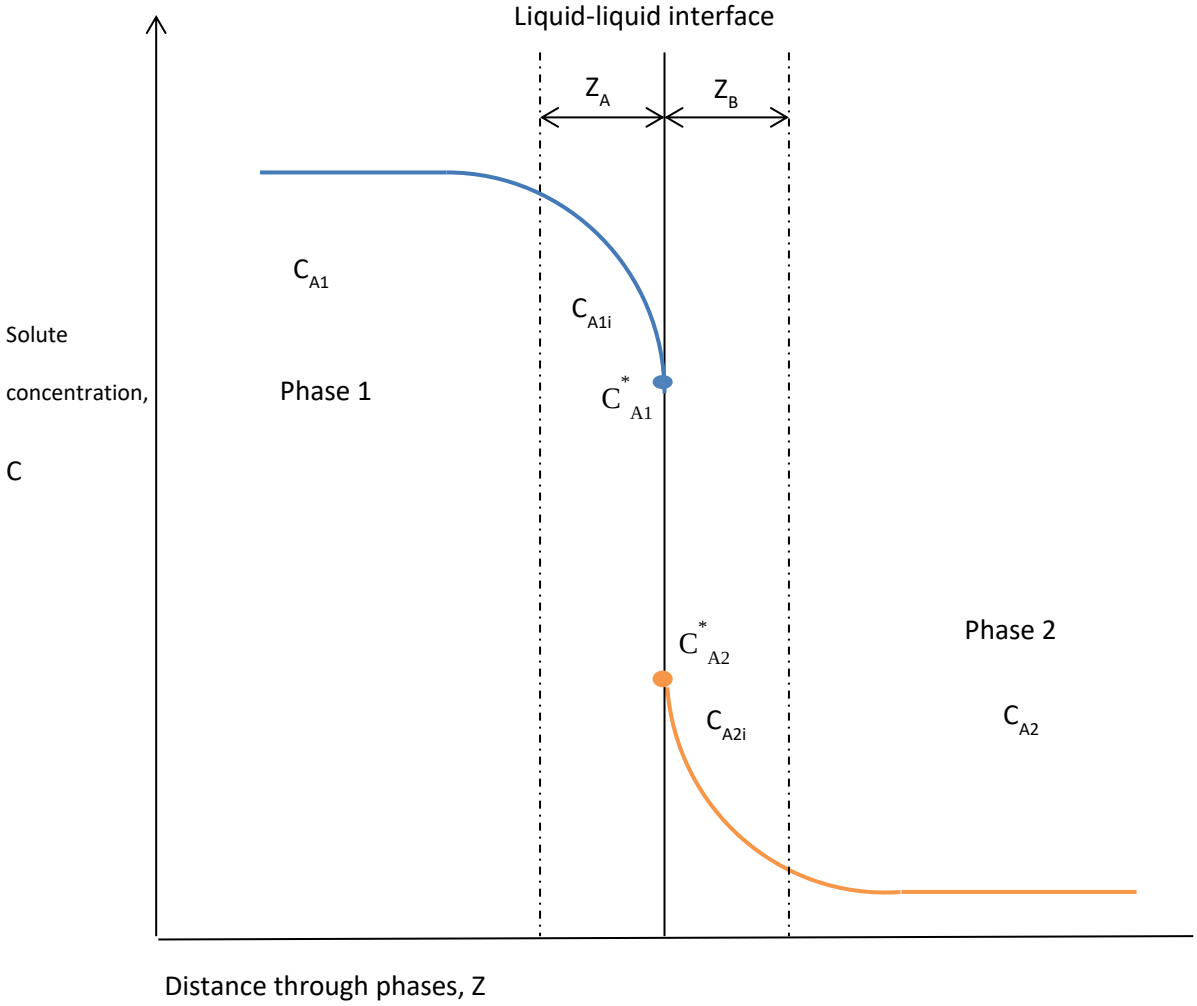

i = interfacial concentration

There is assumed uniform concentration in both bulk phases and the phases are at equilibrium at the interface. The rate of mass transfer of a solute between phase 1 and phase 2 can be described by Equation 4 below.[42] There is firstly the flux of mass transfer through phase 1, from the bulk fluid, M to the interface, C_{Ai}, driven by the concentration gradient and the opposite gradient direction taking the solute away from the interface in the second phase into the bulk fluid.

$$N_A = k_A A(C_A - C_{Ai}) = k_B A(C_{Bi} - C_B)$$

Equation 4. Flux of mass transfer through individual fluids across a boundary

N_A– Flux of mass transfer, g mol s^{-1}
k – Partial mass transfer coefficient for a particular phase, g mol s^{-1} m^{-2}
A – Interfacial surface area, m^2
C – Solute concentration in the bulk of the phase, g mol
C_i – Solute concentration in a phase adjacent to the interface, g mol

C^* – Solute concentration in a phase in equilibrium with other phases in the system, g mol
D

The overall mass transfer between the bulk phase in liquid 1 and the bulk phase in liquid 2 is given below:

$$N_A = KA(C_1 - C_2)$$

Equation 5. Overall rate of mass transfer

K – Overall mass transfer coefficient of system, g mol s^{-1} m^{-2}

Combining Equations 4 and 5, assuming steady state, where the area is constant and the thickness of the interface is ignored, the formula can be rearranged to give the overall mass transfer from the two partial mass transfer coefficients:

$$\frac{1}{K} = \frac{1}{k_A} + \frac{1}{k_B}$$

Equation 6. Overall mass transfer coefficient

The rate of mass transfer of the solute between the two phases depends on the following factors[40,43–45]:

- Phase composition (concentration of solutes)– governing diffusivity and causing interfacial turbulence
- Physical properties of the system (density, viscosity, interfacial tension etc)
- Temperature – affecting diffusion rates due to physical and chemical derived dependencies
- Degree and type of agitation – governs film thickness and interfacial turbulence
- Direction of mass transfer – depending on which phase dispersed
- Phase ratio (volume of dispersed and continuous phase)

2.3.2 Extraction Efficiency

There are typically three ratios used to measure the effectiveness of a solvent extraction process. First is the distribution ratio, *D*, this measures the affinity for the solute in the organic phase over the aqueous phase and is given below in Equation 7, where volumes of both phases are equal. A large distribution ratio indicates favourable extraction of the solute into the organic phase.

$$D = \frac{[S_{org}]_{total}}{[S_{aq}]_{total}}$$

Equation 7. Distribution Ratio[46]

In industrial processes, where one phase is often in volume excess compared to the other to provide control of the continuous and dispersed phase (see Section 2.3.4.4), the distribution ration can be written as:

$$D = \frac{n_{solute\ org} V_{aq}}{n_{solute\ aq} V_{org}}$$

Equation 8. Distribution ratio with respect to volume of solutions

n_{Solute} – Total of solute in organic or aqueous phase

V – Volume of organic or aqueous phase

The overall mass transfer coefficient and distribution ratio can be related, when assuming that the bulk concentration is the total concentration (*i.e* ignoring the interface concentration) and that the system is equilibrium. This provides the below equation (where C1 is substituted to be S_{org} and C2 is S_{aq} with respect to solute concentration in each phase).

$$N_A = KA(D.S_{aq.} - D.S_{org})$$

Equation 9. Combined overall mass transfer and distribution ratio

The distribution ratio can then be further developed to provide a separation factor of one solute over another in the organic phase. This separation factor, S_f, is given in Equation 10 and is made up of the known distribution ratio of two solutes in the extraction process. It is a useful ratio to find the measure the affinity of the extract for a solute over another.

$$S_f = \frac{D_a}{D_b}$$

Equation 10. Separation factor[46]

The distribution ratio, and subsequent ratios, are dependent on many factors in the liquid-liquid extraction process; and values can vary greatly over a range of temperatures and concentrations among other variables. The room temperature PUREX process separation (4 M HNO_3 , 30% TBP) yields the following distribution coefficients of U ≈ 16, Pu ≈ 4.[47]

The final value used as a measure of the ability of the extraction process to remove a contaminant from the product stream is called the decontamination factor. This is given by the concentration or mass of a component in the feed compared with the concentration in the product. The product stream (or streams) is dependent on the process but is typically the separated aqueous actinide stream after back extraction from the organic phase. It is useful for assessing whether the process is effective at removing undesirable constituents in the feed.

$$DF = \frac{[S]_{feed}}{[S]_{product}}$$

Equation 11. Decontamination factor[46]

2.3.3 Solvent and Nuclear Extraction Process Engineering

The successful process design and operation of a liquid-liquid extraction process is dependent on the understanding of the chemical and physical properties of the two liquid phases and how these change across the entire process (solute compositions, solvent degradation, operating temperature etc.). These properties are required at all stages, from the initial screening to the design and finally implementation and operation. Preliminary viability assessments of a solvent extraction system occurs through batch laboratory tests and pilot scale testing before there can be further optimisation of flow-sheets through modelling software.[48,49] Many of the fundamental principles when designing the solvent extraction operation are reliant on the density, viscosity and interfacial tensions of the liquids which are heavily influenced by the shape and size of the component molecules and the strength of any intermolecular forces between these molecules. The types of bonds formed, and their relative strengths are dependent on the structure and elements present in the molecule. This will determine whether dispersion, Van der Walls and dipole forces or hydrogen bonding occurs.[50] These physical properties can also be readily

influenced by the operating conditions associated with the LLE process (temperature, pressure, solute loading etc.).

2.3.3.1 Density

The density of any material is the mass per unit volume it occupies, with the SI of $kg.m^{-3}$, although $g.cm^{-3}$ is commonly used and will be used in this work. The density of a liquid is influenced by its environment and has a relationship with both temperature and pressure.

$$\rho = \frac{m}{V}$$

Equation 12. Equation of Density

The density of a fluid is a caused by a combination of factors. Firstly, it is dependent on the conditions the liquid is present in, such as temperature and to a much lesser degree, pressure. Secondly, the molecular mass of the compounds that are in the composition of the liquid. The density will then be affected by how many of these molecules with their associated molecular masses fit in a volume unit, which is determined by the bond lengths between atoms in the molecule and how tightly these molecules pack between each other. This depends on the types and strengths of both the intra- and intermolecular bonds that form which subsequently influences the size and shape of molecular species and any higher order networks within liquids.[50,51] There is an inverse relationship with density and temperature as the greater the temperature, the more energy and vibrations these molecules have, causing each one to take up a greater amount of space, reducing the density.

Density is important in numerous fundamental engineering expressions, especially in those relating to settling of particles or droplets.[52] For this reason, it is prevalent in solvent extraction engineering and is most influential when looking at the separation of the two phases due to their differences in density be it through gravity or mechanically induced force.

2.3.3.2 Viscosity

The viscosity of a fluid is defined as the measure of the internal resistance to flow (also called shear) of a fluid. It is one of the fundamental properties of a fluid and is required in order to understand its

transport, thermodynamic and intermolecular behaviour. Viscosity can be expressed as either dynamic (absolute) or kinetic viscosity (ratio of viscosity to density). Dynamic viscosity, μ, is the most common version used, and the equation is shown below:[51]

$$\mu = \frac{\tau}{\gamma}$$

Equation 13. Equation of Viscosity

μ - Dynamic viscosity

τ - Shear stress

γ - Shear rate

Differing viscosities of liquids are predominantly due to the differences in the strength of the intermolecular interactions as well as the shape of the molecules within the liquid itself.[50] Strong intermolecular bonding, i.e. hydrogen bonding, will cause a higher viscosity due to a greater energy for the molecules to flow past each other. Whilst as a molecule increases in size the more likely it is to get 'tangled' with other molecules and form intermolecular bonds, thus increasing the viscosity as the resistance to flow is increased.[51] The viscosity of a liquid is dependent on the temperature of the system, so as the temperature increases the molecules have greater energy to overcome these viscous forces causing the viscosity to reduce.[53] Viscosity influences many performance aspects of solvent extraction including mass transfer between phases, diffusion of molecules through a liquid and the operating conditions for flow and agitation. As discussed earlier the Stokes-Einstein equation, shows that as the viscosity of the liquid medium increases, the diffusion coefficient of the solute through the phase will decrease, hindering extraction efficiency. When considering process intensification, viscosity can determine power and separation requirements, with an increase in viscosity increasing the energy costs required for agitation.

For efficient mass transfer and extraction, the droplets in the dispersed phase must be adequately deformed and broken up into smaller droplets. An increase in viscosity results in a greater time for droplet deformation, and agitation requirements. The time for the deformation of a droplet, τ_{def}, to occur

is given in Equation 14 and can be defined as the ratio of the viscosity to the external stress acting on the drop.[54]

$$\tau_{def} = \frac{\mu}{\sigma_{ext}}$$

Equation 14. Deformation time of a droplet

- σ_{ext} – External stress acting on the droplet

The last influencing parameters that will be mentioned in this section, although there are many more areas where viscosity must be considered, are the viscosity ratio and the capillary number (C_a). The viscosity ratio is the ratio between the dispersed and continuous phase (η_D/η_C) and is important when combined with the capillary number in understanding the characteristics of the emulsion being formed between the two phases. The capillary number is the ratio of (shear) stress to Laplace Pressure (σ/R), which develops into the ratio of inertial forces to surface tension.[54]

$$C_a = \frac{\mu_c \dot{\gamma} R}{\sigma}$$

Equation 15. Capillary number

- μ_c – Viscosity of continuous phase
- $\dot{\gamma}$ - Shear rate
- R – Radius of the droplet
- σ – Surface tension

The capillary number should be below the critical capillary number, C_a^*, in order to facilitate an emulsion. Figure 3 represents the emulsion stages depending on the capillary number and phase viscosity ratio ($\frac{\mu_D}{\mu_C}$). When C_a is less than C_a*, it becomes difficult to form an emulsion as the surface tension forces resisting deformation are too great. When the ratio is shown to be 1, it is at the easiest point to form an emulsion. As this ratio is increased it becomes more difficult to form a stable emulsion and beyond 4 it becomes impossible using a shearing process.[55,56]

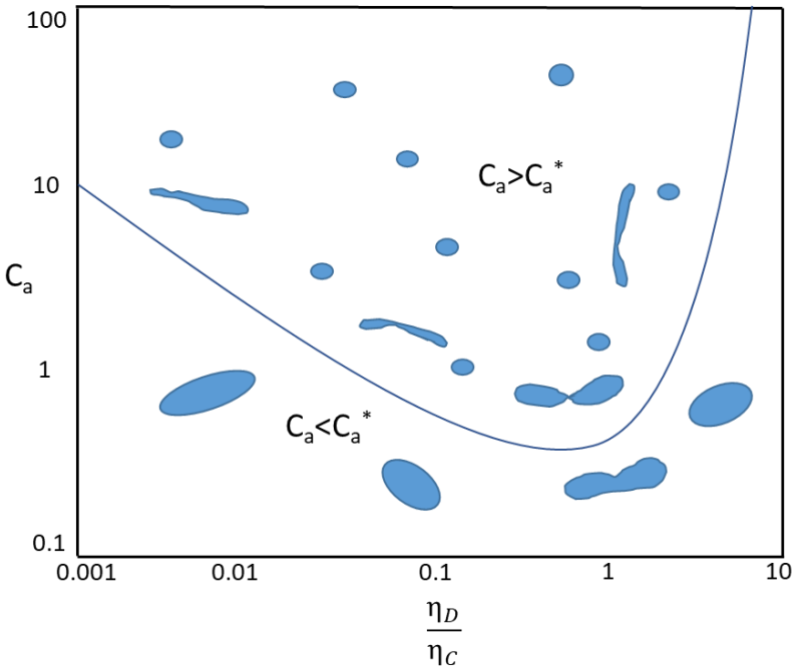

Figure 3. Influence of capillary number and viscosity ratio on emulsion adapted from S. Abbott (2015)[55]

A rapid phase disengagement is beneficial to a solvent extraction process as it reduces the required footprint of separation equipment, reducing cost and increasing the throughput. As mentioned, it is important for the dispersed phase to be broken up into smaller droplets. However, there is a trade-off between how fine the dispersion can be to how long it will take these droplets to coalesce. Referring to the capillary number and Figure 3 it is important that a stable emulsion is not formed, or the two phases will never separate.

2.3.3.3 Surface and Interfacial Tension

The surface tension of a liquid relates to the liquid-gas interface and is defined as the amount of energy required to stretch the liquid by a unit area, $N.m^{-1}$. Interfacial tension is the energy required to increase the size of the interface between two immiscible liquids.[57] This energy is associated with the strength of the intermolecular bonding between the molecules in one phase as well as their affinity to interact with the molecules in the second liquid phase.[50] As with all physical properties, IFT, influences both the extraction and phase separation processes. It can be used to determine the mean diameter of a droplet for each contactor system, given by a function of IFT and density difference ($\sigma/\Delta\rho$) between the two

phases.[58] The interfacial tension can also be used to predict the stability of formed emulsions and phase separation time (PST). A decrease in interfacial tension will reduce the drop size, increasing the interfacial area for mass transfer but increasing the phase separation time, and a trade-off must be established. This value is further influenced by temperature and dissolved solutes in the liquid phases will vary between contactor stages, the specific influences on contactor systems is discussed in Section 1.4.

2.3.3.4 Dispersed and Continuous Phase

An important factor to be determined is which phase will be dispersed and which will be continuous. When an emulsion is formed between the organic and aqueous phase, the dispersed phase will be in the form of droplets within the continuous phase, which will provide the suspension fluid. The dispersed phase, heavy or light, is usually the phase with the smaller volumetric flowrate however it may be that one will not disperse in the other.[43] It is important to understand the effects of which phase is which as mass transfer of the solute can be quicker from the continuous to dispersed and *vice versa*. It is important this is maintained as phase inversion can cause maloperations in a SX process.[59] Once the phase choice has been determined further design processes can be evaluated, as many expressions are specific and dependent to properties of each phase.

The drop size is dependent on many external factors such as the agitation rate and impellor design which in combination with the physical properties of the system determines the behaviour of both liquid phases. Whether regime the droplet is in will also influence the mass transfer of the system, the types of droplet regime as function of droplet diameter and sedimentation velocity is given in Figure 4. In the first regime where the droplets behave as rigid spheres, diffusion within the droplet governs the transfer of the solute from the bulk fluid to the interface. Where there is oscillation and deformation, diffusion in combination with convective motion of the bulk fluid is an influence on the overall mass transfer to the interface.

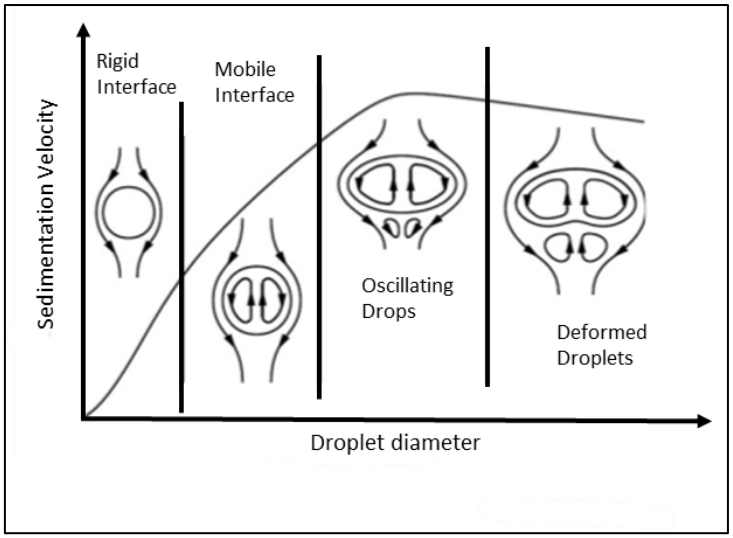

Figure 4. Movement of fluid around and inside droplets as a function of droplet diameter and sedimentation velocity - taken from Kalem *et al. 2009*[60]

2.3.3.5 Emulsion Control and Rate of Separation

The coalescence of a droplets in mixing and separation processes are dependent on multiple factors, some listed below:[61]

- Drop size
- Temperature
- Density difference between phases
- Interfacial tension
- Viscosity ratio
- Vibrational effects

There are various expressions that seek to determine the time taken for coalescence of drops either at an interface or between two droplets. These are dependent on many factors such as the Reynolds number (flow regime) and contactor choice in addition to specialist coalescence equipment that has been developed. An overall liquid coalescence rate is determined by the produce of coalescence rate and coalescence efficiency. However, the physical properties are prominent in this operation. Density and more importantly, density difference are crucial in the separation of the two phases as this is a driving factor of the immiscible layers separating effectively. The coalescence phenomena is the process of the droplet film breaking with another droplet and the drainage occurring to form a single larger drop. The

larger the size of the droplets, the greater the film thickness increasing the coalescence time, however the collision frequency increases with size.[43,61,62]

The coalescence of the dispersed phase and subsequent separation is contactor dependent as intensification techniques such as centrifugal contactor aim to achieved acceptable separation with minimal entrainment in a matter of seconds. There are also subtle effects when considering mass transfer with studies showing that the transfer direction of the solute increases the coalescence efficiency. A greater efficiency is achieved through transfer from dispersed phase to continuous [63]

2.3.3.6 General Operating Considerations

Beyond contactor specific design considerations, the implications of the hydrodynamic properties of a liquid are far reaching through a process. Accurate physicochemical values are necessary for the pumping and flow of any fluid around a plant, where any heat transfer is required and to calculate power and operating costs.[49]

2.4 Liquid-Liquid Contactors in the Nuclear Industry

The purpose of a contactor in solvent extraction operations is to first mix the organic and aqueous phase to facilitate the mass transfer of the elements in the spent fuel. There are three main types of contactor equipment used in the SNF reprocessing industry that will be discussed:

- Mixer-settlers
- Pulsed Columns
- Centrifuges

These contact the two liquid phases by having an initial mixing section or phase achieved through agitation by impellors, pulsing through plates or packing, or through shearing by a centrifugal rotor. This is followed by the separation of the phases due to the differing density of an organic and aqueous phase, droplet coalescence and other factors governing the phase separation. The various configurations that are available within a single contactor system such as choice of impellor blade, number of pulse plates, organic: aqueous phase ratio *etc*. are an indication of how nuanced both the contacting and

separation activity is and the difference between equal volume agitated analytical separation techniques and industrial operations.

2.4.1 Mixer-Settlers

The mixer-settler design was first used in the nuclear industry for reprocessing SNF at Windscale (now known as the Sellafield site in Cumbria, UK).[64] This was a box-type design allowing for the abandonment of inter-stage piping, with purely the density difference between the stages driving the phases through the equipment bank. The design is suitable for use in the nuclear industry due to its reliability, high-stage efficiency and that it does not require a pumping between the stages as the required for maintenance of moving parts is limited only to the agitation mechanism which can be self-contained. This is important as all maintenance work in the nuclear industry is expensive due to the specialist equipment and methods to mitigate against radiation exposure of workers in addition to shut down implications.[48] Mixer-settlers allow for a high-throughput, and are suitable for situations with slow reaction kinetics as the process has a longer residence time in comparison to centrifugal contactors. The lack of intensification of the settling zone is more suitable for liquids with a larger density difference, suitable for gravity separation. These longer residence times can cause challenges within nuclear recycling operations, with increased exposure of the solvent to radiolysis causing increased solvent degradation.

The simplest design of a mixer-settler is shown in Figure 5. The aqueous and organic phases enter from the bottom of the mix box where they are agitated to reduce droplet size and increase the interfacial area, facilitating improved the mass transfer between the two phases. The emulsion then passes into the settling section. This is typically a long, shallow box where gravity separates the two phases according to their densities. There is minimal mass transfer due to a low interfacial area between the two stages in this section. The two phases, post effective separation, leave the mixer-settler stage via their respective light and heavy outlets.

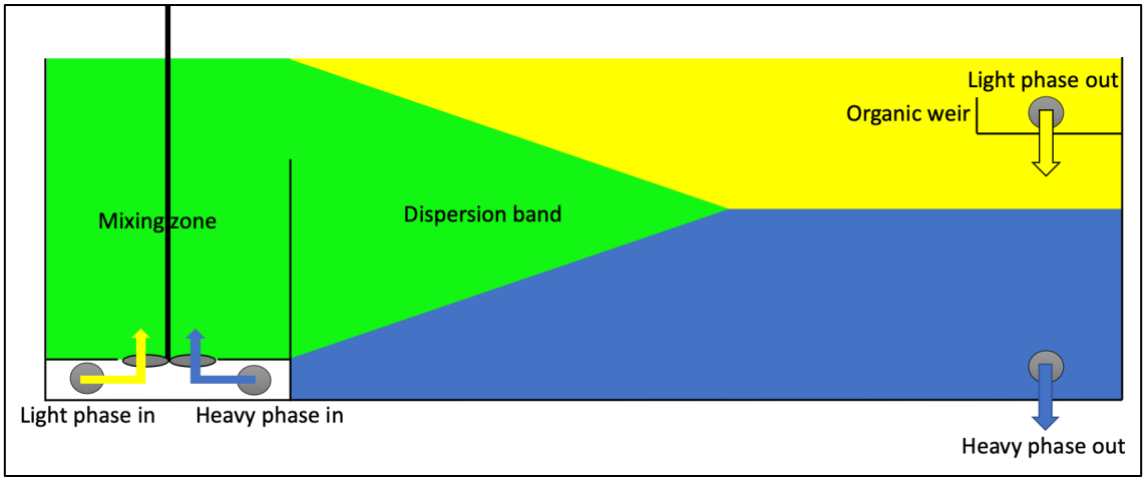

Figure 5. Mixer-settler design

Each mixer-settler unit is viewed as a discrete stage with the number of stages needed dependent on the solvent extraction efficiency and the required extraction performance. The overall flow of the aqueous and organic is counter-current, demonstrated in Figure 6.

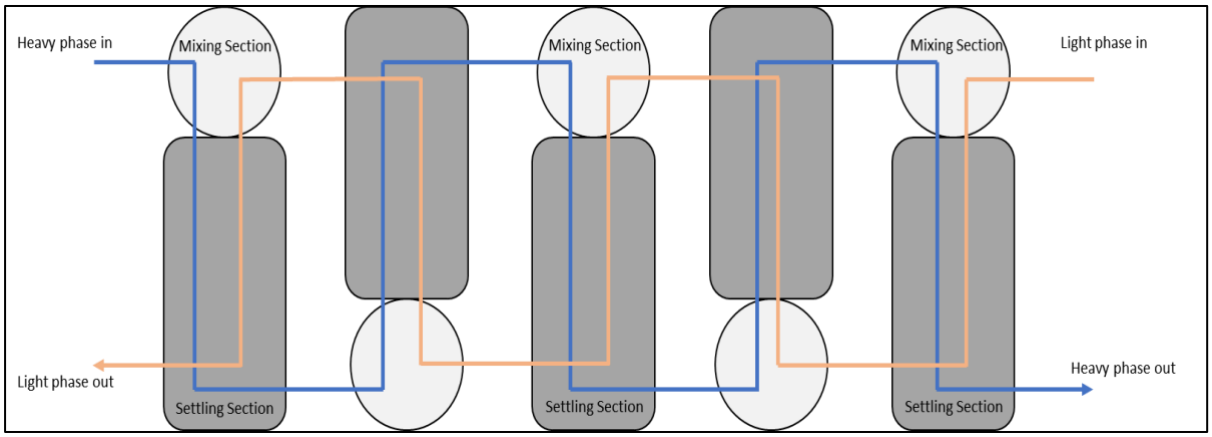

Figure 6. Counter-current 5-Stage Mixer-Settler Cascade

2.4.2 Design Principles of the Mixing Zone

The mixer design is primarily determined by the impeller and tank diameters. How the mixing section is design and operated is governed by the rate of convective mass transfer. This factor is influenced by the size of the droplet, the diffusion coefficient, the viscosity and the velocity.[45]

Skelland and Moeti (1990) then related the Sherwood number to multiple parameters to provide values for the tank and impellor diameter, given in Equation 16.

$$Sh_c = 1.237 \times 10^{-5} \times (Sc)^{\frac{1}{3}} \times (Fr_C)^{\frac{5}{12}} \times (Eo)^{\frac{5}{4}} \times (\emptyset)^{-\frac{1}{2}} \times (Re)^{\frac{2}{3}} \times \left(\frac{D_i}{d_{32}}\right)^2 \times \left(\frac{d_{32}}{D_t}\right)^{\frac{1}{2}}$$

Equation 16. Schmidt number

- Sh_c – Sherwood number
- Fr_C – Froude number
- Eo – Eotvos number
- ϕ – Determined experimental parameter
- d_{32} – Sauter mean diameter of droplet
- Re – Reynolds number
- D_i – Impeller diameter
- D_t – Tank diameter
- S_c – Schmidt number

One of the last primary considerations in the operation of a mixer-settler is the agitation power and associated impellor speed. The implications of increasing the agitation rate on the rate of mass transfer is not as simple as believing it will have purely beneficial consequences. Agitation serves to decrease drop size and film thickness as well as produce a greater blending of the two phases which aid the solute transfer between the phases. However, as the agitation increases the rate of mass transfer can decrease due to multiple reasons. The benefits of a greater interfacial area can be negated by increased agitation as when the drop sizes become too small it reduces interfacial turbulence, reducing the circulation within the droplet until they become r7idged spheres that do not interact.[52] Lastly if agitation is too intense, drops will become too small and will not settle in the required time causing entrainment issues in the settling zone, discussed later.

2.4.2.1 Settling Zone and Interface Control

A drawback of mixer-settlers in comparison to other contactor systems discussed in this section is the required plant footprint due to the settling zone of the equipment (up to 75% of the contactor footprint can be dedicated to the settler depending on throughput).[64] This basic configuration of the settling zone can be manipulated by the addition of inserts such as picket fencing, slopes and other configurations within the settling zone to aid coalescence. These additions hope to increase the efficiency of the mixer-settler by reducing the turbulence in the settling zone, allowing the drops to settle quicker. Maintaining

a low linear velocity in along the settling section also aids efficiency as it reduces entrainment of small drops in the dispersion band.[42]

The primary drive of the separation of the two phases is the density difference and the size of the droplets (interfacial tension). The larger the droplets the quicker the emulsion will separate; however, this larger interfacial area adversely affects the mass transfer in the mixing section. Another aspect to consider in the settling zone is the height of the outlet weir as this can be dependent on the height of the interface. In many designs this outlet weir will be adjustable. Control mechanisms involve adjustable weir height and pressurised stages.[64]

2.4.3 Pulsed Columns

Pulsed columns operate as a continuous differential contactor, and the height of the column was traditionally based on the extraction efficiency or mass transfer rate prior to the introduction of mechanical agitation through multiple techniques.[58] The first pulsed column patent by Van Dijck in 1939 had mechanically moving sieved plates to force the heavy and light liquid phases through holes in the plates.[65] The patent also discussed the possibility of pulsing the liquid in the column rather than moving the plates. It has found suitability in the nuclear industry for solvent extraction of spent fuel due to a variety of factors:[66]

- The pulse design allows for a more compact design in comparison to conventional column contactors reducing head height, this is turn reduces the materials to be used not only for the vessel but also for the area required to be shielded to contain radiation.
- The mechanical design of a pulsed column is suited to use with corrosive and radioactive materials as the moving parts of the pulsing unit can be kept from contacting the column solution, this allows for ease of repair and servicing when required.

The principle of pulsed columns is to increase the area of liquid-liquid contact between the heavy and light phases. The pulsing action achieves this by reducing the drop size of phases as it breaks up the liquid during the pulsing action. There are two types of extraction column, sieve and packed, both

having their own advantages and limitations. The sieve-plate column design is used for all current commercial reprocessing facilities such as THORP, UP3 and RRP.[66] This design uses perforated plates that hold up the liquid under capillary action in the column under non-operating conditions, i.e. no pulsing. This is due small size of the holes in the plates; the liquids are constricted by the interfacial tension and cannot pass due to gravity and density difference. This method is also one of the safest liquid-liquid extraction methods. Relative to the mixer-settler design, the columns have a low hold up time and high surface area to volume ratio. This reduces the risk of third phase formation and possible criticality events, degradation of the solvent, increased extraction efficiency and additional safety features used at THORP are hafnium (a good neutron absorber) lined plates as well as boron carbide filled tubes.[67]

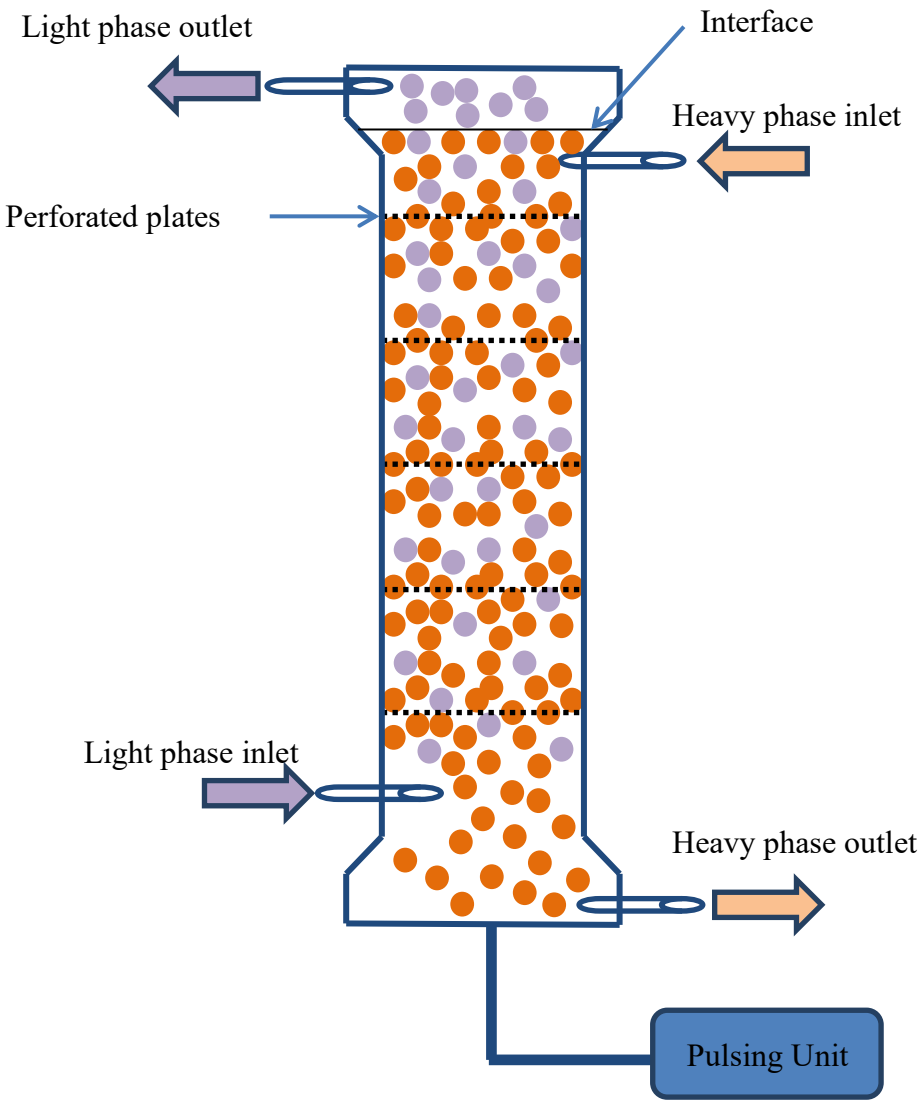

Figure 7. Perforated plate pulsed column adapted from Yadav (2008)[68]

One of the most important factors when optimising pulsed columns is knowledge of the drop size, which is essential in obtaining mass transfer coefficients.[69] The drop size is notoriously difficult to model, with many correlations developed to help estimate it under the various types of column design and operating parameters. In pulsed packed columns, the droplets when contacted with the packing, break down to form smaller drops, which are eventually assumed to be of uniform size. An example equation used to attain the mean droplet size in non-agitated columns is given in Equation 17. In the absence of agitation, the drop size is a ratio of the interfacial tension to buoyancy forces. When introducing agitation, the drop-size was dependent on the previously mentioned parameters and the power dissipation per unit

mass, dispersed phase cohesive forces (IFT and viscosity) as well as the operating regime of the column.[70]

$$d_0 = C_1 \left(\frac{\sigma}{\Delta\rho g}\right)^{0.50}$$

Equation 17 Mean drop size diameter in a non-agitated extraction column[71]

C_1 – Function of the column geometry and mass transfer
d_0 – Mean droplet size, m
σ – Interfacial tension, $N.m^{-1}$
$\Delta\rho$ – Density difference between light and heavy phase, $kg.m^{-3}$
g – Gravitational constant, $m.s^{-2}$

It is accepted that due to the complexities of the operation of an extraction column, pilot-plant data must first be obtained for a greater understanding of the behaviour of the process.[48]

2.4.4 Centrifugal Contactors

Centrifugal contactors (the contactor can be referred to as a centrifugal mixer-settler) were first used for the PUREX process in 1966 at Savannah River Lake (SRL).[72] The 18 stage section was used for extraction and scrubbing of spent nuclear fuel until they were shut down in 2003 (to be replaced by a multistage mixer-settler). Centrifugal contactors are ideal choice for systems with a small density difference and are advantageous in comparison to columns and settling tanks due to their compact size, reducing a plant's footprint (and height) as well as operating at high efficiency and throughput. They also offer other advantages such as a smaller solvent inventory, fast start up (quickly reaches equilibrium), reduced shutdown times, improved criticality safety and reduced solvent degradation due to reduced radiation exposure times. These advantages are predominantly as a consequence of the very short residence time (5-10 seconds) and geometry that centrifugal contactors offer.[73]

The original Savannah River Lake design for a centrifugal contactor has since evolved and the modern centrifugal design is classed as an annular centrifugal contactor, shown later in Figure 8. Both liquid phases enter at the midsection of the contactor, typically 180° apart, and flow downward into the mixing zone. The mixing regime creates turbulent liquid-liquid dispersion promoting effective mass transfer; the mixed phases are then guided into the centrifugal separating zone. Here the dispersion is separated

by density into the two outlets. The denser phase is forced outwards and exits through the top of the contactor, whilst the less dense phase flows through the inner exit. For a given throughput, the design of the contactor is altered by the radii of the inlet below the rotor and outlet weirs of the two phases. What then needs to be considered are the operating conditions such as the density differences, O:A flow ratio and rotor speed which will dictate the dispersion band dimensions and thus the operating threshold. In order to prevent the undesired entrainment and contamination of either phase in the other the density, organic to aqueous flow ratio and rotor speed must operate at the design levels for the outlet weirs.[73–75]

Very high efficiencies can be attained when the operation is staged counter-currently. Advances since the initial SRL contactor into the annual contactor system has allowed for the ability to deal with solids in solution, modular design aspects and improved mechanical endurance. These reasons have led to the centrifugal contactor systems being the favoured equipment of choice in the nuclear recycling industry, especially for future flowsheets.[76] They have since been tested and shown to work with proposed future solvent extraction processes such as uranium extraction process (UREX) and UREX+ [77] and the group actinide extraction process GANEX.[78]

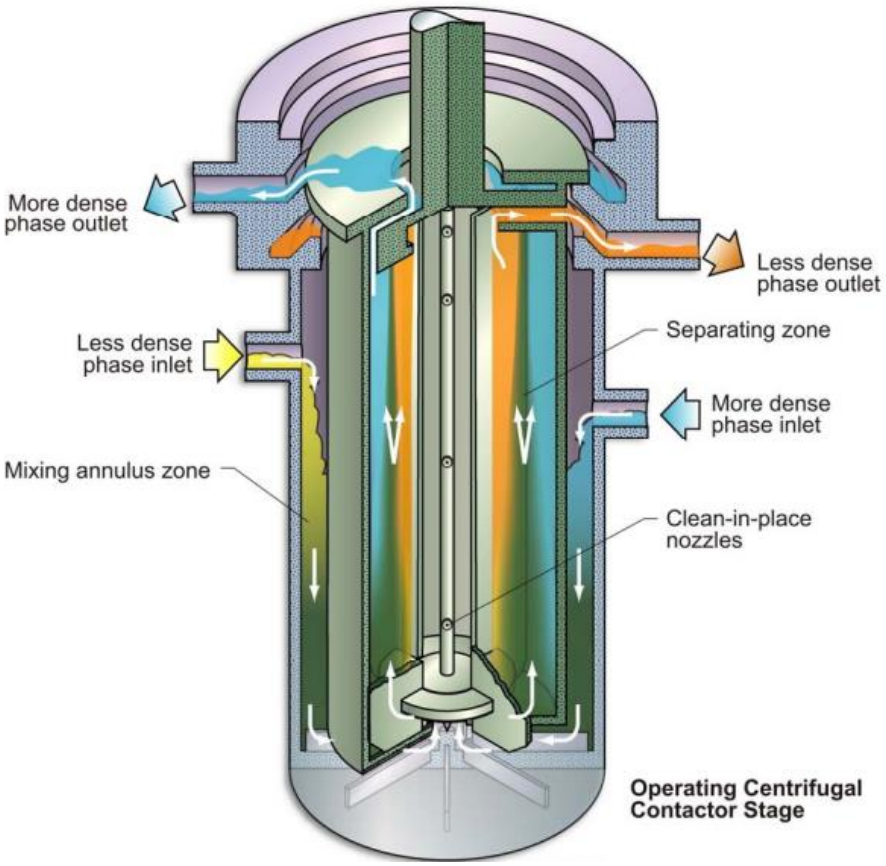

Figure 8. Centrifugal Contactor taken from Simpson et al. [25]

2.5 Waste Strategies and Considerations

2.5.1 The Global Waste Challenge

It is expected that with the current and predicted demand for energy, new reactor designs will be needed by 2040 to relieve existing nuclear power plants. These proposed advanced reactor systems are hoped to increase fuel efficiency, reduce the volumes and radiotoxicity levels of long-lived radioactive waste streams and prolong uranium resources for the nuclear energy programme.[79] With the introduction of advance reactors, the PUREX process now faces problems to be technically feasible.

The step to modernise the whole civil nuclear fuel cycle, including the possible inclusion of recycle operations to close the fuel cycle, was taken in 2000 when the Generation IV International Forum (GIF) was initiated. In addition to develop and deploy new reactor designs between 2020 and 2030 it would also be the catalyst for the transition of the reprocessing era into a recycling, partitioning and

transmutation operation there was to proposal of the Generation IV cycle.[80] This looked to address the following six topics: sustainability, economics, proliferation resistance, and safety and reliability.[81] The advances in reactor design and operating conditions alone will change the recycling process due to a differing spent fuel compositions and the likely physical and chemical properties of these future spent fuels requiring alternative recycling methods. To produce energy through a new generation of nuclear reactors there are six essential areas that must be addressed. These must be implemented for a recycle programme to me compatible and compliant with advanced fuel cycles and energy needs[24,82]:

1. Protection of people from ionizing radiation. This applies to both the wider public and those operating a recycle facility, through enhanced operating procedures, minimised waste volumes and effective shielding.
2. Efficient use and reuse of available natural resources consumed to produce nuclear energy, through effective recycle of fissile materials not consumed in initial burns.
3. Increased proliferation resistance by implementing co-separation of Pu with other actinides.
4. Reduced costs through process intensification, waste arisings and lower environmental impact with carbon, hydrogen, oxygen, or nitrogen based (CHON) extractants, smaller plant footprints (centrifugal contactors) and reduced solvent inventories.
5. Greater flexibility of processes to allow for the spectrum of fuel types in advance reactor systems. Process robustness must be at the heart of a design and tested beyond perceived operating conditions with an ability to retrofit where possible.
6. Reduced impact and time required for waste to be stored in a geological repository. This is achieved by reducing long term heat sources and waste inventories through the effective TRU actinide recycle reducing the inventory of long-lived, high radiotoxicity radionuclides.

2.5.2 Storage and Disposal

Even with the successful implementation of a recycle process with advance reactor systems, there will still be the requirement for the storage of some waste that cannot be consumed during the fission

process. Referring back to Table 2, fission products, plutonium and minor actinides produced in an LWR burn up only constitute around 7% of the composition in the spent fuel. However, these fission products typically possess a very high radiotoxicity but a relatively short half-life in comparison to U, MA and transuranic (TRU) elements in spent fuel. Therefore, it is desirable to segregate the FPs from the long-lived actinides, even if all the actinides are not re-used in fuel, it will minimise waste volumes and the costs of disposal. If this is achieved efficiently and the fissile actinides are recycled and ultimately consumed (or burnt), it can considerably reduce the amount of time the waste from spent fuel requires managed storage/disposal before having an ingestion radiotoxicity level comparable to that of natural uranium (deemed environmentally safe), shown in Figure 9. This could reduce the time needed for a geological disposal facility to safely contain spent fuel waste from 130,000 years to around 1,000 years.[83] This makes the concept of geological disposal a much more realistic proposition as there is increased confidence on geological predictions regarding the future of the storage site for 1,000 years as opposed to over 100,000 years.

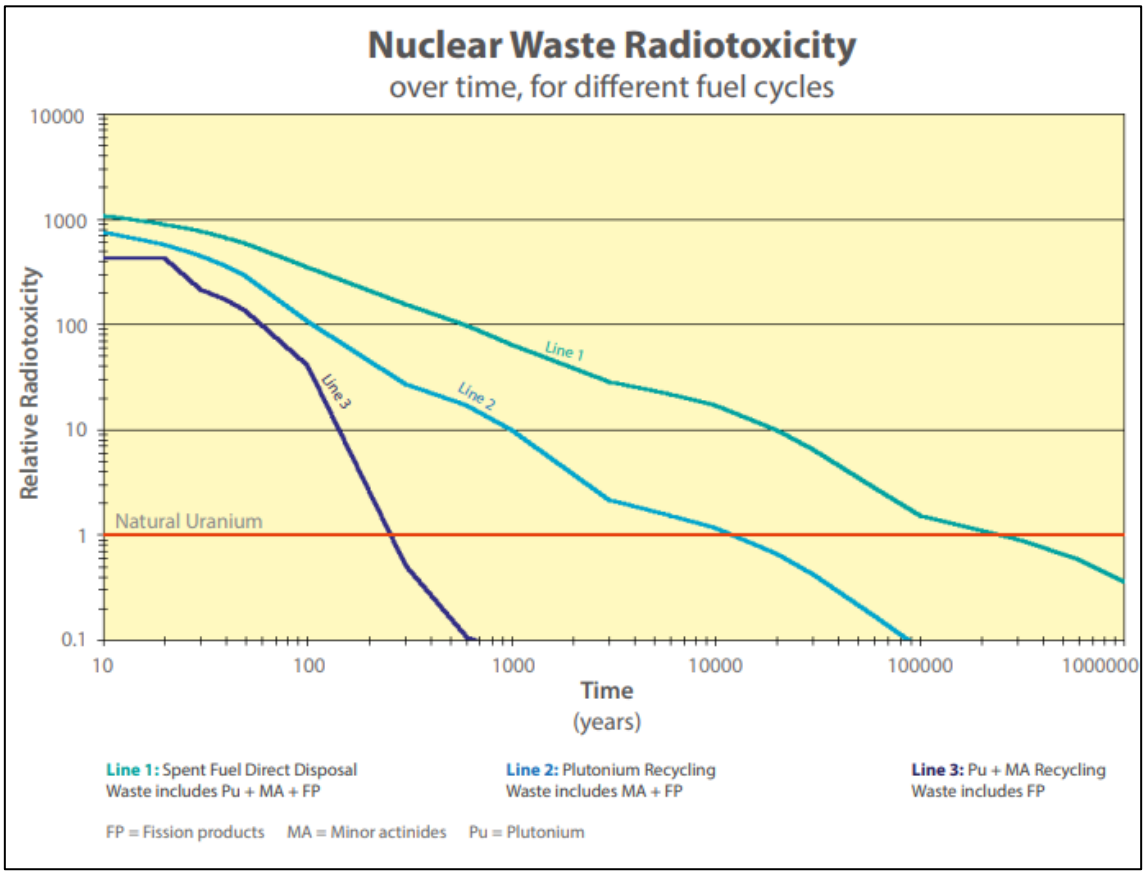

Figure 9. Ingestion radiotoxicity of one tonne of SNF over time[84]

2.5.3 CHON Principle

A new concept is to use extractants that obey the CHON (carbon, hydrogen, oxygen and nitrogen) principle. Through the CHON principle, future extractants could be incinerated producing only CO_2, N_2 and H_2O facilitating a volume reduction in waste streams associated with PUREX solvent which require expensive, managed long-term storage and disposal.[85,86]

To comply with the CHON principle, these concepts look to utilise the extracting ability of amide based extractant systems, which have been evaluated as a potential ligand for the nuclear industry since the 1960's due to their affinity for hexavalent and tetravalent actinides.[87] Siddall's work focused on changing the R and R' groups of the amides, these studies demonstrated simple and inexpensive synthesis route, one of the major problems associated with many extractants.[88] The CHON principle has been harder to implement in MA separations due to the complex chemistry, however advances are being made.[89,90]

2.5.4 Proliferation Resistance Integration

Due to well established chemical route to isolate plutonium through aqueous reprocessing methods, global distribution of recycling techniques is treated with concern with respect to proliferation purposes. There are two ways to integrate proliferation resistance into nuclear recycling operations and realistically requires a combination of both. The first is strict legislation and treaties, enforced by a central international administrative body that would monitor the process to ensure accountancy of the nuclear inventory. This body would be the International Atomic Energy Agency (IAEA) and it already performs this role with an on-site lab at Rokkasho-Mura in Japan.[91]

The second, is the designed in proliferation resistance and safeguards through the separation chemistry. This involves no isolation of plutonium, which is instead coextracted with other species such as the minor actinides.[91] This is the basis of many proposed extraction routes, discussed later in this section, and is seen as an essential feature for the wider application of nuclear recycling.

2.5.5 Process Intensification

Lastly, and what this body of work targets, is the advancement of process intensification within the nuclear recycling sector. This is the improvement of efficiency through a thorough understand of a process which if applied correctly can minimise inventory, waste production and energy costs.[92] Process intensification has already been seen within the nuclear sector with the process-intensifying equipment in contactor technology, moving from mixer-settlers to pulse columns and finally a widespread consensus that centrifugal contactors will be used for future commercial recycling operations.[67,72]

There are many areas of interest to study within liquid-liquid extraction that can bring tangible results to both energy efficiency and extraction efficiency, often focussing on one without consideration for the other can have adverse effects. This is seen with the addition of surfactants to reduce the interfacial tension that can hinder mass transfer across the interface.[93] Within a nuclear sphere there are also more variables to balance, the change of diluent or extractant concentration to reduce the viscosity of an organic extraction in an effort to reduce power consumption could result in a critical third phase forming.[94] In solvent extraction mass transfer is happening within both liquids and across an interface, which presents many opportunities to enhance both dispersed and continuous phase mass transfer, however due to the aggressive process environment, degradation of solvents will occur. Process intensification must look at selecting robust solvents that are able to perform the required separation for as long as possible, whilst balancing cost, regeneration and change to physical properties. Studies into the physical behaviour of both current and proposed advance recycle concepts have occurred,[95–104] however a tangible application as to how these would impact the chemical engineering of a SNF recycle operation is not evident within literature.

2.6 Future Recycling Options

Currently there are over thirteen accepted potential process concepts designed for future recycling operations ranging from the bulk uranium separation to the specialised minor actinide / lanthanide extraction.[105] To address the concerns raised previously in this section, two potential avenues for spent

fuel recycling are discussed here, with the focus on the bulk removal of uranium that would leave a co-extraction of plutonium building in proliferation resistance to the process and simplifying later extraction steps where minor actinide and lanthanide separations become increasingly complex.[106]

2.6.1 UREX

The Uranium Extraction (UREX) process is an advanced version of the PUREX process however as the name suggests it implements a targeted extraction of the uranium from the aqueous raffinate in addition to the removal of technetium. There are nine variations of the process but the core coextraction of U and Tc remains.[107] The extraction of Tc will have the effect of significantly reducing the radiotoxicity of the raffinate main raffinate as well as the heat decay.[106] The Tc is then further removed from the U. The Tc does not contribute significantly to the relative long term dose of HLW and is suitable for geological disposal whilst the partitioning of the uranium allows for it to be recycled or stored at a low dose created a substantially lower high level waste volume.[108]

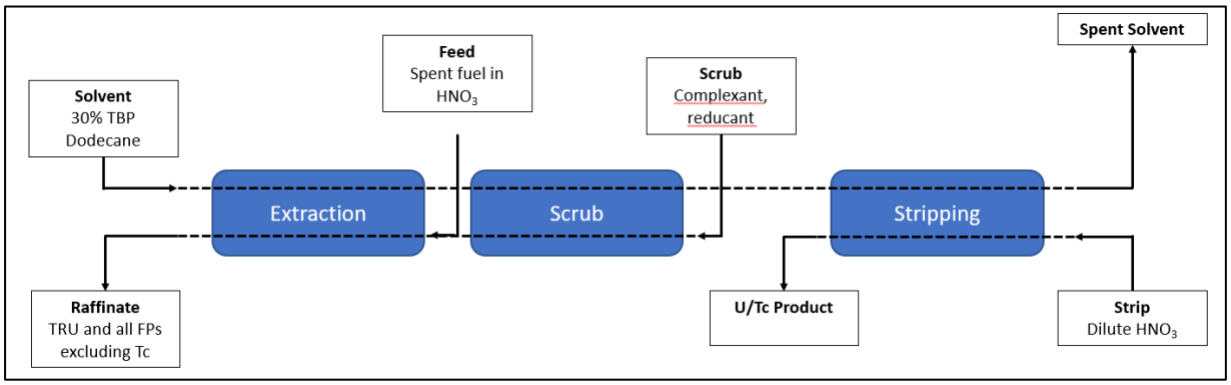

Figure 10. UREX Process Flowsheet[109]

It has been led by development in the United States and successful tests at Savannah River Laboratory have demonstrated its viability using irradiated fuel. As with the PUREX process, the extractant used is a 30% TBP + *n*-dodecane mix which goes against the CHON principle. Following the bulk extraction there is a further removal of Tc with the uranium. Another advantage is that the process chemistry, physical behaviour and general understanding of the solvent system are advanced in comparison to other recycling concepts due to the international level of experience with TBP.

2.6.2 GANEX and EURO-GANEX

The GANEX process is a two-step concept that was developed by CEA, France, to meet the objective of a Gen IV fuel cycle.[110] The first stage is the selective extraction of U(VI) in high purity and concentrations from the aqueous spent fuel solution. This removal of heavy metal masses will also reduce stream volumes and improve the hydrodynamics for next recycle step.[111] The second stage is a bulk removal of the remaining actinides and lanthanides before a targeted strip to remove the Pu and MA for use in MOX fuel types.[112] This coextraction of plutonium with the other MAs will increase the proliferation resistance of the process design and a transmutation pathway to reduce the longevity of radionuclides produced through the nuclear fuel cycle.[112] A monoamide will be used for the first stage and the bulk extraction of U(VI) and it has been widely agreed that *N, N*-di-2-ethylhexyl-butyramide (DEHiBA; Figure 11) is the preferred ligand in a hydrocarbon diluent.[113] Due to the complex extraction behaviour associated with the trivalent actinide and lanthanide series, it has proven a difficult process to accomplish within the future recycle objectives. This challenge has led to several approaches from national and institutional organisations to achieve and effective route, which has delayed a consensus on a preferred system for both the organic and aqueous phases associated with the second cycle objectives, such as the development of the EURO-GANEX concept.

The GANEX 1st stage has focussed on utilising *N,N*-dialkylamides as the extractants of choice to selectively recover U from the other TRUs. From Siddal's work DEHiBA evolved as the primary extractant to be used in the GANEX-1 process. Its desirable properties are, as mentioned, a good extraction ability towards U(VI) and high affinity for U(VI) over Pu(IV).[114] This is believed to be due to steric reasons, with the large and branched DEHiBA struggling to arrange itself with the small Pu(IV) ion.[115] Pathak *et al.* (2010) studied the performance of DEHiBA and other amides in extraction studies focussing on U(VI), Pu(IV) and Th(IV).[116–118] The following extraction mechanism of U(IV) by the amide is generally reported to occur (dependent on acidic conditions):[119]

$$UO_{2\,aq}^{2+} + 2NO_{3\,aq}^{-} + nA \rightarrow UO_2(NO_3)_2.nA$$

where *A* is the monoamide.

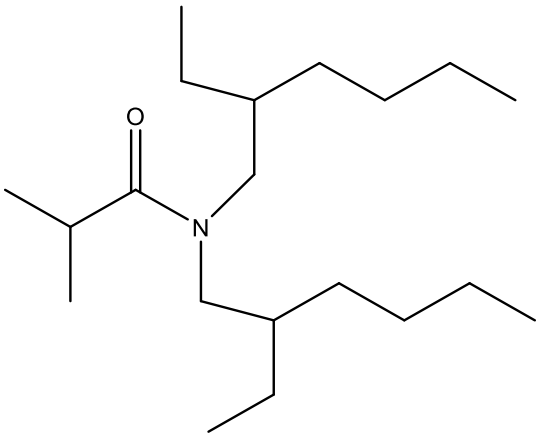

Figure 11. Skeletal diagram of DEHiBA

In addition to its selective properties, it also possesses other attributes that have brought *N*,*N*-di-alkylamides into the focus for future recycling options. DEHiBA obeys the CHON principle, a defining property for next the generation of extractant ligands. The radiolytic stability of monoamides and DEHiBA is at least as good as TBP, and work has shown comparable degradation rates of each ligand. The benefits of selected amide extractants are that the degradation products are less detrimental to the desired separation process involving U(VI) a Pu(IV) in comparison to DBP and MBP associated with TBP as many are water soluble, transferring into the aqueous phase during contact operations.. to the separation of U from the spent fuel.[120–122 123,124] Hydrolysis studies showed a strong resistance to 4 M HNO_3 over circa 600 hours, with no decrease in the D_U value.[117]

Studies have shown that, dependent on the experimental conditions, between 4 - 8 M HNO_3 a peak D_u value is reached. At this critical acidity point, interaction between DEHiBA and the acid competes at a significant rate as which to impair U uptake.[114–117,119,125,126]

Flowsheet studies have demonstrated success, with CEA operating a 28 stage laboratory scale mixer settler system on a highly active raffinate in 2008, using 1 M DEHiBA in a TPH diluent. The results from this attained the an acceptable extraction of U(VI) and an $SF_{U(VI)/Pu(IV)}$ of roughly 80 in 3 M HNO_3.[114] ITU tested the first cycle further in 2012 with a GenIV simulated feel stream (made by dissolving blend of nitride and carbide FR fuels), with an aqueous constitution of 103 g/L U, 22.7 g/L

Pu in 5 M HNO_3.[127] This test accounted for the anticipated higher Pu concentrations in the aqueous feed, as well the anticipated centrifugal contactor extraction equipment to be used in future. A basic flowsheet of the ITU GANEX-1 cycle is given below in Figure 12.

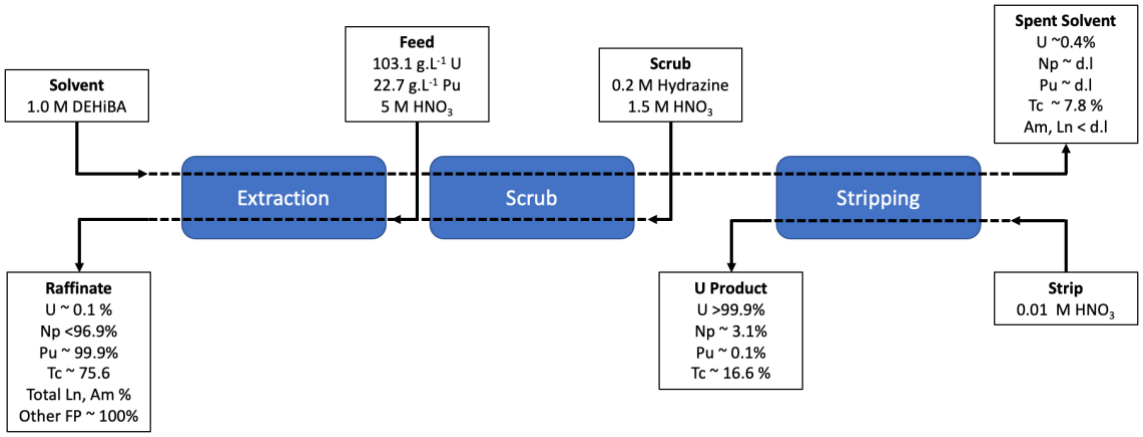

Figure 12. GANEX-1 Flowsheet, ITU 2012.[128]

There are two studies of note that have investigated the physicochemical properties of DEHiBA. Pathak *et. al*. (2002) identified its initial hydrodynamic suitability for extraction systems.[117] This work reported on an exponential increase in viscosity of diakylamides with increasing uranium concentration as well as an increase interfacial tension. However, this study did not explore likely process conditions seen for the GANEX process and limited temperature to only 293 K. Pleins (2020) published a comprehensive paper on the viscosity of dialkylamines and DEHiBA. Pleins investigated the viscosity under a range of temperature and uranyl nitrate concentrations and also attempting to define the molecular to macroscopic behaviour that influences this property.[129] This work agreed with previous studies that viscosity of diakylamide solutions increase exponentially with uranium loading in comparison to that of TBP. The work did not investigate the influence of nitric acid extraction although did acknowledge its role in increasing the viscosity of the organic phase. Pleins describes the structure form in the organic phase as cylindrical, with a polar core. This cylinder increases in length with increasing uranyl nitrate concentration and can form networks at high concentrations, greatly increasing the viscosity of the liquid. These networks suggest similar aggregation mechanisms with which reverse micelles form a

microemulsion on the pathway to eventual third phase formation with the increased extraction of mineral acids and metal salts, as discussed by Chiariza *et. al.* (2007) in TBP in *n*-dodecane.[130]

The second cycle separation involves separation of TRU (Np, Pu, Am, Cm), pioneered by CEA, although there are several solvent systems proposed for the GANEX second cycle. These have been developed generally in collaboration with multiple European partners such as France (CEA), Sweden (Chalmers University) and the UK (NNL) and the solvents systems developed include CEA GANEX, EURO-GANEX and CHALMEX processes.[111]

The feasibility of a TODGA/TBP/OK system was studied by Brown, et al. (2010) for use in the 2nd GANEX extraction step. It was hoped to be able to remove all the actinides from the rest of the fission products in the spent fuel. Studies on this system evaluated the effect of using *N,N,N′,N′*-tetraoctyl diglycolamide (TODGA) as a complexant, on the distribution ratios for various major and minor actinides and lanthanides associated with SNF. A range of concentrations were tested, varying the [TODGA], [TBP], $[HNO_3]_{initial}$ and [U], to determine distribution coefficients and conditions where third phase formation occurs. The conclusions from this work found that for minor actinide and lanthanide extraction the composition of the solvent system as well as heavy metal loading did little to influence the distribution coefficients. There was an impact on TPF (third phase formation) and TODGA has been found to be prone to TPF without phase modifiers.[78] The use of TODGA and a kerosene diluent has been found to be susceptible to TPF at low metal loading concentrations. Brown *et al*. (2010) found through the addition of TBP to the system that the third phase formation was supressed and the heavy metal loading capacity of uranium increased.[78] The addition of TBP still however does not serve to increase the loading capacities of Pu(IV) ions, solutions to this issue have been found by changing the diluent from traditional kerosene and 1-octanol.[131]

Brown *et al*. (2012) followed the previous work by investigating Pu loading of the potential GANEX 2nd cycle solvents and screened a two potential TODGA systems. Initially the work looked at a TODGA + TBP + Octanol + OK solvent system. This was found to form a precipitate when contacted with relatively low Pu(IV) concentrations. The precipitate disappeared when switang to a 0.2 M TODGA + 0.5 M DMDOHEMA in OK and extraction of up to 35 g L^{-1} Pu was achieved. In this work the suitability

of the viscosity and resistance to third phase formation as a function of Pu loading, of TODGA/DMDOHEMA/OK was evaluated. A viable compromise of chemical properties and viscosity was attained using a system of 0.2 M TODGA and 0.5 M DMDOHEMA in OK over a system of 0.4 M TOGDA + 1 M DMDOHEMA due it having a very high viscosity with high Pu loading.[132]

Studies on the degradation of TODGA and DMDOHEMA have showed similar the degradation pathways as with DEHiBA, forming similar associated degradation products, although DMDOHEMA exhibited weaker resistance to acid hydrolysis.[122,133] TODGA, which showed good resistance to acid hydrolysis resistance is also suitability resistant to radiolysis to be considered for extraction techniques.[134,135] Studies have been conducted to understand the hydrodynamic properties of TODGA and DMDOHEMA in multiple diluent systems both before and after undergoing hydrolytic and radiolytic degradation.[97] Irradiation of TODGA solvents was found to lower the IFT in systems contacted with 3 M HNO_3 increasing the phase disengagement rate. Viscosity and density were not found to change significantly. In a 0.5 M DMDOHEMA + 0.3 M HDEHP + TPH system, the density and IFT were found not to alter significantly but there was a 20% increase in viscosity up to a received dose of 800 kGy.[136]

There is still work required to fully evaluate the performance of the various GANEX-2 cycles and the key areas of interest identified are:[137,138]

- Extraction of actinides at oxidation states varying between III and VI.
- Processing fuels with Pu content between 1 wt% - 20 wt%.
- Development of robust separation flow sheets, including operation of centrifugal contactors with fast kinetics.
- Extraction of the acid into the organic phase and ligands.
- Avoiding Pu precipitation and third phase formation.
- The effects of radiolysis on the performance (chemical and physical) of the organic phase and the generation of hydrogen.

2.7 Summary

International recycling strategies have been developed however there is a lack of global consensus on the definitive or shortlisted concepts of preference. There are many reasons for this with the most prevalent due to resource abundance, political driving factors (such as proliferation treaties) or simple safety legislation that result in one recycling avenue being unavailable to a state.[139] It is the authors opinion that without a unity and a common direction for an international recycling strategy where suitable, there will be a continued stall of tangible progress and the industry will lose process expertise in operating nuclear recycling plants.

Although the PUREX process is outdated, the industrial knowledge of both the process and the extraction ability of the TBP ligand has led to its continued consideration in modified versions of the PUREX technique. However, it is still hindered by its associated degradation products and that it does not conform with the CHON principal casts doubts over its continued use in future processes.[140] Some future recycling strategies have been developed on adaptations of the PUREX process whilst others have sought to overhaul the process with new feeds, solvent systems and contactor equipment. In Europe, the focus on the partitioning of the actinides from the other less desirable FPs has led to several potential reprocessing pathways. Another concept, which would overhaul aqueous recycling landscape, is the implementation of a closed fuel concept (CFC). An example of this is the previously discussed Group ActiNide EXtraction process (GANEX), a two-step process which targets a bulk removal of U in the initial separation. This bulk U extraction however will likely cause hydrodynamic issues within the organic phase, have a potential for third phase formation and require good extraction design to maintain a strong concentration gradient for mass transfer. There is still limited understanding of the physicochemical properties, which hinders the ability to understand the properties fundamental behaviour and therefore create models with accurate mass transfer predictions.

European research projects have funded extensive studies analysing the chemical suitability of *di*-alkylamides for spent fuel reprocessing which have shown viable distribution and separation factors

under batch and continuous separation conditions.[113,119] The hot-tests run at CEA indicate that scaling up for both the GANEX and DIAMEX-SANEX processes is feasible.[141,142] DEHiBA can be confidently assessed to be the favoured ligand for the bulk extraction of uranium with multiple papers detailing this. There is still a need for all its appropriate physicochemical properties to be understood. This is even more significant at temperatures above ambient conditions and combined with uranium up to provide a total evaluation of the engineering process.

The individual ligands of the GANEX-2 cycle have been researched with the ambition for use in the nuclear recycling industry for over 20 years, which has provided a strong foundation of understanding of their behaviour. The combination of TODGA and DMDOHEMA is now a likely extractant system for the second GANEX stage. Studies have shown that its behaviour across a wide range of acidic conditions, metal concentrations, diluents and under radiolysis and hydrolysis is not fully documented or understood but is vital for its implementation in a future fuel cycle.

The nuclear reprocessing sector has driven advances in solvent extraction knowledge and technology. From the initial use of mixer-settlers, to pulsed columns and finally the refinement of centrifugal contactors to make them viable for active recycling environments. Literature indicates that the preferential contactor of choice will be the centrifugal contactor in future recycle programmes.[143–147] Centrifugal contactors have been shown to work with proposed European recycle concepts for next generation fuel cycles and will also add safety to flowsheets with higher actinide concentrations, reduce solvent degradation as well reducing the plant footprint in comparison to previous extraction equipment.

To facilitate the implementation of a safe and effective flowsheet, studies must take a holistic approach, seeking to understand the behaviour for both the mixing and separation. Both the chemical extraction behaviour of a ligand and its physical properties in a solvent system (ligand and diluent) must be well defined to correctly design effective contactor equipment. Mass transfer between the continuous and a dispersed phase (droplet) process is driven by the reaction kinetics, concentration gradient and diffusion of the solute through the phases (which is also determined by its physical properties). The physicochemical properties are fundamental when designing the separating specifications of the liquid-liquid emulsion, as the density and interfacial tension are important paraments in dictating the phase

disengagement for both gravity and mechanical techniques. Furthermore, properties like viscosity define many operating principles which can determine the viability of a recycling plant. These properties are vital in preliminary viability assessments of solvent extraction systems, the design of safety and control operations and the optimisation of flowsheets through modelling software.

Process intensification has typically been an afterthought once the technical feasibility of an extraction process has been confirmed, usually through simple extraction experiments. For process intensification to truly optimise a chemical engineering operation a holistic approach much be adopted, which involves the understanding of not only the chemistry of the extraction mechanism but also the physical properties driving mass transfer when being applied at a process scale. All facets of both the dispersed and continuous phase must be understood, operating thresholds calculated and an understanding of the chemical and physical behaviour of the fluids attained to understand first, second and third order effects of manipulating process conditions.

The development of potential aqueous recycling initiatives using novel monoamides by the nuclear industry has provided multiple recycling avenues for consideration with future fuel cycles. Since their initial suitability was established, there has been an evolution in the organic extractant systems to closer fit the requirements of future fuel cycles. Despite the extensive studies we are still unable to predict with certainty which recycling method or process will be widely adopted, it is important for this decision to be made with as much information as possible to implement a safe and effective recycling programme for the common goal of energy security. Studies have started investigating the physical properties of these proposed systems there has still been a focus on the separation chemistry of the processes and not a hand in hand consideration of how to enhance the extraction through the implementation of the principles of mass transfer. Not only will investigations in this area improve the efficiency of the extraction process but can serve to highlight process operating red lines a critical requirement for the nuclear sector. Knowledge of thresholds will improve safety and operation costs, through reducing the chances of maloperation incidents that are costly in both finance and public goodwill.

Finally of note is the lack of physicochemical infrastructure for active studies within the United Kingdom’s research sector. The bulk of physical studies have been performed in India or France on

systems of their choice, leaving a lack of data and choice for researchers within the United Kingdom in their studies of interest. Whilst international collaboration underpins the successful implementation of an advanced fuel cycle, it is important that the UK's research base is continually developed and pursues areas of research relevant to its unique ambitions and contribute to the global picture. As covered throughout this chapter, that can only occur with a total understanding, both chemical and physical, of the extraction process.

3 Project Overview

3.1 Project Aims

1) *Can a simple and robust methodology for physicochemical measurement be developed to give on plant insight into phase transfer behaviour?*

This project aims to investigate the application and practicality of using physicochemical measurements of the organic phase to predict physical and chemical operational behaviours and thresholds and to aid the initial design process of future nuclear solvent extraction systems.

1.1) Can it give insight and determine issues regarding phase transfer in next phase recycling strategies?

Investigations will assess the impact of changing the conditions and parameters of temperature, extractant concentration, extraction of acid and metal loading influence on both the organic and aqueous systems for future recycling strategies. A novel analysis approach will be applied to the data obtained to determine if it is possible to predict or monitor mass transfer, maloperation regimes and operating process thresholds. This will determine the plausibility of applying the interaction between physicochemical properties and transfer kinetics seen within mass transfer theory. This data, where possible, will be obtained in conditions that are likely to be encountered in process environments as this will give the most accurate indication of how the process will operate. As such, the experiments are designed to provide a replication of what could be seen in a likely extraction process, an area with limited published research.

1.2)Can it give insight and determine issues with respect to radiolysis effects in recycling?

Work will evaluate how added system complexity affects the ability to perform physicochemical measurements and its implications on industrial operations by determining an operating threshold. This will be achieved through subjecting the organic system to progressive radiolytic degradation gaining insight to the behaviour of these systems when exposed to irradiation fields.

1.3) Can a method be readily identified and deployability determined?

Through the establishment of a physicochemical research suite to facilitate the physical studies of nuclear recycling systems, of both equipment and knowledge, at the University of Manchester this project will assess the practically of both commercial (off-the-shelf) equipment and innovative techniques. The project seeks to produce a reliable method and apparatus that can obtain measurements using low sample volumes and to operate in the harsh nuclear recycling environment. It will identify if these measurements can be applied to provide on-line understanding and monitoring of nuclear solvent extraction recycling processes and their limitations in use. This will provide novel research on the viability of a range of current physicochemical measurement techniques for nuclear separation research and their suitability within laboratory and process conditions.

This project will focus on developing the above aims by studying the behaviour of the GANEX solvent extraction systems, both the proposed GANEX-1 and the EURO-GANEX cycle providing enhanced physicochemical knowledge of a novel extraction system. The primary identified extractants for use in a GANEX closed fuel cycle are the amides, *N',N'-di*-2-ethyl-hexyl-isobutyamide (DEHiBA), *N,N,N',N'*-tetraoctyl-3-oxapentanediamide (TODGA) and dimethyl-dioctyl-hexylethoxy-malonamide (DMDOHEMA). Amide extractants have yet to be used in the recycling of spent nuclear fuel at plant scale and understanding the physicochemical properties of these novel solvents is needed if such systems are to be deployed in the heavily regulated nuclear industry.

3.2 Thesis Overview

This thesis has been organised in alternative paper format. Below is a brief synopsis of the aims and contents of each chapter.

Chapter 4 – Experimental and Analytical Procedures

An explanation of the experimental and analytical techniques and equipment used for the work in this thesis. This chapter details the fundamental procedures used to prepare the systems for testing, contacting of solutions and separation analysis. Further details of the physicochemical procedures developed during the project are covered in Chapter 5.

Chapter 5 – Evaluation of the Physicochemical Experimental Procedures

The chapter takes an optioneering approach to the development, identification of experimental challenges encountered and the refinement of techniques to overcome these issues and obtain reliable results. It aims to evaluate from methods undertaken and exploration through research of other equipment and techniques suitable techniques to obtain physicochemical measurements in both current industrial recycling processes and research environments.

Chapter 6 – Physicochemical properties of extraction solvents for the advanced recycling of spent nuclear fuel

This paper is a study of the changing physicochemical behaviour of DEHiBA and TBP as a function of their composition in a *n*-dodecane binary system. It aims to provide a basic model to predict both the density and viscosity across a range of temperatures and solvent compositions. This work was conceived as a way to build a foundation of understanding of physicochemical analytical techniques which could be compared with literature values for TBP + *n*-dodecane whilst expanding the knowledge of the behaviour of DEHiBA in a binary system.

Chapter 7 – Studies on the Physicochemical Properties of the GANEX-1 Solvent with the Extraction of Nitric Acid and Uranium (VI) for the Advanced Recycling of Spent Nuclear Fuel

Extraction and physicochemical studies of the effect of uranium and nitric acid uptake into a 1 M DEHiBA + *n*-dodecane organic system. The influence of temperature is also studied to evaluate the hydrodynamic suitability of the organic system in process conditions. This is related to the assessed

impact that these changing properties will have on behaviour of the fluid during a solvent extraction process.

Chapter 8 – Effects of Gamma Irradiation on the Physicochemical Properties of the GANEX Solvent Systems

Both proposed GANEX-1 and GANEX-2 extractant systems were subjected to gamma radiolysis to simulate the radiolytic degradation conditions over a prolonged period in a recycle process. The effects on the physicochemical properties were analysed and related to literature degradation analysis

Chapter 9 – Conclusions and Further Work

A summary of what the project has achieved and its hoped contribution to the wider nuclear recycling industry understanding. Areas of the work are discussed that would complement and build on research from this thesis are also identified.

4 Experimental and Analytical Techniques

4.1 Sample Preparation

4.1.1 PUREX Organic Phase

Tributyl phosphate (≥99.0%) and *n*-dodecane (≥99.0%) were obtained from Sigma Aldrich. The densities of both compounds were tested in the density meter and compared to known literature values. TBP was measured as a volume percent using an autopipette and made up to the required volumes by the addition of *n*-dodecane into a volumetric flask.

4.1.2 GANEX Organic Phase

DEHiBA, TODGA and DMDOHEMA were obtained from Technocomm and confirmed by HPLC documentation to be of ≥99.0% purity and were used as received. The *n*-dodecane diluent (≥99.0%), was purchased from Sigma Aldrich.

When investigating the effects of increasing ligand concentration in the organic phase on the physicochemical properties, DEHiBA was pipetted to make the desired volume percentage of between 0-100%. DEHiBA was pipetted at room temperature using an autopipette technique made up to the required volumes by the addition of *n*-dodecane into a volumetric flask.

For extractant systems requiring exact ligand molarities, the ligand was weighed at room temperature using a Kern mass balance (±0.0001 g) and diluted to the appropriate volume with appropriate diluent in a volumetric flask.

Organic solutions that were to be used in any contacting work were pre-contacted with a nitric acid solution in a 3:1 aqueous to organic ratio at 293 K. The contacting procedure is described later in this chapter.

The use of DEHiBA, TODGA and DMDOHEMA as well as any potential future studies using novel ligand systems required the careful consideration of experimental procedures and equipment to maximise the research for the minimum volume. This was due to the cost of the ligands to work within project funding constraints. Cost mitigation and evaluation of long-term benefits is seen in this section

through the development of experimental techniques and procurement of equipment that could measure the physicochemical properties of small sample volumes (less than 1 mL).

4.1.3 Uranyl Nitrate

All uranyl nitrate was prepared from the conversion of a uranyl acetate stock. Uranyl acetate was dissolved in a 15 MΩ deionised water and filtered under gravity. 1 M sodium hydroxide is then added to form the precipitate sodium diuranate, which is vacuum filtered through a sintered glass funnel. The remaining solid is washed through with excess deionised water to remove any remaining NaOH. The sodium diuranate was then dissolved with nitric acid and the solution collected before being dried by heating in excess of 150 °C, crystallised and stored before further dissolution in desired nitric acid concentrations. Stock solutions of up to 180 $g.L^{-1}$ U nitric acid concentrations were confirmed by ICP-OES before being diluted down to any required metal concentrations, these were then further confirmed by ICP-OES.

4.1.4 Aqueous Phase Solutions

Nitric acid (>68 wt.%) received from Sigma Aldrich was diluted the required concentrations between 2-6 M HNO_3 with 15 MΩ deionised water. These dilutions were confirmed by titration using a T5 Mettler Toledo auto titrator with 1.0 M NaOH as the titrant. The free nitric acid concentrations of the uranyl nitrate stock solutions were confirmed through the precipitation of uranium metal with excess potassium oxalate, supplied by Flurochem, and a subsequent acid base titration.

4.2 Acid and Metal Extraction into the Organic Phase

Contacting of phases was achieved using an Eppendorf Thermomixer® which was capable of maintaining a temperature of up to 333 K at 1000 RPM. For pre-contacting of organic samples with acid a volume of up to 10 mL organic was used in a 50 mL vial. This was performed in a 3:1 volume ratio of aqueous to organic against the desired HNO_3 concentration. Extraction studies used an organic: aqueous volume ratio of 1:1. 3 mL of each phase was pipetted into glass vials and brought up to the desired temperature before being agitated at 1000 RPM for 45 minutes and left to stand for an hour before being carefully separated to minimise entrainment in either phase.

Aliquots (0.1 mL) were taken from the aqueous sample after to determine a mass balance using ICP-OES of the amount of U extracted into the organic phase. Concentrations in the organic phase were obtained through the back extraction of 0.1 mL of organic with 10 mL of 0.01 M HNO_3 and separated at 4000 RPM for 4 minutes in a centrifuge and an overall mass balanced performed.

4.3 ICP-OES

The concentration of metals in the aqueous phase were measured by ICP-OES (Inductively Coupled Plasma – Optical Emission Spectrometry). Samples were prepared by dilution into 2% HNO_3 in 15 mΩ deionised water and set to be the concentration range of 1 - 20 ppm. These were compared to a calibration curve calibrated from the dilution of a Fisher Scientific 1000 ppm U standard in 2% HNO_3. The ICP-OES instrument was an Analytik Jena PlasmaQuant PQ 9000.

The emission peak for the determination of the concentration of U was chosen after an analysis of peaks at 294 nm, 385 nm and 409 nm. The emission peak at 385 nm was decided on through consultation with analytical technicians, a consistently low RSD error and a lack of interference with any trace elements present.

4.4 Karl Fischer Titrations

The water content of the organic systems was analysed using a Mettler-Toledo C10S Karl Fischer Columetric Titrator which can detect between 1 ppm – 5 % water content. This was calibrated weekly using 1.0 mg/L^{-1} Aquastar® water standard. The determination method involved the addition of between 0.1 – 0.2 g of sample into the sealed vessel and the Hydranal™ Coulomat catholyte solution which is then mixed and analysed. The exact mass added was recorded at each stage and this is repeated three times to give an average water content in ppm.

4.5 Acid Titrations

Titrations were carried out using a Mettler-Toledo T5 Auto Titrator with a DGi-115SC pH probe. All titrations were carried out at ambient temperature between 290 – 298 K, using 15 MΩ deionised water and a 1.0 M or 0.1 M NaOH as the titrant. The titrant concentration was calibrated weekly against

potassium phthalate (≥99.5%) supplied by Sigma Aldrich. An aliquot of 0.1 mL of sample or stock acid solution was pipetted into a beaker for titration.

The concentration of the acid absorbed into the organic phase was obtained through a wash with pure water. 0.1 mL of organic phase was washed with 1 mL of 15 MΩ deionised water for 30 minutes at 1800 rpm at 298 K. The samples were separated by centrifuge for 2 minutes at 4000 rpm and a 0.1 mL aliquot of the aqueous phase is taken for titration against 0.1 M NaOH.

4.6 Physicochemical Measurements

The experimental techniques and their refinement for use in this project are detailed in Chapter 5, section 3. Chapter 5 is an optioneering paper detailing the approach and performance to the experimental work. This paper aims to provide insight into applicable physicochemical measurement techniques for the reader and allow for an informed method assessment. This paper was written at the conclusion of the project and provides a retrospective analysis, combing both literature and learnt experimental techniques.

5 Evaluation of the Physicochemical Experimental Procedures

Paper Overview

The paper presented in this chapter provides an optioneering evaluation of the physicochemical measurement techniques available and insight gained from both literature and experimental practice. The techniques are compared against an assessment criteria for the purposed of presenting recommendations for techniques to measure the physical properties of radioactive liquids for the purpose of spent nuclear fuel recycling.

It is anticipated that this paper will be submitted to Journal of Chemical Engineering Data.

Author Contributions:

R. Blundell – Experimental work, data collection and data analysis, manuscript drafting.

H. Lambert – Experimental advice

K. George – Manuscript review

C. A. Sharrad - Principal investigator and manuscript review

Evaluation of the Physicochemical Experimental Procedures

*R. J. Blundell *a, H. Lambert, K. George, and C. A. Sharrad*a*

a. School of Chemical Engineering and Analytical Science, The University of Manchester, Oxford Road, Manchester, M13 9PL, U.K .

5.1 Abstract

Techniques to measure the physicochemical properties of active liquids were evaluated both from literature and experimental practice. These techniques were assessed with their ability to perform in both research and industrial environments, the approach included cost, technique application and an overall suitability assessment. It was found that the techniques evaluated in a research setting did not show the suitability to replace and current industry standard methods, however leading techniques did emerge for each property which are recommended for work with active liquids with a laboratory environment.

5.2 Introduction

The nuclear recycling environment, both research and industrial, requires harsh operating conditions[85], potentially expensive extractants[148] (currently) and unique challenges not seen in most liquid-liquid extraction systems due to the nuclear element. Equipment is required to be robust to withstand the harsh radiolytic and chemical environments used or, conversely, cheap enough to be replaced (providing any replacement is safely accessible either remotely or by an operator) and any technique or item is simple enough for consistent and safe operation.

The importance of knowing the physicochemical properties of solvents overall operating conditions is applicable across all liquid-liquid extraction processes and supporting operations, from the pumping and transportation of the reagents from storage, to the power requirements for the agitation and

contacting of the phases and finally, the separation of the two phases. This understanding is fundamental in facilitating a safe and efficient process environment. This is achieved by accurate measurements from reliable equipment and trained staff who understand the process and can correctly interpret the data they are presented with. This is no more important than in a nuclear recycling plant where the potential consequences of maloperation are severe.[48] This approach must start at the smaller scale, research setting as reliable and accurate measurements are fundamental in the design and scale up of a process to pilot and full-scale operation.[48]

Any techniques developed and proven within a laboratory environment can subsequently be integrated for the on-line monitoring of a continuous process or off-line batch samples taken for quality control. There are various methods available to both researchers and industry to measure density, viscosity, and interfacial tension, however, these vary significantly in their application suitability and access.

To the best knowledge of the author, there is no combined work that has evaluated techniques for the physicochemical research of liquid-liquid extraction systems used in the nuclear industry. This paper uses available research and industry literature to provide an informed evaluation of data acquisition techniques and their potential use within the research and process sphere. Secondly, it details work undertaken using a selection of the equipment, how these were refined in a research environment to facilitate the measurement of the physical properties of both the aqueous and organic phases.

5.3 Review and Paper Approach

Available methods for the acquisition of physicochemical measurements will be obtained from a literature review along with the stated costs, technical specifications and resulting advantages and constraints associated with each technique.

The literature review of the techniques will look at the technologies currently available and in established use in research and industry and where possible, evaluate their use within the nuclear sphere. The review will not be exhaustive and will be limited to commercial off the shelf (COTS) instruments and techniques available to the typical research institute and the nuclear industry. There are three

assessment criteria being evaluated that aim to provide insight into the performance and suitability of the instruments and techniques for nuclear research and industry application, these are discussed in detail in the next section.

It most continuous operation circumstances equipment as a Coriolis flowmeter[149] would be used to measure the density and viscosity of a fluid. These have also seen application at pilot-level testing within the nuclear recycling research environment.[150,151] This paper looks to present novel and or research approaches to physicochemical measurements and where possible relate their potential use to continuous, pilot or industrial level operations.

5.4 Assessment Criteria

Three overarching criteria have been selected to evaluate and assess the application of various physicochemical measurement techniques in both research and industry. These are the cost of the method, a technique assessment, and the compatibility with recycling research and process conditions (resistance to chemical attack, radiolysis *etc*.). These aim to provide a measure of the availability, ease of use and robustness of a method within for the purposes of research and application within the nuclear recycling sector. Although the use within industry is considered, especially when considering on-line measurements, the use within research does take precedent as cost, consumables, ability to research multiple processes and conditions are viewed as important for the current position of the advanced nuclear recycling sector.

The scoring system used is subjective and derived from the author's experience when performing experiment work and its assessment of importance with a research and industrial sphere. Typically, a maximum score of four is given for any criteria however due to some subjective areas of assessed importance of that factor, *e.g.* cost, a higher total possible score is allocated. Due to the nature of the work of work being performed in a laboratory setting it should be noted that this could weight assessments towards their use within research setting. The evaluation of the application of the

techniques to an industrial environment has been derived from published reporting and the author's assessment of the feasibility of their translation.

It is possible with the evolving nature of the field that the importance of some factors become obsolete such as improvement of remotely operated techniques, a reduction in cost in automated sampling techniques or novel extractant prices or even the cost of the measuring equipment itself. This would subsequently impact the relevance of the scores given.

5.4.1 Cost Assessment

The cost scoring system is judged on the capital costs required to obtain a viscosity measurement using a manual technique from a standard industry supplier of viscometers and must include all ancillary consumable costs associated with equipment commissioning. Automated systems or integrations have been ignored due to the excessive cost they can add to any experimental system, while "manual" systems still offer the same. A low-cost system scores highly as it facilitates implementation and utilisation within research environments (see Table 3). This criterion has a greater possible score due to the assessed weighting of cost on the ability to perform a measurement technique. Within research, cost is a primary consideration as it can determine the outright feasibility of a technique in industry which will, typically, have a greater expenditure budget. The figure of £2,500 is given as this was the figure arrived at to produce a reliable interfacial tension measurement system and is the lower end of a yearly consumables research budget. Items above £100,000 would be typically a research school procured item, that would be required for wider use which would detract from the ability to perform active studies.

Table 3. Initial Cost of Technique Evaluation Criteria

Score	Evaluation Criteria
5	< £2,500
4	£2,500 – 10,000
3	£10,000 – 25,000
2	£25,000 – 50,000
1	£50,000 – 100,000
0	> £100,000

Costs of systems are based on either available open-source information or quotes obtained from industry leading suppliers up to the month of December 2020.

5.4.2 Technique Assessment

For a technique to be used within research it must be simple enough to reproduce data reliably and when used in industry it must be easy operate or monitor for the process operators of a plant, all of whom will have differing levels of experience, process background and understanding. Most modern instruments will communicate results through a software interface either on the instrument itself or through a computer interface. These forms must be intuitive in nature, clear in data presentation and provide a level of insight that allows for the ready identification of problems or concerns during operation. At research level it is not always possible for automation to be afforded with an instrument resulting in a technique requiring manual cleaning and replacement of consumables between sample measurements.

Ease of Use

Measurements are likely to be performed by operators with a range of experiences from seasoned laboratory workers who still might have no experience with a specific technique, or plant operators who have been exposed to ruggedised industrial hardware. Ease of use is typically dictated by digital control with fail safe designs, minimal manual interaction and provide a high level of repeatability. These

features are universal to both research and industry, although typically more dextrous or complex operations are part of academic research and are not viable for high-throughput operational performance. Manual interaction can also become a concern due to nuclear safety concerns and shielding requirements for operators, this applies to both environments.

Table 4. Technique Assessment Criteria

Score	Evaluation Criteria
3	Simple technique and software interface. At most daily calibration required. No or only one part required for simple cleaning in-between measurements. Easily integrated with thermostatic control. Fully automated control. High reproducibility.
2	More complex technique and software interface, more than one part required to be cleaned / replaced between runs. At most daily calibration required. Easily integrated with thermostatic control. Minimal manual interaction. Satisfactory reproducibility.
1	More complex technique and software interface, more than one part required to be cleaned / replaced between runs. Zeroing required between each sample run. Thermostatic control can be achieved. Heavy manual interaction. Satisfactory reproducibility.
0	More complex technique and software interface, whole instrument requires to be cleaning / replacement between runs. Zeroing required between each sample run. Thermostatic control can be achieved with some difficulty or inaccuracy. Heavy manual interaction. Low reproducibility.

Thermostatic control

Thermostatic control is the ability to set and maintain a desired temperature for the experimental measurement to take place at. Achieving thermostatic control is a requirement for accurate research that can replicate process conditions. Integration with measurement recording is a key benefit for a technique performance, in industry this is dictated by the process conditions and is irrelevant except for off-line monitoring. Due to the importance but also binary nature of thermostatic control is applicable, the below scoring system assigns four as the highest, two as difficult to attain and zero as not feasible.

Table 5. Thermostatic Control Evaluation Criteria

Score	Thermostatic control
4	Yes
2	Inconsistent or difficult to implement / achieve
0	No

Sample Size

An area that is more relevant for research activities is the amount of sample required and if the sample can be retrieved with minimal disturbance to its intrinsic properties. The sample can then be used for further analysis to provide a cost-efficient method, this is particularly applicable to some ligands being investigated for future aqueous recycling cycles.

Table 6. Size of Sample Required Evaluaion Criteria

Score	Evaluation Criteria
4	< 0.5 mL
3	0.5 - 5 mL
2	5 – 25 mL
1	25 – 100 mL
0	> 100 mL

5.4.3 Operation within a Nuclear Recycling Environment

The process conditions of an aqueous recycling plant require instruments to operate in a harsh chemical and radiolytic environment. The radiation can interfere with both the materials themselves, causing weakness, fractures and eventual failure or the radiation can damage the electronic operation of the instruments due to the interaction with the electrons within the equipment.[152] The degree of interaction with the electronics depends upon the type of radiation, alpha (α), beta (β) or gamma (γ). The first two can be mitigated with low level shielding such as aluminium on circuit components or the lenses on

cameras. The greatest challenge to electrical equipment and the shielding required is due to the effects of gamma radiation, which causes an ionizing phenomena by removing electrons from atoms. [152,153]

In addition to radiolysis, the chemical environment caused by the aqueous and organic used to dissolve and separate the metals will also have an impact on the materials and operation of the measurement instruments. Acidic corrosion within a radiolytic environment is a complex area of study[58,154] and is beyond the scope of this assessment. All equipment is assumed to have operational capability with the acid concentration ranges used within the nuclear sector (0 – 6 M HNO_3) due to its likely construction from glass or stainless steel. Over time, almost all materials will be adversely affected by operating within this hostile environment, however, this evaluation focuses on the short to medium-term operation, *i.e.*, can the equipment perform or even function at all.

Radiolytic Resistance

As discussed, the nuclear operating environment offers a high level of attack to an equipment relative to the majority of chemical processes. To mitigate operational failure (which can result in severe safety concerns), cost of constant replacement of hardware and overall added expense, any equipment should be able to withstand differing levels of radiolytic degradation depending on its desired operating environment. Radiation interferes with all physical and electrical properties of materials and degradation is an expectation. This criterion range assesses whether an item could likely be placed within an operating process to perform on-line measurements through to the infrequent use or use in low radiation environments.

Table 7. Radiolytic Resistance Evaluation Criteria

Score	Evaluation Criteria
4	Can operate in high radiation environment for sustained periods of time with limited adverse effects
3	Can operate in high radiation environment for sustained periods of time with frequent replacement of components
2	Can only operate in low to mild radiation environments for sustained periods of time with limited adverse effects
1	Can only operate in low to mild radiation environments with frequent replacement of components
0	Not suitable

Suitability for operation in the Nuclear Recycling Environment

The assessment for a technique to be used in industry or research will consider previous performance indicators mentioned in this chapter but ultimately must be suitable for implementation in the nuclear sector. The harsh operating conditions associated with nuclear processes require a higher standard of robustness for equipment and measurement instruments. Over time the chemical and radiolytic environment will degrade materials and lead to eventual failure, if not replaced. Due to inherent risk to plant personnel, all techniques must either be fully remote or safe to carry out with a level of shielding that allows for appropriate dexterity and control for the operator. Suitability for the use in a research environment will typically involve small quantities and batch conditions or small-scale continuous pilot tests. This final assessment of the technique (Table 8) is a holistic evaluation of all the previous performance indicators covered and determines whether, in a research environment, what the level of replication the technique and instrument can operate at and its constraints. It summarises the previous considerations, assesses its suitability and is used to highlight the level of application, relative to nuclear research or operation that a technique can be applied to.

Table 8. Suitability for use in Nuclear Recycling Environment

Suitability	Evaluation Criteria
Yes	Can be performed at or near process conditions manually or automatically with effective mitigating safety procedures (*e.g.* glovebox)
Yes	Can be performed with extensive safety procedures, specially adapted equipment or using substitute process constituents
No	Not suitable

This assessment matrix allows for the use of glove boxes as a standard safety procedure.

5.5 Density Technique Assessment

5.5.1 Literature

Two approaches of note for the measurement of density of a fluid are given in below in Table 9.

Table 9. Density Measurement Techniques

Instrument	Description
Pycnometer	Sample liquid is used to fill a special glass bulb of accurate volume and known mass. The simple relationship between volume and mass is then used to calculate the density.[155] Low-cost method, with a 5 mL glass bulb
Densimeter	Special instrument that uses the frequency of the oscillation of a filled u-tube of known volume to determine the density of the sample liquid.

Pycnometer

The pycnometer is a simple and, typically, manual technique. It uses a glass or metal bulb of a known volume and weight, and is filled with the testing liquid and subsequently weighed, providing the density of the fluid.[155] The technique is heavily dependent on manual input, produces a relatively low sample throughput and cannot be integrated to a continuous measurement technique. The benefit of its low cost (e.g. a 5 mL bulb typically costs £20 – 50) (FischerScientific), simple technique would be sacrificed

when implementing temperature control as the fluid would be required to reach thermal equilibrium which the mass balance must also sit within. There would also be an associate change in the volume of the glass bulb with temperature, and each pycnometer would have to be unique for the temperature condition. Sources of error include human error in establishing the correct volume level, errors associated with the calibration and accuracy of the scales which must also be located in an environment that is deemed to be at thermal equilibrium. The instruments are inexpensive without temperature control and can use small sample sizes (5 mL). As a manual technique requiring direct handling of sample solutions, it is ideally not suitable for active studies although early research into uranium solutions was performed using specially designed pycnometers.[156–158]

Densimeter

The densimeter instrument is based on the relationship between mass of the sample which influences the oscillation frequency of a small hollow U-tube of known volume. The change in oscillation is used to determine the mass of the fluid occupying the U-tube and therefore the density can be derived. (REF) Technique is simple and the only manual interaction is the injection of sample into the side port of the equipment. The U-tube standard material is borosilicate glass, which offers satisfactory resistance to most chemicals, although erosion will take place over time and calibration of the instrument is important to mitigate this.[159] The material of the tube can be customised to allow for measurement of particularly corrosive chemicals. Cleaning the tube requires rinsing with water and a solvent such as acetone before drying. Temperature control is achieved through heating and cooling elements in the vicinity of the tube and thermal equilibrium can be achieved relatively quickly. Advantages of the densimeter are the small sample size, high repeatability and accuracy when routinely calibrated, thermal equilibrium can be reached relatively quickly and high throughput of samples. The unit is typically relatively small in dimensions and is able fit on a workbench or within a glove box, as discussed later, some designs are compatible with viscometers.

The technique is now the research standard[103,160–167] and has been used extensively for the measurement density of active and corrosive materials.[96,99,168–171] The principle is also implemented as a method for continuous measurement, with the fluids diverted through a special U-tube cell. These have been used

in highly corrosive conditions, proven safe to operate and offer reliable density data with no moving parts requiring regular maintenance or replacement.[172,173]

5.5.2 Experimental

A densimeter was used in the experimental activities on density data acquisitions presented in this thesis due to the uranium containing samples studied and for its potential to be used in gloveboxes for measuring high active samples. Density measurements were obtained using a Mettler Toledo DM40 densimeter. The DM40 densimeter was procured for its wide temperature range, precise measurements, and small sample volumes. Its ability to record density for samples over 323.15 K allowed measurements to replicate solvent extraction process conditions.

This instrument measures density of liquids up to 3.000g cm^{-1} using an oscillating U-tube technique. Temperature is controlled across a range of 273.15 – 364.15 K through Peltier temperature control. The Eigen frequency of the oscillation tube is influenced by the mass in the sample tube. Knowing the volume of the tube, the density can be calculated.

$$T = 2\pi \sqrt{\frac{\rho V_c + m_c}{K}}$$

ρ = density of sample in cell

V_c = internal volume of the U-tube

m_c = mass of empty U-tube

K = U-tube specific constant

With the correct technique it is possible to limit the required volume of a sample to 0.8 - 1 mL, however a simple fill, and natural technique requires approximately 1.2 mL. This is injected into the densimeter using a Luer lock syringe. Care should be taken for viscous solutions as there is a risk of trapping air-bubbles within the fluid, which becomes evident when the solution is elevated to a higher temperature. A way to mitigate this risk is to insert the fluid at the highest temperature of measurement and decrease the temperature, as this decreases the viscosity of the fluid and allows for a visual inspection of the

sample chamber at the most problematic point. Alternatively, pre-wetting the U-tube and reinserting the sample can overcome this issue, at the expense of losing some sample. An estimated 80-90% of the sample is recoverable for further analysis on other instruments. For the more viscous organic solvents, the technique requires some familiarity to retrieve as much sample as possible. First there is a bulk removal of the organic liquid and a secondary residue removal. This is the only area that required familiarity with the technique as a residue would coat the walls of the u-tube but when left for a short period of time (15 – 30 seconds) the fluid merges forming larger droplets allowing for careful retrieval. Once the sample is removed, the instrument is washed through with deionised water, followed by acetone before being dried with an air pump. The density meter was calibrated once a week during periods of use with air and ultrapure water. The uncertainty of the instrument is reported to be ± 0.1 K and ± 0.0006 $g.cm^{-3}$ and repeat density measurements never varied beyond this given value.

Figure 13. Mettler-Toledo DM40 Density Meter

5.6 Viscosity Technique Assessment

5.6.1 Literature

Methods for obtaining viscosity measurements have developed significantly from the earliest techniques using capillary tubes and measuring the time taken for the fluid to flow between two points to the use of pressure sensors in a microfluid channel.[53,174,175] The type of measurement equipment depends on the requirements and constraints of the desired sample or process monitoring conditions. Inline or flow-loop systems can be integrated for continuous monitoring of the fluids or samples can be drawn and batch testing can be performed, as is the case for many measurement techniques. Listed below (Table 10) are the methods used to deliver viscosity data in research and industrial applications.

Table 10. Viscometer measurement background description

Instrument	Description
Rotational viscometer	The torque for the required rotation of a spindle immersed in the fluid at a set rate, typically a plate or cylinder, is measured by a calibrated spring. This converts the resistance to rotate the object at known torque into viscosity.[53] The various spindle set-ups can be used to tailor the procedure to the fluid and conditions.
Rolling ball viscometer	A sphere of known density falls through the sample fluid of known density, and the velocity is determined from the time taken for the sphere to fall between two points. This is related to density through the Stokes equation.
Gravity viscometers	The known volume of fluid is placed in tube (Otswald / Ubbelohde) or a cup (orifice flow) and the efflux time for the fluid to flow between two points, or empty below a certain level is measured. This is a relatively low cost and reliable method for measuring viscosity but does not allow for continuous measurement of a liquid.[53,174]
Vibrational viscometer	Typically used for online viscosity measurement in industry and the instrument is placed inside a vessel. This is set to resonate at a frequency and the dampening due to resistance provided by the viscosity of the fluid, this instrument can also be used to measure the density.[53]
VROC® pressure sensor viscometer	A sample of liquid is forced through a microfluid channel, fitted with pressure sensors. The drop in pressure is related to shear rate and stress at the boundary walls through the Hagen–Poiseuille equation.[175]

The listed methods in Table 10 have been applied in both industry and research with two common candidates, the rolling ball viscometer, and the rotational viscometer along with Ubbelohde also seen in research.

Rotational Viscometers

A rotational viscometer is a simple technique producing a digital measurement reading from the torque required to turn a spindle in a fluid. The technique requires the filling of a sample chamber, attachment and immersion of the spindle, followed by cleaning or the spindle and chamber between samples. Of note is the attachment of the spindle as the spring is calibrated and incorrect attachment technique can damage the spring. This is a point of weakness for the technique as prolonged and frequent changing is likely to cause some distortion in the calibration over time. The cleaning procedure of the rotational viscometer, through manual operation, involves the removal and cleaning of the chamber and spindle, although with automated integration the sample can be retrieved, and the spindle chamber and spindle are flushed in-situ. Temperature control is typically maintained through the immersion of the sample chamber in a water bath or water pumped through a jacketed sample chamber. Evaporation effects can interfere with the accuracy of measurements and this is seen especially within the cone and plate method, as described in section 5.4.2.[174] This method is seen commonly in research and allows for continuous measurement and is suitable for measurement of non-Newtonian fluids as the shear rate can be manipulated.[174] It has proven use over the last 30 years measuring high level waste in a research environment, up to temperatures of 1300 K when analysing glass vitrification, demonstrating the robustness of the technique[97,169,170,176–178] and has been used for the determination of the viscosity of uranium in amide extractants previously by Pleins (2018).

Rolling Ball Viscometers

The rolling-ball technique can be performed manually, but modern techniques allow for automatic optical, electronic, or magnetic measurement for the time for the ball to fall between two points. The cleaning procedure for the rolling-ball is straight forward, involving a rinse through of the capillary tube housing the ball. The benefits of adequately designed modern rolling-ball allow for a high throughput

of measurements, due to the small sample size required (0.5 mL) allowing for a quick thermal equilibrium to be establish and short measurement distance. For opaque liquids, electrodes or magnetic sensors are used to detect the ball falling between the set distance.[174] It is unknown how a highly active sample would interfere with this procedure although it has been used previously in some studies with radioactive samples, although none could be identified which used a HAR or HLW component.[97–99,168,170,179] There would be some mitigation of radiation effects due the glass barrier between the fluid and sensors, although the influence of γ radiation has yet to be accurately assessed. One common model of the rolling ball viscometer, the Anton Paar Lovis 2000 M/ME, is easily integrated with a densimeter, allowing for the automated measurement of two physicochemical properties with a single sample, creating a compact physicochemical suite.

Capillary viscometers

Capillary viscometers are simple in design and measure the time taken for the sample liquid to flow through a vessel, either a tube or cup. The two most common designs of the gravity type viscometers are the Ostwald and Ubbelohde viscometers. These are relatively inexpensive, long glass u-tube designs, with reservoir bulbs. Here the determination of viscosity is given by the Hagen–Poiseuille flow equation for Newtonian fluids under laminar flow conditions. The fluid is released and the efflux time for the fluid to pass a mark in the tube is measured with the velocity of the fluid being determined and finally, by the Poiseuille equation, the dynamic viscosity. These viscometers typically require greater than 10 mL of sample for sufficient filling of the bulbs.[53] Automated measurements can be taken, with infrared or thermal sensors used to detect the fluids efflux time through the vessel. Temperature control can be integrated and requires the tube to be placed in a water bath or thermostatic box. If performed manually, this task requires dexterity and control when changing out and cleaning the capillary tubes between measurements. Cleaning of gravity tubes typically requires flushing or changing of the tube being used. This, again, is relatively simple procedure for automated systems however can become lengthier if done manually. Automated measurement systems typically require a large area for the equipment to be housed, potentially limiting the use of the instrument within research environments for highly radioactive samples, such as a glove box. There are multiple studies of viscosity within the

nuclear recycling field have used an Ostwald or Ubbelohde [23,101,117,168,180] viscometer which measures the time taken for the fluid to travel between two points although none have been performed on highly active material. A limiting factor in the application of this method is the amount of operator interaction required and space required for a thermostatic viscometer set-up in comparison to a rotational or rolling ball viscometer and that it can only be used for Newtonian fluids.

Vibrational Viscometers

Typically used for online measurement within industry[53], vibrational or oscillating viscometers are an oscillating instrument utilising either a rod or fork, immersed within the sample liquid or process vessel. A less established method relative to the previous techniques described, the instrument forces the rod or fork to oscillate and the dampening exerted by the fluid is recorded, which is related to the viscosity of the fluid. Sample sizes as low as 2 mL have been used with this approach [181] and there are also recent studies showing the suitability of the design for measuring both density and viscosity[182] which would make it a promising candidate for the suite of physicochemical measurements. Research instrument options are limited in variety but are cheaper in comparison to rotational and rolling ball.[183] The technique is simple, compact and the equipment is able to provide a digital viscosity measurement. The instrument must be cleaned in-between samples as frictional effects are a source of error and build-up of contaminants will contribute to these inaccuracies. Temperature control is non-specialist and is performed through immersion or a jacketed sample chamber with a water bath, like the other described methods. An assessed benefit is the location of the electrical signal transforming location, which is placed outside a vessel and behind the vessel wall, making it suitable adaption with shielding for the measurement of highly active material. There are no studies within the nuclear field of research utilising this method as it is a relatively new approach for viscometry measurements although use in high-temperature metallic melts have shown promise.[184]

Microfluidics Viscometer

The last method of note is the microfluidics viscometer. This measures viscosity through pressure sensors across a microchannel in which the sample is forced through and the drop in pressure is

converted into a viscosity measurement by Poiseuille flow law.[175] The instrument is extremely portable and the measurement technique is relatively simplistic in terms of sample manipulation as it merely requires the injection of a sample across a channel. This technology is very new when compared with the other techniques previously described in this section, although a study on uranium and plutonium extraction has demonstrated viability within the nuclear sector.[185] The most identifiable benefit is the small sample size, only 50 μL is required, although the cost of the equipment is considerably more in comparison to all other techniques. A long-term cost analysis would be economical, although to obtain the full host of physicochemical measurements the technique would be limited by the largest sample size required across the differing measurements which is likely to be much higher.

5.6.2 Experimental

There were two rotational viscometers used for the measurement of fluid viscosity in this thesis. A rotational viscometer was chosen for this research for three reasons: 1) It was an existing piece of hardware available that initially required a small retrofit for temperature control and there was no discernible difference upon commencing the project that would justify the procurement of a new instrument; 2) The rotational technique allowed for shearing of the fluid, something seen within industry, and; 3) The shear rate could be varied which allowed for further investigation of the properties of the fluids of interest, *i.e.* non-Newtonian behaviour which was a characteristic to investigate for third phase formation.

The requirements evolved through the body of work and it became unfeasible to carry out work on the relatively large volumes of the organic and metal loaded aqueous phases needed for the rotational viscometer that was first purchased for this work. All subsequent work was completed using its equivalent system that required much smaller sample volumes when there was the opportunity to procure a more suitable viscometer.

The viscosity for the first experimental chapter was measured using a Brookfield LVDV-I Prime Viscometer using an UL (ultralow viscosity) adaptor. This instrument uses a torsion spring to measure the torque by rotating the spindle through a volume of liquid at a given rotational speed. The measured

values, their rheological significance, and the equation to relate to the fluid viscosity are given in Table 11 and Equation 18 below.

Table 11. Values recorded and calculated using the rheometric viscometer method

Viscometer Value	**Calculated Value**
Torque / Nm	Shear stress / Pa
Rotational speed of spindle / min^{-1}	Shear rate / s^{-1}

$$\tau = \eta . \dot{\gamma}$$

Equation 18. Newton's Law of Viscosity

η – Dynamic viscosity

τ – Shear stress

$\dot{\gamma}$ – Shear rate

The sample holder is immersed in a circulating water-bath, measured independently by two K-type thermocouples. The temperature controlled is assessed, from the average reading, to be ±1.0 K. The operational set up is shown below in Figure 14. A source of potential error when measuring across a range of temperatures is the expansion and contraction of the metal chamber and spindle. The spindle rotates at a set distance from the chamber wall. There is no ability for the operator to quantify any effects seen due to this distance being altered.

Figure 14. Brookfield LVDV-I Viscometer

The stainless-steel UL adaptor is filled with 16 mL of the desired sample using a 10 mL auto pipette. The cylindrical spindle is then immersed into the holder and the spindle and sample are rotated to allow for any trapped air bubbles to come to the surface before being attached the viscometer and the sample measured. Problems with this experimental procedure were the large quantities of solvent that were required (16 mL) and the amount of time for the sample to reach the desired temperature equilibrium and a temperature difference from the water bath of up to 2 K due to the open sample. These samples sizes would become problematic for future contacting and radiolytic degradation studies and therefore it became important to source a more viable viscometer set up.

For samples involving a small volume (Chapter 7 onwards) a LVDV2T Viscometer with a Wells Brookfield Cone/Plate system was used for viscosity measurements. This viscometer operates in a similar manner to the previously described system with a spring mechanism used to record the torque which is proportional to the shear stress in the fluid before converting this into a viscosity reading (mPa.s). However, the design of the sample chamber and spindle allows for accurate readings using sample volumes of 0.5 mL. A temperature control system is built into the Wells Brookfield chamber and a digital reading is provided within ±0.1 K, maintained by a circulating water-bath. The smaller sample volume also allowed for thermal equilibrium to be attained rapidly and a faster measurement time.

Figure 15. Brookfield Wells Viscometer with small sample attachment.

When measuring conditions were in excess of 323 K for studies of the viscosity of the aqueous with nitric acid concentrations reaching 6 M it was evident that corrosion of the steel elements of the viscometer was occurring on the underside of the sample chamber. This area is not supposed to be in contact with the liquid sample and is likely due to evaporation of the acid, shown in Figure 16.

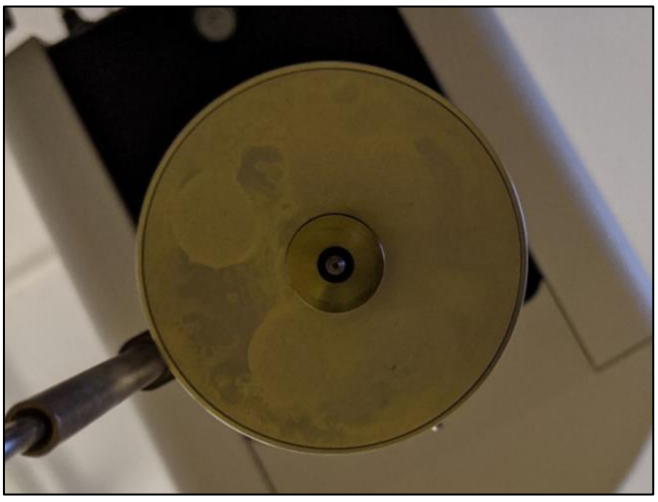

Figure 16. Underside of Wells-Brookfield Small Sample Viscometer (showing slight superficial corrosion)

If this corrosion occurs further within the equipment, it can possibly damage the calibrated internal spring and affect the readings of the equipment. It was decided to stop further measurements of concentrated aqueous acid samples above 323 K to mitigate this risk.

All compounds were tested across a range of shear rates (dependent on the viscosity of the fluid) to ensure they exhibited Newtonian fluid behaviour (viscosity was independent of shear rate). Table 12 shows that across shear rates the viscosity does not differ beyond the associated error for each measurement. As the fluids differed in viscosity it was not possible to accurately measure at one shear rate for each solvent system, instead the fluid was measured at 80 ± 5% of the torque range of the viscometer. Keeping the torque high and minimising the range of the reading reduces the associated equipment uncertainty for each measurement.

Table 12. Viscosity of liquids of note with different shear rates at 298 K

Liquid	Shear rate	Shear Stress	Viscosity
n-dodecane	375	5.13	1.37 ± 0.06
	750	10.25	1.37 ± 0.03
	1125	15.38	1.37 ± 0.02
DEHiBA	22.50	6.12	27.29 ± 1.02
	45.00	12.14	26.98 ± 0.54
	82.50	22.60	27.37 ± 0.28
TBP	150	5.20	3.46 ± 0.15
	375	12.70	3.39 ± 0.09
	563	19.04	3.38 ± 0.06
TODGA	3.75	4.46	118.9 ± 6.1
	7.50	8.76	116.8 ± 3.0
	11.25	14.07	119.4 ± 2.0
DMDOHEMA	3.75	4.18	113.4 ± 6.1
	7.50	8.53	114.7 ± 3.0
	11.25	12.48	111.4 ± 2.0

5.7 Surface / Interfacial Tension Technique Assessment

5.7.1 Literature

Surface (air-liquid) and interfacial (liquid-liquid) tension measurements vary through direct and indirect measurement techniques. Direct techniques focus on the determination of the tension of the surface layer through the use of a microbalance whilst the advances of imagery and understanding of capillary dynamics use the formation of a bubble or droplet and its capillary effects as a technique to find the tension.[186] Listed in Table 13 are common technique used for interfacial studies.

Table 13. Surface and interfacial tension measurement techniques

Technique	Instrument	Description
Direct microbalance measurement	Du Nouy Ring	A microbalance is used to determine the force required to detach a thin ring from the interface is measured, from which the interfacial tension is calculated. [57,186]
	Wilhelmy Plate	A similar procedure that used by the Du Nouy ring approach but a thin roughened plate is used instead of a ring to achieve maximum wetness. [57,186]
Drop analysis	Drop volume	A drop is allowed to form and detach from a capillary tube with a known radius *r*. The volume measured (usually by analysis of the mass and known density) is then related through gravity and buoyant forces to the interfacial tension between the liquids.
	Pendant drop	Using the curvature analysis of an image of a hanging (or floating) drop from an interface, dimensions of the drop can be calculated. These dimensions can be used in the Bashford-Adams equation, providing the interfacial tension. The method does not require advanced instrumentation, just a camera capable of a clear image and software to analyse the drop shape.[186]
	Spinning drop	Liquid system with the immiscible droplet is spun around its axis, the resulting cylindrical form is analysed through imaging and the interfacial tension is calculated.

Direct Microbalance Measurement

Direct microbalance measurements require a specialist tensiometer instrument to measure the force required to detach either a thin metal probe (ring or plate) from the interface using a microbalance. The two main methods are known at the Du Nouy ring or Wilhemy Plate method and depend on the probe being used which subsequently utilise equations specific to the probe used due to change in the interfacial interactions.[186,187]

The determined force required is measured with a microbalance which is then used to calculate the interfacial tension. When performed by the instrument the method is relatively simple in data acquisition and does not require the density of the liquids to be known, however a more complex and delicate experimental procedure is required for the cleaning of the ring or plate as it is not robust and must be correctly aligned with the interface for an accurate measurement and any deformation can lead to experimental errors. For use with organics the cleaning of the probe is important as a source of error of note is insufficient cleaning of the plate from adsorbed organics on the surface of the probe.[57,186,187] This is typically performed with a solvent wash followed by flaming. Small sample adaptors are available reducing samples to less than 5 mL however, in practice this was difficult to achieve in tests conducted within this project with an organic/aqueous nitric acid system performed as discussed later in the experimental stage. Temperature control can be integrated into the instrument however, without control of the surround air temperature, reperformance is hard to achieve as there will be heat transfer to the environment, causing inconsistencies with interface temperatures. There are some issues with the technique, and it is not best suited for interfacial tension measurements compared to some drop analysis methods. This is due to associated contact angle errors between the probe and the liquid interface cause by either inadequate wetting of the probe or the curvature in the meniscus. There are also known challenges with the ability of the scale to determine the weight of the plate or ring in liquid-liquid systems. The mentioned issues are more common with viscous or strong polar and nonpolar layers. [186,187]

The method is well established and common practice in SNF recycling research, and although the equipment cost is relatively expensive it can produce data quickly with a high degree of repeatability due to the performance capabilities of modern instruments. [55,56,97,104,162,187–196]

Drop Volume and Shape Analysis

Drop volume technique is based on the theory when gravitational forces acting on the drop are equal to the capillary forces and reach their critical size.[187] The drop is allowed to form and detach from a capillary tube with a known radius *r*. The volume measured (usually by analysis of the mass and known density) and this force related to the capillary force. This method is simple and relatively inexpensive, however can be sensitive to the operating environment, such as vibrations causing premature detachment and adsorption in liquid-liquid phases if the system has not reached equilibrium.[186] This technique has been used for the study of promising extractants and the effect of acid and metal loading, demonstrating its functionality.[117,197]

Pendant drop technique (PDT) performs an image analysis of the droplet to calculate the dimensions of the droplet formed at critical volume and relate this to the interfacial tension. The PDT captures and image of the droplet when suspended and still attached to a needle or capillary. It is important for the PDT that the needle is well cleaned to mitigate climbing, reducing the accuracy on the measurement.[186] Density of both liquid phases are required for the calculation (at the recording temperature). The method require advanced instrumentation, just a camera capable of a clear image and software to analyse the drop shape.[186] The production of droplets can be an automated or manual procedure. The use of automation allows for greater control and reproducibility of the droplet volume and removes any dexterity issues that would be associated when operating in hazardous environments. It is reported that the PDT is the one of the most suitable methods for liquid-liquid IFT measurements as there is no associated error with the contact angle between the liquid and the needle.

The last measurement system of note is the spinning drop tensiometer (SDT), which is particularly useful for systems with an ultralow interfacial tension and has found use for measurement of petrochemical systems.[187] Like all previously mentioned drop analysis methods, using a digital camera,

the dimensions of a drop are analysed however, the technique differs in that is does not use gravity to deform the droplet. The two liquid samples (typically 4 μL is required of the suspended {light phase} sample and 1 mL of the flooding {heavy phase} sample) are injected into a small horizontal tube with a Peltier element temperature control. The machine spins a small glass tube with the liquid-liquid system along its rotational axis sufficiently fast enough that the gravitational effects on the droplet can be ignored. Under increasing centripetal forces the droplet overcomes surface tension forces and will form a cylinder in the immiscible liquid, the dimensions of which are subsequently correlated to the interfacial tension with the rotational force.[187] The SDT uses a relatively complex and expensive operating instrument however, it does remove operator errors and allows for a fully automated measurement. The technique uses an extremely small sample size which will not only increase the safety of highly active experiments but also reduce the cost.

There are limited studies within nuclear recycling research that use either the PDT or SDT, although published liquid-liquid interfacial studies of radioactive samples are relatively rare. There have been unloaded liquid system studies and studies with low active fuel metals [102,198] in addition to a technical report demonstrating the ability of the PDT to measure changing IFT between the two unloaded phases over time.[199]

5.7.2 Experimental

A Krüss K11 Tensiometer (shown in Figure 17) was initially planned to be used to record both the surface and interfacial tension measurements for the work in this project due to the prior availability of the instrument. For the purposes of this research a Krüss temperature control unit combined with a Grant LT ecocool 100 circulating water-bath was purchased to maintain the temperature within the sample vessel to ensure thermostatic conditions. This offered temperature control to within ±0.1 K for measurements using this tensiometer.

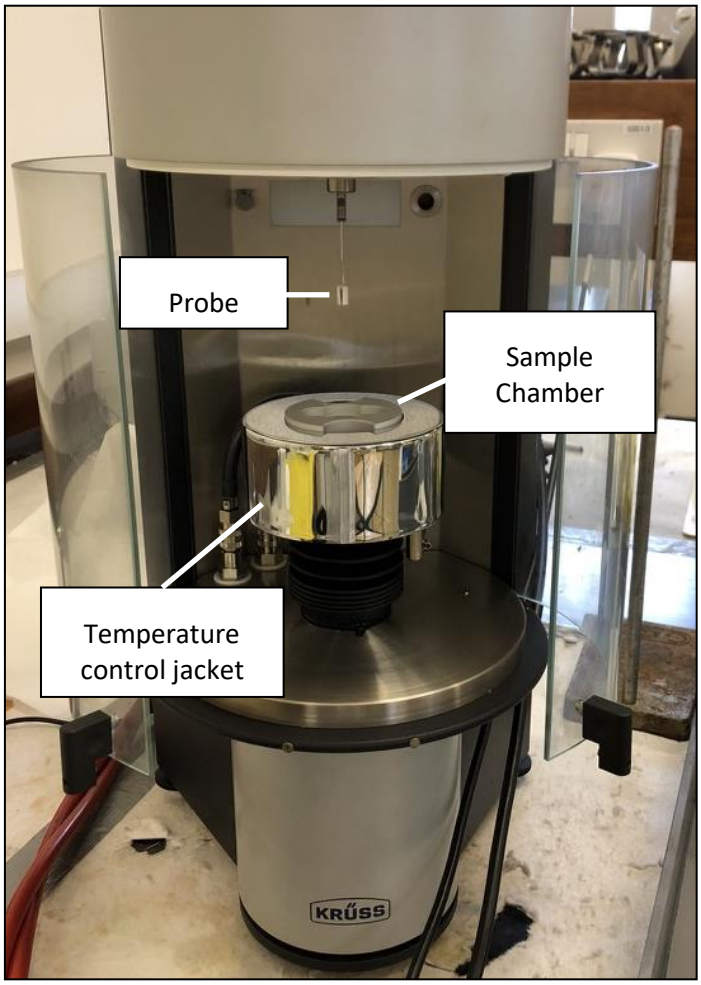

Figure 17. Kruss K11 Tensiometer

Surface tension measurements (air-liquid interface) were obtained using a Krüss PL02 curved plate, measuring made from roughed platinum. The curved plate allowed for smaller sample sizes to be measured. Sample solution (10 mL) was pipetted into the sample holder which fitted into the temperature control unit. The temperature of the sample was maintained through thermal conduction between the sample holder and the water jacket which led to inefficiencies. The method is relatively slow to reach thermal equilibrium and was also difficult to maintain the desired temperature due to the exposed surface area of the sample. This identified experimental limitation was that there was a slight temperature gradient at the surface of the sample and the air temperature of inside the glass case of the equipment, which could not be overcome but could be mitigated. The developed technique used was that a direct temperature measurement of the sample using a K type thermocouple connected to a Pico temperature recorder, ± 0.1 K, with the circulating water bath adjusted accordingly.

The procedure of acquiring the interface is performed by the instrument however, especially in the case of liquid-liquid IFT measurements, the combination of small sample volumes and the resulting liquid meniscus resulted in the accuracy of interface detection being impaired. This lowered the reproducibility of the technique.

Samples were then left to equilibrate to the set temperature for 30 minutes before measurements were taken. Each value recorded required a standard deviation of less than 0.1 $mN.m^{-1}$ of the last five readings as they varied randomly around the true value. This method was repeated in triplicate for each desired test condition. After each measurement the Pt plate was cleaned to remove impurities which are known to cause problems with organic samples. This involved being rinsed with acetone, deionised water before being heated by a Bunsen burner until glowing red for 30 seconds.

This approach utilises the Wilhelmy plate method to establish the force acting on the immersed plate between the two phases or the liquid interface and air, which applies the following equation to determine surface tension.

$$\sigma = \frac{F}{L \cdot cos\theta}$$

Equation 19. Wilhelmy surface tension equation

θ is the contact angle between the plate and the surface (i.e. 0° for the solvents studies here), L is the wetted length of the plate and F is the force required for the plate to break the surface of the liquid.

A slightly different technique involving a small platinum rod was used to measure the interfacial tension (liquid-liquid interface) between the organic and aqueous phase. Each phase (10 mL per phase) was required to fully immerse the Pt rod in the heavy phase, just below the meniscus at the organic – aqueous interface. The rod is then withdrawn and the force to break the interface is converted into an interfacial tension value. This method was first tested during the interfacial work presented in this thesis in Section 7. Table 14 shows the recorded IFT of water / *n*-dodecane and water / 1-octanol for two different experimental methods and the equivalent values reported in previous work.

Table 14. Interfacial Tension using K11 Tensionmeter vs. Literature at 298 K

System	IFT_{K11} / $mN.m^{-1}$	$IFT_{Literature}$ / $mN.m^{-1}$
Water / *n*-dodecane	49.0 ± 1.2	52.67[200], 53.7 [201]
Water / 1-octanol	11.7 ± 0.7	8.52[202], 8.19[164]

During the initial method testing it became evident that the method using the K11 Tensiometer was inadequate to produce accurate readings as the minimum deviation from previously reported work was 7.49%. There were also secondary issues encountered such as the requirement to reduce the volume of phases being tested due to the expense and availability of extractants to be studied and the wish to minimise the quantities of uranium to be handled during these measurements. As mentioned previously a requirement to minimise the volume of samples meant it would not be feasible to use the K11 Tensiometer in its standard set up (minimum of 10 mL of each phase) when analysing the IFT of GANEX ligands or aqueous phases with a high uranyl nitrate content.

To overcome these issues an optical, in-house pendant drop technique was developed using freely available drop analysis software.[203] The set-up of this technique is shown below in Figure 18 with a full schematic provided in Figure 19.

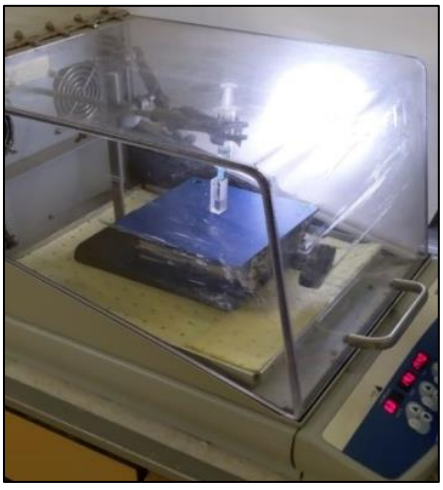

Figure 18. Initial set up of Pendant-Drop IFT

This set up used a LED white light source placed 0.3 m away from a diffuser on the side a thermostatic Perspex box within ± 1 K. A Sony DSC8100 with a 20.1 MP camera was placed on the other side of the Perspex box, approximately 0.2m from the sample chamber. A UV-Vis quartz cell chosen sample

chamber was chosen as the sample chamber, as it reduced the required volume of the light phase to 2 mL and allowed for a non-distorted image of the droplet. The heavy phase was gradually syringed out of a 1 mL syringe with a 1.68 mm internal diameter blunt needle (purchased from Adhesive Dispensing) to allow for maximum control of the droplet. It is important to record the droplet at its maximum stable size as this reduces the associated error for the measurements.[204]

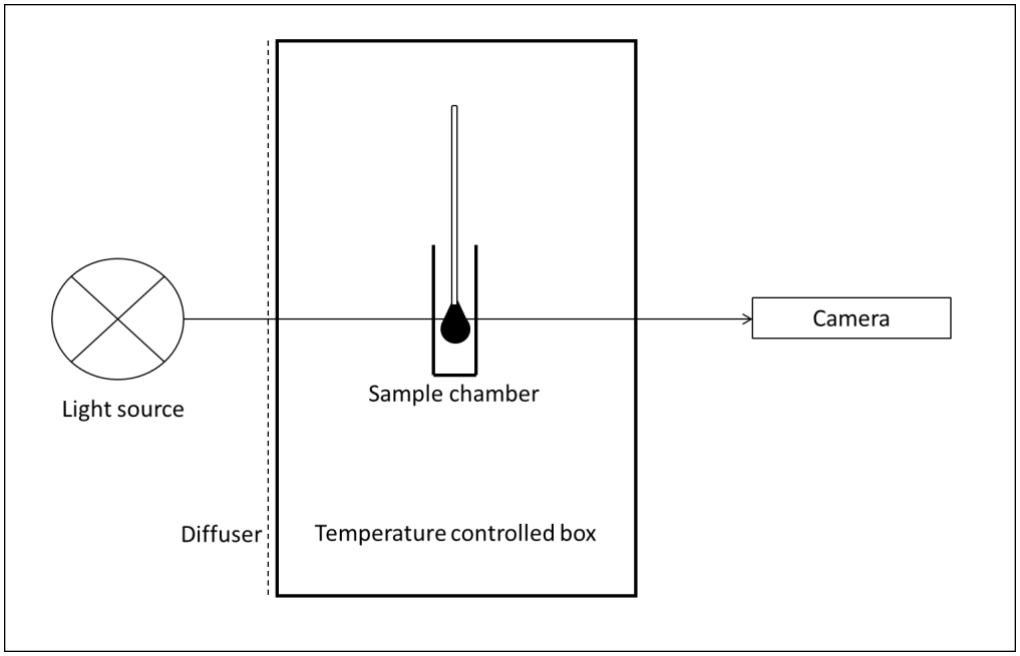

Figure 19. Schematic of initial Pendant drop experimental set up

Obtained images are analysed using the pendant drop downloadable plugin for Fiji (ImageJ) Software. Densities of both phases were required at the temperatures being investigated as well as a set length for the plugin to convert pixel size at the point of focus to an actual unit of length, this was chosen as the diameter of the needle. The software detects the droplet boundary (through colour contrast) and performs a Young-Laplace fit to analyse the dimension of the drop and establish the capillary length, *l*. The interfacial tension is then calculated using the following equation:

$$\sigma = \Delta\rho . g . l^2$$

Equation 20. Drop profile surface tension equation

This method was first tested using known systems such as water-air interface, dodecane-air interface and water-dodecane interface. These values are shown in Table 15 and example of an image obtained

from these tests is shown in Figure 20. The deviations from previously established values for the tested systems were found to be up to ± 13%.

Table 15. Surface Tension values of liquids at ambient conditions using first Pendant Drop Technique with Sony DSC8100

System	Experimental Value / mN.m^{-1}	Literature value / mN.m^{-1}
Water + Air	63.9 ± 4.2	72.59[205], 72.76[206]
n-Dodecane + Air	21.2 ± 3.1	25.3[201]

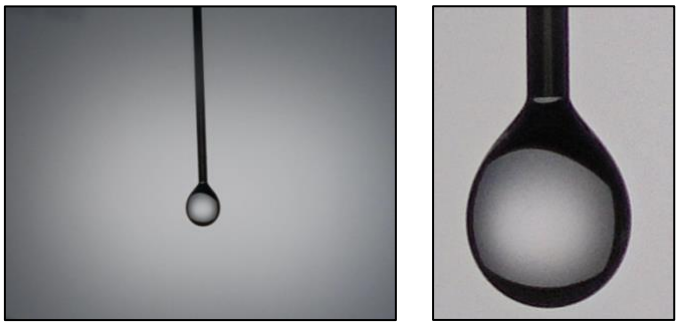

Figure 20. Image of water droplet in air taken with Sony DSC8100

The scale of error for these systems was troubling and could not be used for further studies. Further probing of the technique was undertaken to find the cause for the large difference in true and obtained results. Literature suggested that the greatest cause of error is the inaccurate measurement of the droplet, as the capillary length is squared, as shown in Equation 20, to give the surface tension result. The first iteration of the method was the addition of a condensing lens from Thorlabs, Germany. This technique involved the addition of a condenser to create near parallel light rays to reduce the incidence rays that can cause a distorted droplet size measurement. This was not found to change the SFT measurement of water significantly for the Sony DSC8100. This led to the imaging device being changed from the Sony DSC8100 to an iPhone X. This switch increased the pixel: mm ratio from 78 to 95 (at the perceived best distance from droplet and focus) and provided an improvement in the accuracy and repeatability of the SFT value however the results were still not acceptable (see Table 16).

Table 16. Surface Tension values of liquids at ambient conditions using a Pendant Drop Technique with iPhone X

System	Experimental Value / $mN.m^{-1}$	Literature value / $mN.m^{-1}$
Water + Air	71.4 ± 3.4	72.59[205], 72.76[206]
n-Dodecane + Air	23.9 ± 1.0	25.3[201]

Although the value of error was not large and results were relatively consistent, it was decided to further enhance the imaging set-up to further improve accuracy and confidence in the method. Greater probing of imaging techniques highlighted the benefits of telecentric lenses and discussions with EHD Imaging™ provided a bespoke camera and telecentric lens set up for greater accuracy for the image capture of the droplet (see Figure 21 for an example droplet image). A 6.3 MP monochrome CMOS-Camera was purchased for the specific purpose of close objectives against an illuminated background. This was used in combination with a telecentric lens, working distance 70 mm, field of view 6 × 8 mm (see Figure 22 for an image and the full schematic diagram of the set-up used).

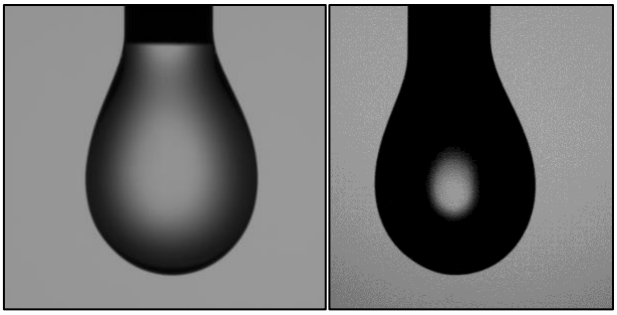

Figure 21. Image of water droplet in air without condenser lens (L), with condenser lens (R). Taken with a 6.3 MP CMOS Camera with 0.8 X Telecentric Lens

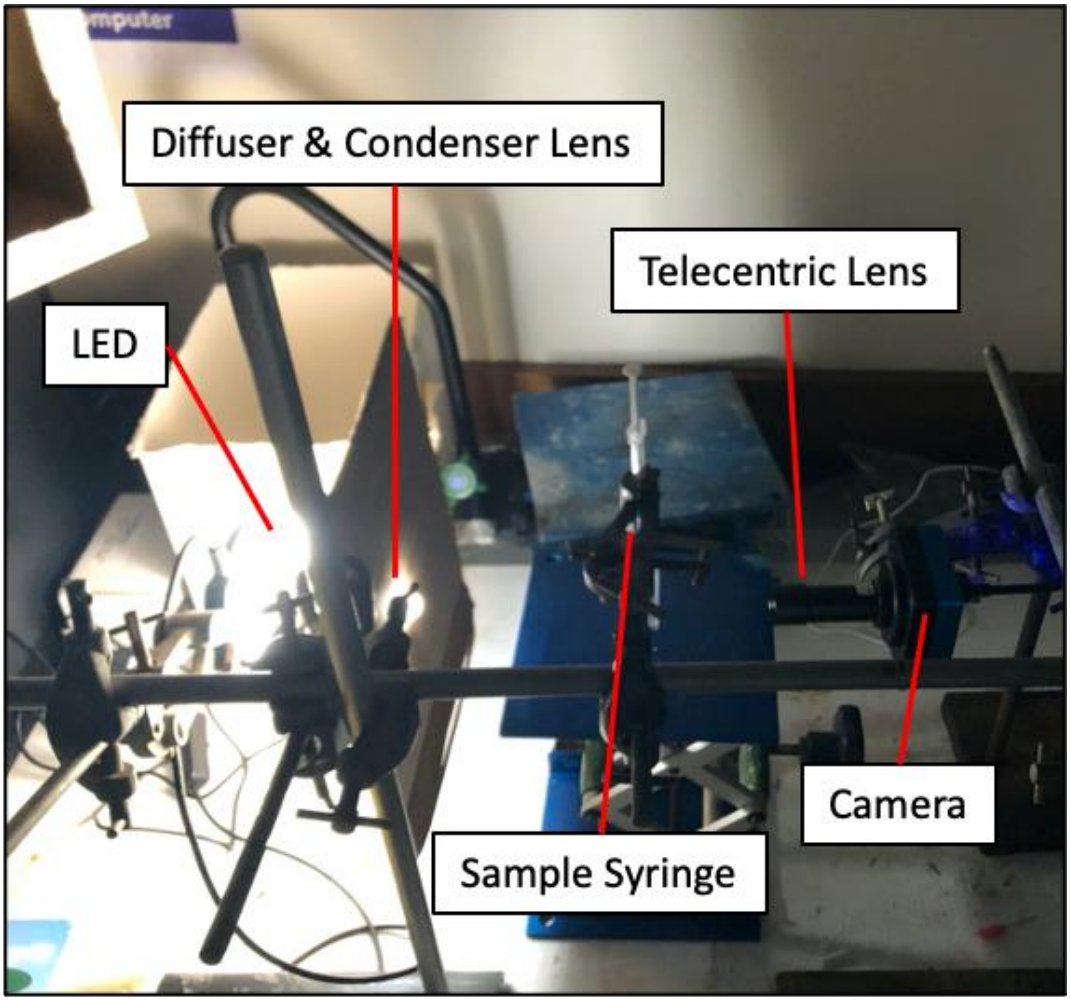
Diffuser & Condenser Lens
Telecentric Lens
LED
Camera
Sample Syringe

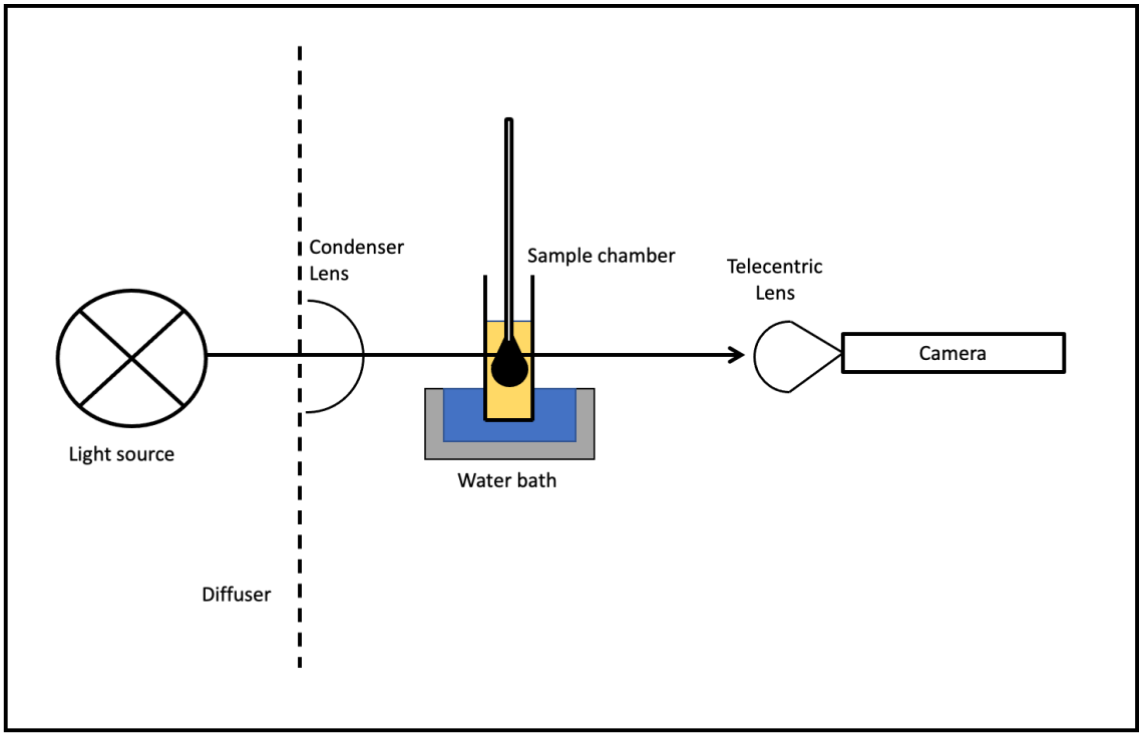

Figure 22. Final Pendant Drop schematic of set up above with added water-bath

This increased the pixel : mm ratio to 330. The following results (Table 17) for the interfacial tension results of water + air, *n*-dodecane and 1-octanol at ambient conditions were recorded using the above method. Temperature control was achieved through the submersion of the cuvette in a small water bath. The temperature of the bulk organic phase was measured using a K type thermocouple to ±0.1 K.

Table 17. Surface and Interfacial Tension values of liquids at ambient conditions using a Pendant Drop Technique with 6.3 MP CMOS Camera with 0.8 X Telecentric Lens

System	Experimental Value / mN.m^{-1}	Literature value / mN.m^{-1}
Water + Air	72.8 ± 0.3	72.59[205], 72.76[206]
n-Dodecane + Air	25.5 ± 0.2	25.3[201]
n-Dodecane + Water	52.7 ± 0.2	52.67[200], 53.7 [201]
1-Octanol + Water	8.03 ± 0.1	8.52[202], 8.19[164]

The results in Table 16 demonstrated a high degree of accuracy combined with a high-level repeatability with documented systems. From these baseline studies the technique was deemed acceptable for experimental investigations.

After this body of work was completed a final design of the pendant drop was completed which aimed to add simplicity to the setup, allowing more confidence in the stability, distances and measurement technique seen in Figure 23. This involved the purchase of an aluminium breadboard fitted with special rubber feet aimed to reduce vibrations, a cause for premature detachment from the needle. The board allowed for all pieces of equipment to be screwed into place combined with a minute incremental distance control, a high level of precision over distance movements for the camera, and therefore lens was achieved. This provided easily attainable focus for the set telecentric lens, which is critical for a clear picture of the droplet to be obtained.

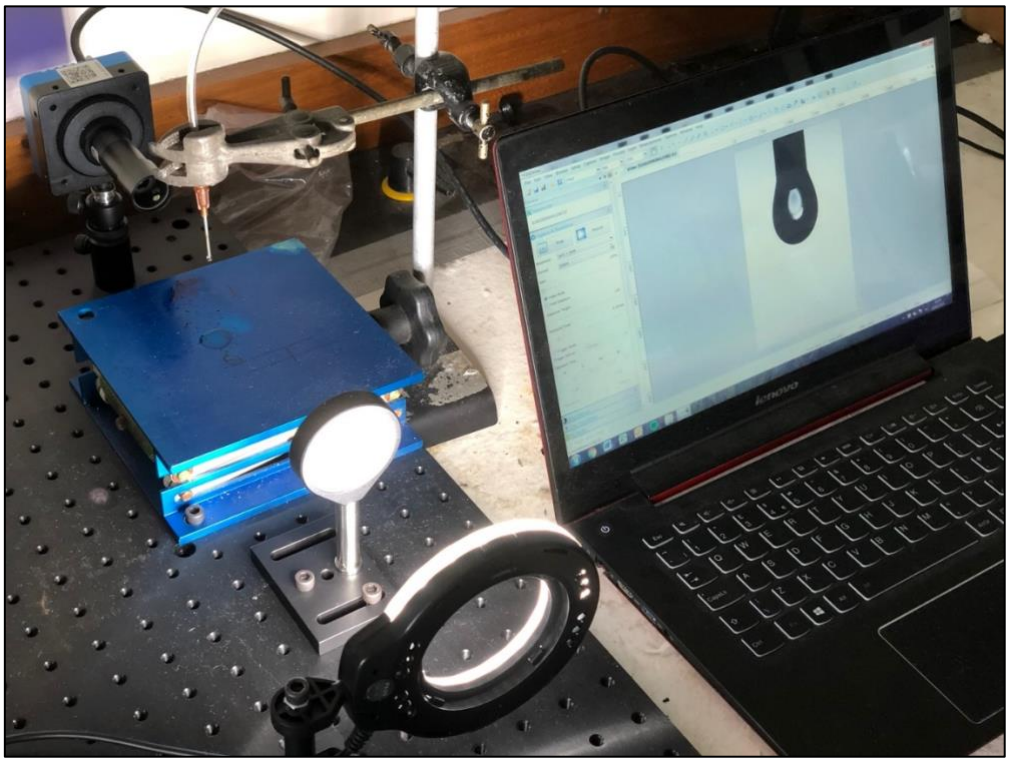

Figure 23. Updated set up of in-house pendant drop technique

The technique used in this project utilised free software developed to work with Fiji image analysis and required experience and learned judgement to provide a high level of performance with the analysis. This post-measurement analysis is an area which can be improved through procurement of specialist droplet analysis software. This will allow for the analysis through commercial and dedicated tools,

which are typically intuitive and add a high level of automation and accuracy to droplet boundary analysis (even with noise and shadows as seen with some images) which is an area of high importance for an accurate IFT calculation.

5.8 Results and Discussion

Assessment of all the various physicochemical measurement techniques described previously has been performed using the criteria based templates described in Section 5.3. The allocated scores (Tables 17-19) are based against assessment criteria and have been judged against previous statements available in the literature and, when applied experimentally, learned experience of the techniques.

5.8.1 Density Measurements

A clear conclusion can be the choice of an oscillating u-tube densimeter over a pycnometer for density measurements. Table 18 shows the full distinction between the two techniques in score when assessing the key performance indications.

Table 18. Scoring of Density Measurement Techniques

Instrument / Technique	Cost	Technique Assessment	Thermostatic control	Sample Volume	Operation in Radiolytic Environment	Suitability for Operation within Nuclear Sector	Total
Pycnometer	4	1	3	1	4	Yes	13
Densimeter	3	3	3	3	3*	Yes	15

The cost for the pycnometer can be seen as one of the only benefits to the technique, although over the medium term this advantage would be negated as typically five times the sample size is required in comparison to the densimeter. Therefore, the cost for a densimeter can be justified when accounting for the ligand demand of a research laboratory over a medium-term period. The pycnometer lacks the suitability for the operation with nuclear materials due to the manual interaction with both the measurement technique and sample preparation and cleaning. Removal of manual operation is key if performing this measurement when operating with highly active materials within a glove box or other

shielding technique. The simple injection method for a densimeter, which can be upgraded for fully automated measurement allows for safe and fast automated measurement with thermal control quickly obtained through small sample sizes. The integration of densimeters with a rolling ball viscometer is the most suitable option for measurement of density.

5.8.2 Viscosity Measurements

All techniques discussed in this chapter are suitable for viscosity measurements of active materials for the purposes within research or industry. The allocated scores assigned to the techniques is provided in Table 19.

Table 19. Summary of Viscometer Assessment

Instrument / Technique	Cost	Technique Assessment	Thermostatic control	Sample Volume	Operation in Radiolytic Environment	Suitability for Operation within Nuclear Sector	Total
Rotational sheer	3	2	3	3	4 †	Yes	15
Rolling ball	3	3	3	4	3 †	Yes	16
Capillary tube (Otswald / Ubbelohde)	3	2	3	0	3 †	Yes	11
Vibrational viscometers	4	3	3	1	4 †	Yes	15
m-VROC®	2	3	3	4	3 †	Yes	15

† - It is unknown how the electronic elements of these techniques would function in a highly active environment. An assessment of the method that the measurement is obtained has been used to provide this score.

The assessed least suitable techniques and instruments are rotational and capillary viscometers. Although basic capillary viscometers are inexpensive and expendable these are not suitable for reproducibility, or accuracy and automated viscometers are required increasing the instrument cost. These are relatively bulky and do not allow for repeat measurements with a single sample when testing

a range of temperatures as the sample must be removed and the equipment cleaned in between each measurement. This increases operator interaction, sample requirements and data acquisition time.

The small-sample rotational viscometer used during the work proved reliable and accurate in measurements and allows for a single sample to move through the entire testing temperature range. This technique has the potential to cause zeroing errors with the contraction and expansion of the sample chamber and spindle. Investigations were not performed into this aspect and quantification of any errors are not available although it can be expected to be low between 278 – 333 K. The experimental technique used in this paper requires manual operational where equipment in direct contact with samples are handle. This technique would not be suitable for a highly active environment, though the viscometer would be suitable with an automated measurement and cleaning upgrade. The additional requirement of a water bath for temperature control negates the cost saving advantage the technique has over a rolling ball viscometer. It is possible that this technique could be the most suitable for highly active samples due to the sensors being located away from the sample chamber. However, this could be inconsequential to the other higher scoring options should they be able to operate in a high radiation environment.

There is little to distinguish the three highest scoring options, and currently there is not enough literature or available industry reporting, to assess their operating capabilities when exposed to high levels of radiation. On the basis of current literature, the assessed most suitable viscometer for industrial use is the vibrational viscometer due its reported ability for modification to operate in harsh conditions and *in-situ* measurement capability. Within a research environment both the rolling ball and microfluidics techniques are suitable and offer fast data acquisition with small sample sizes (less than 1 mL).

The microfluidics approach is relatively new within research but its use within the nuclear sphere shows suitability for research. Small sample volumes could be very useful for certain aspects of recycling research such as initial ligand screening; however, it does not stand it above other techniques as 4 μL is not an appropriate minimal sample size for extraction and subsequent physicochemical studies. Therefore, although the small sample size for microfluidic viscometers is beneficial, the required

sample size for densimeter or interfacial tension measurement is likely to restrict the minimum volumes use in an experiment the additional cost for the instrument does not justify this parameter.

5.8.3 Surface and Interfacial Tension Measurements

All drop analysis techniques, pending further investigation into the effects of the radiation on the imaging equipment, appear suitable for use with active materials. However, it is not recommended to use direct balance measurement techniques due to unsuitability for small sample interfacial tension measurements, difficulty achieving thermal equilibrium and cleaning requirements for the instruments probe. Table 20 displays the allocated scores against the identified key performance criteria for all the surface and interfacial measurement techniques described.

Table 20. Summary of Interfacial Tension Assessment

Instrument / Technique	Cost	Technique Assessment	Thermostatic control	Sample Volume	Operation in Radiolytic Environment	Suitability for Operation within Nuclear Sector	Total
Direct microbalance measurement	3	2	1	1	4	No	11
Drop volume	4	1	3	1	3‡	Yes	12
Pendant drop	3**	1	3	3	3‡	Yes	13
Spinning drop	2	3	3	3	3‡	Yes	14

** - This was achieved in-house using a system costing between £2,500 – 10,000 which would increase its score to 4 and overall by 1 point.

‡ - Estimate score given as the effects on imaging equipment and techniques are unknown

All techniques require extremely clean apparatus for accurate results due to the nature of interfacial tension measurements. Due to the delicate physical properties of the probes used in the microbalance methods extreme care must be taken with the cleaning process, the dexterity and naked flame required make it unsuitable working with the appropriate safety techniques for highly active materials. The needles and tubes used for pendant drop technique and drop volume respectively are inexpensive and

can be disposed of after use. Whilst the spinning drop technique apparatus just requires the sample chamber to be flushed and rinsed which is a simple procedure. All techniques require a level of measurement expertise and would require a high level of instruction before confidence in the measurement results can be attained. Even high-specification pendant drop equipment requires an atypical level of manual interaction in comparison to the other physicochemical measurement techniques. The spinning drop tensiometer is the most automated instrument, at the expense of capital cost.

Glove boxes typically operate at below atmospheric pressure and maintenance of this will cause instability in the interface. This is a particular problem for direct measurement techniques as accuracy on correct interface detection is required for appropriate submersion of the probe. This was seen when operating within a fume cupboard causing prolonged measurement time and poor repeatability in results. This is also problematic for surface tension measurements using the pendant drop technique as the droplet can be distorted or detach prematurely but with sufficient volume of the immersing phase does not interfere with liquid-liquid measurements. Vibrations within the immediate environment or large pressure changes should be considered as they will interfere with any droplet equilibrium.

5.9 Recommendations

Due to the ease of use and relatively high throughput in comparison to a pycnometer a densimeter is recommended for laboratory studies for active studies. It is also recommended for it to be combined with a viscometer set-up to allow for dual measurements, intensifying the throughput of samples, minimising wastage, and reducing required footprint within a laboratory or glovebox.

The most appropriate technique for viscosity in a research setting can be assessed to be the automated rolling ball viscometer although the effects of a highly active sample on any electrical measurement equipment would need further investigation. It allows for both Newtonian and non-Newtonian fluids to be measured using a small sample size (less than 1 mL) and crucially allows integration with a

densimeter. The size requirement that this would save is crucial for work within areas such as gloveboxes and the technique is an injection and subsequent removal of sample which is advantageous over the rotational technique. The standard Peltier temperature control option removes requirement for a water-bath reducing required space and additional cost to the instrument. This technique within industry would require sampling from the process line and is not recommended over the standard Coriolis flowmeter techniques.

The recommended technique for interfacial tension studies is a spinning drop tensiometer. The automation for the measurements far surpasses other options and can be performed with ease in comparison to the other techniques which require skill and experience from the operator in both the technique and subsequent analysis. Both the drop volume and pendant drop are relatively simple techniques if using commercial equipment, in house methods can substantially drop the price to 10% compared to off the shelf, sacrifices are made in operation ease which will be exaggerated with active liquids and shielding equipment. If an in-house system is to be used, it is recommended to purchase droplet analysis software as this aids standardisation of the analysis and enhances reproducibility.

5.10 Acknowledgements

A studentship for RJB was funded by an EPSRC DTP awarded to the University of Manchester. Funding for consumables and equipment used in this work was provided by the EPSRC as part of the PACIFIC consortium (EP/L018616/1), and the Department of BEIS Energy Innovation Programme that has supported the National Nuclear Laboratory led Advanced Fuel Cycle Programme.

6. Physicochemical properties of extraction solvents for the advanced recycling of spent nuclear fuel

Paper Overview

The paper presented in this chapter provides a physicochemical study of the binary systems of both TBP and DEHiBA in a *n*-dodecane diluent. The viscosity, density and surface tension were investigated at varying extractant composition between 278 – 333 K. The aim of the paper was to establish a robust data set for DEHiBA in a hydrocarbon diluent and, where possible, create accurate empirical expressions to aid computational methods that could incorporate the extractant system. TBP was studied as a comparison extractant system owing to the wide availability of literature on its behaviour.

It is anticipated that this paper will be submitted to Journal of Chemical Engineering Data.

Author Contributions:

R. Blundell – Experimental work, data collection and data analysis, manuscript drafting.

H. Lambert – Experimental advice

K. George – Manuscript review

C. A. Sharrad - Principal investigator and manuscript review

Physicochemical properties of extraction solvents for the advanced recycling of spent nuclear fuel

*R. J. Blundell *a, H. Lambert, K. George, and C. A. Sharrad*a*

a. School of Chemical Engineering and Analytical Science, The University of Manchester, Oxford Road, Manchester, M13 9PL, U.K .

6.1 Abstract

Densities, viscosities and surface tension of various compositions of the binary mixtures of tributyl phosphate (TBP) (0.92 – 3.66 M) + *n*-dodecane and *N,N*-di (2-ethyl hexyl)isobutyramide (DEHiBA) (0.69 – 2.78 M) + *n*-dodecane were measured at atmospheric pressure between 278.15 to 333.15 K. Through these measurements, empirical expressions to predict the density and viscosity at any molar composition of these solvents within the studied temperature range were constructed and shown to be in good correlation with all experimental data across the studied variables. The relationship between temperature and viscosity of pure TBP and DEHiBA can be described by the Arrhenius equation for viscosity in the temperature range studied. Surface tension measurements (air-liquid interface) were obtained for varying extractant concentrations between 278.15 – 333.15 K, which showed DEHiBA acts as a surfactant when mixed with *n*-dodecane whilst TBP exhibited a higher surface-tension than *n*-dodecane.

6.2 Introduction

Over the last 60 years, the bulk of spent fuel reprocessing has been accomplished at plant scale using the PUREX (Plutonium and Uranium Redox EXtraction) process.[17,47] This is a liquid-liquid solvent extraction process using TBP (tributyl phosphate) as the selective extractant in a kerosene or dodecane hydrocarbon diluent.[207] Uranium and plutonium are stripped from the aqueous phase from the rest of

the fission products. After this step plutonium is back extracted and separated from the uranium through control of the redox chemistry. Future recycling methods hope to transition away from the historic and current reprocessing aims that resulted in the isolation of Pu(IV) for proliferation purposes. Proposed recycling methods, under the Gen IV International Forum, look to improve the efficiency, safety, sustainability and proliferation resistance through the implementation of new nuclear fuel cycles and reactor designs.[208] In addition to the focus of an improved recycling process there are also proposed Gen IV advanced reactor systems. These reactors are likely to operate at a higher temperature (between 800 -1300 K) relative to currently operating reactors. There is likely to be an elevated need to implement actinide recycling in such reactor systems not only to improve sustainability but also to safely manage spent fuel obtained from high burnups. The ambition is to provide conditions capable of recycling the majority of the actinides present in spent fuel and make it feasible to reuse a greater proportion of the fissile material that remains.[79] Effective P&T (partitioning and transmutation), combined with proliferation resistant recycling of Pu, most likely as MOX fuel, will reduce the long term radiotoxicity of the non-useful proportion of spent nuclear fuel resulting in improved confidence in waste management strategies that may only require timescales of < 500 years as opposed to potentially up to 100,000 years without any spent fuel recycling. [209]

One such proposed recycling method is the GANEX (Group ActiNide EXtraction) process. This process is composed of two cycles. The first cycle is a selective bulk removal of the U(VI) in the spent fuel feed using, almost certainly, a *N*,*N*-dialkylamide.[110] The isolated removal of U in the first step will not only increase the proliferation resistance of reprocessing but additionally aid the hydrodynamic properties of the waste stream in further processing stages. The second cycle is a group separation of the transuranic elements (Np, Pu, Am, Cm).[112] The potential of *N*,*N*-dialkyl monoamides for the extraction of the tetravalent actinide series and their synthetic route has been studied since the 1960s.[87,120,210] One extractant, DEHiBA (*N*,*N*- di(2-ethylhexyl)isobutyramide), has shown significant promise for suitability in achieving the objectives of the 1st GANEX cycle. The extractant has a high affinity for the extraction of U(VI) over other major actinides and FPs (fission products) in the spent fuel in acidic conditions between 3-6 M HNO_3, while the back extraction of U(VI) from DEHiBA continuous organic

phase is more amenable in comparison to back extraction from TBP.[113,114,116,117,119,125,179,210,211] DEHiBA also obeys the CHON principle (contains only C, H, O and N atoms). This is a desirable attribute to all new solvent systems as it allows the extractant to be completely incinerated when present in radioactive waste streams leaving the remaining residues without any problematic elements with regards to waste form production and performance. The radiolytic stability of the *N*,*N*-dialkylamides is at least as strong as TBP and the associated degradation products of the monoamines do not hinder the extraction process.[120,121,212]

Physicochemical properties such as density and viscosity are fundamental when designing and optimising process operations. Values that reflect the properties as near to operating conditions as possible are required for the development of accurate predictive process models as they dictate such properties as mass and heat transfer, as well as the numerous parameters that influence fluid flow. Understanding the variation of both chemical and physicochemical parameters with temperature across a whole operation (pumping from storage, mixing in the reaction vessel etc.) is essential but is often overlooked during the development of novel processes for the partitioning of spent nuclear fuel in favour of separation performance of the extractant mixture.

There are many published studies presenting slightly varied but similar results on the physicochemical properties of TBP + *n*-dodecane systems at various temperatures [22,165]. In contrast, with regard to available experimental data on DEHiBA, there are few extensive studies above 303.15 K. [117,213] This restricts the ability to accurately predict, design and model systems that will be used at the varied conditions seen across an operational process. This work presents viscosity, density and surface tension data for solutions of DEHiBA up to temperatures of 333.15 K in a varied binary *n*-dodecane system composition. The observed tests are benchmarked and discussed against those obtained for equivalent solutions of TBP in dodecane. The PUREX process conditions use 1.1 M TBP (30% vol) at the extractant concentration, with the most advanced tests on the GANEX system using 1 M DEHiBA in an alkane diluent.[128,141] The skeletal diagrams of both extractants are shown below in Figure 24.

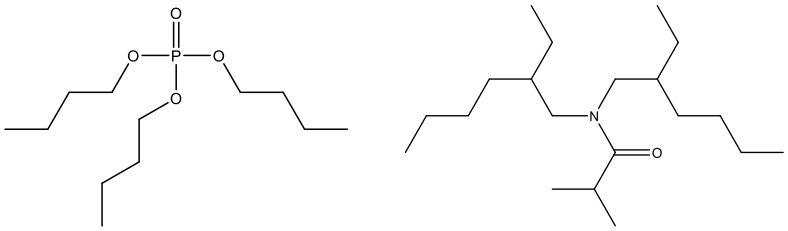

Figure 24. Skeletal diagrams of tributyl phosphate (TBP, left) and *N,N*,-di(2-ethyl hexyl) isobutyramide (DEHiBA, right).

6.3 Experimental

6.3.1 Materials

N,N-di (2-ethyl hexyl) isobutyramide was provided by Technocomm. Tributyl phosphate (≥99.0 %) and dodecane (≥99.0 %) were obtained from SigmaAldrich. All these chemicals were used as received. The extractants were diluted in dodecane using automatic pipettes (±0.70% associated error) to appropriate volumes. Initial sample concentrations represented 1.0, 0.75, 0.50 and 0.25 vol. fractions in *n*-dodecane, with the molar concentrations calculated from these. Further sample ranges were investigated depending on the requirement to investigate further trends within the DEHiBA + *n*-dodecane mixture.

6.3.2 Apparatus and Procedure

Solution densities were measured using a Mettler-Toledo DM40 densimeter with a Peltier temperature control (± 0.1 K) unit. The instrument was calibrated throughout the experimental work using standard water provided by the instrument supplier. Density measurements were reproducible to ±0.0006 g.cm^{-3}.

Viscosity measurements were obtained using a Brookfield LVDV-I viscometer connected to water heated unit at temperatures between 278 and 333 K. A Brookfield stainless steel closed sample chamber (16 mL) was connected to the temperature control unit set at the desired temperature for one hour to allow the temperature to equilibrate before viscosity measurements were taken. The temperature in the surrounding jacket was monitored using two K type thermocouples, providing an accuracy of ± 1 K. The viscometer was calibrated using 5 mPa.s standard silicone fluid provided by AMTEK Brookfield.

Surface tension measurements were made using a Krüss K11 tensiometer with a curve platinum plate. The surface tension was calculated by the Wilhelmy plate method. The plate is a roughened platinum probe designed to achieve maximum surface wettability. The temperature was maintained using a circulating water-bath and measured by the K11 to within ±0.1 K. Samples (10 mL) were left to equilibrate for 30 minutes at the desired temperature before triplicate measurements were recorded. All measurements were taken at atmospheric pressure.

6.4 Results and discussion

The physicochemical properties of the pure compounds were found to be in good agreement with those in literature and are shown in Table 21. There are minor variations within the surface tension which are likely due to the experimental error associated with the apparatus and methods used in previous work.

Table 21. Comparison of Experimental and Literature Values of Density (ρ), Viscosity (μ) and Surface Tension (SFT) at T = 298 K

		ρ (g.cm^{-3})		μ (mPa.s)		SFT (mN.m^{-1})	
	M_r	Exp.	Lit.	Exp.	Lit.	Exp.	Lit.
TBP	267.2	0.9726	0.9725 [165] 0.97083 [22] 0.9732 [103]	3.47	3.44 [165] 3.399 [22] 3.43 [103]	27.67	27.2 [188]
DEHiBA	311.3	0.8617	0.86 [101]	27.8	n.d.	23.93	n.d.
n-Dodecane	170	0.7455	0.74579 [22] 0.7453 [214]	1.44	1.336 [22] 1.330 [214]	25.50	25.35 [162]

6.4.1 Density

Experimental densities and dynamic viscosities of TBP and DEHiBA + *n*-dodecane binary systems over the temperature range T = 278 – 333 K are shown in Figures 25 and 26. Pure TBP, DEHiBA and *n*-dodecane all show an inverse linear relationship with temperature of R^2 = 0.999. This is an expected liquid relationship of an increase in temperature resulting in a decrease in density. This temperature

dependence is extended into the binary mixtures of the extractants in *n*-dodecane. All measurements gave a calculated 95% confidence value less than the ±0.001 g.cm^{-3} and as a result all error bars have been omitted as they are too small to show on the presented plots.

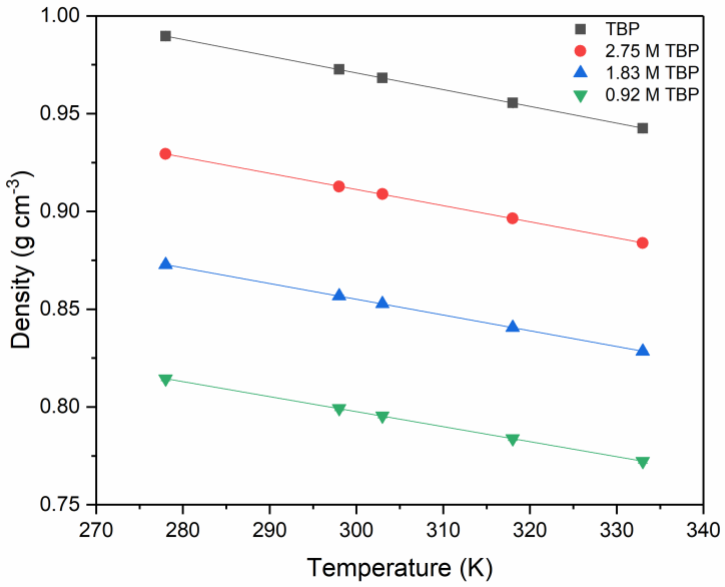

Figure 25. Plot of the density of TBP (0.9 – 3.66 M) in *n*-dodecane *vs* temperature (T) **between T = 278 – 333 K. The best fit lines show an inverse linear relationship between density and temperature for both neat TBP and TBP in *n*-dodecane.**

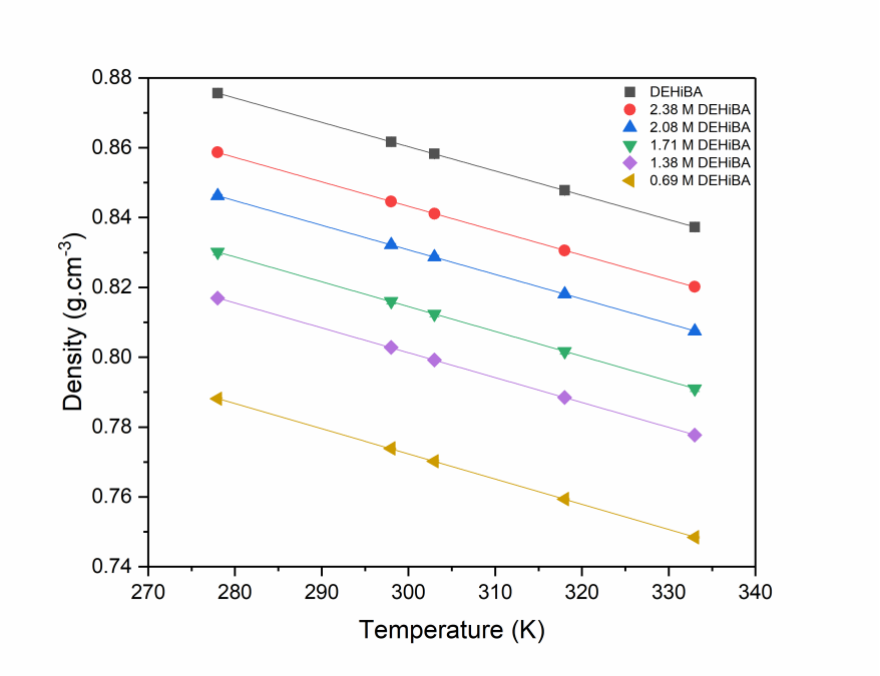

Figure 26. Plot of the density of DEHiBA (0.7 – 2.77 M) in *n*-dodecane *vs* temperature (T) between T = 278 – 333 K The best fit lines show an inverse linear relationship between density and temperature for both neat DEHiBA and DEHiBA in *n*-dodecane.

Pure compounds of TBP and DEHiBA have a greater density due to stronger intermolecular interactions in comparison to *n*-dodecane. The polar molecules of TBP and DEHiBA solutions both interact with dipole-dipole bonds and the greater density of TBP is due its smaller molecular size and ability to pack closer together, reducing the free volume. All correlations had an $R^2 > 0.999$.

Using a fundamental formula for the relationship between density, molar fraction and temperature:[166]

$$\rho = a_1(x_f) + b_1(x_f) \times T$$

Equation 21. Relationship of density of a fluid with molar fraction and temperature

Where a_1 and b_1 are calculated parameters, x_f is the molar fraction of DEHiBA in *n*-dodecane and T is the temperature.

The values graphs of a_1 and b_1 against the mole fraction of the extractant in the TBP + *n*-dodecane and DEHiBA + *n*-dodecane binary systems are shown below in Figures 27 – 30. The predicted density at 273 K, found by the intercepts in Figures 26 and 27, are plotted against their respective mole fraction in Figures 29 and 30 to provide an expression for a_1. The linear gradients, provided by the best fit

analysis from Figures 27 and 28, are plotted for the values of b_1 plot in Figures 29 and 30 against mole fraction. Levenberg-Marquardt least-square methods was performed to provide a fit for each plot which was used for the respective a_1 and b_1 expressions. These expressions are combined in the form of Equation 21, complete with their respective parameter values, shown in Table 21.

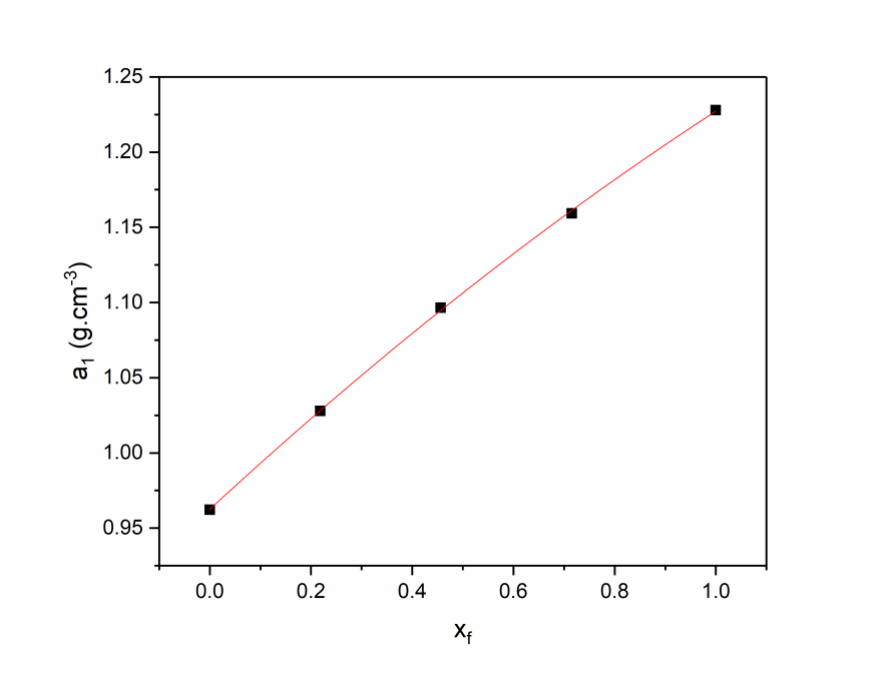

Figure 27. Values of density of TBP in *n*-dodecane at 273 K against the mole fraction of TBP in *n*-dodecane. The equation of the curve is used to provide the expression for a_1.

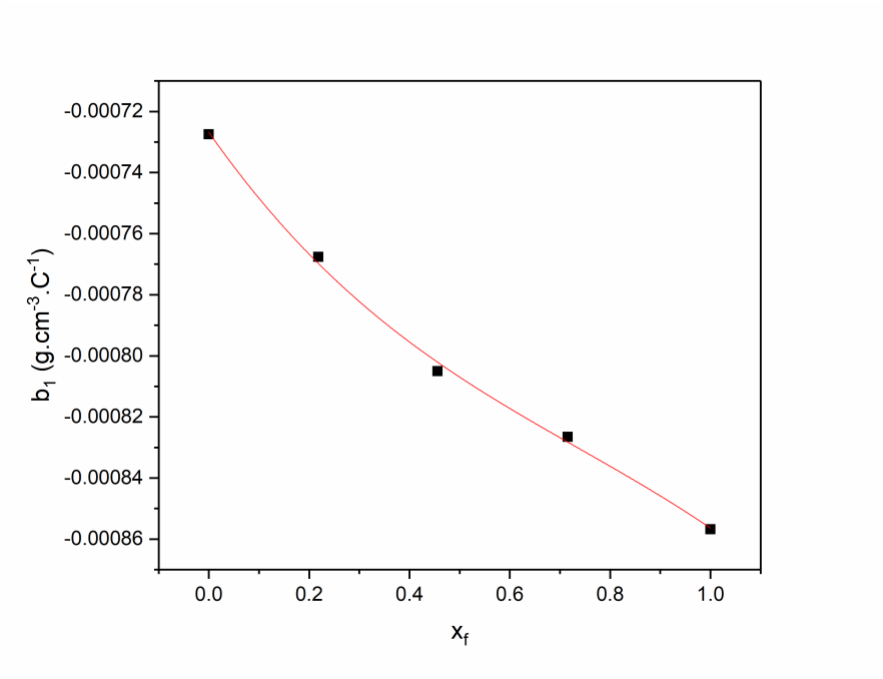

Figure 28. Gradient of the relationship of density with temperature plotted against the mole fraction of TBP in *n*-dodecane. The equation of the curve is used to provide the expression for b_1.

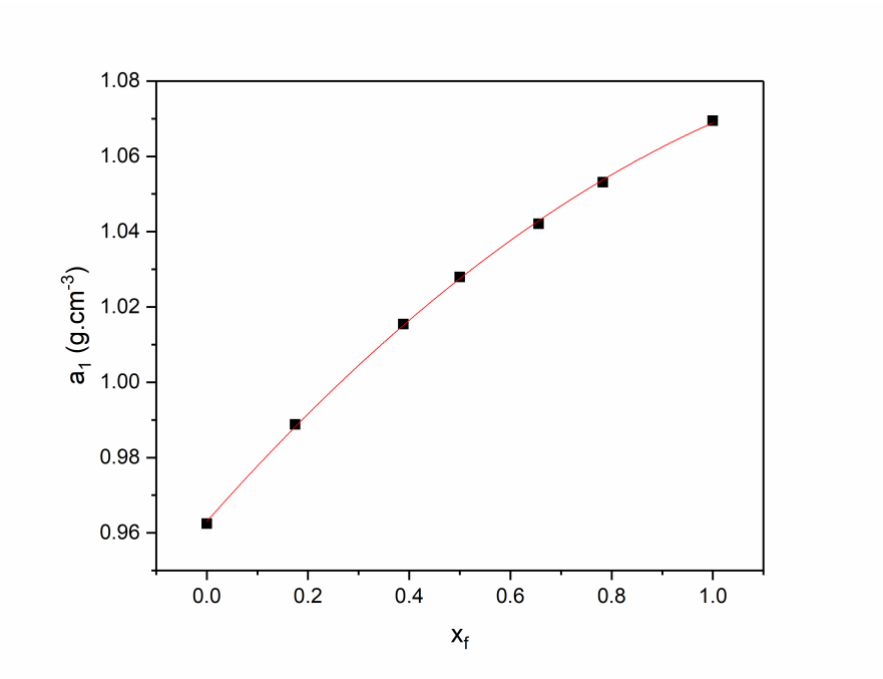

Figure 29. Values of density of DEHiBA in *n*-dodecane at 273 K against the mole fraction of DEHiBA in *n*-dodecane. The equation of the curve is used to provide the expression for a_1.

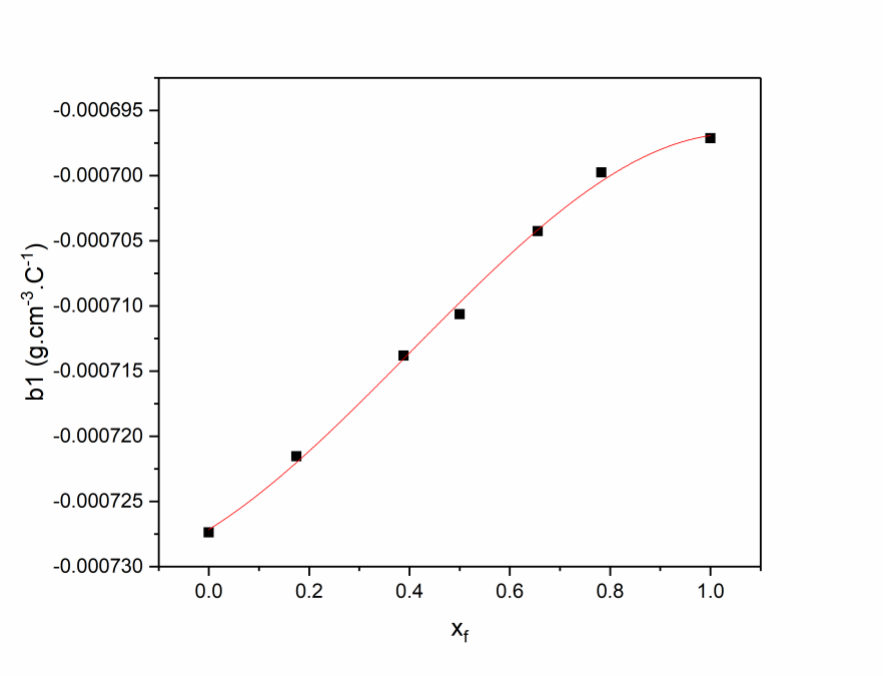

Figure 30. Gradient of the relationship of density of DEHiBA in *n*-dodecane with temperature plotted against the mole fraction of DEHiBA in *n*-dodecane. The equation of the curve is used to provide the expression for b_1.

Table 22. Density expressions for TBP in *n*-dodecane and DEHiBA in *n*-dodecane with respect to mole fraction and temperature of the system.

TBP + *n*-dodecane
$\rho = \left(0.9625 + 0.3107x_f - 0.0459x_f^2\right) + \left(-7.27 \times 10^4 - 2.34 \times 10^{-4}x_f + 1.91 \times 10^{-4}x_f^2 - 8.63 \times 10^{-5}x_f^3\right) \times T$
$\sigma = \pm 6 \times 10^{-4}$
DEHiBA + *n*-dodecane
$\rho = \left(0.9623 + 0.1522x_f - 0.0463x_f^2\right) + \left(-7.27 \times 10^4 - 2.37 \times 10^{-5}x_f + 3.77 \times 10^{-5}x_f^2 - 3.13 \times 10^{-5}x_f^3\right) \times T$
$\sigma = \pm 6 \times 10^{-4}$

The overall standard deviation for each expression of density in Table 22 was found from the difference between the experimental and calculated value and the total number of measurements.

$$\sigma = \sqrt{\left[\frac{\sum(P_{Exp} - P_{Calc})^2}{N}\right]}$$

As mentioned in the introduction, the working concentration of DEHiBA in the GANEX system is likely to be in the region of 1.0 M. Using the expression provided in Table 22, calculated values from the empirical model are compared with literature values of TBP and DEHiBA at 298 K. All results are found to be within 1% error from recorded known values, and are given in the Supplementary Information. The expression was used compared to previously reported density values for 0.5 and 1.0 M DEHiBA in *n*-dodecane shown in Table 23.

Table. 23 Comparison of calculated DEHiBA in *n*-dodecane system densities (see Table 21) with previously published values, T = 298 K.

[DEHiBA] M	$\rho_{calculated}$ / g.cm^{-3}	$\rho_{literature}$ / g.cm^{-3}
0.5	0.7652	0.768 [117]
1.0	0.7854	0.782[117]

6.4.2 Viscosity

The brief definition of the viscosity of a solution is a measure of its resistance to flow. This property is present in many of the expressions which define the operating conditions, equipment parameters and dimensionless numbers seen in a liquid-liquid extraction process. This difference in viscosity between DEHiBA and TBP can be explained by primarily by two factors: intermolecular attractive and intermolecular repulsive (within which steric effects are present) forces. The stronger the intermolecular force, the greater the resistance for molecules to flow. If the repulsive intermolecular forces are also greater, it again is harder for the molecules to move past one another.

Effect of Diluent

Figures 31 and 32 shows the addition of the diluent greatly reduces the viscosity of both the TBP and DEHiBA binary system, reducing the power requirements of any pumping and contacting process.

When comparing the viscosity of the two pure extractants, DEHiBA is the most viscous fluid. DEHiBA is a bulkier, less planar molecule in comparison to TBP. This structure causes increased steric resistance for the molecules and a resulting greater viscosity relative to TBP. Furthermore, DEHiBA is a longer chain molecule with its branched alkyl groups relative to TBP (see Figure 24). This chain combined with branching provides a larger area to form more intermolecular bonds with other DEHiBA molecules again increasing the viscosity of the solution.

Effect of Temperature

The relationship between temperature and dynamic viscosity is best described as an Arrhenius-type equation and first was proposed by de Guzman (1913), though this relationship is best known now as the Andrade equation given in Equation 22[215,216]

$$\eta = \eta_{\infty}\, e^{\frac{E_a}{RT}}$$

Equation 22. Andrade Equation

(2)

Where R is the universal gas constant and η_{∞}, the pre-exponential factor (viscosity at infinite temperature). The expression is an A high value of E_a indicates a high value of energy associated with flow of the liquid whilst $\eta\infty$ is linked to the disorder, entropy and motion of the solution.

Figures 31 and 32 show the changes in viscosities with increasing temperature for both TBP and DEHiBA in *n*-dodecane, which exhibit the Arrhenius relationship as described by the Andrade equation. At lower temperatures (< 290 K) and reduced energy of the molecules there the greatest difference between the viscosity of the DEHiBA and TBP. As the temperature is increased up to 333 K, the difference in viscosities between the neat extractants is gradually reduced. This difference is further reduced with the dissolution of the solvent in the *n*-dodecane diluent. The exponential relationship results in both extractants diluted with *n*-dodecane reaching values within 1 mPa.s of each other at 333 K.

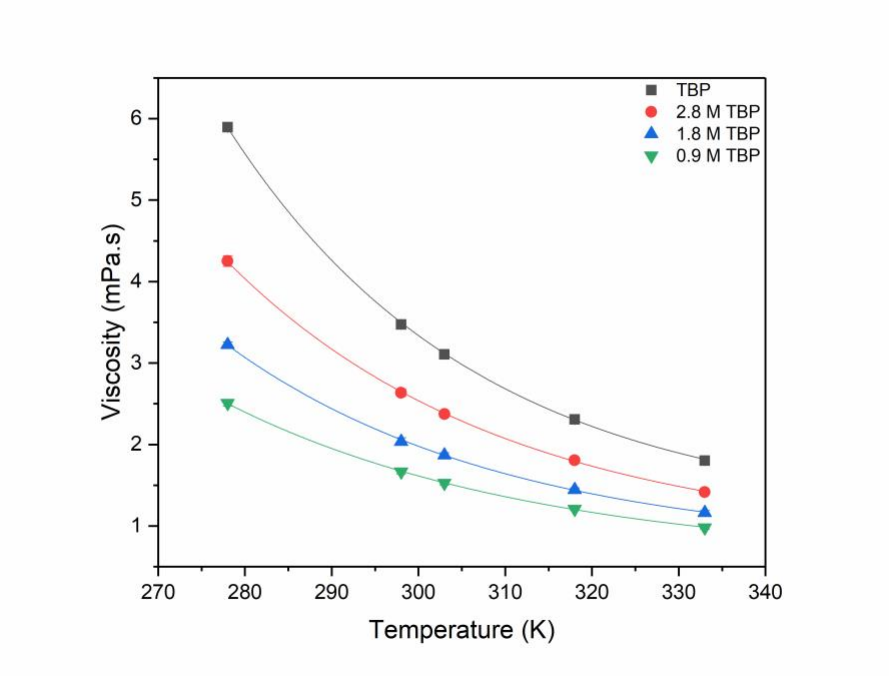

Figure 31. Plot of viscosity (η) of TBP in *n*-dodecane (0.92 – 3.67 M) *vs* temperature (T) between T = 278– 333 K. Viscosity of pure TBP and a binary mixture of TBP in *n*-dodecane decrease is fitted to the Andrade equation.

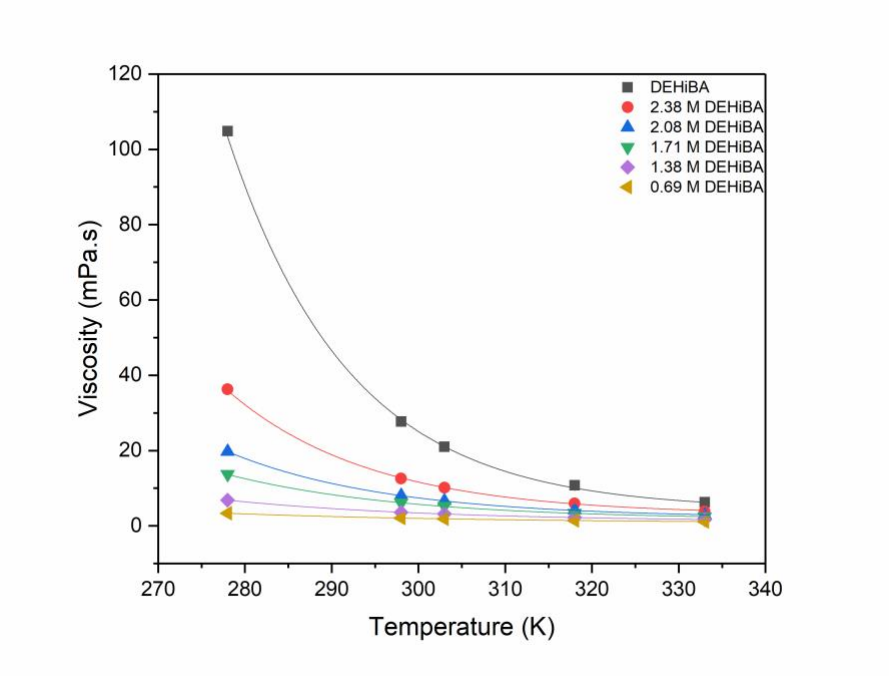

Figure 32.Plot of viscosity of (η) DEHiBA in *n*-dodecane (0.7 – 2.77 M) *vs* temperature (T) between T = 278 – 333 K. Viscosity of pure DEHiBA and a binary mixture of DEHiBA in *n*-dodecane decrease is fitted to the Andrade equation.

Developing on Eq. 1, when the natural logarithm of viscosity is taken and plotted against the absolute temperature (1/T), the plotted data is should exhibit a straight line from which the activation energy for viscous flow (E_a) is can be calculated. This equation is presented in Equation 23 below.

$$\ln(\eta) = \ln(\eta_\infty) + \frac{E_a}{R}\frac{1}{T} \quad (3)$$

Equation 23. Natural log of Andrade equation

Figures 33 and 34 is the plot of the natural log of the viscosity *vs.* 1/T which shows a linear relationship of the behaviour of the solvents TBP and DEHiBA in relation to Equation 23. Between T = 278 – 333 K, both TBP and DEHiBA the binary systems can be observed to adhere to the Andrade equation with an $R^2 \geq 0.989$.

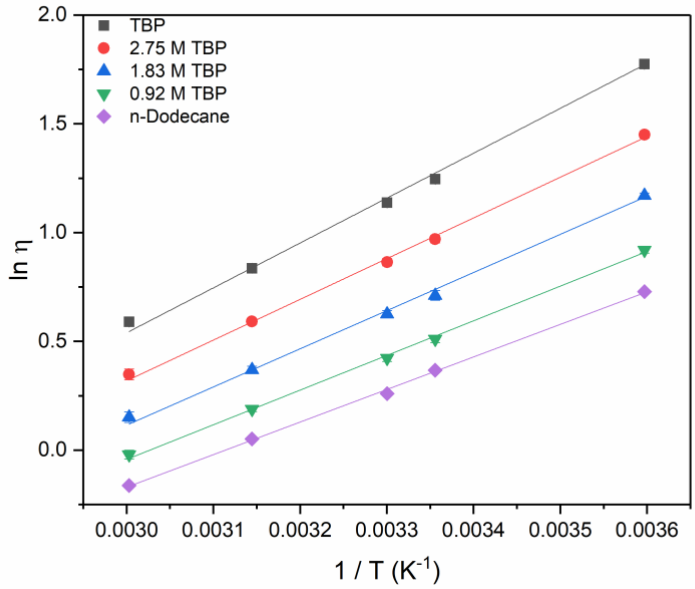

Figure 33 Plot of ln η vs 1/T showing the Andrade equation for TBP in *n*-dodecane between T = 278.15 – 333.15 K

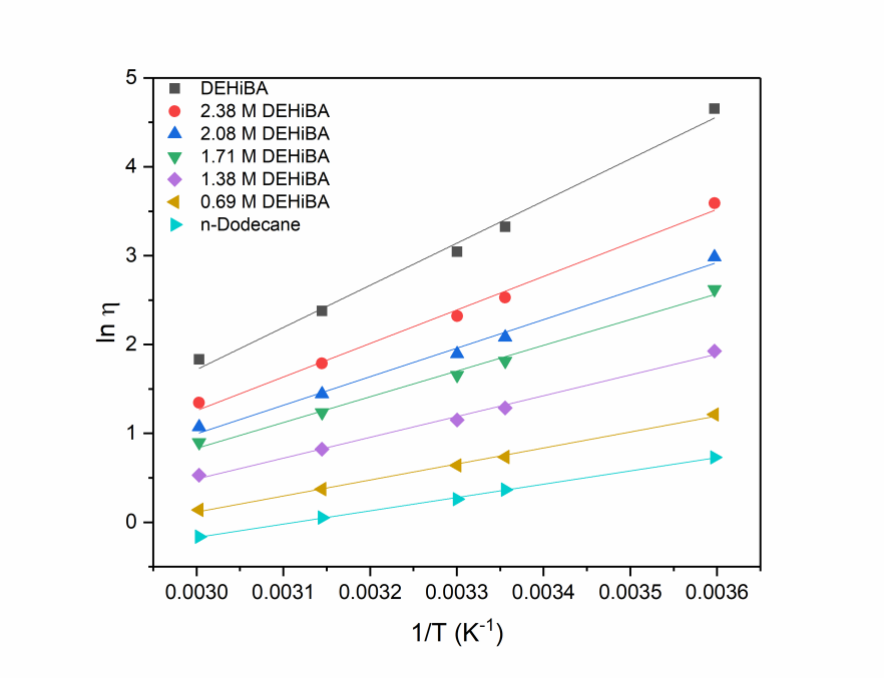

Figure 34. Plot of ln η vs 1/T showing the Andrade equation of DEHiBA in *n*-dodecane between T = 278.15 – 333.15 K

Table 24. Results of the fitting viscosity data from TBP and DEHiBA in *n*-dodecane using the Andrade equation

[TBP] / M	**x_f**	**ln η∞**	**B**	**E_a / kJ.mol^{-1}**
3.67	1.000	-3.126	1.995×10^3	16.59
2.75	0.714	-2.913	1.846×10^3	15.35
1.83	0.455	-2.685	1.704×10^3	14.17
0.92	0.217	-2.475	1.579×10^3	13.13
[DEHiBA] / M				
2.78	1.000	-10.199	4.740×10^3	39.41
2.38	0.796	-7.790	3.782×10^3	31.44
2.08	0.656	-6.395	3.229×10^3	26.85
1.71	0.504	-5.565	2.899×10^3	24.10
1.38	0.388	-4.246	2.344×10^3	19.49
0.69	0.175	-2.985	1.801×10^3	14.97
n-dodecane	1.000	-4.66	1.497×10^3	12.45

Predicting Viscosity

TBP viscosity as a function of mole fraction (TBP) and temperature (K) could be predicted using the Andrade in Equation 23 as it obeyed this behaviour within the studied temperature range. The expression used to predict both temperature and mole fraction based on viscosity is given below in Equation 24 and presented in Table 25. Values for a_2 and b_2 were plotted against mole fractions (of extractant) in the method previously described for the density expression.

$$\ln(\eta) = \ln(a_2)(x_f) + \frac{b_2(x_f)}{T}$$

Equation 24. Relationship of viscosity with molar fraction and temperature

Table 25 . Viscosity expressions for TBP in*n*-dodecane and DEHiBA in *n*-dodecane with respect to mole fraction and temperature (K) of the system

TBP + *n*-dodecane
$\ln(\eta) = \left(-4.650 - 0.865x_f - 0.127x_f^2\right) + \frac{\left(1490 + 512x_f + 58.4x_f^2\right)}{T}$ σ = ± 0.044
DEHiBA + *n*-dodecane
$\ln(\eta) = \ln(\eta) = \left(-4.614 - 3.676x_f - 4.202x_f^2\right) + \frac{\left(1477 + 1820x_f + 1435x_f^2\right)}{T}$ σ = ± 2.117

Viscosity Deviation

The viscosity deviation, Δη, is the difference between the ideal viscosity of a mixture and the actual value, as determined experimentally. A positive or negative deviation can indicate the types of interactions between the molecules in a mixture. A positive deviation is reported to occur when there

are stronger bonds being formed between unlike molecules (such as hydrogen bonds) and a negative deviation indicates weaker bonds being formed through the mixing of the two components.[217] The viscosity deviation is calculated using the following equations:

$$\Delta\eta = \eta_{exp} - (\eta_1 x_1 + \eta_2 x_2) \qquad (6)$$

Where η_{exp} is the measured experimental viscosity of the binary solution, η_i is the viscosity of the pure extractant as measured during the experiments and x_i is the molar fraction of the respective components.

The deviation of the viscosity for both binary systems at varying temperatures as a function of the mole fraction, x_f are shown in Figures 35 and 36. Both systems exhibit a negative viscosity deviation, becoming less negative with increasing temperature. The addition on non-polar *n*-dodecane indicates the bonding in the mixture are not as strong as those between like molecules when pure, hence a negative change upon mixing.[217,218] The minimum viscosity deviation for the TBP in *n*-dodecane system occurs at around x = 0.5 – 0.6 mole fraction and is of a small magnitude when compared to that of DEHiBA, as the viscosity difference between TBP and dodecane is not as great it is to be expected that the binary mixture of the two does not produce a great deviation. The curve shape is similar to that presented by Tian *et al.* [22], although by a slightly increased amount (-0.3 mPa.s). The DEHiBA in *n*-dodecane system exhibits a much greater Δη, at its lowest between x = 0.6 - 0.7 mole fraction around -50 mPa.s. A large negative deviation is to be expected when there is large difference between the viscosities of the two liquids. For both liquids the greatest deviation occurs at the lowest temperature, due to the relationship of viscosity and temperature, determined by the strength dependence of intermolecular bonding and thermal motion with temperature, described previously.

Fitting of curves Figures 35 and 36 was performed using the Redlich-Kister polynomial expansion below:

$$\Delta\eta = x_f(1 - x_f)\sum_{i=0}^{n} A_i(2x_f - 1)^i$$

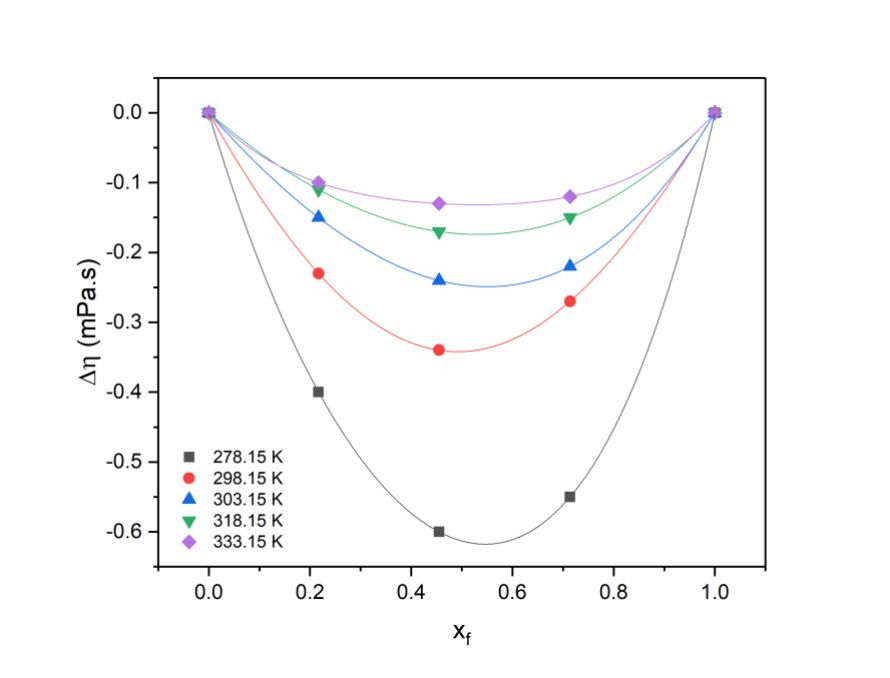

Figure 35. Plot of the negative deviation of viscosity in the binary TBP in *n*-dodecane system *vs* mole fraction fitted with Redlich-Kister expansion

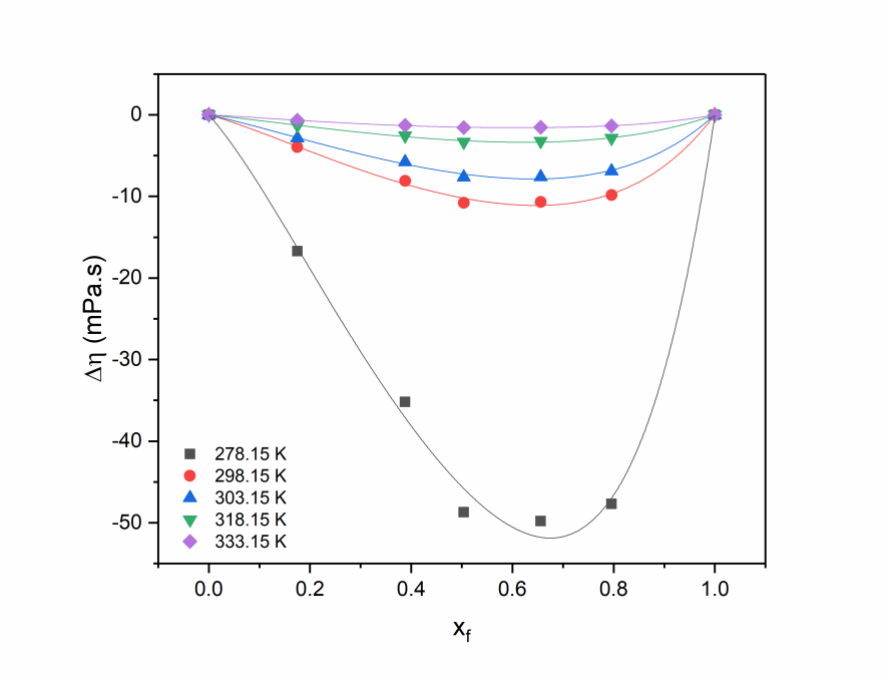

Figure 36. Plot of the negative deviation of viscosity in the binary DEHiBA in *n*-dodecane system *vs* mole fraction fitted using Redlich-Kister expansion

6.4.3 Surface Tension

The air-liquid interface was measured at different intervals between 283 – 333 K. The SFT of pure compounds are in the order TBP > *n*-dodecane > DEHiBA. Studies on both systems showed the expected inverse linear relationship between SFT and temperature, with the SFT decreasing as the temperature increased, data is presented in Table 26. However, the influence of the addition of *n*-dodecane on SFT was varied in the two mixtures due to the surfactant effect of DEHiBA.

Table 26. Surface Tension of TBP + *n*-dodecane and Surface Tension of DEHiBA + *n*-dodecane

		T / K			
[TBP] / M	x_1	283.15	293.15	313.15	330.15
		SFT / mN.m^{-1}			
3.67	1.000	28.57	27.84	26.64	25.01
2.75	1.000	27.44	26.78	25.52	24.07
1.83	0.714	26.70	25.92	24.54	23.05
0.92	0.455	26.58	25.77	24.43	22.73
0.00	0.217	26.49	25.49	23.60	22.17
[DEHiBA] / M		**SFT / mN.m^{-1}**			
2.78	1.000	24.48	23.93	22.90	21.84
2.08	0.656	24.32	23.89	22.67	21.75
1.38	0.388	24.50	24.03	22.85	21.71
0.69	0.175	24.43	23.87	22.83	21.68
0.00	0.000	26.49	25.49	23.60	22.17

Figures 37 and 38 shows this inverse relationship with temperature as well as the behaviour with respect to varying concentrations of *n*-dodecane with the two extractants. The SFT of the TBP-*n*-dodecane system decreases as the concentration of TBP is reduced. The SFT is reduced in a consistent pattern until the concentration of TBP < 1.83 M or 50 vol%, where the system approaches the recorded SFT of

n-dodecane. The binary system of DEHiBA + *n*-dodecane behaves differently in comparison to TBP, as the dodecane diluent has a higher SFT than the amide. It would be expected that the addition of the diluent would increase the SFT. At the concentrations studied, the SFT does not vary enough from experimental error to suggest that the SFT of the binary solutions deviates from the value recorded for neat DEHiBA and that at values as low as 0.25 vol %, the DEHiBA has saturated the interface.

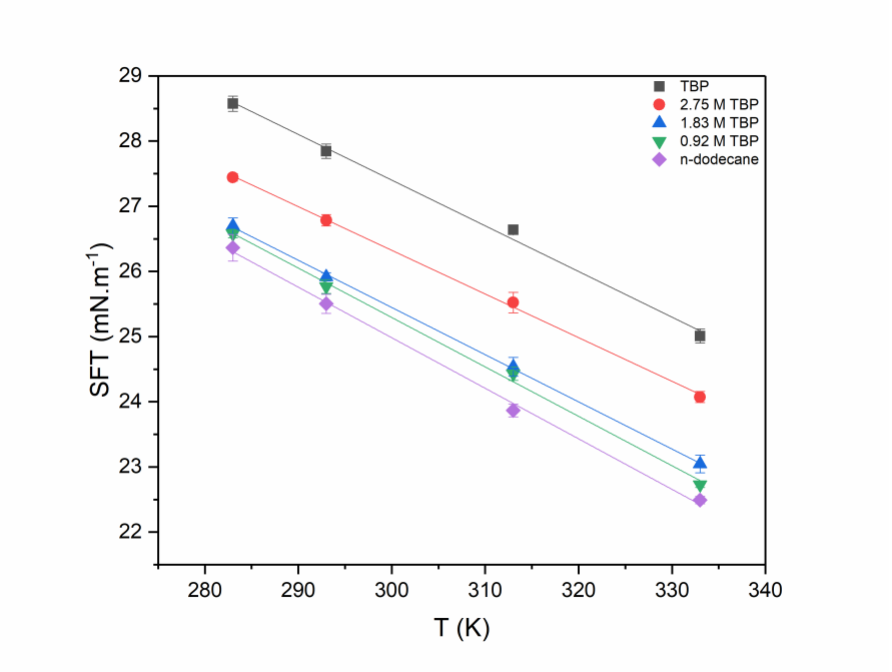

Figure 37. Plot of surface tension of the binary DEHiBA in *n*-dodecane system *vs* temperature

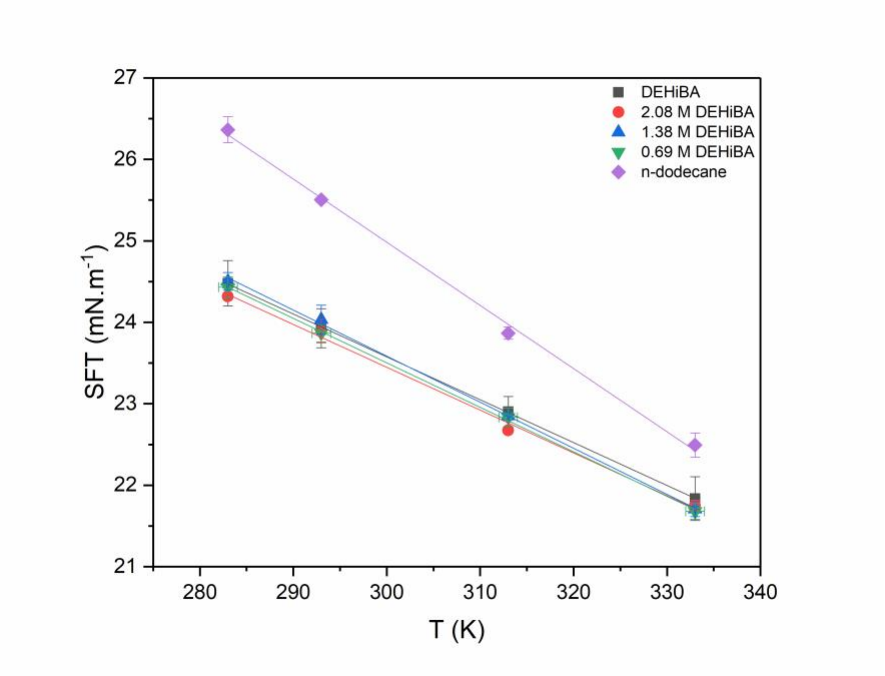

Figure 38 Plot of Surface tension of the binary DEHiBA in *n*-dodecane system *vs* temperature.

6.5 Conclusions

The physicochemical properties of TBP and DEHiBA in *n*-dodecane binary systems have been ascertained allowing expressions to be determined that can predict these physicochemical parameters at different molar composition at temperatures between 278 – 333 K. These novel expressions provide close agreement to values recorded through experimental studies and will allow for accurate estimates to be computed without the requirement of further empirical research. The examined and derived physical properties of the TBP system showed good alignment with previously reported values. The TBP in *n*-dodecane system exhibited Arrhenius behaviour and was fitted through the Andrade equation. Where available, all data compared well to known literature values. The reduction in viscosities of both systems with *n*-dodecane diluent relative to the neat extractant indicated weaker interactions occur between the extractant and *n*-dodecane diluent than those between extractant molecules in neat solution. Surface tension results shows DEHiBA to be more surface-active than TBP with a relatively low interfacial tension of the air-liquid interface. This understanding in the changes of physicochemical properties for DEHiBA in *n*-dodecane across various conditions will help further computational work that can better predict the behaviour and performance of this extractant system.

6.6 Acknowledgements

A studentship for RJB was funded by an EPSRC DTP awarded to the University of Manchester. Funding for consumables and equipment used in this work was provided by the EPSRC as part of the PACIFIC consortium (EP/L018616/1), and the Department of BEIS Energy Innovation Programme that has supported the National Nuclear Laboratory led Advanced Fuel Cycle Programme.

6.7 Supplementary Information – Chapter 6

Table 27. Density and viscosity values of TBP at varying compositions in *n*-dodecane between 278 - 333 K

[TBP] / M	x_1	T / K 278	298	303	318	333
			η/ mPa.s			
3.67	1.000	5.90 ± 0.01	3.49 ± 0.02	3.10 ± 0.06	2.32 ± 0.01	1.80 ± 0.02
2.75	0.714	4.25 ± 0.03	2.64 ± 0.05	2.36 ± 0.04	1.81 ± 0.02	1.42 ± 0.01
1.83	0.455	3.21 ± 0.04	2.03 ± 0.05	1.87 ± 0.03	1.45 ± 0.02	1.16 ± 0.03
0.92	0.217	2.51 ± 0.03	1.66 ± 0.03	1.53 ± 0.02	1.21 ± 0.01	0.98 ± 0.02
0.00	0.000	2.08 ± 0.06	1.44 ± 0.03	1.29 ± 0.03	1.03 ± 0.04	0.88 ± 0.01
			ρ / g.cm^{-3}			
3.67	1.000	0.9897	0.9727	0.9684	0.9555	0.9426
2.75	0.714	0.9294	0.9131	0.9089	0.8964	0.8839
1.83	0.455	0.8727	0.8568	0.8527	0.8407	0.8285
0.92	0.217	0.817	0.8021	0.7982	0.7866	0.775
0.00	0.000	0.7599	0.7455	0.7419	0.7273	0.7199

Table 28. Density and viscosity values of DEHiBA at varying compositions in *n*-dodecane between 278 - 333 K

[DEHiBA] / M	x_1	**T / K** 278	298	303	318	333
			η/ mPa.s			
2.78	1.000	105 ± 0.64	27.8 ± 0.34	21.1 ± 0.03	10.8 ± 0.07	6.28 ± 0.01
2.38	0.796	36.4 ± 0.17	12.6 ± 0.06	10.2 ± 0.03	5.98 ± 0.02	3.83 ± 0.04
2.08	0.656	19.8 ± 0.07	8.02 ± 0.03	6.65 ± 0.05	4.23 ± 0.04	2.90 ± 0.04
1.71	0.504	13.8 ± 0.11	6.13 ± 0.02	5.24 ± 0.03	3.44 ± 0.06	2.46 ± 0.02
1.38	0.388	6.88 ± 0.06	3.59 ± 0.03	3.18 ± 0.02	2.27 ± 0.03	1.70 ± 0.02
0.69	0.175	3.36 ± 0.06	2.09 ± 0.01	1.90 ± 0.03	1.45 ± 0.02	1.15 ± 0.02
0.00	0.000	2.08 ± 0.06	1.44 ± 0.03	1.29 ± 0.03	1.03 ± 0.04	0.88 ± 0.01
			ρ / g.cm^{-3}			
2.78	1.000	0.8756	0.8617	0.8582	0.8478	0.8373
2.38	0.796	0.8587	0.8446	0.8411	0.8306	0.8202
2.08	0.656	0.8462	0.8322	0.8287	0.8181	0.8075
1.71	0.504	0.8304	0.8163	0.8127	0.8020	0.7913
1.38	0.388	0.8304	0.8029	0.7992	0.7883	0.7778
0.69	0.175	0.7881	0.7739	0.7702	0.7594	0.7484
0.00	0.000	0.7599	0.7455	0.7419	0.7273	0.7199

* All density errors were less than ± 0.0006 g.cm^{-3}

7. Studies on the Physicochemical Properties of the GANEX-1 Solvent with the Extraction of Nitric Acid and Uranium (VI) for the Advanced Recycling of Spent Nuclear Fuel

Paper Overview

This paper presents the observations of the density, viscosity and interfacial tension of the proposed first Group Acinide Extractions (GANEX) liquid-liquid extraction process. This paper aims to study the physicochemical behaviour across a range of metal and acid concentrations to attempt to simulated potential aqueous feed conditions. Both the aqueous and organic phases were examined to give a total overview for the process. Batch extraction experiments were conducted across the following conditions, 0 – 180 $g.L^{-1}$ U, 293 – 333 K and 2 – 6 M HNO_3. Implications for all observed phenomena, with relation to their impact in an industrial context are described to provide insight into the effects on mass transfer and separation.

It is anticipated that this paper will be submitted to Solvent Extraction and Ion Exchange.

Author Contributions:

R. Blundell – Experimental work, data collection and data analysis, manuscript drafting.

K. George – Manuscript review

C. A. Sharrad - Principal investigator and manuscript review

Studies on the Physicochemical Properties of the GANEX-1 Solvent with the Extraction of Nitric Acid and Uranium (VI) for the Advanced Recycling of Spent Nuclear Fuel

R. J. Blundell[*a], *K. George*[a] *and C. A. Sharrad*[*a]

a. School of Chemical Engineering and Analytical Science, The University of Manchester, Oxford Road, Manchester, M13 9PL, U.K .

7.1 Abstract

Aqueous phase concentrations of 2, 4 and 6 M nitric acid and 0, 60, 120 and 180 $g.L^{-1}$ U(VI) were contacted in batch experiments with an organic phase of 1 M DEHiBA in *n*-dodecane diluent at 293, 313 and 333 K in order to understand the physicochemical behaviour of both phases of the potential solvent extraction system. Uranium distribution ratios showed the peak extraction conditions at the higher acidities (4-6 M),lower temperatures (293 K) and lower initial aqueous uranium concentrations (60 $g.L^{-1}$) of those condition studied here. Uptake of acid increased with initial acidic concentration. Density and viscosity of the 1 M DEHiBA in *n*-dodecane system increased with the extraction of HNO_3 and uranium but even under high loading has shown compatibility with contacting equipment when operating above 313 K. Interfacial tension between the two phases was not found to alter significantly across the conditions studied. Exhibited properties have been tied to mass transfer and separation behaviour to provide insight into possible behaviour when under industrial operations. Third phase was observed at initial aqueous concentrations 6 M HNO_3 and at 293 K resulting a viscous and dense heavy phase in comparison to the formed light phase. This data provides accurate values to facilitate the modelling of both phases of the GANEX 1^{st} cycle and design for process conditions in addition to the implications on industrial operations.

7.2 Introduction

The Group ActiNide EXtraction (GANEX) process is a promising, European led, homogenous liquid-liquid extraction concept being considered for future spent nuclear fuel recycling techniques.[106] GANEX is termed a consolidated flow concept (CFC) and is being developed to satisfying the requirements of Generation IV reactors.[106] This process utilises at a two stage cycle, the first cycle is a bulk removal of uranium from the aqueous phase whilst the second is the group extraction of the transuranics (Np, Pu, Am and Cm).[111] This is achieved using an *N*,*N*-dialkyamide, with *N*,*N*-di(ethylhexyl) isobutyramide (DEHiBA) as a likely candidate, as it can selectively extract U(VI) over Pu(IV) and Th(IV) following complexation with the $\{UO_2\}^{2+}$ ion.[87,119] The use of diakylamides adheres to the carbon, hydrogen, oxygen and nitrogen (CHON) principle where the extractant molecule is only composed of these atoms, a defining property for next generation solvent extraction recycling. This principle allows such compounds to be completely incinerated after their useful lifetime, minimising secondary waste.[86] *N*,*N*-diakylamides are also proven to be as resistant to both hydrolysis and radiolysis when compared to TBP, in addition to this their degradation products have been show not to hinder the selective extraction of uranium.[219] The degradation products of *N*,*N*-diakylamides have been shown to have little interference with the selective extraction of U.[220] Over the past 20 years, research has shown the suitability for *N*,*N*-diakylamides to achieve the required selective extraction of U over other metal species found is dissolved spent fuel liquors in both batch studies and continuous flow contactor tests.[114–117,119,126,221–224]

The nuclear reprocessing industry has seen the evolution of solvent extraction equipment, from packed and pulse columns to mixer settlers and centrifugal contactors.[73,225,226] Each system has unique characteristics, through which the physicochemical properties of the aqueous and organic phases interact and influence with varied importance. There is no parameter that carries more weight over another across the whole extraction process, rather each one is more pertinent in certain aspects, from mixing which has a focus on mass transfer and power requirements to separation either through gravity or mechanical where density and phase separation is key.

A well-defined understanding of the physical properties of a liquid-liquid solvent system are as important as knowing its extraction behaviour when determining the suitability of the solvent extraction process.[103] These properties not only allow for the extraction design and optimisation but also underpin its safe operation. Continuous flow study by Y. Ban *et al.* (2012) evaluating the extractant *N,N*-di(2-ethylhexyl)butanamide (DEHBA), showed that at high U loading in the organic phase operation issues arose in centrifugal contacting equipment. This was associated to the increased viscosity and density with an increased uranium concentration in the organic.[227]

Studies on both the extraction and physicochemical properties of *N,N*-dialkylamides, and DEHiBA in particular, have been reported previously. These have investigated how the structure of the ligand and metal loading affects the physical behaviour of the organic phases.[95,101] Vidyalakshmi *et al.* (2003) studied the interfacial tension (IFT) of various *N,N*–dialkylamides in *n*-dodecane diluent against aqueous phases of water and 3 M HNO_3 at 303 K. The change of IFT was also measured with increasing acid and uranium concentration in the organic phase. It was found that an increase in amide concentration decreases the IFT between the two phases. An increase in IFT occurs with increasing acid and metal concentration in the organic phase as well as structural changes to the amides such as branching of the carbon chains on either the acyl or nitrogen side.[95] Interfacial studies of DEHiBA are also available, investigating the unloaded metal behaviour of the amide extractants at the interface with 3 M HNO_3 at 293 K.[101,194,198] Pleines *et al.* (2019) studied the viscosity of DEHiBA and other amide extractants in the presence of uranyl nitrate in 3 M nitric acid, whilst Pathak *et al.* (2009) looked at uranium uptake from uranium/thorium feeds with a focus on interfacial tension of DEHiBA.[101,129] Organic phase viscosity was seen to rise exponentially with $[U]_{org}$ which was attributed to aggregation effects between the classical 1:2 (metal:amide) complexed entities (shown in Figure 39) and free amide in the organic phase.[97,129,179,228]

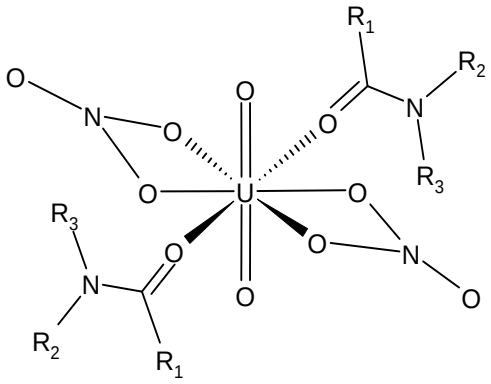

Figure 39.$UO_2(NO_3)_2$(Amide)$_2$ extractant complex.[228]

This paper aims to give a comprehensive study of the key physicochemical properties of the organic DEHiBA in *n*-dodecane under varying process conditions likely to be encountered in Gen IV fuel cycles with variables such as the uranyl concentrations, aqueous nitric acid concentration across counter-current contactor unit operations and the temperature with different fuel burnups and cooling requirements.

7.3 Experimental

7.3.1.1 Materials

N,N-di(2-ethyl hexyl)isobutyramide (DEHiBA) was provided by Technocomm and *n*-dodecane (≥99.0 %) was obtained from SigmaAldrich. DEHiBA was weighed and subsequently diluted in *n*-dodecane to a concentration of 1.0 M. Aqueous solutions of 2, 4 and 6 M HNO_3 were prepared using 68% nitric acid, used as received, from SigmaAldrich. These were diluted using 15 MΩ deionised water and concentrations were confirmed by titration using a Mettler-Toledo T5 auto titrator and standardised 1 M NaOH as the titrant. All chemicals were used as received. Uranyl nitrate ($UO_2(NO_3)_2$) was converted from a uranyl acetate stock using the method described in Section 3.1.3.

Uranyl nitrate was dissolved at each required nitric acid concentration to make stock solutions with a uranium concentration of 180 $g.L^{-1}$. This was subsequently diluted to prepare further aqueous batches of 120 and 60 $g.L^{-1}$ U across the three desired nitric acid concentrations. All U concentrations in the aqueous phase were measured using ICP-OES at the 385 nm peak.

7.3.1.2 Physicochemical Measurements

Density measurements were obtained from a Mettler-Toledo DM40 densimeter as described in Section 3.4.

A Wells Brookfield Cone and Plate Viscometer was employed to take viscosity readings. Samples of 0.550 mL were pipetted into the sample chamber. In situ temperature control was achieved using a Brookfield water bath and a specially adapted sample chamber allowing for readings of ± 0.01 K. All samples tested were found to obey Newtonian behaviour and samples were measured at 80 ± 5% of the torque range of the viscometer. Keeping the torque high and minimising the range of the reading reduced the associated equipment uncertainty for each measurement, giving an uncertainty error unique for each measurement.

Interfacial tension (liquid-liquid interface) was measured using an inhouse pendant drop technique as described and developed in Section 3.8. The samples and experiment were kept in a thermostatic Perspex box within ± 1 K. Images were taken using a 6.3 MP CMOS Camera with 0.8 X Telecentric Lens. Images were analysed using the pendant drop tool in Fiji Software[203], utilising the Young-Laplace equation for mean curvature of the drop. Deviation for all measurements were found to be within ± 5%. Recorded density values were used in the calculation of the interfacial tension between both organic and aqueous phase. Optical calibration was obtained by the length of the outer diameter of the needle measured by a micrometer. Due to limitations with the temperature control technique, measurements could not be obtained at 333 K.

Preparation and Analysis of Solutions

Solutions of DEHiBA (1 M) in *n*-dodecane were pre-contacted with an aqueous HNO_3 solution of the appropriate acid concentration in a 3:1 aqueous to organic volume ratio at room temperature using the contacting procedure discussed in Section 3.2. Each sample was subsequently contacted using an aqueous uranyl nitrate solution between 0 and 180 $g.L^{-1}$ at a given HNO_3 concentration of 2 M, 4 M and 6 M at 293, 313 and 333 K. Sample volumes of 3 mL in a 1:1 volume ratio with the pre-contacted

organic phase were used. Samples were left for 15 minutes to reach the desired temperature before the contacting of both phases using an Eppendorf Thermomixer for 30 minutes at 1000 rpm .

Solutions were placed in the temperature-controlled mixer and brought to the required temperature before being contacted at 1000 rpm for 45 minutes. Contacted solutions were left to settle for 30 minutes at the set temperature before being further separated by centrifuge for 4 minutes at 4000 rpm at room temperature and each phase was carefully removed into separate vials.

All samples post-extraction were stored in in a refrigerator at 278 K before being brought up to the desired temperature for physicochemical analysis.

Post-extraction concentrations were determined using ICP-OES of the aqueous phase and a back-extraction of the organic phase was performed using 0.1 mL of organic with 10 mL of 0.01 M HNO_3. Extracted acid concentrations were determined by a back extraction of an 0.1 mL aliquot into 1 mL of 15 MΩ deionised water for 30 mins at 1800 rpm. The phases were separated using a centrifuge at 4000 rpm for 4 minutes. 0.1 mL of this solution was titrated against 0.1 M NaOH using a Metter-Toledo T5 auto-titrator. Water concentrations were determined using a Metler-Toledo C10S Karl Fischer titrator.

All errors were calculated to 95% confidence, if this was less than the uncertainty associated with the equipment, the larger value was used.

7.4 Results and Discussion

7.4.1 HNO_3 and H_2O extraction

The extraction concentrations of water and HNO_3 by 1 M DEHiBA in *n*-dodecane are given in Table 29. There is seen to be a small increase in the concentration of water with the contacting of 1 M DEHiBA with deionised water in a 3:1 (aqueous: organic) ratio in comparison to a fresh 1 M DEHiBA solution. There is a notable increase in water co-extraction when contacting under acidic aqueous conditions. This co-extraction of water is at its greatest at 2 M HNO_3, decreasing gradually to 6 M. his is in agreement with previous studies that place the acidic conditions for maximum water co-extraction at 3 M.[219,229,230]

Table 29. Extraction and co-extraction of water and nitric acid into 1 M DEHiBA in n-dodecane at 293 K.

$[HNO_3]_{aq.\ initial}$ / M	$[H_2O]_{org}$ / M	$[HNO_3]_{org}$ / M
Uncontacted	0.041 ± 0.003	-
0	0.061 ± 0.007	-
2.028	0.117 ± 0.001	0.38 ± 0.06
3.958	0.114 ± 0.001	0.70 ± 0.06
5.979	0.102 ± 0.002	0.98 ± 0.01

The extraction of nitric acid by DEHiBA increases with acidity up to the studied limit of 6 M. These results follows the studied behaviour of DEHiBA in alkane diluent which is known to extract nitric acid and form the following adduct species $(HNO_3)(DEHiBA)$, $(HNO_3)(DEHiBA)_2$ and $(HNO_3)_2(DEHiBA)$ through hydrogen bonding.[219]

7.5 Uranium (VI) Extraction

The extraction of U(IV) with 1 M DEHiBA in *n*-dodecane when assessing the influence of temperature and aqueous nitric acid concentration shows similar uranium distribution trends to previous studies.[113,115,221] Figures 40 - 42 show the distribution ratios recorded against a changing nitric acid concentrations, extraction temperature and initial concentration of uranium in the aqueous phase at 293, 313 and 333 K. For initial concentrations of 60 $g.L^{-1}$ U the trend shows increasing $D_{U(IV)}$ with increasing aqueous phase acidity up to the maximum studied, with the distribution ratio decreasing with increasing temperature. When the initial aqueous concentrations of uranium are 120 and 180 $g.L^{-1}$ and for extraction temperatures of 313 K the distribution ratio is closer between 4 and 6 M HNO_3 and appears to level off and at 333 K and the distribution ratio for 4 M HNO_3 is greater than that at 6 M. This is reported to be due to saturation phenomena associated with high initial uranium concentrations in the aqueous phase, combined with competition for extraction of the proton at high acidities.[113] This has some agreement with previous studies which show a maximum U(VI) extraction was achieved up to an

aqueous nitric acid concentration of 5 M.[113,221] This work also confirms the inverse relationship between uranium distribution behaviour and temperature with amide extractants.[171,179]

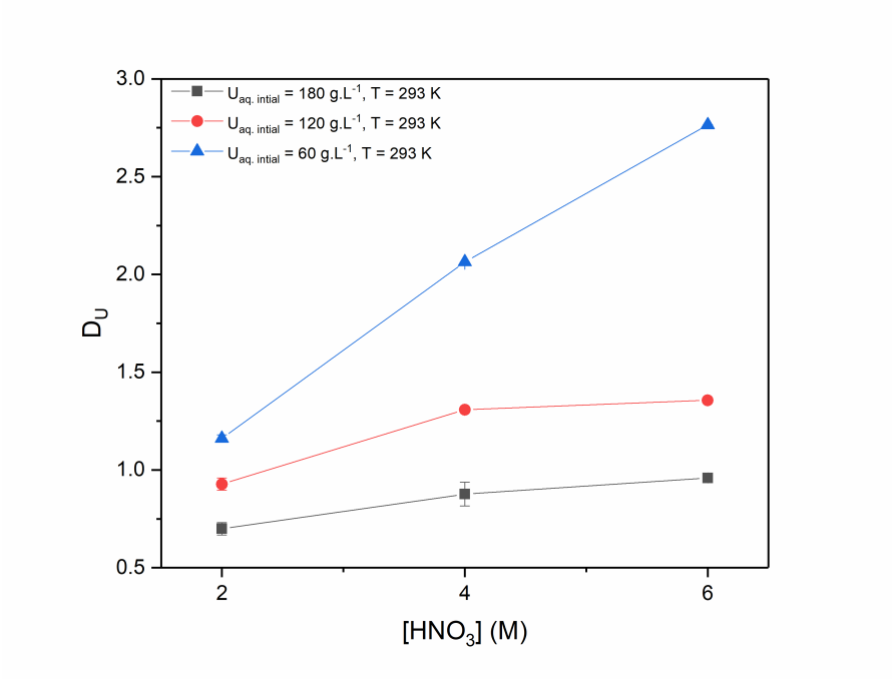

Figure 40. Uranium (VI) Distribution Ratios of 1 M DEHiBA in n-dodecane organic phase and 2 – 6 M HNO_3 aqueous phase. T = 293 K.

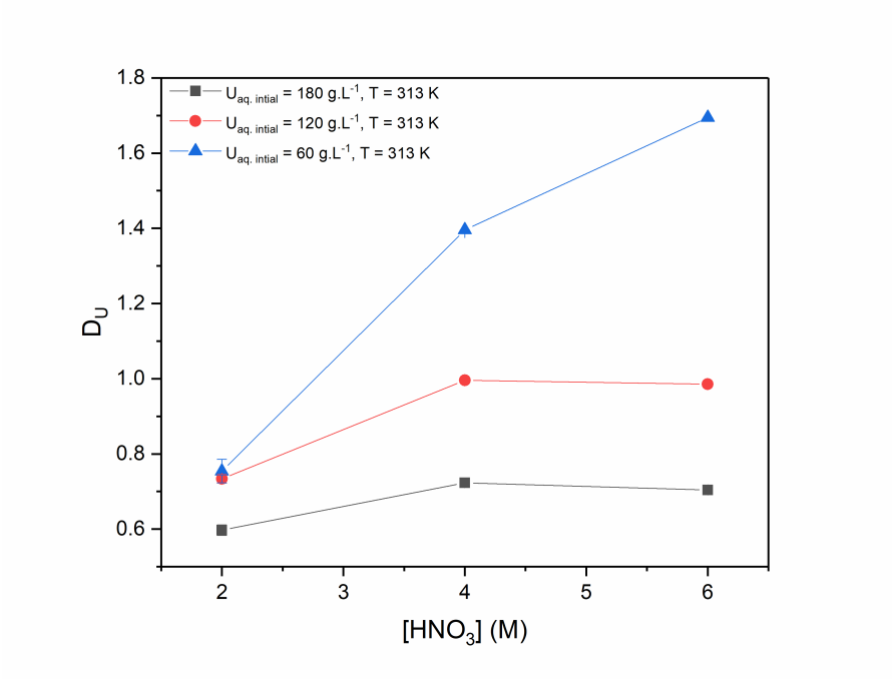

Figure 41. Uranium (VI) Distribution Ratios of 1 M DEHiBA in n-dodecane organic phase and 2 – 6 M HNO_3 aqueous phase. T = 313 K.

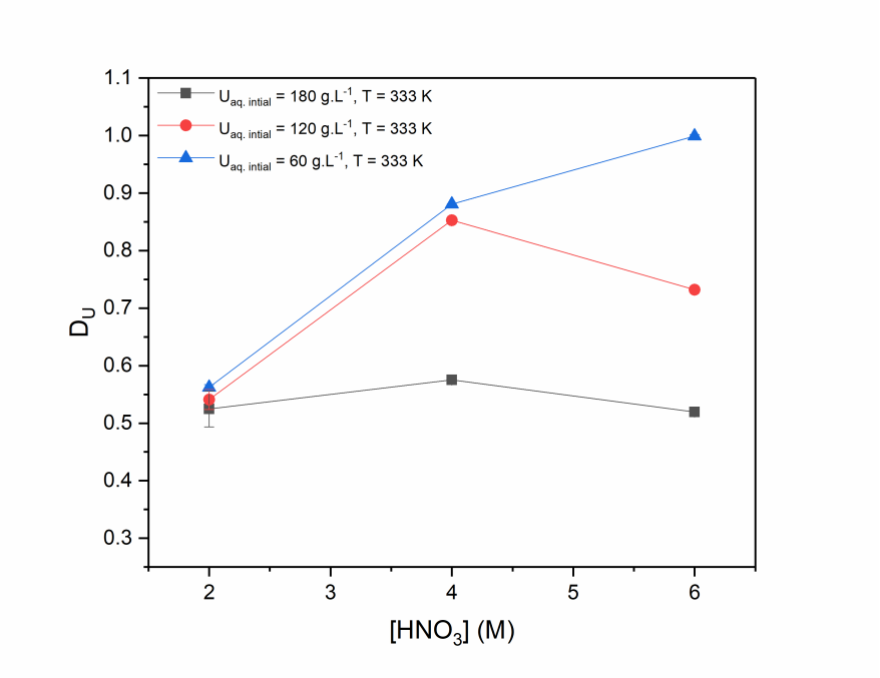

Figure 42 Uranium (VI) Distribution Ratios of 1 M DEHiBA in n-dodecane organic phase and 2 – 6 M HNO_3 aqueous phase. T = 333 K.

7.5.1 Third Phase Formation

Previous third phase formation (TPF) studies on DEHiBA + *n*-dodecane have been carried out for [HNO_3] = 4 M at 298 K, which found the LOC to be ~ 90 g.L^{-1} U.[231] Other research on TPF of *N*,*N*-diakylamides in the presence of uranyl nitrate have identified increased acidity of the aqueous phase reduces the limiting organic concentration (LOC) whilst increasing temperature is found to increase the U(VI) loading capacities of *N*,*N*-diakylamide containing organic phases.[232]

The range of conditions studied in this work found that third phase was only formed when 1 M DEHiBA in *n*-dodecane was contacted with an initial aqueous phase of 180 g.L^{-1} U in 6 M nitric acid at 293 K. This was found to extract 92.1 ± 1.3 g.L^{-1} U. The viscosity increased by such a value that it was not possible to obtain a reading for the viscosity of 1 M DEHiBA post-extraction when using the nominal shear rate for the experimental procedure. This was due to the phenomena within the organic phase and what appeared to be third phase formation or aggregation just prior to the splitting of the organic phase as a translucent haze was observed. TPF was also observed when the extraction condition was 313 K, however only once separated and the organic phase allowed to settled overnight between 278 – 283 K.

The organic phase could be seen to split and stayed in this state when raised to ambient temperature (293 ± 2 K).

Figures 43 – 45 show the separated organic phases post-extraction and once allowed to settle over night before being brought to ambient temperature. TPF is observed at 293 K when $T_{extraction}$ = 293 and 313 K. Extraction conditions of $[HNO_3]$ = 6 M, $[U]_{aq.\ intial}$ = 180 $g.L^{-1}$ and T = 293 K were recreated to create a third phase in greater volumes for further study.

Figure 43. Third phase observed for organic phase with extraction conditions of 6 M HNO_3, U 180 $g.L^{-1}$ T = 293 K. Photographed at ambient conditions. Clear boundary can be seen between top, lighter layer and heavy bottom phase.T = 293 K

Figure 44. Third phase observed for organic phase with extraction conditions of 6 M HNO_3, U 180 $g.L^{-1}$ T = 313 K only when brought to 293 K. Photographed at ambient conditions. Boundary can be seen between top, lighter layer and heavy bottom phase.

Figure 45. No third phase observed for organic phase with extraction conditions of 6 M HNO_3, U 180 $g.L^{-1}$ T = 333 K. Photographed at ambient conditions. K

Both the heavy and light phases were separated before being studied against a range of temperatures to provide an indication of potential issues when being used in contactor systems such as phase inversion or viscosity incompatibility.

The density of the organic leading up to TPF against initial uranium concentration in the aqueous phase is shown in Figure 46 shows the density of the organic and subsequent TPF. The density of the organic phase increases, with the uptake of $UO_2(NO_3)_2$ until such a point is reached that the organic phase splits.

At this point the density of the lighter phase falls to 0.8428 g.cm^{-3} whilst the heavy phase increases to 0.9639 g.cm^{-1}, still not able to induce phase inversion in this studied system. However, the ability for third phase formation to occur in the organic phase at conditions of U = 180 g.L^{-1}, T = 293 - 313 K, albeit once at 293 K, could be a maloperation concern.

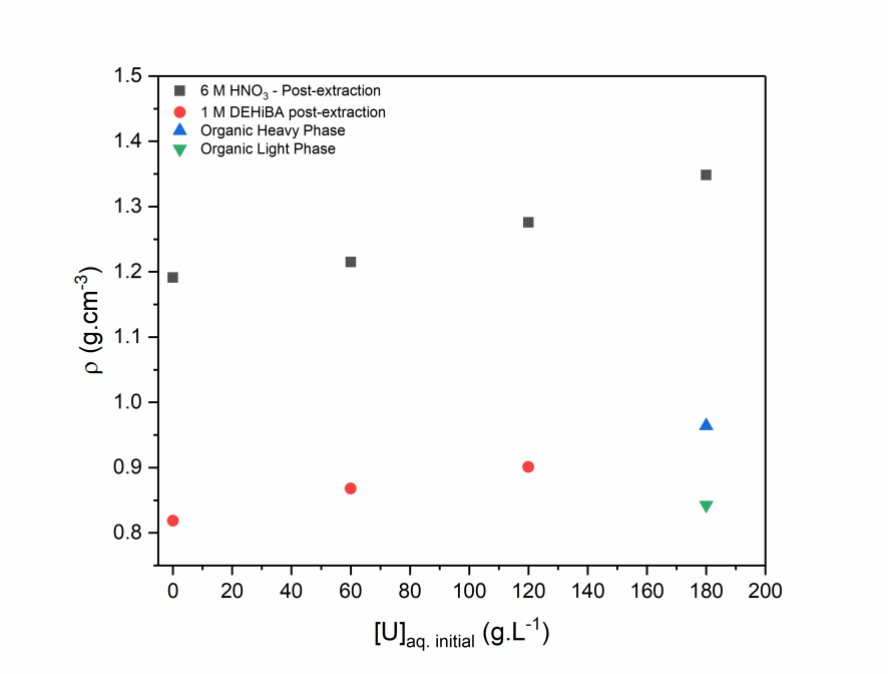

Figure 46. Density of aqueous 6 M HNO_3 with $UO_2(NO_3)$, 1 M DEHiBA post-extraction and subsequent third phase (light and heavy) against the initial uranium concentratoin in the aqueous phase.

TPF also causes two phases of differing viscosities, the more viscous heavier phase having most of the metal, acid and ligand present in comparison to the lighter, less viscous, diluent rich phase. The viscosities of the two phases against temperature and its plotted Arrhenius relationship are shown below in Figure 47.

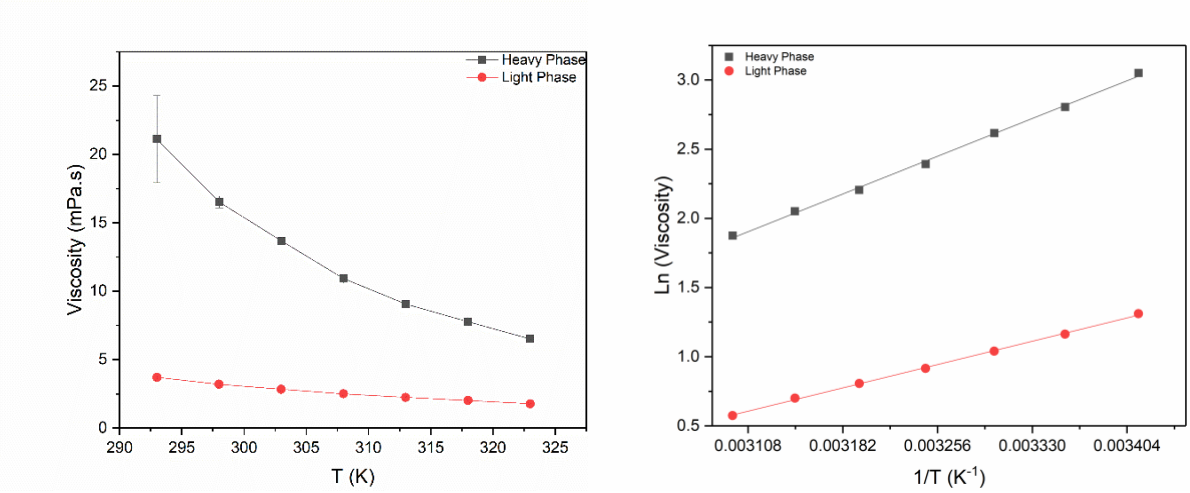

Figure 47. Viscosity against temperature of heavy and light phases of 1 M DEHiBA after TPF (left). Plot of natural log of viscosity against 1/T to give Arrhenius plot (right) relationship given by linear best fit.

Table 30 Arrehnius values of the heavy and light phase

Phase	ln η∞	E_a / kJ.mol^{-1}
Heavy	-9.558 ± 0.231	30.68 ± 0.07
Light	-6.473 ± 0.095	18.96 ± 0.02

Both phases appear to exhibit a common exponential relationship with temperature, and when the natural log η is plotted against 1/T, the expected straight line is given across the temperature range studied. This shows that both phases show Arrhenius behaviour. Using this relationship to find the value for viscosity at infinite temperature as well as the activation energy for viscous flow, some conclusions can be made about the phases. The energy required to facilitate viscous flow is much higher in the heavy phase as is reflected by the larger activation energy. The viscosity at infinite temperature is lower than that of the lighter phase indicating a greater organisation of the molecules within the heavy phase, likely due to the aggregation and associated organisation of the extractant and the uranyl metal.

Table 31. Phsyical Properties of Third Phase Formation of 1 M DEHiBA – HNO_3 – $UO_2(NO_3)_2$

Heavy Third Phase – 1 M DEHiBA + *n-dodecane*, T = 298 K	
ρ / $g.cm^{-3}$	η / mPa.s
0.9599 ± 0.0006	16.52 ± 0.43
Light Third Phase – 1 M DEHiBA + *n-dodecane*, T = 298 K	
ρ / $g.cm^{-3}$	η / mPa.s
0.8390 ± 0.0006	3.20 ± 0.05

7.5.2 Density Studies

7.5.2.1 Effect of acid and water uptake on density

1 M DEHiBA in *n*-dodecane was found to increase in density after contacting with increasing aqueous HNO_3 concentration in a 3:1 (aq:org) ratio. A slight increase in density was observed after contacting the pre-contacted organic phase with 0 $g.L^{-1}$ U at all measured nitric acid concentrations in a 1:1 volume ratio. This increase was found to be within the experimental error of these measurements (±0.0006 $g.cm^{-3}$) and the organic phase is assumed to be at equilibrium with HNO_3 at the specific aqueous acidity after pre-contacting. Figure 48 shows an increasing density change with increasing nitric acid concentration up to the maximum 6 M HNO_3 measured. This density increase can be attributed to the extraction of HNO_3 and coextraction of water into the organic phase reported in Table 31. Comparing the values in Table 29 with Figure 48, it is evident that water accounts for a negligible increase in density, and is present in a lower concentration at the higher acidities measured, indicating increase greatest change in density of the organic phase is due to a larger concentration of $[HNO_3]_{org}$. Previous work has detailed that an increasing concentration of aqueous HNO_3 up to 8 M in results in an increased uptake of the 1:1 (HNO_3)(DEHiBA) adduct, with $(HNO_3)(Amide)_2$, $(HNO_3)_2$(Amide) contributing to a lesser extent but rising with increasing $[HNO_3]_{aq}$ which go on to form small aggregates in the organic phase.[219,233]

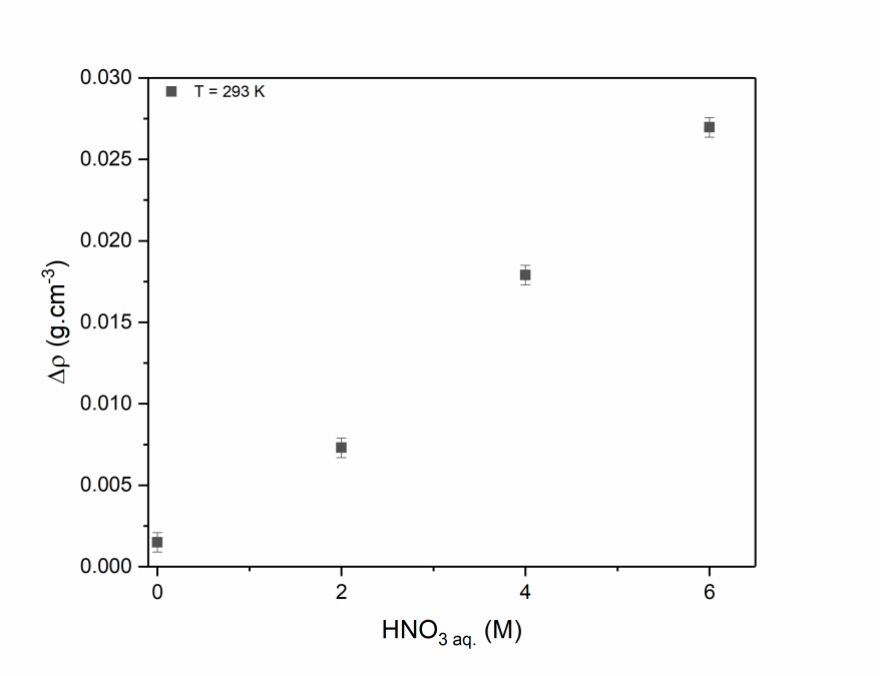

Figure 48. Density change of the organic phase after pre-contacting with water and HNO_3

7.5.2.2 The Effect of Uranium Extraction on Density

The extraction of uranyl nitrate notably increases the density of the organic phase due to the resulting extractant adduct, $(UO_2(HNO_3)_2)(DEHiBA)_2$ and the greater associated density of the uranyl metal ion and extracted nitric acid. Figures 49-51 show the density of both phases of the solvent system against their recorded U(IV) concentrations for each temperature condition studied. The density of all aqueous phases post-contacting is found to be greater for their respective uranium concentrations than the stock solutions with a trend of a greater increase seen with acidity. A potential reason for this could be the transfer of (most likely only small) quantities of DEHiBA or *n*-dodecane into the aqueous phase and its interaction with uranyl nitrate inducing a change in the organisation of molecules in the aqueous phase.

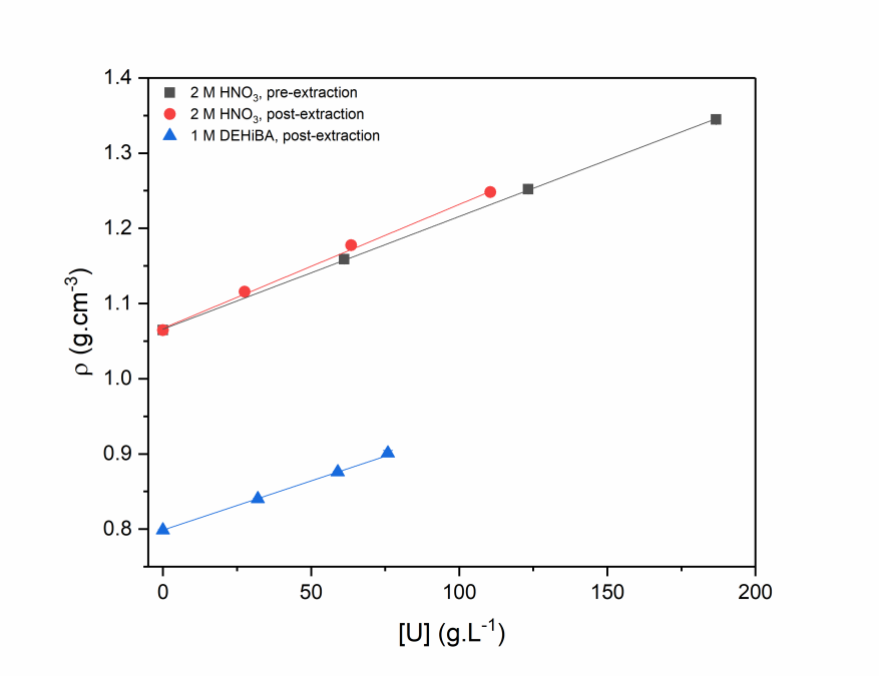

Figure 49. Density of the aqueous and organic phase of the 2 M HNO_3 and 1 M DEHiBA solutions against the concentration of uranium present in the liquid phase. T = 293 K. The best fit for the data indicates a linear relationship with concentration of dissolved uranium and density.

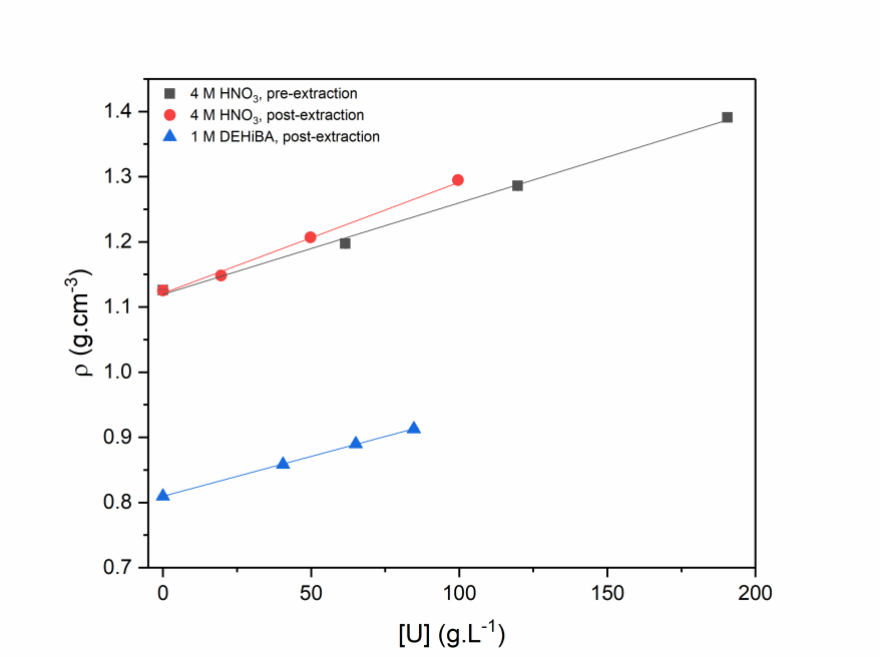

Figure 50. Density of the aqueous and organic phase of the 4 M HNO_3 and 1 M DEHiBA solutions against the concentration of uranium present in the liquid phase, T = 293 K. The best fit for the data indicates a linear relationship with concentration of dissolved uranium and density.

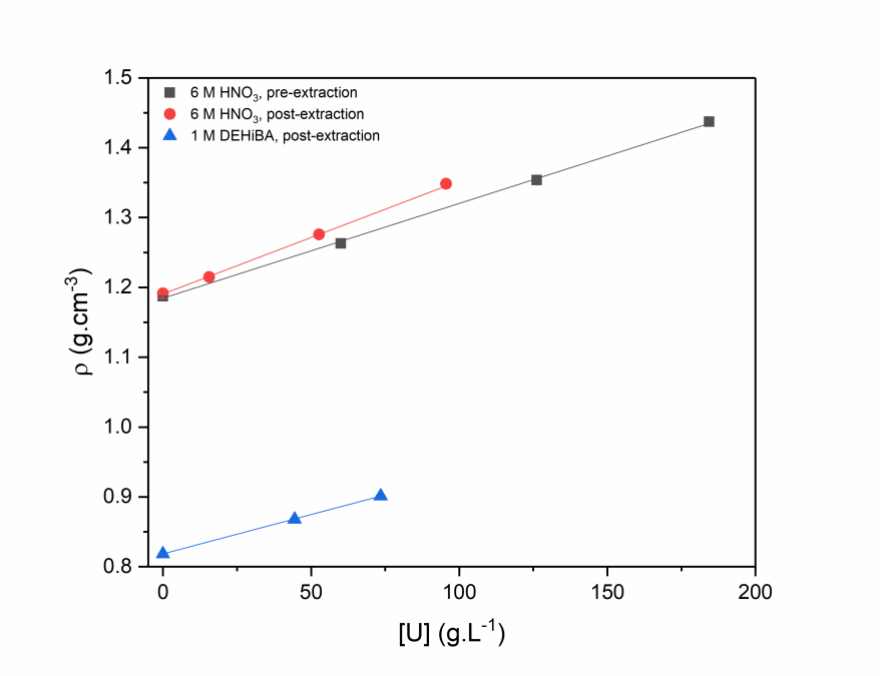

Figure 51. Density of the aqueous and organic phase of the 6 M HNO_3 and 1 M DEHiBA solutions against the concentration of uranium present in the liquid phase, T = 293 K. The best fit for the data indicates a linear relationship with concentration of dissolved uranium and density. $U_{aq.\ intial}$ 180 g.L^{-1} at 293 K not recorded..

When the initial aqueous conditions of extraction were 180 g.L^{-1} U and 6 M HNO_3 with contact at 293 K, it was difficult to record the density of the loaded organic phase. An initial density value was recorded however the measured density would drift downwards, in what has been described as a 'living network',[129] and fail to stabilise with a translucent haze observed in the sample measuring chamber due to formation of third phase.

Densities were observed to decrease as the temperature is increased for both the organic and aqueous phases, keeping with the known relationship of density and temperature.

Despite the decrease in aqueous phase density and increase in organic there is no condition where the density difference of the two phases come fall within 10% of each other, a threshold value for the operating conditions of a centrifugal contacting system.[73] This in addition to the counter-flow techniques implemented for solvent extraction ensures a safe operating profile with respect to density difference would be maintained.

7.5.3 Viscosity Studies

7.5.3.1 Effect of extraction of water, HNO_3 and uranium

The extraction of nitric acid increases into the organic phase induces an increase in viscosity of the organic phase by varying magnitudes dependent on acidity. Water was observed not to have an impact outside of experimental error. This can be attributed to the interactions of the $(HNO_3)_x(Amide)_y$ adducts in the organic phase described earlier. Any adduct formed will result in a larger molecule, resisting flow to a greater extent than in uncontacted 1 M DEHiBA. The generally accepted understanding of the formation of small aggregates between the adducts in the organic phase is also a likely reason for the observed increase in viscosity with increase uptake of acid by DEHiBA.[219,230]

Table 32. Viscosity of 1 M DEHiBA in n-dodecane before and after contact with an aqueous phase of increasing acidity at 293 K

$[HNO_3]_{aq.\ initial}$ / M	η / mPa.s
Uncontacted	3.13 ± 0.02
0	3.14 ± 0.02
2	3.24 ± 0.03
4	3.44 ± 0.06
6	3.69 ± 0.07

The extraction of uranyl nitrate can be seen to increase the viscosity of the organic phase, as shown in Figures 52 – 54, to a much greater degree than nitric acid uptake. The magnitude of this change with increasing uranyl concentration in the organic phase is dependent on the temperature of the system. As increased thermal energy allows the system to overcome the friction forces and fits to an exponential trend with $[U]_{org}$ as a result temperature can be seen to dampen the exponential rise of the relationship between metal concentration and viscosity. At the conditions of T = 293 K and initial aqueous conditions of 2 M HNO_3 and 180 $g.L^{-1}$ U, the organic phase extracted uranium to an equilibrium concentration of 75.92 ± 2.7 $g.L^{-1}$ which corresponded to an increase in organic phase viscosity of 4.53 mPa.s. In contrast, the higher temperature of 333 K and initial aqueous conditions of 2 M HNO_3 and

180 g.L^{-1} U which delivers a post contacted $[U]_{org}$ of 63.29 ± 1.0 g.L^{-1}, only offers a maximum organic phase viscosity change of just 0.74 mPa.s.

The reason for this seeming exponential increase in viscosity with the uptake of uranium into the organic phase is a combination of an increase in size of complexes, increased intermolecular bonding and organisation of the molecules in a similar but exaggerated manner to HNO_3 extraction.[129,230] Stronger intermolecular attractions from more polar molecules in the organic phase in addition to the larger complexes formed with their increased steric resistance within the solution both contribute to a greater viscosity. Lastly the formation of aggregates in the organic phase[234] will contribute the most to the viscosity increase due to the potential aggregate structures (dependent on the condition specific aggregation number) forming between the uranium-acid-amide complex shown in Figure 39 $UO_2(NO_3)_2(DEHiBA)_2$, inducing greater steric resistance between the movement of molecules.

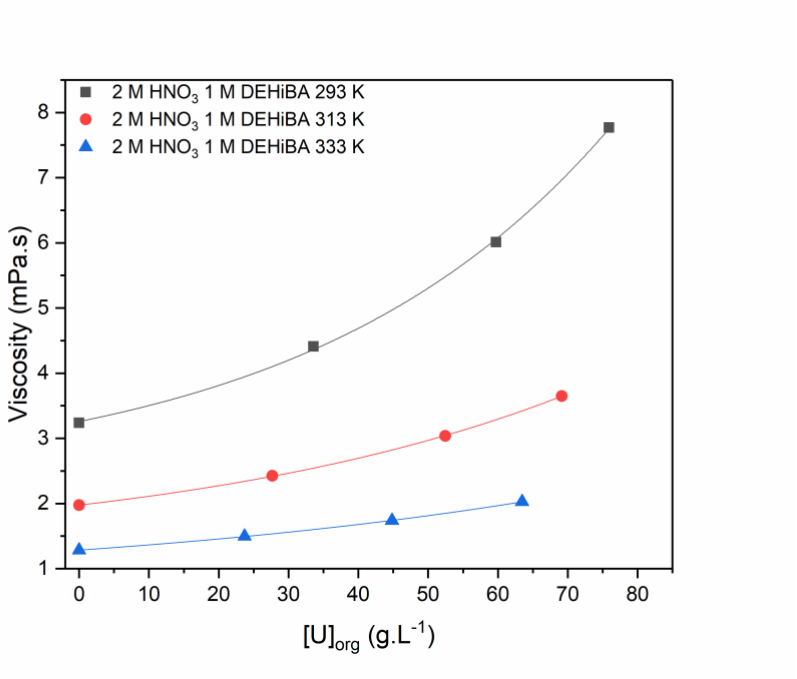

Figure 52. Plot of organic phase viscosity against post contact $[U]_{org}$ of 1 M DEHiBA in *n*-dodecane after contacting with aqueous uranyl nitrate (0 -180 g.L^{-1} $[U]_{aq, initial}$) in 2 M HNO_3, at 293, 313 and 333 K.

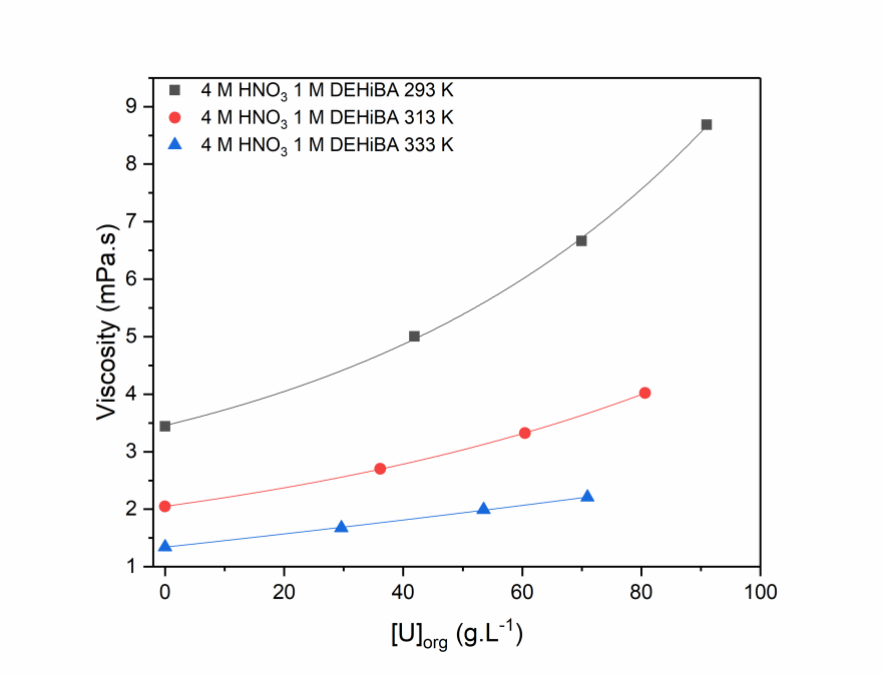

Figure 53 Plot of organic phase viscosity against post contact$[U]_{org}$ of 1 M DEHiBA in *n*-dodecane after contacting with aqueous uranyl nitrate (0 – 180 g.L^{-1} $[U]_{aq, initial}$) in 4 M HNO_3, at 293, 313 and 333 K.

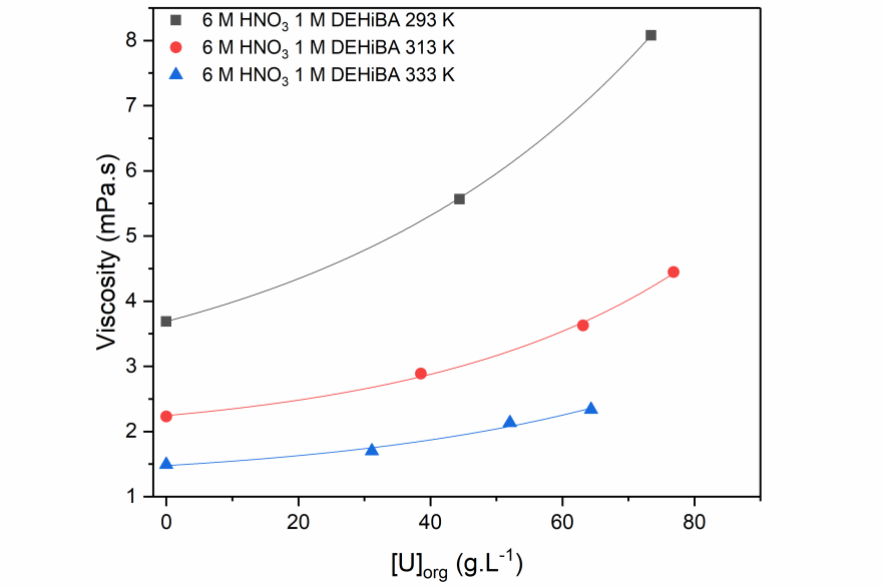

Figure 54. Plot of organic phase viscosity against post contact$[U]_{org}$ of 1 M DEHiBA in *n*-dodecane after contacting with aqueous uranyl nitrate (0 – 180 g.L^{-} $[U]_{aq, initial}$) in 6 M HNO_3, at 293, 313 and 333 K. $U_{aq. intial}$ 180 g.L^{-1} at 293 K not recorded.

Figures 52 – 54 show the maximum loading between at 293 K for all acidic conditions of the aqueous phase more than doubles the initial pre-contacted viscosity due to the apparent exponential relationship between η_{org} and $[U]_{org}$. The viscosity ratio (η_D/η_C) between each extraction equilibrium condition is

shown in the Supplementary Information section. The organic was noted to be the dispersed phase after settling observation post equal volume mixing, confirming the tendency of a higher viscosity phase to become dispersed.[235]

7.5.4 IFT

The post-extraction interfacial tension (IFT) of the unloaded and loaded organic phases with their respective aqueous phases at 293 ± 2 K and 313 ± 2 K are shown in Figure 54 and 56. IFT measurements with water as the aqueous phase was recorded at 293 K to provide a baseline measurement in order to explore the influence of acid uptake on the interfacial tension of the extractant system and is provided along with all IFT values in the Supplementary Information section. All IFT values did not alter significantly enough to cause potential mass transfer or phase separation concerns.

The increased extraction of acid into the organic phase can be seen to decrease the interfacial tension between the two phases. This can be explained by reduction in the hydrophobicity of the organic phase due to the extraction (and co-extraction) of nitric acid and water which has been observed previously in other liquid-liquid extraction systems.[98] A relatively the low water content was found in all organic phases studied here so it can be concluded that nitric acid is the dominant cause of the observed reduction in IFT.

The extraction of uranium is seen to increase the interfacial tension for systems with 2 and 4 M aqueous acid phases which is attributed to the formation of uranyl-amide reducing the concentration of the surface active free amide as the complex moves away from the interface post extraction.[189] An opposite effect can be seen in the IFT measurements of the system with the initial uptake of uranium from 6 M nitric acid. Condamines *et. al* (1988) reports more that less than half the concentration of free amide exists in the organic phase after a DEHiBA extractant system is contacted with 6 M HNO_3 compared with 4 M HNO_3. In addition to this there is increased formation of $(HNO_3)_2$(Amide) complexes which would be more polar than the other (HNO_3)(Amide) and $(HNO_3)(Amide)_2$ found in the presence of all acidic conditions, indicated by the lower interfacial tension at 6 M aqueous nitric acid equilibrated without metal loading. Uranium extraction at the interface appears to prefer free amide, less polar

molecules which could be replaced with the more polar acid-amide adducts from the bulk organic phase, reducing the IFT. Other phenomena such as aggregation could be the cause for the seen IFT decrease at the high acidity studied. Further studies that characterise the interfacial region are required to prove if this interpretation is valid. As uranium concentrations increase and there is greater uptake of uranium and complexation of all surface active extractant species into the bulk organic phase and the interfacial tension is increases, and is observed at both 293 and 313 K.

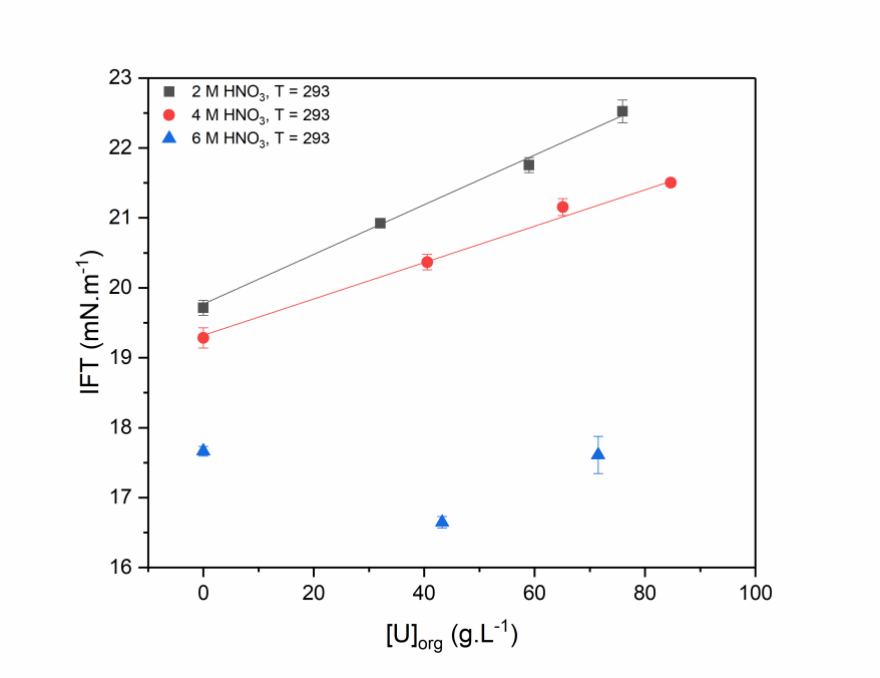

Figure 55.Interfacial tension vs $[U]_{org}$ of 1 M DEHiBA in *n*-dodecane and 2, 4 and 6 M nitric acid aqueous phase conditions at 293 K. Linear best fits were achieved for 2 and 4 M aqueous acidities. No definitive trend line is fitted for the 6 M HNO_3 conditions.

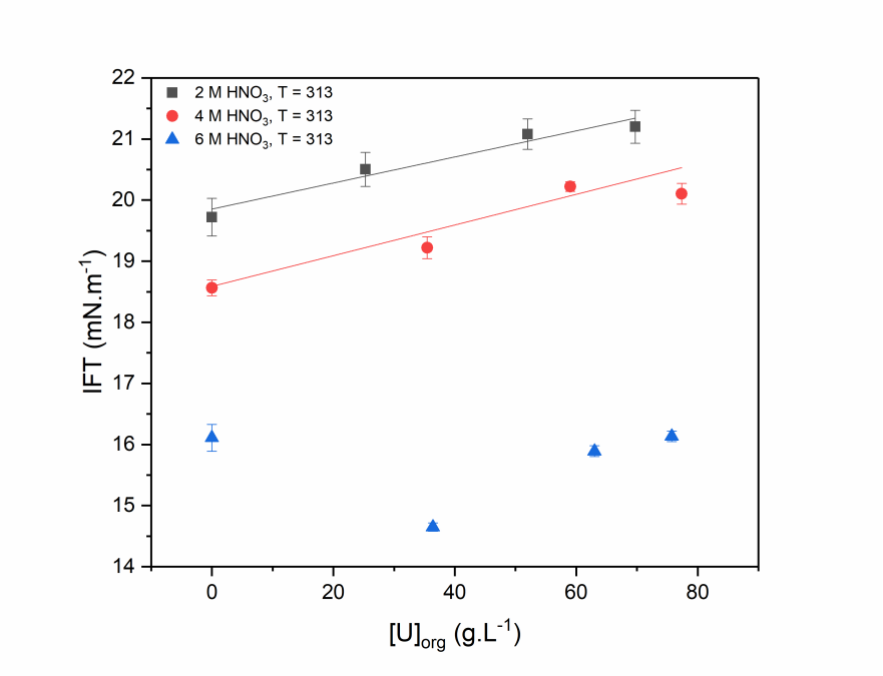

Figure 56. Interfacial tension vs $[U]_{org}$ of 1 M DEHiBA in *n*-dodecane and 2, 4 and 6 M nitric acid aqueous phase conditions at 313 K. Linear best fits were achieved for 2 and 4 M aqueous acidities.

Increased temperature reduces the IFT between the organic and aqueous phases as the intermolecular bonds weaken and allowing greater miscibility[236], this is seen across all conditions with a reduction in IFT between both unloaded and loaded metal 1 M DEHiBA and its respective aqueous phase.

7.6 Influence on Process Operations and Intensification

The separation process that is presented within this paper is based on equal volume, agitated batch samples and therefore inferences to contactor systems and their operating regimes, due to their characteristics cannot be made. However, the physical properties do provide an understanding into the fluid behaviour and areas that could cause concern if operating near process thresholds. Discussed are impacts of the physical properties on the extraction (mass transfer) and separation of a liquid-liquid process. The discussion within this section assumes a continuous organic phase with the aqueous droplets dispersed within.

7.6.1 Mass transfer

The mass transfer from the loaded aqueous phase into the organic extractant will be dictated by the kinetics of the chemical reaction of the ligand extraction (which is not in the scope of this work) and

the physical properties which dictate the diffusion of molecules within a fluid and the transfer across the interface. The physical properties studied in this paper will contribute to both an enhancement and hinderance of the mass transfer properties, and conclusions from the observations in sections 7.4.1 to 7.4.5 are discussed.

The first parameter to consider is influence of the properties on the interfacial area for mass transfer, which is dictated by the droplet size. Assuming an aqueous dispersed phase, a decrease in the size of the droplets can be induced through reducing the interfacial tension, increasing the density of the continuous phase, a change in viscosity ratio ($\frac{\mu_d}{\mu_c}$)[61] or through external influence by increasing the agitation or a change in mixing design (*e.g.* impellor diameter).

Within turbulent dispersions it is accepted that the dominant force driving droplet break up is that cause by turbulent breakage, an increase in continuous phase viscosity can either increase or decrease the droplet size depending on the conditions. Further work is required in this area with a specific contactor system to study droplet formation as a function of the observed viscosity increase in the organic phase related to $[U]_{org}$. As is discussed later, an increase in μ_c can hinder coalescence of the droplets, increasing the number of dispersed droplets (decreasing average droplet size) with a resulting the surface area available for mass transfer. However, this continues to a maximum point when the viscous forces become too great that it contributes to a decrease in the droplet break rate of the dispersed phase. At this point it will increase droplet size[237], decreasing the surface area and will being to reduce mass transfer. This is likely to be offset by a higher resistance to diffusive movements to the DEHiBA-U adducts in the organic phase hindering the concentration gradient. This is a complex area and both liquid-liquid system and extraction system dependent, which would require further work in both understanding the undergoing droplet formation of the dispersed phase at varying conditions. This droplet formation is further influenced by the interfacial tension. Typically, a reduction in IFT reflects a decrease in cohesive forces and will contribute to a smaller drop size. Both the viscosity and changing IFT are plotted below in Figures 57 and 58 show a decrease interfacial tension and increase in viscosity with uranium uptake at 293 K. Relatively, there is a much greater change in viscosity of the continuous phase with variation of $[U]_{org}$ and a subsequent reduction in the viscosity ratio. This physical property

variance is greater in magnitude than the deviation of the IFT with $[U]_{org}$. It is likely from these observations that this viscosity change will have a much greater impact than the IFT, although further work would be required to establish this within a contactor setting.

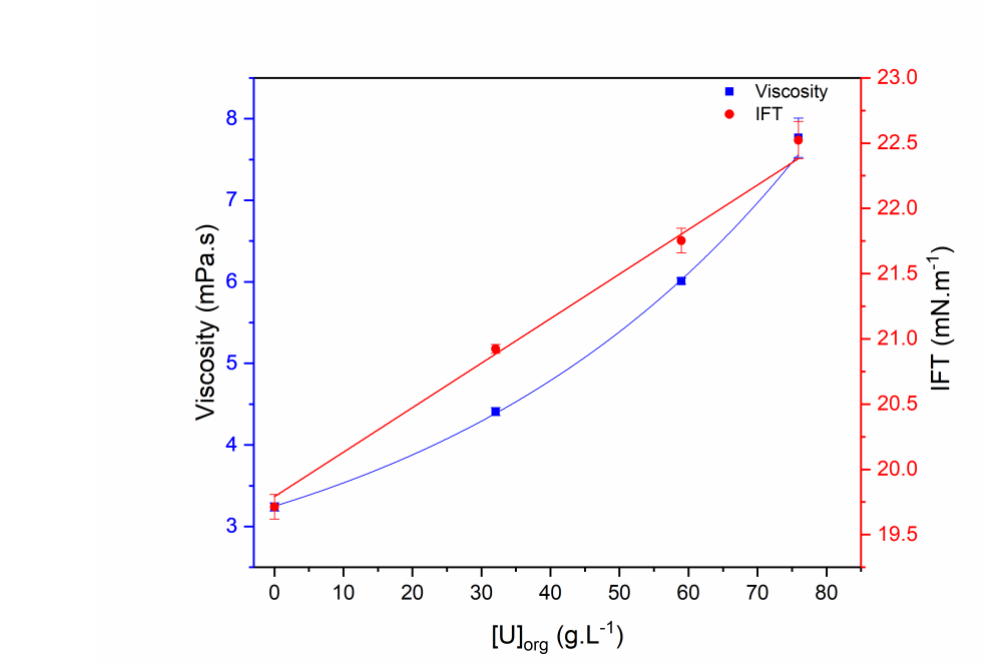

Figure 57. Viscosity (organic) and interfacial tension of 1M DEHiBA extraction of U from 2M HNO_3 aqueous phase

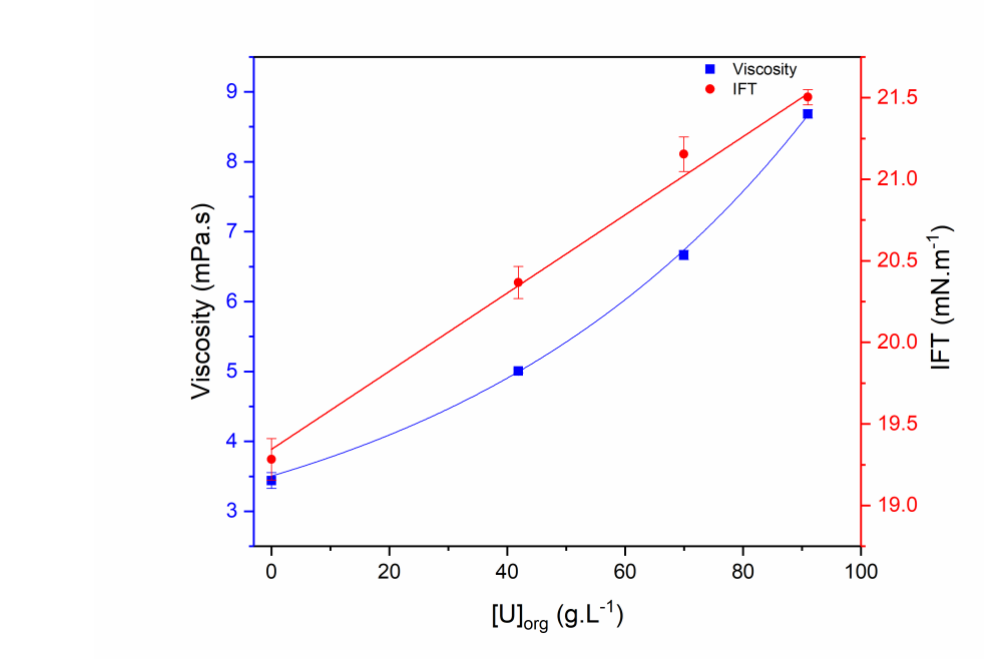

Figure 58. Viscosity (organic) and interfacial tension of 1M DEHiBA extraction of U from 4M HNO_3 aqueous phase

The second influence on the mass transfer is the movement of the molecules both within the fluids and across the interface. Referring to the Stokes-Einstein equation from the introduction to this project and provided below, an increase in viscosity in the continuous phase will reduce the diffusion coefficient and impede mass transfer away from the interface, if the unicomponent extraction is into the continuous phase. Both a decrease in concentration gradient as the organic phase extracts uranium and its subsequent increase in viscosity will hinder the mass transfer seen in the studied system. This is due to the increase in the time taken for molecules to naturally move away from the interface and maintain a concentration gradient in favour of mass transfer, decreasing the overall mass transfer.

$$D = \frac{k_B T}{6\pi\mu R}$$

Equation 25. Stokes-Einstein Equation

k_B – Boltzmann constant
T – Absolute temperature
μ – Viscosity
R – Radius of the particle

The last consideration is the influence of temperature on the mass transfer. From previous studies and as demonstrated within this paper, the increase in temperature is unfavourable to the extraction of uranium by DEHiBA. It is evident that any influence to the physical properties such as reduction in IFT and viscosity does not overcome the dominance of the associate chemical kinetics of the system When considering the process intensification of the operation, a detailed cost-performance analysis would be required that investigated the power consumption for running at higher temperatures, lowering the viscosity and increasing mass transfer area against the natural extraction equilibrium of the chemical reaction occurring.

7.6.2 Separation

Within industry the separation of the two immiscible phases will be dominated by differing physical properties, the importance of which are determined by the implemented contacting and separating system.[61] If separation is not efficient it is likely there will be entrainment issues within the exit feeds resulting in a process inefficiency, economic loss (as extractants cannot be recycled) and in certain instances, safety issues due to high activity metals in the wrong process stream. The process deviation

of physical properties is highly influential on phase separation and droplet coalescence. Tied to these properties are the droplet size, generally a smaller droplet size results in an increased coalescence time.[62,238,239] Droplet size relating to this system has been discussed in the above section and the observations on determination of the size are consistent for this section.

The density of the phases and their difference is a primary factor in both gravity and mechanical separating operations. The greater the density difference between the two phases, the more readily the separation. Although, as discussed in Section 7.4.4, at no point is the observed no conditions saw the densities of both phases within a 5% or 10% difference that are typically used as a rule of thumb for centrifugal and mixer settlers respectively. Although this is a feasibility threshold of the equipment for operation and other aspects that could cause entrainment should be considered. The observed decrease in density difference between the loaded organic extractant and stripped aqueous phase would increase the separation time in both gravity and mechanically driven segregating processes however, a counter-current extractor system would mitigate this and ensure the largest density difference within each stage. Whether this would be an issue would have to be determined in lab or pilot scale contactor conditions.

The associated viscosity increases with metal loading of the continuous organic phase will influence the separation of the two phases in all solvent extraction equipment. The impact of an increase in μ_c will hinder coalescence of the nitric acid as the droplets face increased resistance to movement, decreasing collision and increasing coalescence time. The continuous viscosity increase also resists drainage of the film between the dispersed droplets,[61] further increasing coalescence time. The last influence of note will be the type of droplets formed by the shearing of the loaded nitric acid with respect to primary and secondary drop distributions. These distributions are heavily dependent on the viscosity ratio of the liquid-liquid system, a lower viscosity ratio increasing the secondary distribution or “satellite” drops.[240,241] These drops can be view as fragments of the larger drops and in this system would increase the volume of aqueous entrainment in the organic phase.

Interfacial tension typically has countering effects on coalescence and separation but the overall effect is that a lowering IFT will increase coalescence time.[61,242] The lower IFT will disrupt the coalescence of any secondary dispersions, decrease drop size and increase the probability of coalescence resulting

from collisions. Therefore, the lowering of the interfacial tension observed between the two liquids with metal and acid loading will increase the stability of the emulsion form between the two phases. The values found between all systems however when combined with large density differences, would not concern serious entrainment issues within centrifugal contactor. This natural lowering of IFT though would need to be considered when choosing flow rates, agitation requirements and phase ratios to mitigate entrainment as much as reasonably possible.

7.6.3 Maloperation

The most concerning result with respect to potential maloperation for the process has been the aggregate formation and susceptibility to form third phase under certain conditions. In comparison to Pu(IV) extractant systems, there is a relative reduced criticality threat with the extraction of just U(VI) however it is still a key concern with any nuclear process. The aggregation seen within the organic phase will slow mass transfer as the viscosity is increased and the diffusion of the $UO_2(NO_3)_2(DEHiBA)_2$ away from the interface into the bulk phase slows. There is also an increased chance of entrainment of the loaded heavy organic phase in the aqueous outlets of a contactor system as the separation kinetics are impeded. If third phase is formed, this would have serious consequences on the operation of the contactor system designed for two phase flow. A potential way to monitor the system would be to implement density measurements between each stages. As it seen with the 4M acid conditions, density of the loaded phase goes above 0.9100 $g.cm^{-3}$ at 293 K, whilst no data is obtained due to the aggregates disrupting the density measurements at 6M HNO_3 for the same conditions, it can be confidently predicted that it will be above this mark. Process conditions should therefore aim to keep the organic phase density below this mark to mitigate against the formation of a third phase.

7.7 Conclusions

Studies on the uranyl extraction performance by 1 M DEHiBA in *n*-dodecane show similar trends to previous work, indicating a peak acidic extraction condition between nitric acid concentrations of 4 and 6 M. Temperature was observed to have an inverse relationship on extraction performance.

Conditions were discovered at which third phase formation is observed, due to the extraction of uranium and nitric acid for 1 M DEHiBA at 6 M HNO_3. This would not likely lead to phase inversion (with respect to heavy and light phase) but the formation itself would be a concern for maloperations in large scale processing. However, as it approaches third phase it is likely mass transfer and entrainment issues would arise. Processes should look to monitor the behaviour of the organic phase through density measurements as an indicator that the organic phase could be approach maloperation regimes.

Physicochemical studies have provided values for the density and viscosity of both the aqueous and organic phases with varied uranium concentrations associated with GANEX-1 process between 293 – 333 K. The extraction of water was seen to be negligible in concentration and influence on the physicochemical properties. The density of the organic phases increased post contacting with nitric acid, with a greater density increase attributed to increasing nitric acid uptake up to an aqueous phase of 6 M HNO_3. Density of the organic phase increased with increasing uranium concentrations and it was evident that the density of the organic phase as it approaches the LOC will not be problematic to process operations with respect to the density difference between the two liquids.

The uranium loading effect on viscosity was shown to be most pronounced at room temperature within the concentrations studied. Aqueous nitric acid concentration has the least impact on the viscosity of the organic phase post-contact. Viscosity ratio of an increasingly loaded organic phase can be kept to below 4 for loading conditions when operating above between 313 K.

The interfacial tension between phases decreased with nitric acid uptake and with temperature. For acidic conditions between 2 – 4 M nitric acid and uranium uptake was observed to increase the interfacial tension marginally. Across all conditions studied measured the interfacial tension did not alter significantly to concern solvent extraction process operations.

This comprehensive study on the uptake of acid and uranium has established the foundation of physical properties of the GANEX uranium extraction cycle for a range of potential operating conditions. These observations have shown that with loaded of the organic phase mass transfer will be impacted at high viscosities although studies beyond vial shaking would need to be performed. The relative changes of density and interfacial tension are unlikely to present operation issues in the conditions studied. This

data can be used to determine the physical and chemical properties to aid further experimental work and operational control to determine mass transfer fundamentals when applied to specific contacting and separation equipment. A density value for which is it likely that a process would begin to exhibit maloperation has been identified, although further work with contactor systems would provide greater insight into the effects of aggregation and potential third phase formation.

7.8 Further Work

As the system studied is relatively simple in comparison to an active feed solution, the purpose of the GANEX 1st cycle is the bulk extraction. Further work should be used to compare the densities and uranium concentration of the loaded organic phase with that recorded in this work. Should they be within acceptable agreement the expressions derived will prove useful as an on-line monitoring tool for in-situ process control.

Many aspects within both the mass transfer, coalescence and separation of the phases will offset each other or can be manipulated through operating conditions such as agitation power, shear rates and phase ratios. As is accepted, it is very difficult to create a standard environment in which a single physical parameter can be changed and the impact on the entire mixing and settling regime studied in isolation. It is recommended that further work build on the physical foundations discovered in this paper and apply these to an industrial system of interest. This would allow for process conditions to be studied and the altered to aid the understanding of the mass transfer and separation kinetics during near predicted operating processes. It would also allow for threshold and intensification studies to be performed using the data obtained in this paper with the aim developing potential pilot systems and designing extraction processes.

7.9 Acknowledgements

A studentship for RJB was funded by an EPSRC DTP awarded to the University of Manchester. Funding for consumables and equipment used in this work was provided by the EPSRC as part of the PACIFIC consortium (EP/L018616/1), and the Department of BEIS Energy Innovation Programme that has supported the National Nuclear Laboratory led Advanced Fuel Cycle Programme.

7.10 Supplementary Information – Chapter 7

Table 33. Physicochemical Properties of 1 M DEHiBA + *n*-dodecane contacted and 2 M HNO_3 pre and post-contact with uranium loading at 293, 313 and 333 K

1 M DEHiBA + *n*-dodecane, [HNO_3] – 2 M, T – 293 K									
$[U]_{aq.\ initial}$ / $g.L^{-1}$	$[U]_{aq}^{Post\ Ext.}$ / $g.L^{-1}$	$[U]_{org}^{Post\ Ext.}$ / $g.L^{-1}$	D_U	$\rho_{aq.}$ / $g.cm^{-3}$	$\rho_{org.}$ / $g.cm^{-3}$	η_{aq} / mPa.s	η_{org} / mPa.s	η_D/η_C	IFT / $mN.m^{-1}$
180	110.82 ± 2.69	75.92 ± 0.35	0.69 ± 0.02	1.2481 ± 0.0026	0.9011 ± 0.0018	1.54 ± 0.04	7.77 ± 0.24	0.198 ± 0.012	22.52 ± 0.09
120	63.59 ± 1.22	58.98 ± 1.07	0.93 ± 0.03	1.1773 ± 0.0006	0.8758 ± 0.0006	1.33 ± 0.04	6.01 ± 0.04	0.222 ± 0.009	21.75 ± 0.36
60	27.58 ± 0.27	32.05 ± 0.85	1.16 ± 0.03	1.1155 ± 0.0006	0.8402 ± 0.0006	1.22 ± 0.05	4.41 ± 0.05	0.278 ± 0.015	21.12 ± 0.11
0	0.00	0.00	0.00	1.0645 ± 0.0006	0.7988 ± 0.0006	1.09 ± 0.04	3.24 ± 0.05	0.337 ± 0.018	20.75 ± 0.16
1 M DEHiBA + *n*-dodecane, [HNO_3] – 2 M, T – 313 K									
$[U]_{aq.\ initial}$ / $g.L^{-1}$	$[U]_{aq}^{Post\ Ext.}$ / $g.L^{-1}$	$[U]_{org}^{Post\ Ext.}$ / $g.L^{-1}$	D_U	$\rho_{aq.}$ / $g.cm^{-3}$	$\rho_{org.}$ / $g.cm^{-3}$	η_{aq} / mPa.s	η_{org} / mPa.s	η_D/η_C	IFT / $mN.m^{-1}$
180	117.59 ± 1.56	75.21 ± 0.70	0.64 ± 0.01	1.2415 ± 0.0006	0.8764 ± 0.0006	1.02 ± 0.04	3.65 ± 0.04	0.28 ± 0.015	21.20 ± 0.27
120	70.86 ± 0.55	51.98 ± 0.57	0.73 ± 0.01	1.1742 ± 0.0006	0.8510 ± 0.0006	0.89 ± 0.04	3.04 ± 0.08	0.294 ± 0.021	21.08 ± 0.25
60	33.48 ± 2.03	25.26 ± 0.22	0.75 ± 0.05	1.1118 ± 0.0006	0.8179 ± 0.0006	0.81 ± 0.04	2.43 ± 0.04	0.334 ± 0.022	20.50 ± 0.28
0	0.00	0.00	0.00	1.0556 ± 0.0019	0.7838 ± 0.0006	0.71 ± 0.04	1.97 ± 0.03	0.36 ± 0.026	19.72 ± 0.31
1 M DEHiBA + *n*-dodecane, [HNO_3] – 2 M, T – 333 K									
$[U]_{aq.\ initial}$ / $g.L^{-1}$	$[U]_{aq}^{Post\ Ext.}$ / $g.L^{-1}$	$[U]_{org}^{Post\ Ext.}$ / $g.L^{-1}$	D_U	$\rho_{aq.}$ / $g.cm^{-3}$	$\rho_{org.}$ / $g.cm^{-3}$	η_{aq} / mPa.s	η_{org} / mPa.s	η_D/η_C	IFT / $mN.m^{-1}$
180	123.29 ± 1.04	63.29 ± 0.33	0.51 ± 0.01	1.2387 ± 0.0006	0.8504 ± 0.0006	0.73 ± 0.04	2.03 ± 0.04	0.362 ± 0.027	Nd.
120	78.48 ± 1.88	42.46 ± 0.35	0.54 ± 0.01	1.1708 ± 0.0006	0.8265 ± 0.0006	0.66 ± 0.04	1.74 ± 0.04	0.382 ± 0.032	Nd.
60	37.45 ± 0.14	21.06 ± 0.25	0.56 ± 0.01	1.1066 ± 0.0006	0.7981 ± 0.0006	0.60 ± 0.04	1.50 ± 0.04	0.401 ± 0.038	Nd.
0	0.00	0.00	0.00	1.0437 ± 0.0006	0.7693 ± 0.0006	0.52 ± 0.04	1.29 ± 0.04	0.39 ± 0.044	Nd.

Table 34. Physicochemical Properties of 1 M DEHiBA + n-dodecane contacted and 4 M HNO3 pre and post-contact with uranium loading at 293, 313 and 333 K

1 M DEHiBA + *n*-dodecane, $[HNO_3]$ – 4 M, T – 293 K									
$[U]_{aq.\ initial}$ / $g.L^{-1}$	$[U]_{aq}^{Post\ Ext.}$ / $g.L^{-1}$	$[U]_{org}^{Post\ Ext.}$ / $g.L^{-1}$	D_U	$\rho_{aq.}$ / $g.cm^{-3}$	$\rho_{org.}$ / $g.cm^{-3}$	η_{aq} / mPa.s	η_{org} / mPa.s	η_D/η_C	IFT / $mN.m^{-1}$
180	99.60 ± 0.98	84.66 ± 0.58	0.85 ± 0.01	1.2948 ± 0.0015	0.9129 ± 0.0018	1.72 ± 0.04	8.68 ± 0.07	0.362 ± 0.027	21.16 ± 0.12
120	49.77 ± 0.77	65.11 ± 1.02	1.31 ± 0.04	1.2069 ± 0.0008	0.8900 ± 0.0006	1.45 ± 0.04	6.67 ± 0.08	0.382 ± 0.032	19.92 ± 0.11
60	19.65 ± 0.46	40.56 ± 0.78	2.06 ± 0.09	1.1484 ± 0.0006	0.8584 ± 0.0006	1.27 ± 0.04	5.01 ± 0.04	0.401 ± 0.038	20.37 ± 0.29
0	0.00	0.00	0.00	1.254 ± 0.0006	0.8098 ± 0.0006	1.14 ± 0.04	3.44 ± 0.11	0.39 ± 0.044	19.76 ± 0.15
1 M DEHiBA + *n*-dodecane, $[HNO_3]$ – 4 M, T – 313 K									
$[U]_{aq.\ initial}$ / $g.L^{-1}$	$[U]_{aq}^{Post\ Ext.}$ / $g.L^{-1}$	$[U]_{org}^{Post\ Ext.}$ / $g.L^{-1}$	D_U	$\rho_{aq.}$ / $g.cm^{-3}$	$\rho_{org.}$ / $g.cm^{-3}$	η_{aq} / mPa.s	η_{org} / mPa.s	η_D/η_C	IFT / $mN.m^{-1}$
180	109.95 ± 2.68	77.35 ± 0.54	0.70 ± 0.02	1.2877 ± 0.0007	0.8878 ± 0.0006	1.14 ± 0.04	4.02 ± 0.04	0.284 ± 0.013	20.10 ± 0.17
120	59.29 ± 0.75	59.02 ± 0.91	1.00 ± 0.02	1.2024 ± 0.0018	0.8657 ± 0.0006	0.98 ± 0.04	3.32 ± 0.06	0.296 ± 0.018	20.33 ± 0.11
60	25.40 ± 0.72	35.45 ± 1.11	1.40 ± 0.06	1.1428 ± 0.0007	0.8358 ± 0.0006	0.87 ± 0.04	2.70 ± 0.04	0.323 ± 0.02	20.36 ± 0.12
0	0.00	0.00	0.00	1.1123 ± 0.0006	0.7955 ± 0.0006	0.74 ± 0.04	2.05 ± 0.04	0.361 ± 0.027	20.18 ± 0.15
1 M DEHiBA + *n*-dodecane, $[HNO_3]$ – 4 M, T – 333 K									
$[U]_{aq.\ initial}$ / $g.L^{-1}$	$[U]_{aq}^{Post\ Ext.}$ / $g.L^{-1}$	$[U]_{org}^{Post\ Ext.}$ / $g.L^{-1}$	D_U	$\rho_{aq.}$ / $g.cm^{-3}$	$\rho_{org.}$ / $g.cm^{-3}$	η_{aq} / mPa.s	η_{org} / mPa.s	η_D/η_C	IFT / $mN.m^{-1}$
180	119.62 ± 0.71	67.07 ± 0.89	0.56 ± 0.01	1.2813 ± 0.0009	0.8607 ± 0.0006	0.83 ± 0.04	2.21 ± 0.04	0.378 ± 0.025	Nd.
120	66.23 ± 1.59	56.48 ± 0.97	0.85 ± 0.03	1.1969 ± 0.0018	0.8388 ± 0.0006	0.72 ± 0.04	1.99 ± 0.05	0.363 ± 0.03	Nd.
60	31.92 ± 0.83	28.12 ± 1.00	0.88 ± 0.04	1.1359 ± 0.0008	0.8134 ± 0.0006	0.64 ± 0.04	1.68 ± 0.04	0.379 ± 0.033	Nd.
0	0.00	0.00	0.00	1.0968 ± 0.0006	0.7807 ± 0.0006	0.54 ± 0.04	1.34 ± 0.04	0.402 ± 0.042	Nd.

Table 35. Physicochemical Properties of 1 M DEHiBA + n-dodecane contacted and 6 M HNO3 pre and post-contact with uranium loading at 293, 313 and 333 K

1 M DEHiBA + *n*-dodecane, [HNO_3] – 6 M, T – 293 K									
$[U]_{aq.\ initial}$ / $g.L^{-1}$	$[U]_{aq}^{Post\ Ext.}$ / $g.L^{-1}$	$[U]_{org}^{Post\ Ext.}$ / $g.L^{-1}$	D_U	$\rho_{aq.}$ / $g.cm^{-3}$	$\rho_{org.}$ / $g.cm^{-3}$	η_{aq} / mPa.s	η_{org} / mPa.s	η_D/η_C	IFT / $mN.m^{-1}$
180	95.62 ± 1.29	92.00 ± 1.43	0.96 ± 0.01	1.3484 ± 0.0043	Nd.	2.00 ± 0.06	Nd.	Nd.	Nd.
120	52.72 ± 0.81	71.51 ± 0.33	1.36 ± 0.03	1.2759 ± 0.0006	0.9012 ± 0.0006	1.68 ± 0.04	8.08 ± 0.08	0.209 ± 0.008	17.32 ± 0.13
60	15.65 ± 1.06	43.27 ± 0.35	2.77 ± 0.19	1.2150 ± 0.0006	0.8679 ± 0.0006	1.43 ± 0.05	5.56 ± 0.11	0.257 ± 0.015	16.65 ± 0.07
0	0.00	0.00	0.00	1.1912 ± 0.0006	0.8185 ± 0.0006	1.19 ± 0.04	3.69 ± 0.14	0.323 ± 0.024	17.88 ± 0.55
1 M DEHiBA + *n*-dodecane, [HNO_3] – 6 M, T – 313 K									
$[U]_{aq.\ initial}$ / $g.L^{-1}$	$[U]_{aq}^{Post\ Ext.}$ / $g.L^{-1}$	$[U]_{org}^{Post\ Ext.}$ / $g.L^{-1}$	D_U	$\rho_{aq.}$ / $g.cm^{-3}$	$\rho_{org.}$ / $g.cm^{-3}$	η_{aq} / mPa.s	η_{org} / mPa.s	η_D/η_C	IFT / $mN.m^{-1}$
180	107.54 ± 1.08	75.72 ± 0.43	0.70 ± 0.01	1.3368 ± 0.0007	0.8891 ± 0.0017	1.32± 0.06	4.45 ± 0.11	0.297 ± 0.021	16.13 ± 0.09
120	63.05 ± 1.07	63.00 ± 0.54	1.00 ± 0.02	1.2683 ± 0.0006	0.8742 ± 0.0006	1.11 ± 0.04	3.63 ± 0.04	0.306 ± 0.015	16.05 ± 0.07
60	21.47 ± 0.56	36.38 ± 1.10	1.69 ± 0.07	1.2050 ± 0.0006	0.8454 ± 0.0006	0.96 ± 0.04	2.8 ± 0.07	0.334 ± 0.022	15.94 ± 0.12
0	0.00	0.00	0.00	1.1751 ± 0.0006	0.8034 ± 0.0006	0.78 ± 0.04	2.23 ± 0.04	0.35 ± 0.025	18.53 ± 0.55
1 M DEHiBA + *n*-dodecane, [HNO_3] – 6 M, T – 333 K									
$[U]_{aq.\ initial}$ / $g.L^{-1}$	$[U]_{aq}^{Post\ Ext.}$ / $g.L^{-1}$	$[U]_{org}^{Post\ Ext.}$ / $g.L^{-1}$	D_U	$\rho_{aq.}$ / $g.cm^{-3}$	$\rho_{org.}$ / $g.cm^{-3}$	η_{aq} / mPa.s	η_{org} / mPa.s	η_D/η_C	IFT / $mN.m^{-1}$
180	120.05 ± 2.53	62.36 ± 0.78	0.52 ± 0.01	1.3277 ± 0.0006	0.8610 ± 0.0006	0.95 ± 0.04	2.34 ± 0.04	0.408 ± 0.025	Nd.
120	74.14 ± 1.50	54.27 ± 0.62	0.73 ± 0.02	1.2615 ± 0.0006	0.8461 ± 0.0006	0.81 ± 0.04	2.14 ± 0.04	0.378 ± 0.026	Nd.
60	28.91 ± 0.94	28.78 ± 0.53	1.00 ± 0.04	1.1916 ± 0.0011	0.8237 ± 0.0026	0.70 ± 0.04	1.70 ± 0.05	0.409 ± 0.036	Nd.
0	0.00	0.00	0.00	1.1586 ± 0.0006	0.7886 ± 0.0006	0.58 ± 0.04	1.49 ± 0.08	0.389 ± 0.048	Nd.

8. Effects of Gamma Irradiation on the Physicochemical Properties of the GANEX Solvent Systems

Paper Overview

This paper presents the effects of γ-radiation induced degradation of proposed GANEX-1 and EURO-GANEX extractant systems. Samples were irradiated up to 750 kGy with a ^{60}Co source both uncontacted and contacted with likely aqueous acidic concentrations. The viscosity, density and interfacial tension were evaluated and qualitatively explained with reference to literature degradation studies.

It is anticipated that this paper will be submitted to Separation Science and Technology or the Journal of Radioanalytical and Nuclear Chemistry.

Author Contributions:

R. Blundell – Experimental work, data collection and data analysis, manuscript drafting.

K. George – Data analysis and manuscript review

R. Edge – Irradiation experiments

C. A. Sharrad - Principal investigator and manuscript review

Effects of Gamma Irradiation on the Physicochemical Properties of the GANEX Solvent Systems

*R. J. Blundell [*a], K. George,[a] R. Edge[b] and C. A. Sharrad[*a]*

a. School of Chemical Engineering and Analytical Science, The University of Manchester, Oxford Road, Manchester, M13 9PL, U.K .

b. Dalton Cumbrian Facility, The University of Manchester, Westlakes Science and Technology Park, Whitehaven, Cumbria, CA24 3HA, U.K.

8.1 Abstract

The organic extractant systems of the GANEX-1 and EURO-GANEX process were subjected to gamma radiation in order to induce solvent degradation to simulate process conditions of the spent nuclear fuel (SNF) recycling operation. Physicochemical properties were investigated at 293 K both before and after irradiation. Organic solvents were irradiated with and without pre-contract with nitric acid, and showed little change in the density and viscosity other than what could be attributed the loss of $[HNO_3]_{org}$. The interfacial tension (IFT) of the GANEX-1 system was observed to decrease with total dose, with sufficient deviation from the initial, non-irradiated solvent value to indicate that the solvent, if used in process operations, will require regeneration in order to maintain the IFT required for use in centrifugal contactors. The IFT of the EURO-GANEX process did not deviate significantly up to total dose of 750 kGy.

8.2 Introduction

8.2.1 Overview

Future spent nuclear fuel (SNF) recycling objectives seek to reduce the potential impact of radioactive waste on the environment and lessen the cost of deep geological disposal through a reduction in the volume of high-level waste (HLW) and heat load associated with this waste. Future recycling aims to

achieve these objectives whilst also improving proliferation resistance and process safety compared to currently established methods for reprocessing spent fuel at process scales.[137,243,244] Ideas for a future nuclear fuel recycling programme involve the implication of a consolidated flow concept (CFC).[243] One proposed method is the Group ActiNide Extraction (GANEX) process.[110] The GANEX cycle can be divided into two stages, the first involving the bulk U(VI) separation from the rest of the spent fuel and the second is a Pu(IV) and minor actinide (MA) strip followed by a scrub.[106,111,224,245] This proposed separation aims to facilitate the recycle of all the actinide elements opening the possibility of producing and recycling fuels for fast reactor systems. A particular challenge is to separate the minor actinides from the lanthanide fission products due to their similar chemical properties. The lanthanides, in particular, cannot be present in recycled fuel due to their strong neutron absorption cross-section.

The first GANEX cycle is almost certain to use the diakylamide, N,N-diethylhexyl isobutylamide (DEHiBA), which has shown favourable properties for the selective extraction of U(VI) over other transuranic (TRUs) and fission products (FPs) present in spent fuel.[113] In addition to its uranium extraction ability, DEHiBA obeys the carbon, hydrogen, oxygen and nitrogen (CHON) principle which leads to reduced waste volumes, and, in the correct concentration and diluent, has shown suitable extraction kinetics and hydrodynamic properties for liquid-liquid extraction techniques.[106] A wider consensus is yet to be reached on the preferred system for the GANEX 2nd cycle and methods under consideration are still being developed and evaluated. The ambition of the second cycle is to strip the actinides from the remaining lanthanides and FPs in the spent fuel solution. The three leading routes are CEA GANEX (developed by the French Alternative Energies and Atomic Energy Commission {CEA}), EURO-GANEX and CHALMEX (developed by Chalmers University).[111] The EURO-GANEX system, which is the focus of this study, uses an organic solvent containing *N,N,N′,N′*-tetraoctyl diglycolamide (TODGA) and *N,N′*-dimethyl-*N,N′*-dioctylhexylethoxymalonamide (DMDOHEMA) in hydrocarbon diluents to co-extract the TRUs.[246,247] The An(III) are then selectively stripped into the aqueous phase containing water soluble sulfonated bistriazinylpyridine molecule, SO_3-Ph-BTP,[248] and acetohydroxamic acid (AHA) in weak nitric acid.[138,249] Both the initial group extraction

and the scrubbing steps of the 2nd GANEX cycle have been successfully demonstrated in a 32 stage centrifugal contactor hot-test environment.[127]

This work explores the CEA developed, GANEX-1 cycle with DEHiBA as the extractant and *n*-dodecane as the diluent, instead of hydrogenated tetrapropene (TPH) which has been previously proposed as the organic phase diluent in this cycle, and an aqueous phase of unloaded 4 M HNO_3. There are variations in proposed techniques on how to deal with the challenging extraction of minor actinides and plutonium after the initial selective uranium extraction. The GANEX-2 cycle, used for the separation of TRUs will evaluate the EURO-GANEX process. The EURO-GANEX process uses this 0.2 M TODGA + 0.5 M DMDOHEMA organic extractant system to co-extract the TRU.[246,247] The An(III) are then selectively stripped into the aqueous phase by SO_3-Ph-BTP[248] and acetohydroxamic acid (AHA) in weak nitric acid.[138,249] Work on the EURO-GANEX hot-tested in a 16 stage centrifugal contactor bank with an aqueous phase containing 10 $g.L^{-1}$ Pu in 5.9 M HNO_3, the increased acidity of the aqueous phase to aid the extraction of Np.[250] Two flowsheets in Figures 59 and 60 illustrate this process.

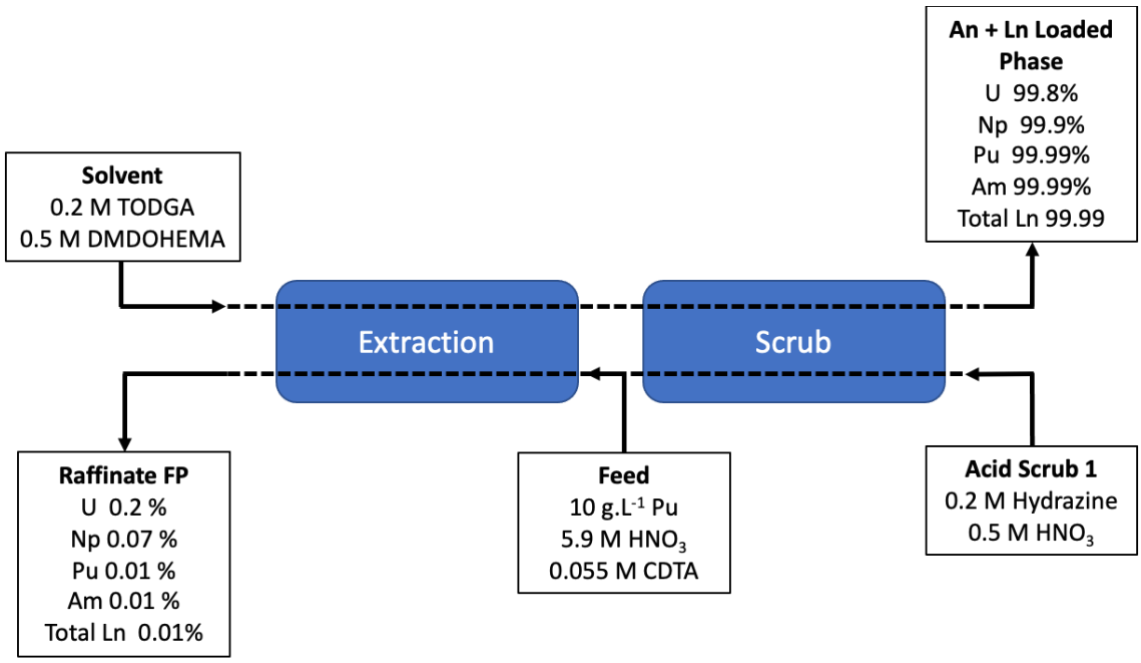

Figure 59. EURO-GANEX Hot-Test Flowsheet, removal of TRU from FP. [250]

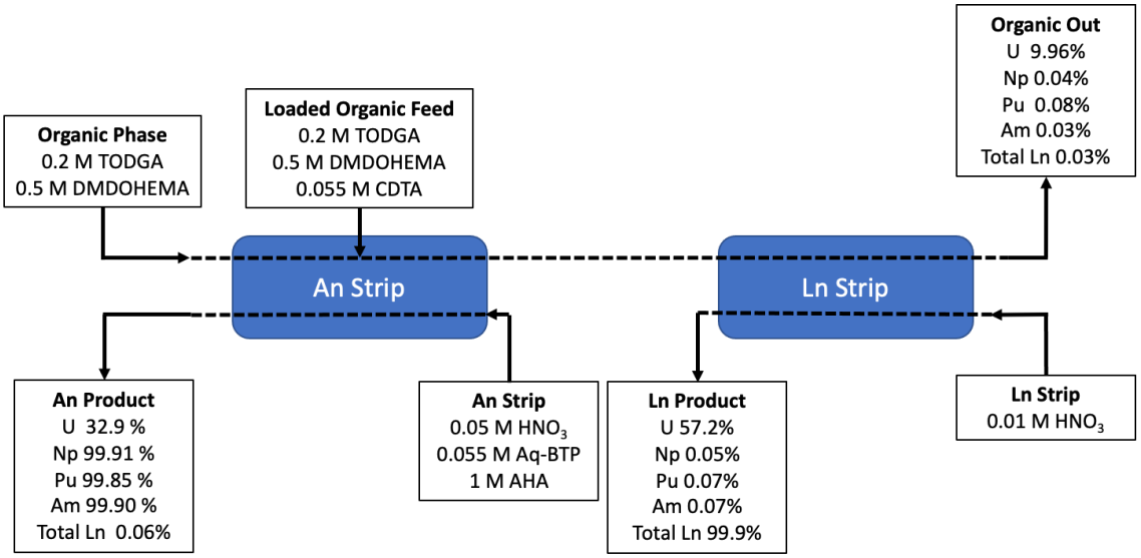

Figure 60. EURO-GANEX Hot-Test Flowsheet, Actinide and Lanthanide separation.[250]

This uses an organic phase of 0.2 M TODGA and 0.5 M DMDOHEMA in *n*-dodecane diluent with an aqueous phase of 5.9 M HNO_3. The structures of the organic soluble extractants studied here are shown below in Figure 61.

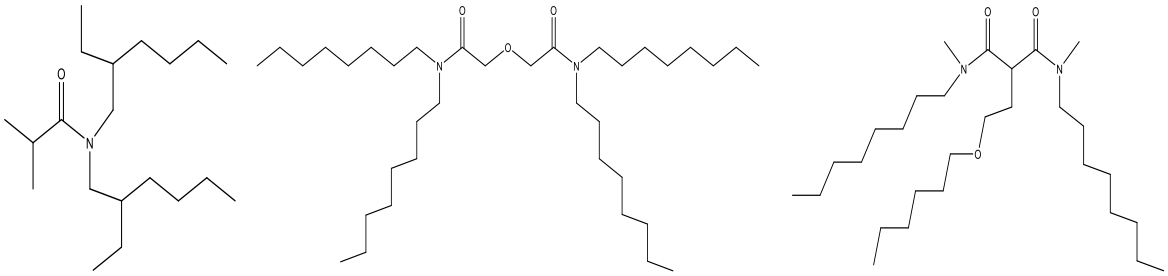

Figure 61. Structure of DEHiBA (left), TODGA (middle) and DMDOHEMA (right).

Future recycling processes will have to contend with the implications of high burn-up/ fast reactor fuels which will expose the organic phase to elevated radiation intensities.[251] Therefore, the impact of radiolysis on the extraction behaviour of these extractants needs to be fully understood. Not only is it important to have a rigorous understanding of how radiolytic degradation products of the solvent affect the selective extraction of target elements, the presence of these degradation products can also impact the hydrodynamic suitability of the solvents in liquid-liquid separations and ultimately the overall process performance.[251] The goal of this work it to quantify the effect of radiolytic degradation on the

GANEX process with respect to the physiochemical thresholds likely to be encountered in operational conditions.

8.2.2 Previous Degradation Studies

8.2.2.1 Radiolytic Degradation of DEHiBA in n-dodecane (GANEX-1 solvent)

The suitability of DEHiBA as the extracting ligand for the GANEX-1 cycle has been previously studied with respect to both acid hydrolysis (nitric acid) and radiolysis. Under contact with nitric acid DEHiBA showed good resistance to both hydrolysis and radiolysis.[122] When absorbing a total gamma dose of 1250 kGy there was up to 85% of the ligand still remaining.[121,122,220,252] Drader *et al.* (2017) produced a comprehensive study on the radiolysis and degradation products of DEHiBA in *n*-dodecane in the presence and absence of both acidity and aeration. This work reported that bond cleavage primarily occurs at the C-N junction in monoamide extractants resulting in primary radiolytic degradation products being a carboxylic acid and its corresponding amide.[220] Drader's study showed similar degradation kinetics were observed under all conditions but explained differences between the fresh and pre-contacted phases by the favoured degradation pathways in the presence and absence of nitric acid.[220] The uncontacted samples had an ability to form higher molecular weight species attributed to the interaction of DEHiBA with *n*-dodecane degradation products and vice versa instigated by irradiation. Prominent degradation species were identified as diethylhexylamine (DEHA) and monoethylhexylisobutyramide (EHiBA). Two additional heavier molecular ion species of note were identified from the interaction between dodecane and DEHiBA at m/z = 480.5 and the interaction between dodecane and the degradation product DEHA at m/z= 410.5 .[220] The radiolysis degradation products of DEHiBA were found to be relatively unproblematic in extraction processes in contrast to the radiolytic degradation products of tributylphosphate (TBP) in the well established PUREX (Plutonium Uranium Reduction Extraction) process.. The degradation products of DEHiBA are water-soluble and thus transfer into the aqueous phase upon formation. These DEHiBA degradation products have been shown to have little impact on the selective extraction of U(VI).[220,253]

8.2.2.2 Radiolytic Degradation of 0.2 M TODGA + 0.5 M DMDOHEMA in n-dodecane (GANEX-2 solvent)

Previous studies have documented the gamma ray induced radiation chemistry and degradation products of both TODGA and DMDOHEMA, although there are currently no published studies of the combined extractant system as proposed in the EURO-GANEX process.[135,254]

The degradation pathway of TODGA is provided in Figure 62 from Sugo *et al.* (2002) where products include dioctylamine (DOA), *N,N*-dioctyl-3-oxapentan-1.5-amide acid, *N,N*-dioctylacetamide (DOAA), *N,N*-dioctylglycoamide (DOGA) and *N,N*-dioctylformamide (DOFA).[254,255] The degradation rate of TODGA was found to be unaltered by the presence of HNO_3 but enhanced by the diluent *n*-dodecane.[254] Conversely, Galan *et al.* (2012) found the degradation of TODGA was impaired with the pre-equilibration with 3 M HNO_3.[135] It was concluded that the overall resistance of TODGA to acid hydrolysis and to both gamma and heavy particle radiolysis make it suitable for process scale solvent extraction of spent nuclear fuel.[134,135,254]

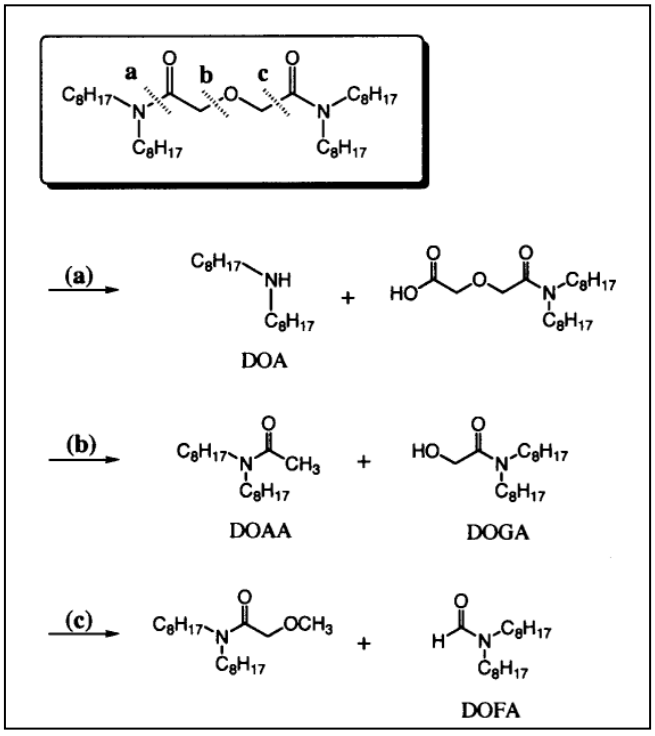

Figure 62. Radiolytic degradation pathway of TODGA taken from Sugo et. al (2002) [254]

Degradation studies of DMDOHEMA show a multitude of degradation products that have been previously identified using mass spectrometry, the main products being the amide-acid compound C-$_8$H$_{17}$N(CH$_3$)COCH(C$_2$H$_4$OC$_6$H$_{13}$)COOH, monoamide C$_8$H$_{17}$N(CH$_3$)COC$_3$H$_6$OC$_6$H$_{13}$, a variety of carboxylic acids and the amine C$_8$H$_{17}$N(CH$_3$).[133,256] Studies of both the radiolytic and hydrolytic degradation of DMDOHEMA showed similar degradation pathways and associated products to that of the monoamide DEHiBA although DMDOHEMA showed weaker resistance to acid hydrolysis.[122,133]

8.3 Experimental Procedure

8.3.1 Materials

Nitric acid (68% wt.), supplied by SigmaAldrich, was diluted using a 15 MΩ deionized water to desired concentrations. These acid concentrations were confirmed using Mettler T5 Autotitrator with standardised 1 M NaOH as the titrant. DEHiBA, TODGA and DMDOHEMA were procured from Technocomm (99% pure confirmed by HPLC) and used as received. Samples were weighed before being diluted to desired concentrations using *n*-dodecane (>99%) from SigmaAldrich. The measured physicochemical properties of neat extractants and diluent are given in Table 36.

Table 36. Physicochemical properties of pure extractants and n-dodecane

Compound	Formula	Molar Mass / g mol^{-1}	Density / g.cm^{-1} *	Viscosity / mPa.s *
n-dodecane	C$_{12}$H$_{26}$	170	0.7493	1.53 ± 0.03
DEHiBA	C$_{20}$H$_{41}$NO	312	0.8652	35.76 ± 0.61
TODGA	C$_{36}$H$_{72}$N$_2$O$_3$	518	0.9112	164.47 ± 2.56
DMDOHEMA	C$_{29}$H$_{58}$N$_2$O$_3$	482	0.9234	152.13 ± 2.56

* As recorded using Mettler-Toledo DM40 densitometer and a Wells Brookfield Cone and Plate Viscometer at 293 K. Associated density error for all measurements was ± 6 x 10^{-4} g.cm^{-1}

8.3.2 Methods

Density and viscosity measurements were obtained using previously described methods. Triplicate interfacial tension (liquid-liquid interface) measurements followed the same method previously described for analogous studies. The method required the values of density at 293 K for both the organic and aqueous phases. Measurements were taken between the interface of the organic samples and a droplet of fresh aqueous solution.

The sealed samples were exposed to γ-irradiation using a ^{60}Co source at the University of Manchester's Dalton Cumbrian Facility (DCF) achieving total doses of 250, 500 and 750 kGy. Samples were irradiated using a Foss Therapy Service 812 ^{60}Co gamma irradiator with a calculated average dose rate for each sample of 6.14 kGy.h^{-1}. The chamber is at a temperature of approximately 314 K during sample irradiations. Absorbed dose rates were determined using a Radcal Corporation Accu-Dose unit calibrated to national standards. Calculated actual dose rates show all irradiation targets were met within ±2% of the desired total dose.

Nitric acid is known to influence the degradation of extractants, hence samples of the organic phase were irradiated as both 'fresh' (uncontacted with nitric acid) and 'pre-contacted'. DEHiBA and TODGA – DMDOHEMA systems were pre-contacted with 4 M HNO_3 and 5.9 M HNO_3, respectively. Contacting with acid was carried out in a 3:1 (aqueous: organic) volume ratio for 30 minutes at 293 K using an Eppendorf Thermomixer at 1000 rpm. The contacted mixtures were centrifuged at 400 rpm for two minutes at room temperature. The organic phases were carefully separated from the aqueous phase and subsequently irradiated as sealed organic samples only.

All measurements were taken in triplicate and the error stated is the largest between that of the 95% confidence interval calculated or the technique uncertainty of the measurement. Linear best fit analysis was undertaken and presented in plots to aid the viewing of observed trends unless otherwise stated.

8.4 Results and Discussion

All recorded physiochemical measurements for the conditions studied are provided in the Supplementary Information section.

8.4.1 Qualitative Sample Observations Post-Irradiation

Figures 63 – 66 show visual observations to the change in colour of the extractant systems with increased exposure to γ-radiation. Solutions of 1 M DEHiBA uncontacted with nitric acid can be seen to have negligible changes with irradiation. Uncontacted EURO-GANEX samples (0.2 M TODGA + 0.5 M DMDOHEMA in *n*-dodecane) shown in Figure 65 show a slight change from colourless to pale yellow with increasing total dose. Both solvents studied here when contacted with nitric acid show a clear increase in intensity of a yellow/brown colour with increasing dose. On the opening of all irradiated solvents contacted with nitric acid, notable gas in the form of bubbles from the organic phase were observed to be released, possibly NO_2 or H_2.

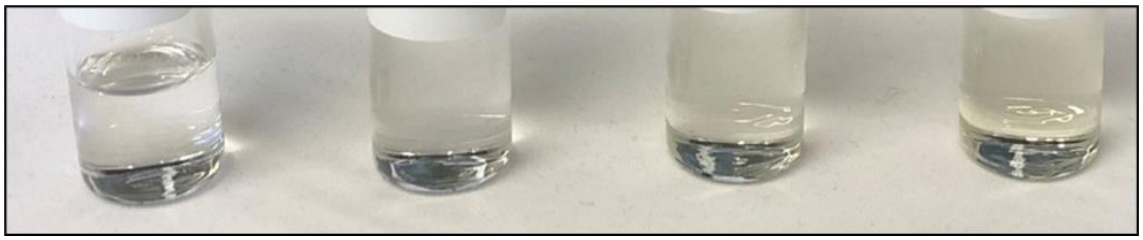

Figure 63. Samples of 1 M DEHiBA in n-dodecane (uncontacted) after undergoing γ-radiolysis with respective total doses (left to right) of 0, 250, 500, 750 kGy irradiation

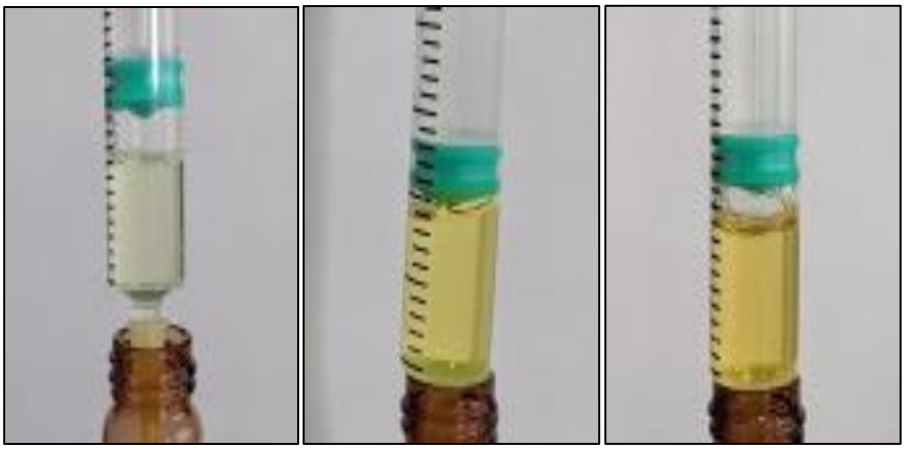

Figure 64. Samples of 1 M DEHiBA in n-dodecane (pre-contacted with 4 M HNO_3) after undergoing γ-radiolysis with respective total doses (left to right) of 250, 500, 750 kGy irradiation

Figure 65. Samples of 0.2 M TODGA + 0.5 M DMDOHEMA in n-dodecane uncontacted after undergoing γ-radiolysis with respective total doses (left to right) of 0, 250, 500, 750 kGy irradiation

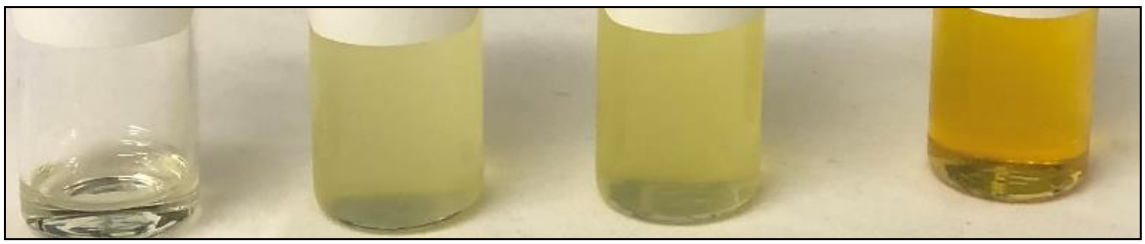

Figure 66.. Samples of 0.2 M TODGA + 0.5 M DMDOHEMA in n-dodecane (pre-contacted with 5.9 M HNO_3) after undergoing γ-radiolysis with respective total doses (left to right) of 0, 250, 500, 750 kGy irradiation

8.4.2 Acid Extraction and Change with Total Dose

The uptake of acid due to the pre-contacting of the GANEX solvent systems with nitric acid was confirmed and the quantity of acid present in both solvent systems seen to decrease as total dose increases. Table 37 provides the acid content of the pre-contacted organic samples after gamma irradiation showing the organic phase acid content was partially consumed during irradiation. The most significant change in $[HNO_3]_{org}$ for both systems is observed between 0 – 250 kGy after which there is a more gradual decrease in organic phase acid content with respect to dose.

Table 37. Acid content in the organic phase of 1 M DEHiBA in n-dodecane and 0.2 M TODGA + 0.5 M DMDOHEMA in n-dodecane with increasing dose

	1 M DEHiBA in *n*-dodecane (contacted with 4M HNO_3)	0.2 M TODGA + 0.5 M DMDOHEMA in n-dodecane (contacted with 5.9M HNO_3)
Total Dose / kGy	$[HNO_3]_{org}$ / M	$[HNO_3]_{org}$ / M
0	0.61 ± 0.02	0.88 ± 0.02
250	0.41 ± 0.05	0.46 ± 0.05
500	0.36 ± 0.03	0.37 ± 0.01
750	0.31 ± 0.04	0.34 ± 0.01

Previous pulsed and gamma radiation studies of aqueous NO_3^- and HNO_3 identified the primary formation of the following products: NO_2^-, HNO_2, NO_3•, NO_2 and O_2 and water radiolysis products; all which can contribute to a decrease in acidity for these previous aqueous studies and are likely to also cause the observed decrease in acidity present in the organic solvents studied here after irradiation.[35,257]

8.4.3 Density

8.4.3.1 GANEX-1 Density Studies

The pre-contacting of the organic phase and the extraction of nitric acid by the organic phase without irradiation results in a density increase of 0.0102 ± 0.0006 $g.cm^{-3}$ (see 0 kGy values in Figure 67).

Densities of uncontacted samples were found to be almost unaltered across all doses received. A change in density with absorbed dose for the pre-contacted solutions is clearly evident and decreases with increasing dose up to 500 kGy. This negative deviation in organic density can be attributed to the reduction of nitric acid content in the organic phase. There may be a slight increase observed in the density of the pre-contacted organic phases with gamma exposure from 500 to 750 kGy, but it is noted this change is within error of the measurements.

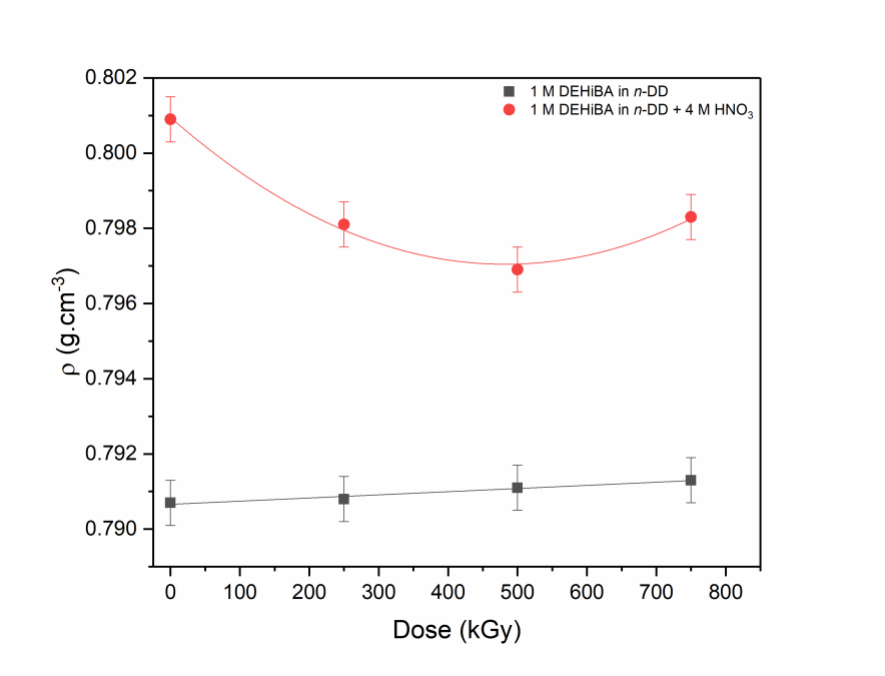

Figure 67. Density of 1 M DEHiBA + n-dodecane vs. absorbed dose of γ radiation at 293 K. Nonliear and linear best fits were applied respectively to both uncontacted and acid pre-contacted sample series (Regression data provided in Supp. Info.)

Although there was an observed variation in density for pre-contacted samples with gamma irradiation, the maximum variation from the non-irradiated solvent was only 0.0040 ±0.0006 g.cm^{-}, between unirradiated and 500 kGy [3]. When considering the impact this will have on process operations the density is most influential during the separation of the immiscible liquids. A decrease in density would aid this the separation as it would increase in the density difference between the two phases. This is only the case if no other properties were impacted, which is not the case and discussed later. There the changes seen can be dismissed as unlikely to have the potential to cause problems in process scale conditions.

8.4.3.2 GANEX-2 Density Studies

The uptake of HNO_3 is observed to cause the greatest deviation in density across all conditions for the proposed GANEX-2 solvent exhibiting an increase in density by 0.0289 g.cm^{-3} (3.54%), as seen in Figure 68. Uncontacted samples exhibit a slight increase in density with dose, which could be associated with previous reports of increased degradation of the extractants with total dose[133,254] and the resulting

formation of stronger intermolecular bonds between degradation compounds, although the increase is within experimental error across the dose range. The densities of the pre-contacted samples can be seen to significantly decrease with increasing dose, in contrast with the density trend of the uncontacted samples with increase dose. Previous studies[254] detailing that degradation of TODGA is relatively constant regardless of the presence of nitric acid suggests that the change in density across the total dose range is primarily due to the further loss of $[HNO_3]_{org.}$ Despite this clearly observed deviation in density, it is unlikely to be problematic in the industrial solvent process setting for the same reason discussed for the deviation seen in the GANEX-1 solvent system.

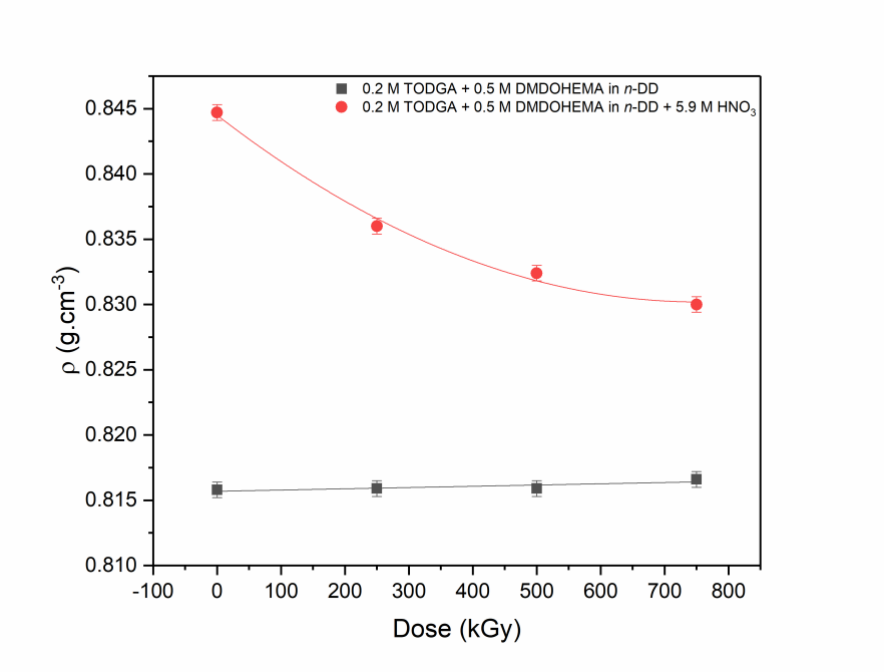

Figure 68. Density of 0.2 M TODGA + 0.5 M DMDOHEMA in n-dodecane vs. absorbed dose of γ radiation at 293 K. Nonliear and linear best fits were applied respectively to both uncontacted and acid pre-contacted sample series (Regression data provided in Supp. Info.)

8.4.4 Viscosity

8.4.4.1 GANEX-1 Viscosity Studies

Figure 69 displays the induced viscosity deviation with radiolysis of the uncontacted and nitric acid contacted 1 M DEHiBA in *n*-dodecane samples. The expected viscosity increase with the uptake of nitric acid is clear between the two samples and discussed previously in Chapter 7. It can be observed

from Figure 69 that there is a change in viscosity with absorbed dose for both uncontacted and pre-contacted solutions, both following a similar trend where there is a relatively sharp decrease in solvent viscosity for 0 to 250 kGy, with viscosities then increasing slightly with further doses. For the pre-contacted solutions, there is a sharper drop in the viscosity from 0 to 250 kGy relative to that observed for the uncontacted solvent, which is attributed to both the reduced nitric acid concentration in the organic phase, and the formation of lower mass molecular species reducing the resistance that can occur between large molecules. This then climbs with total dose to 2.90 mPa.s ± 0.04 at 750 kGy. The changes in viscosity observed across the absorbed doses studied indicates that radiolysis on the GANEX-1 solvent is unlikely to cause an operational concern as the deviation observed is minimal compared to the changes in viscosity due to the effects of metal loading, as we have reported previously (see Section 7). Further work will attempt to explore the combined influence of radiolysis and metal loading on solvent viscosity.

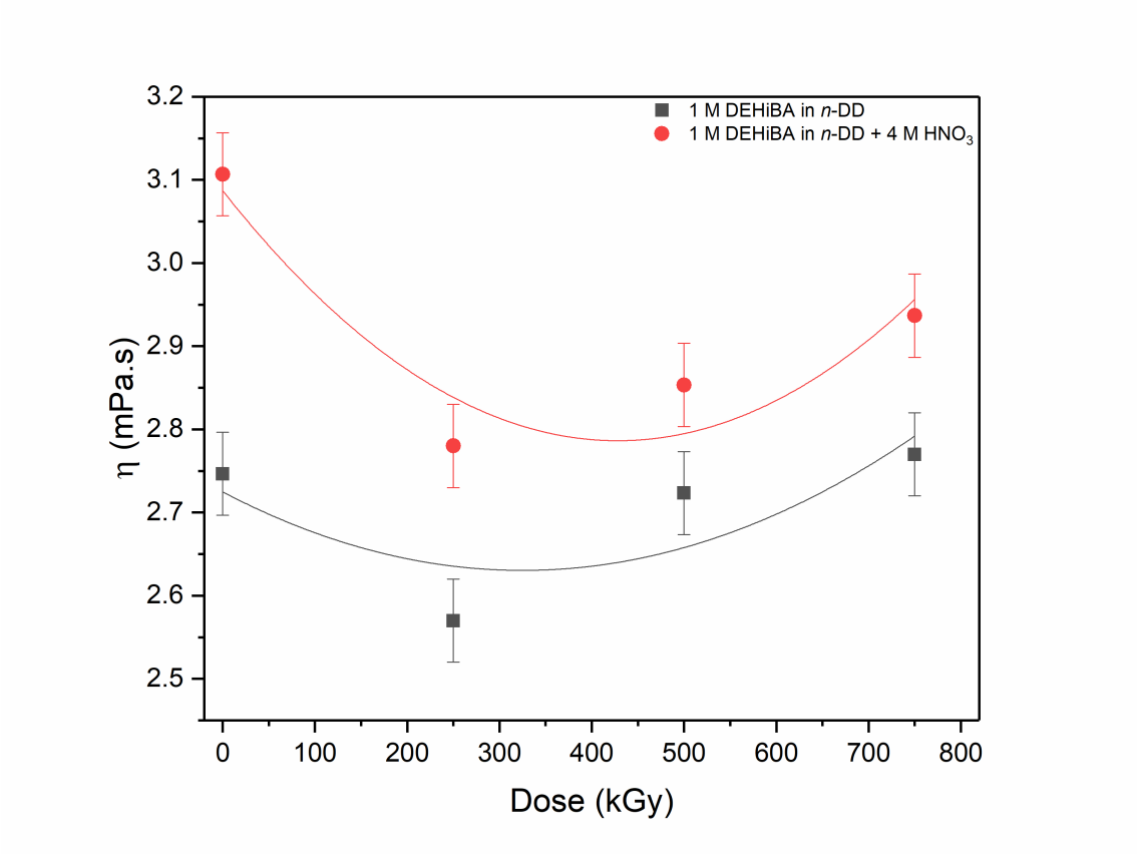

Figure 69. Viscosity of 1 M DEHiBA + n-dodecane against absorbed dose for uncontacted and pre-contacted (4 M HNO_3) phases at 298 K. Non-linear fits were attempted respectively to both uncontacted and acid pre-contacted sample series (Regression data provided in Supp. Info.).

8.4.4.2 GANEX-2 Viscosity Studies

The observed changes in viscosity of 0.2 M TODGA + 0.5 M DMDOHEMA in *n*-dodecane with absorbed dose up to 750 kGy are shown in Figure 70. The influence of extracted nitric acid on solvent viscosity is remarkable and is responsible for an increase of 3.77 mPa.s (67.4%). The irradiation follows a similar trend to the density deviation of this solvent with absorbed dose system with a linear trend exhibited for both contacted and uncontacted conditions. Acid pre-contacted samples exhibit a relatively sharp decrease in viscosity with increasing dose, which could be attributed to the degradation of the nitric acid in the organic phase. The uncontacted phase maintains a stable viscosity, within error, across the range of absorbed doses studied.

Pre-contacted samples can be seen to decrease in viscosity with increasing dose. The data obtained suggest a possible linear trend in viscosity with respect to dose, but this will require further investigation as there are some departures from this linear trend. The general decrease in viscosity can be explained by the reduction in nitric acid content in the organic phase, as was seen in our previous work with the attributed viscous effects most likely caused by the formation of amide-acid adducts. Both GANEX-2 ligands in pure form are relatively viscous in comparison to pure DEHiBA, shown in Table 36, due not only to the greater size of TODGA and DMDOHEMA molecules but as they also exhibit larger dipole moments. The formation of smaller degradation products from the degradation of TODGA and DMDOHEMA will most likely have two outcomes. Firstly, the reduction in molecule size promotes a decrease in the viscosity of the solvent. The other outcome is that some of the degradation products are able to form stronger intermolecular interactions, such as hydrogen bonds, relative those observed in the non-degraded solvent due to the formation of amines and carboxylic acid containing degradation products (see Figure 62). These stronger intermolecular interactions will cause an increase in viscosity, which competes against the influence of the reduction of molecule size. It can be seen however that the $[HNO_3]_{org}$ content dominates the viscosity behaviour of the pre-contacted phase. The viscosity increase in the uncontacted samples suggests that the viscosity due to the size of TODGA and DMDOHEMA

does not contribute as much as the formation of stronger bonds between its degradation products as it increases with total dose and extractant degradation.

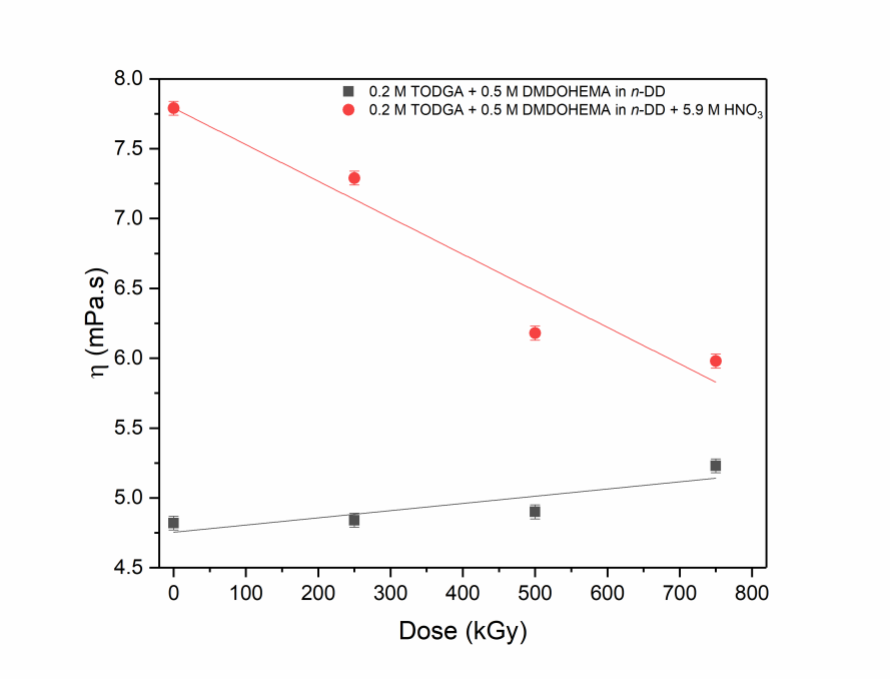

Figure 70. Viscosity of 0.2 M TODGA + 0.5 M DMDOHEMA + n-dodecane against absorbed dose for uncontacted and pre-contacted (4 M HNO_3) phases at 298 K. Linear best fits were applied to the both uncontacted and acid pre-contacted sample series (Regression data provided in Supp. Info.)

8.4.5 Interfacial tension

8.4.5.1 GANEX-1 IFT Studies

Interfacial studies between 1 M DEHiBA in *n*-dodecane at 4 M nitric acid demonstrated a decrease in interfacial tension with total dose for both uncontacted and contacted samples (Figure 71). The interfacial tension was initially lower in the pre-contacted samples due to the effects of nitric acid uptake as previously discussed. There is an intial linear decrease in the IFT with total dose in both uncontacted organic solutions, with a relatively stronger effect seen for acid pre-contacted solvents. This the decreases in the uncontacted samples, indicating further degradation products are no longer interacting with the interfacial phenomena. Increasing length of the hydrocarbon chains on both the nitrogen side and acyl side are known to contribute to larger IFT values in *n*-*n*-dialkyl amides[103] and thus, the breaking of these bonds could be a contributing factor to this observed decrease with total dose. Formation of

amines and degradation products with the hydroxyl group will contribute to the seen decrease in IFT due to the ability to form hydrogen bonds with the aqueous phase. In the absence of acid, DEHiBA in dodecane is reported to form high molecular weight species with long hydrocarbon chains[220] which could also contribute to the arrest in the decline of the IFT with increasing dose for the uncontacted samples.

The decreasing trend of interfacial tension with radiolysis suggests that the IFT values between the organic and aqueous phase will reach a point that will cause process concerns due to the difficulty in separation of the two phases without appropriate solvent regeneration techniques. From the dose range studied it is not possible to say when that point would be reached or whether this potential challenge is effectively mitigated with regeneration techniques.

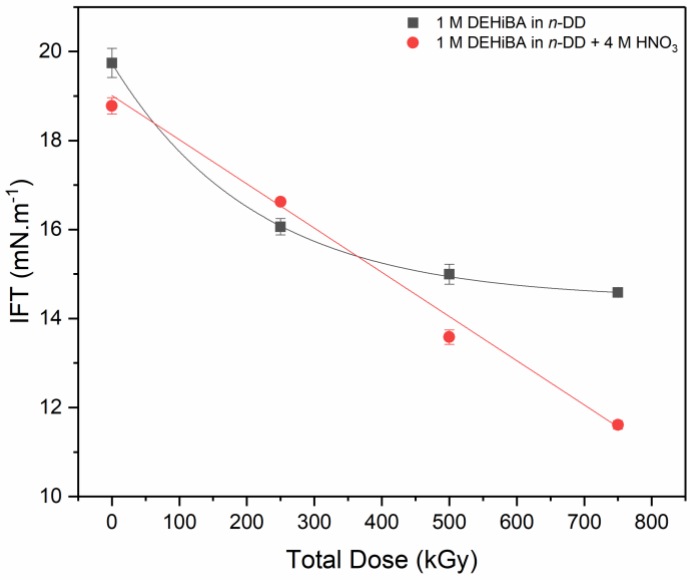

Figure 71. Interfacial tension of 1 M DEHiBA in dodecane vs. total gamma dose. Both uncontacted and acid contacted systems show a decrease with irradiation at 293 K. Linear best fits were applied to the both uncontacted and acid pre-contacted sample series (Regression data provided in Supp. Info.)

8.4.5.2 GANEX-2 IFT Studies

It was not possible to record the IFT value for the unirradiated, pre-contacted sample with confidence due to the disturbance within the organic phase disrupting the imagery technique (given in the

Supplementary Information). This phenomenon is only seen in this system and not in the GANEX-1 cycle and is related to the solvent used and is a result of the initial radiolysis as continued radiolytic degradation clears visibility in the liquid.

The formation of surface-active degradation products with polar functional groups, similar to those discussed with DEHiBA are likely to account for the observed decrease in IFT for the uncontacted samples. This becomes more pronounced with increasing total dose, which is indicative of further degradation and the production of the surface-active compounds. The gradual increase in IFT for pre-contacted samples could be a result of the protective effects of HNO_3 on TODGA, discussed by Galan *et al.* (2012) reducing the formation of its respective surface-active degradation products in addition to the reduction of $[HNO_3]_{org.}$, reducing the polarity of acid-organic species.

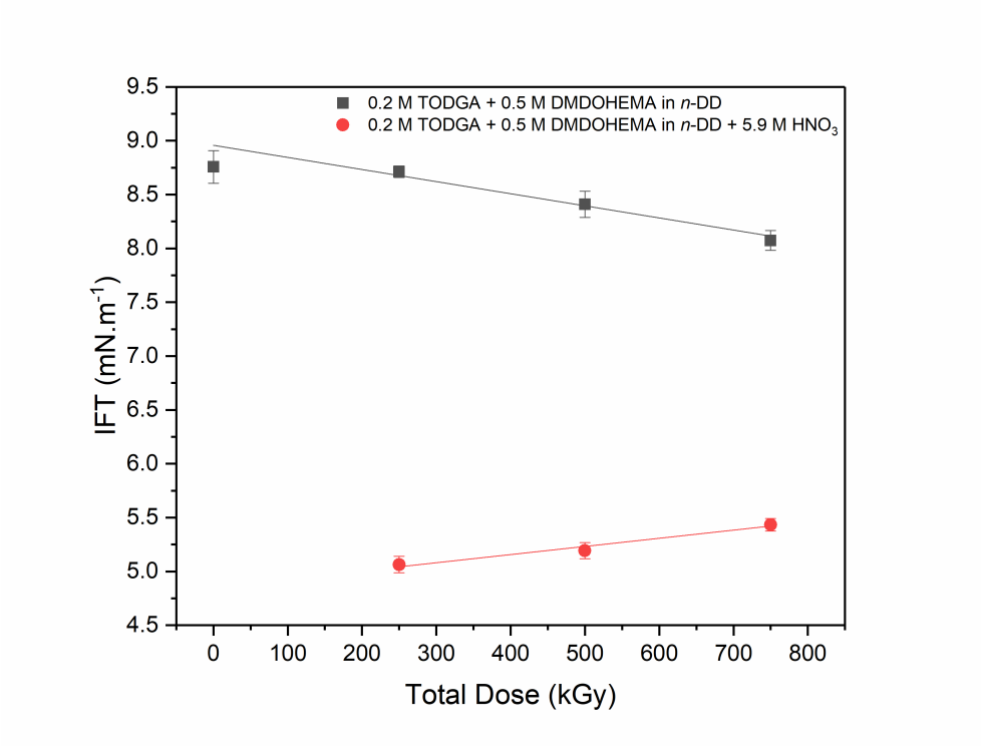

Figure 72. Interfacial tension of 0.2 M TODGA + 0.5 M DMDOHEMA in n-dodecane vs. total gamma dose at 293 K. Linear best fits were applied to the both uncontacted and acid pre-contacted sample series (Regression data provided in Supp. Info.).

8.5 Conclusion

The viscosity and density of both the extractant systems showed little deviation with gamma doses up to 750 kGy that would indicate a concern for industrial extraction operations. IFT studies of the proposed GANEX-1 solvent system indicate that IFT needs to be considered as a limiting factor on their use in recycling of high burn-up fuels due the relatively intense radiation field solvent would be exposed to. In contrast, the IFT of the EURO-GANEX system does not alter significantly to change the hydrodynamic performance of a contacting and separation process it is likely that the degradation can be mitigate with effective management of individual stages.

8.6 Further work

To better understand the role that individual degradation products have on the behaviour of the extractant systems must include identification of each degradation product and a quantitative assessment of these products with respect to total dose, dose rate and dose type. In order to better replicate process conditions, irradiation should be performed on biphasic samples. This could also readily lead to a targeted exploration of solvent regeneration techniques. This would discount the role that any water-soluble degradation products are having on the observed data. Degradation products seen in this work are likely to have less of an impact on organic phase behaviour in a biphasic system due to the likely aqueous solubility of many of these degradation compounds. This is required to establish which degradation products are soluble in the aqueous phase and the resulting impact on the physical behaviour. The evaluation of a solvent regeneration technique is also fundamental to the viability of the extractant systems. The ability to regenerate the physical properties are important for process intensification (reducing the volume of solvent required and subsequent cost) and also for efficient and safe operating conditions.

8.7 Acknowledgements

The University of Manchester's Dalton Cumbrian Facility is acknowledged for providing access to the ^{60}Co irradiator. A studentship for RJB was funded by an EPSRC DTP awarded to the University of

Manchester. Funding for consumables and equipment used in this work was provided by the EPSRC as part of the PACIFIC consortium (EP/L018616/1), and the Department of BEIS Energy Innovation Programme that has supported the National Nuclear Laboratory led Advanced Fuel Cycle Programme.

8.8 Supplementary Information – Chapter 8

Table 38. Physiochemical Properties of GANEX-1 Solvent System at 293 K with calculated total γ-dose

1 M DEHiBA in *n*-dodecane, uncontacted			
Calculated Total Dose/ kGy	ρ / g.cm^{-3}	η / mPa.s	IFT / mN.m^{-1}
0	0.7907 ± 0.0006	3.14 ± 0.04	19.74 ± 0.33
248	0.7908 ± 0.0006	2.90 ± 0.04	16.06 ± 0.18
491	0.7911 ± 0.0006	3.08 ± 0.04	15.00 ± 0.16
756	0.7913 ± 0.0006	3.12 ± 0.04	14.57 ± 0.03
1 M DEHiBA in *n*-dodecane, pre-contacted with 4.0 M HNO_3			
Calculated Total Dose/ kGy	ρ. / g.cm^{-3}	η / mPa.s	IFT / mN.m^{-1}
0	0.8009 ± 0.0006	3.60 ± 0.04	18.78 ± 0.18
247	0.7981 ± 0.0006	3.16 ± 0.04	16.62 ± 0.07
503	0.7970 ± 0.0006	3.32 ± 0.04	13.58 ± 0.16
758	0.7983 ± 0.0006	3.38 ± 0.04	11.61± 0.10

Table 39. Physiochemical Properties of EURO-GANEX Solvent Systems at 293 K with calculated total γ-dose

0.2 M TODGA + 0.5 M DMDOHEMA in *n*-dodecane, uncontacted			
Calculated Total Dose/ kGy	ρ / g.cm^{-3}	η / mPa.s	IFT / mN.m^{-1}
0	0.8158 ± 0.0006	5.59 ± 0.07	8.75 ± 0.15
253	0.8159 ± 0.0006	5.61 ± 0.07	8.71 ± 0.05
490	0.8159 ± 0.0006	5.64± 0.07	8.41 ± 0.12
759	0.8166 ± 0.0006	6.07 ± 0.07	8.07 ± 0.09
0.2 M TODGA + 0.5 M DMDOHEMA in *n*-dodecane, pre-contacted with 5.9 M HNO_3			
Calculated Total Dose/ kGy	ρ / g.cm^{-3}	η / mPa.s	IFT / mN.m^{-1}
0	0.8447 ± 0.0006	9.36 ± 0.07	8.21 ± 0.15
254	0.8360 ± 0.0006	8.80 ± 0.07	5.13 ± 0.07
502	0.8324 ± 0.0006	7.34 ± 0.07	5.24 ± 0.07
761	0.8300 ± 0.0006	7.50 ± 0.07	5.43 ± 0.06

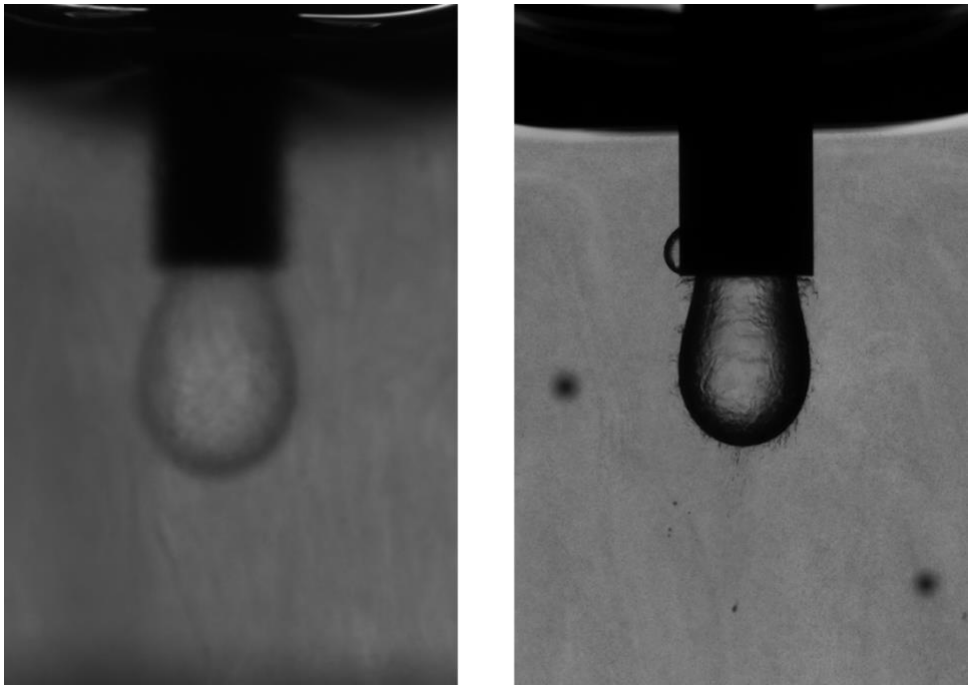

Figure 73. Left - Pendant drop of unirradiated, 0.2 M TODGA + 0.5 M DMDOHEMA pre-contacted with 5.9 M HNO3¬. Right - Pendant drop of 0.2 M TODGA + 0.5 M DMDOHEMA pre-contacted with 5.9 M HNO3¬ exposed to 250 kGy gamma radiation

9. Conclusions and Further Work

9.1 Experimental Overview

1) *Can a simple and robust methodology for physicochemical measurement be developed to give on plant insight into phase transfer behaviour?*

The work presented in this thesis was achieved through the development and implementation of a physicochemical suite at The University of Manchester within an active laboratory with the purpose of evaluating and predicating the behaviour of advanced nuclear recycling liquid-liquid extraction systems. This project firstly evaluated experimental techniques both from literature reviews and technical examination before investigating proposed solvent extraction systems for the purpose of advanced recycling processes. The work established suitable techniques for the measurement of the physical properties of active solutions across a range of operating conditions that would be seen in a recycling process.

The project explored solvent behaviour in potential process-like conditions through uranium and acid loading and finally through radiolytic degradation to understand extractant and process operation thresholds with respect to the relationship of the physical properties, investigating mass transfer and phase separation performance. This project has focussed on the ability to gain an understanding into the process performance, extraction and separation, through the measurement of the fundamental physical properties, density, viscosity and interfacial tension. The work was able to use these properties to give an insight in the behaviour of the extraction process through relating these properties to the basics of mass transfer and its dependence on fluid properties. It was found that measuring these properties alone could not provide enough detail to predict and monitor mass transfer behaviour due to the multiple independent and co-dependent relationships related to specific contactor designs. The work has however been able to provide, through tying to fundamental mass transfer theory, the influence of these properties on the extraction and separation performance within a nuclear setting. This information and predictive expressions derived from the work can form the foundation of uranium extraction in the GANEX-1 cycle and, with small amounts of further work, can give deep insight into the liquid-liquid

physical conditions across an extraction operation. For example, density, in single element uranium extraction work, has been shown to accurately predict the concentration at set acidic conditions. This could be further evaluated to provide measurement techniques to derive distribution coefficients and extraction efficiency can be monitored on-line purely through the liquids' density, however, the addition of other TRUs and possible interference of any undesirable co-extraction would have to be quantified on this ability.

1.1) Can it give insight and determine issues regarding phase transfer in next phase recycling strategies?

The study of TBP and DEHiBA across a variety of extractant concentrations provided an empirical expression for the density and viscosity of the binary mixtures for any molar composition between 278 – 333 K. The analysis of the excess viscosity of mixing provided an insight into the intermolecular behaviour of DEHiBA with its diluent, *n*-dodecane, and the physicochemical limits of the extractant concentration in unloaded conditions. This viscosity of DEHiBA is a crucial parameter in determining its ability for implementation in recycling processes and was shown to be satisfactory at appropriate dilutions (less than 1.4 M). A large data set has been populated that will allow researchers and design engineers access to these values for future use in research and industry tasks. This data can facilitate predictive process intensification studies into the behaviour of both current and proposed solvent systems through the utilisation of the physical properties in fundamental mass transfer and separation relationships in addition to plant design and operation considerations.

Problematic third phase formation was observed in 1 M DEHiBA in *n*-dodecane systems when contacted with 6 M HNO_3 and high uranium concentrations at 293 K. This phase splitting identifies a potential maloperation regime concern. The partitioning of the organic phase produced a heavily loaded, dense and viscous 'heavy' phase with a 'light' organic phase. Mitigations to this are a reduction in the acidity of the spent fuel feed and sustained process temperatures of over 313 K in order to increase the LOC of the organic phase. There is promise in the application of physicochemical measurements to produce online monitoring systems that can alert when a process approaches maloperation regimes.

Such as when the density of the organic phase approaches a threshold value. Uranium extraction studies showed the uranium distribution ratios were influenced by both aqueous nitric acid concentration and temperature. The highest uranium distribution ratios were achieved for acidities between 4 - 6 M HNO_3 depending on other varied parameters.

Both the density and viscosity of 1 M DEHiBA increased with acid and uranium extraction. This emphasised that aqueous acidity must be considered to mitigate the risk of third phase formation whilst providing optimum extraction performance at high metal concentrations.

The exponential increase of the viscosity of the extractant phase, due to the metal-acid-amide complexes formed, will require limitations on the metal concentration allowed in the organic phase to achieve a sufficient dispersion of the organic and facilitate diffusion of the metal within the continuous organic phase if favourable mass transfer conditions are to be maintained, especially when using contactors with short residence times.

Pre-contacting of the two phases showed a trend of increasing the aqueous phase acidity resulting in a decrease in IFT but this was not found to alter the IFT sufficiently to cause concern in process operations. Increasing the temperature also caused a reduction in IFT. Uranium uptake showed an increasing IFT between the organic and aqueous layers for aqueous conditions between 2-4 M nitric acid. For 6 M aqueous nitric acid there was an unexplained initial decrease with uranium uptake before an increase with further uranium loading. Further studies are required to fully understand the observed initial decrease. Overall, minimal deviation in the IFT provides confidence in its predicated use in mixing and separating operations.

The influence of extracted water in the organic phase for all studied solvents was found to have negligible effects on the physicochemical properties of solvents studied in this project

1.2) Can it give insight and determine issues with respect to radiolysis effects in recycling?

The gamma irradiation of both 1 M DEHiBA in *n*-dodecane and 0.2 M TODGA + 0.5 M DMDOHEMA in *n*-dodecane showed differing impacts to the studied physicochemical properties. The studies require further degradation product analysis as initial GC-MS studies have been deemed inconclusive. The

observed phenomena can be explained by comparison of previously reported studies of irradiated solvents. Acid concentration in the organic samples was seen to decrease with increasing total dose, which is explained by the radiolytic degradation of the $[HNO_3]_{org.}$ No certain trend was observed for density deviation with total dose in the uncontacted samples. However, a reduction in density was observed in pre-contacted solutions, attributed to the loss of acid concentration in the organic phase which would not be seen in biphasic process conditions.

Viscosity of the GANEX systems saw a similar trend with total dose for both uncontacted and contacted samples. There was little overall deviation that would cause a concern for prolonged use of the solvent. The viscosity of contacted EURO-GANEX solvents had a negative deviation with dose whilst uncontacted samples increased slightly with dose. Neither of these observations provided a significant change from the measurements obtained for the non-irradiated equivalent solvents.

A decreasing interfacial tension due to the formation of surface-active degradation products however should be noted. All samples GANEX-1 and EURO-GANEX samples exhibit a decreasing IFT trend with total dose. This is more pronounced decrease with acid contacted samples, with the IFT of 1 M DEHiBA in *n*-dodecane with aqueous nitric acid phases falling by up to 40% of its initial value. The deterioration of its interfacial properties without regeneration will lead to separation and phase entrainment issues in the contactor units.

1.3) Can a method be readily identified and deployability determined?

An important objective of this work was to develop the ability to undertake measurements using small volumes, due to the current cost of novel organic extractants, and utilising a relatively simple technique for compatibility with active samples. The work produced a novel review that has contrasted techniques that can be used in both laboratory and industrial environments to record physicochemical data for both process development and operational monitoring for active samples. The studies compared a range of indicators ranging from cost to technical feasibility, with a focus on understanding the measurements applicability to both low-level and high-level radioactive environments. Density and viscosity

measurements were obtained through the procurement of small volume apparatus that allowed for precise measurements between 278 – 333 K. Interfacial tension techniques were developed using a low-cost, high accuracy pendant drop technique with limited temperature control ability. The combination of low sample volume and thermostatic measurement techniques allows for the collective analysis of the extraction performance of a future recycling LLE process and its physicochemical behaviour.

9.2 Further Work and Recommendations

The work performed provides a platform for several avenues of research to develop the understanding the proposed GANEX extraction cycle and other future solvent extraction processes for recycling spent nuclear fuel. Whilst there should be an immediate focus on further work to investigate the radiolysis effects on the physicochemical behaviour of the solvent under biphasic irradiation conditions, a long term priority should be to utilise the techniques and data developed through this project to inform the selection of contactor system/s (e.g. centrifugal contactors, pulsed columns, mixer-settlers) and associated operational parameters by implementing an iterative process to record, develop and document a detailed understanding of the variation in transfer and separation kinetics through the variation of contactor conditions such as agitation power, shear rates and phase ratios.

To gain a greater understanding of the physiochemical behaviour of the GANEX system, future work must involve organic and aqueous phases with closer representations of likely phase compositions with respect to metals present and their compositions, with a requirement to provide a robust understanding that relates mass transfer and separation kinetics to physical behaviour using process equipment. While this work was limited with its focus on uranium, being able to use either Pu(IV) or a surrogate to replicate phase behaviour that is expected in GenIV processes and should be an attainable ambition. As was seen with the studies, the type of metal and its quantity present can have significant effects on extraction behaviour and there is a clear need to be able to accurately predict mass transfer behaviour when processing fissile material. There are also other additives such as masking agents which would all contribute to varied physical properties that have the potential to interfere with the extraction

dynamics of system. To achieve these measurements with Pu and other minor actinides, determinations would need to be performed in a glove-box environment imposing restrictions on equipment space. It is recommended that for glove-box studies the procurement of an Anton Paar density meter with rolling-ball viscometer attachment is necessary to facilitate a compact data acquisition ability. IFT measurements could be obtained with the technique developed in this paper, although further understanding and quantification of the effects of radiation on imagery technology will be required. There must also be consideration of the ambient pressure in a glovebox environment and interference on droplet formation. Further refinement of techniques developed in this project would include the provision of elevated temperature control ability for IFT measurements. A method involving a semi-encasing jacket for the UV cuvettes has since been developed to improve the consistency of the temperature profile of the fluids in addition to achieving up to 333 K.

The literature survey provides confidence that future recycling processes are likely to use counter-current, staged, centrifugal contactor operations and this should be targeted for further studies, but established contactor operations may still be considered. This would allow for a range of process conditions to be studied to aid the understanding of the mass transfer and separation kinetics under predicted operating regimes. It would also allow for threshold and intensification studies to be performed using the data obtained in this paper with the aim developing potential pilot systems and designing extraction processes. The physicochemical expressions developed from the analysis for density and viscosity, allow for accurate predictions of these properties for uranium extraction into the GANEX-1 solvent over a range of acidic conditions. These provide a foundation when integrating focussed studies of contractor systems with their dedicated expressions for fluid behaviour. Combined studies on contactor extraction behaviour and operating regimes are a priority to extend understand and facilitate robust modelling capability. Experimental work should therefore focus on determining operation regimes by investigating the variance of contactor properties like agitation or process conditions such as the organic:aqueous phase ratio. The most effective optimisation work would allow for samples to be taken across the stages in a pilot set up to develop a physiochemical profile across the

process. As the process progresses each stage will have its own unique equilibrium that should be characterised in order to maximise safe and efficient operating parameters. This should involve tailoring contactor operations to the physical properties to maintain favourable mass transfer and separation conditions whilst using a process intensification approach to minimise power and solvent consumption. There should also be a focus on determination of droplet size formation within the dispersion zones. Studies have shown this to be possible[258,259] through differing techniques and this application should be investigated. The information gained from such studies can be used to improve existing prediction models and provide essential knowledge required to quantitate the system changes undergone during process scale-up.

It is also of interest to develop and test on-line monitoring techniques for the measurement of physicochemical properties, as recommended in Section 5, to maintain contactor performance and avoid maloperation conditions. On-line monitoring in nuclear processes generally focusses on quantifying fissile material content (for security and safeguards) and radioactivity levels (for safety and disposal). The integration of physicochemical measurements into process monitoring tools for solvent extraction processes provides an opportunity to significantly enhance safety control systems through the identification of departures from ideal operational conditions which could be more prevalent in the recycle of higher burn-up or alternative fuels in potential future reactor systems. Such monitoring can also assist in process intensification developments.

10. References

1. World Nuclear Association. World Energy Needs and Nuclear Power. (2020).
2. Brook, B. W. *et al.* Why nuclear energy is sustainable and has to be part of the energy mix. *Sustain. Mater. Technol.* **1**, 8–16 (2014).
3. Poinssot, C., Rostaing, C., Greandjean, S. & Boullis, B. Recycling the Actinides, The Cornerstone of Any Sustainable Nuclear Fuel Cycles. *Procedia Chem.* **7**, 349–357 (2012).
4. Miller, S. E. *et al. The Global Nuclear Future Volume 1*. (2009).
5. Orszag, P. R. Costs of reprocessing versus directly disposing of spent nuclear fuel. *Rethink. Nucl. Power United States* 85–98 (2010).

6. Law, E. What is reprocessing? *NDA* (2018).

7. Roitto, M., Nevalainen, P. & Kaarkoski, M. Fuel for commercial politics: the nucleus of early commercial proliferation of atomic energy in three acts. *Bus. Hist.* **0**, 1–44 (2020).

8. World Nuclear Association. Processing of Used Nuclear Fuel. https://world-nuclear.org/information-library/nuclear-fuel-cycle/fuel-recycling/processing-of-used-nuclear-fuel.aspx (2020).

9. Nikitin, M. B., Andrews, A. & Holt, M. Managing the nuclear fuel cycle: Policy implications of expanding global access to nuclear power. *Nucl. React. Hist. Fuel Cycle Manag. Propos.* 63–113 (2013).

10. Fetter, S. How long will the world's uranium supplies last? *Scientific American* (2009).

11. World Nuclear Association. The Nuclear Fuel Cycle. http://www.world-nuclear.org/information-library/nuclear-fuel-cycle/introduction/nuclear-fuel-cycle-overview.aspx (2017).

12. World Nuclear Association. Uranium Mining Overview. https://world-nuclear.org/information-library/nuclear-fuel-cycle/mining-of-uranium/uranium-mining-overview.aspx (2022).

13. World Nuclear Association. Nuclear Power Reactors. (2020).

14. World Nuclear Organisation. Nuclear Power Reactor Characteristics. http://www.world-nuclear.org/uploadedfiles/org/pocketguide/Pocket Guide 2009 Reactors.pdf (2009).

15. Feiveson, H., Mian, Z., Ramana, M. V. & von Hippel, F. Spent Fuel from Nuclear Power Reactors: An Overview of a New Study by the International Panel on Fissile Materials. *Int. Panel Fissile Mater.* 1–21 (2011).

16. Bonin, B. The Scientific Basis of Nuclear Waste Management. *Handb. Nucl. Eng.* 3253–3419 (2010) doi:10.1007/978-0-387-98149-9_28.

17. Lanham, W. B. & Runion, T. . *PUREX process for plutonium and uranium recovery*. (1949).

18. Schulz, W. W. *Science and technology of tributyl phosphate*. (CRC Press, Inc, 1987).

19. Naylor, A. & Eccles, H. Tri-n-butyl phosphate - the universal solvent for the nuclear fuel cycle. *Int. solvent Extr. Conf.* **20**, 31–36 (1988).

20. Schulz, W. W. & Navratil, J. D. Science and technology of tributyl phosphate. Vol. I: Synthesis, properties, reactions and analysis. (1984).

21. Wright, A. & Paviet-Hartmann, P. Review of physical and chemical properties of tributyl phosphate/diluent/nitric acid systems. *Sep. Sci. Technol.* **45**, 1753–1762 (2010).

22. Tian, Q. & Liu, H. Densities and viscosities of binary mixtures of tributyl phosphate with hexane and dodecane from (298.15 to 328.15) K. *J. Chem. Eng. Data* **52**, 892–897 (2007).

23. Tripathi, S. C. & Ramanujam, A. Effect of radiation-induced physicochemical transformations on density and viscosity of 30% TBP - n-dodecane - HNO3 system. *Sep. Sci. Technol.* **38**, 2307–2326 (2003).

24. Nash, K. L. & Nilsson, M. 1 - Introduction to the reprocessing and recycling of spent nuclear fuels A2 - Taylor, Robin BT - Reprocessing and Recycling of Spent Nuclear Fuel. in *Woodhead Publishing Series in Energy* 3–25 (Woodhead Publishing, 2015). doi:http://dx.doi.org/10.1016/B978-1-78242-212-9.00001-0.

25. Simpson, M. F. & Law, J. D. Reprocessing of Nuclear Fuel. in *Nuclear Energy: Selected Entries from the Encyclopedia of Sustainability Science and Technology* (ed. Tsoulfanidis, N.) 153–173 (Springer New York, 2013). doi:10.1007/978-1-4614-5716-9_5.

26. Carrott, M. J., Maher, C. J. & Taylor, R. J. Purex Process Improvements for PU and NP Control in Total Actinide Recycle Flowsheets J.E. (2006).

27. Nuclear Energy Agency. Organisation for Economic Co-operation and Development. NEA Accelerator-driven Systems (ADS) and Fast Reactors (FR) in Advanced Nuclear Fuel Cycles: A Comparative Study. *Book* (2002).

28. Lyseid Authen, T. *et al.* An overview of solvent extraction processes developed in Europe for advanced nuclear fuel recycling, Part 2 — homogeneous recycling. *Sep. Sci. Technol.* **57**, 1724–1744 (2022).

29. Mckibben, J. M. Chemistry of the Purex Process. *Radiochim. Acta* **36**, 3–16 (1984).

30. Natarajan, R. 9 - Reprocessing of spent fast reactor nuclear fuels A2 - Taylor, Robin BT - Reprocessing and Recycling of Spent Nuclear Fuel. in *Woodhead Publishing Series in Energy* 213–243 (Woodhead Publishing, 2015). doi:http://dx.doi.org/10.1016/B978-1-78242-212-9.00009-5.

31. Pleines, M. Viscosity-control and prediction of microemulsions. (Universite de Montpellier, 2018).

32. Plaue, J., Gelis, A. & Czerwinski, K. Plutonium third phase formation in the 30% TBP/nitric acid/hydrogenated polypropylene tetramer system. *Solvent Extr. Ion Exch.* **24**, 271–282 (2006).

33. Lane, E. S. Performance and Degradation of Diluents for TBP and the Cleanup of Degraded Solvents. *Nucl. Sci. Eng.* **17**, 620–625 (1963).

34. Neace, J. C. Diluent Degradation Products in the Purex Solvent. *Sep. Sci. Technol.* **18**, 1581–1594 (1983).

35. Katsumura, Y. *et al.* Pulse radiolysis study of aqueous nitric acid solutions. Formation mechanism, yield, and reactivity of NO3 radical. *J. Phys. Chem.* **95**, 4435–4439 (1991).

36. Ladrielle, T., Wanet, P. & Lemaire, D. Alpha and gamma induced radiolysis of tributyl phosphate. *Radiochemistry* 335–364 (1983).

37. Danesi, P. R. *Solvent extraction principles and practice*. (M. Dekker, 2004).

38. Dreisinger, D. B. & Charles Cooper, W. THE USE OF THE ROTATING DIFFUSION CELL TECHNIQUE FOR THE STUDY OF SOLVENT EXTRACTION KINETICS. *Solvent Extr. Ion Exch.* **4**, 135–147 (1986).

39. Rydberg, J., Cox, M., Musikas, C. & R Choppin, G. *Solvent Extraction Principles and Practice*. (2004). doi:10.1201/9780203021460.

40. Raju, K. S. N. Mass Transfer. in *Fluid Mechanics, Heat Transfer, and Mass Transfer: Chemical Engineering Practice* 455–469 (John Wiley & Sons, Inc., 2011).

41. Heertjes, P. M. & De Nie, L. H. Chapter 5 - Mass Transfer to Drops. in *Recent Advances in Solvent Extration* (ed. Hanson, C.) 367–406 (Elsevier Ltd, 1971). doi:https://doi.org/10.1016/C2013-0-02337-7.

42. Schweitzer, P. *Handbook of separation techniques for chemical engineers / Philip A. Schweitzer editor-in-chief. SERBIULA (sistema Librum 2.0)* (2018).

43. Kislik, V. S. Modern (Classical) Fundamental Principles of Solvent Extraction. in *Solvent Extraction* 3–67 (2012). doi:10.1016/b978-0-444-53778-2.10001-9.

44. Varfolomeev, B. G., Zelenchev, A. V. & Pebalk, V. L. Mass transfer in liquid-liquid systems. *Theor. Found. Chem. Eng.* **36**, 360–364 (2002).

45. Karwa, R. *Heat and mass transfer: Mass transfer. CRC Handbook of Thermal Engineering, Second Edition* (Springer, 2017). doi:10.4324/9781315119717.

46. Aguilar, M. & Cortina, J. L. *Solvent extraction and liquid membranes : fundamentals and applications in new materials*. (New York : CRC ; London : Taylor & Francis distributor, 2008).

47. Irish, E. R. & Reas, W. H. The PUREX Process - A Solvent Extraction Reprocessing Method for Irradiated Uranium. 33 (1957).

48. Hanson, B. 6 - Process engineering and design for spent nuclear fuel reprocessing and recycling plants A2 - Taylor, Robin BT - Reprocessing and Recycling of Spent Nuclear Fuel. in *Woodhead Publishing Series in Energy* 125–151 (Woodhead Publishing, 2015). doi:http://dx.doi.org/10.1016/B978-1-78242-212-9.00006-X.

49. Sinnott, R. & Towler, G. *Design Information and Data*. *Chemical Engineering Design* (2020). doi:10.1016/b978-0-08-102599-4.00008-4.

50. Chang, R. *General Chemistry - Chang 5th Edition*. (2006).

51. Brown, T. L., Eugene LeMay, H. & Bursten, B. E. *Chemistry : The Central Science*. (Pearson/Prentice Hall, 2006).

52. Schweitzer, P. A. *Handbook of separation techniques for chemical engineers*. (McGraw-Hill, 1997).

53. Viswanath, D. S., Ghosh, T. K., Prasad, D. H. L., Dutt, N. V. K. & Rani, K. Y. Theories of Viscosity. in *Viscosity of Liquids: Theory, Estimation, Experiment, and Data* 109–133 (Springer Netherlands, 2007). doi:10.1007/978-1-4020-5482-2_3.

54. Tadros, T. F. *Emulsion Formation and Stability*. *Emulsion Formation and Stability* (Wiley, 2013). doi:10.1002/9783527647941.

55. Abbott, S. Surfactant Science : Principles and Practice. *Surfactant Sci. Princ. Pract.* 1–249 (2015).

56. Karam, H. J. & Bellinger, J. C. Deformation and Breakup of Liquid Droplets in a Simple Shear Field. *I E C Fundam.* 576–581 (1968).

57. Kruss. Interfacial Tension. https://www.kruss-scientific.com/services/education-theory/glossary/interfacial-tension/ (2020).

58. Logsdail, D. H. & Lowes, L. *Industrial Contacting Equipment*. *Recent Advances in Liquid–Liquid Extraction* (Pergamon Press Ltd, 1971). doi:10.1016/b978-0-08-015682-8.50009-2.

59. Kislik, V. S. Engineering Development of Solvent Extraction Processes. in *Solvent Extraction* 157–184 (2012). doi:10.1016/b978-0-444-53778-2.10004-4.

60. Kalem, M., Altunok, M. & Pfennig, A. Sedimentation Behavior of Droplets for the Reactive Extraction of Zinc with D2EHPA. *AIChE J.* **59**, 215–228 (2012).

61. JEFFREYS, G. V. & DAVIES, G. A. Coalescence of Liquid Droplets and Liquid Dispersion. in *Recent Advances in Liquid–Liquid Extraction* 495–584 (Pergamon Press Ltd, 1971). doi:10.1016/b978-0-08-015682-8.50018-3.

62. Lang, S. & Wilke, C. A hydrodynamic mechanism for the coalescence of liquid drops. Theory of coalescence at a planar interface [6]. *Ind. Eng. Chem. Fundam.* **11**, 430 (1972).

63. Kamp, J. & Kraume, M. Influence of drop size and superimposed mass transfer on coalescence in liquid/liquid dispersions - Test cell design for single drop investigations. *Chem. Eng. Res. Des.* **92**, 635–643 (2014).

64. Lo, T. C., H. I Baird, M. & Hanson, C. *Handbook of solvent extraction*. (Wiley, 1983).

65. Van Dijck, W. J. D. Extraction Apparatus.

66. Arm, S. & Phillips, C. 3 - Chemical engineering for advanced aqueous radioactive materials separations. in *Advanced Separation Techniques for Nuclear Fuel Reprocessing and Radioactive Waste Treatment* (eds. Nash, K. L. & Lumetta, G. J.) 58–94 (Woodhead Publishing, 2011). doi:https://doi.org/10.1533/9780857092274.1.58.

67. Phillips, C. Development and design of the Thermal Oxide Reprocessing Plant at Sellafield.

Chem. Eng. Res. Des. **71**, 134–142 (1993).

68. Yadav, R. L. & Patwardhan, A. W. Design aspects of pulsed sieve plate columns. *Chem. Eng. J.* **138**, 389–415 (2008).

69. Yaparpalvi, R., Das, P. K., Mukherjee, A. K. & Kumar, R. R. Yaparpalvi, P. K. Das, A. K. Mukherjee and R. Kumar Department of Chemical Engineering, Indian Institute of Science, Bangalore 560012, India. *Differentiation* **41**, 2547–2553 (1986).

70. Kumar, A. & Hartland, S. Unified correlations for the prediction of drop size in liquid-liquid extraction columns. *Ind. Eng. Chem. Res.* **35**, 2682–2695 (1996).

71. Gayler, R. L. & Pratt, H. R. C. S. *LIQUID-LIQUID EXTRACTION. PART 5. FURTHER STUDIES OF DROPLET BEHAVIOUR IN PACKED COLUMNS*. (1953).

72. Webster, S. Performance of Centrifual Mixer-Settler in the Reprocessing of Nuclear Fuels. in *Chemical Engineering Progress Symposium Series* (1969).

73. Leonard, R. A. Design Principles and Applications of Centrifugal Contactors for Solvent Extraction. in *Ion Exchange and Solvent Extraction* (ed. Moyer, B.) 564–610 (CRC Press, 2012).

74. Leonard, R. A., Pelto, R. H., Ziegler, A. A. & Bernstein, G. J. Flow over circular weirs in a centrifugal field. *Can. J. Chem. Eng.* **58**, 531–534 (1980).

75. Wardle, K. E. Liquid–Liquid Mixing Studies in Annular Centrifugal Contactors Comparing Stationary Mixing Vane Options. *Solvent Extr. Ion Exch.* **33**, 671–690 (2015).

76. Duan, W., Zhao, M., Wang, C. & Cao, S. Recent Advances in the Development and Application of Annular Centrifugal Contactors in the Nuclear Industry. *Solvent Extr. Ion Exch.* **32**, 1–26 (2014).

77. Vandegrift, G., Regalbuto, M. & Aase, S. Designing and demonstration of the UREX+ process using spent nuclear fuel. *Atalante 2004* 1–8 (2004).

78. Brown, J. *et al.* Screening of TODGA/TBP/OK solvent mixtures for the grouped extraction of actinides. *IOP Conf. Ser. Mater. Sci. Eng.* **9**, 012075 (2010).

79. GIF. GIF R&D Outlook for Generation IV Nuclear Energy. *Nucl. Energy* (2010).

80. World Nuclear Association. Generation IV Nuclear Reactors. https://www.world-nuclear.org/information-library/nuclear-fuel-cycle/nuclear-power-reactors/generation-iv-nuclear-reactors.aspx (2019).

81. *GEN IV 2007 Annual Report*. https://www.gen-4.org/gif/jcms/c_43518/2007-annual-report (2007).

82. Birkett, J. E. *et al.* Recent developments in the purex process for nuclear fuel reprocessing: Complexant based stripping for uranium/plutonium separation. *Chimia (Aarau).* **59**, 898–904 (2005).

83. IAEA. Implication of Partioning and Transmutation in Radioactive Waste Management. *Tech. Reports Ser.* STI/DOC/010/435 (2004).

84. IAEA. Implication of Partioning and Transmutation in Radioactive Waste Management. *Tech. Reports Ser.* STI/DOC/010/435 (2004).

85. Nash, K. L. A Comparison of New Reagents and Processes for Hydrometallurgical Processing of Actinides. *Back-End Fuel Cycle From Res. To Solut.* (2001).

86. Madic, C. Overview of the Hydrometallurgical and Pyro-Metallurgical Processes Studied Worldwide for the Partitioning of High Active Nuclear Wastes. *NEA/OECD 6th Inf. Exch. Meet. Actin. Fission Prod. Partitioning Transmutat.* 53–64 (2000).

87. Siddall, T. H. Effects of Structure of N,N-Disubstituted Amides on Their Extraction of Actinide and Zirconium Nitrates and of Nitric Acid'. *J. Phys. Chem.* **64**, 1863–1866 (1960).

88. Drader, J. A. *et al.* Assessment of monoamide extractants and solid supports as new extraction chromatographic materials. *Sep. Purif. Technol.* **163**, 352–356 (2016).

89. Macerata, E. *et al.* Hydrophilic Clicked 2,6-Bis-Triazolyl-pyridines Endowed with High Actinide Selectivity and Radiochemical Stability: Toward a Closed Nuclear Fuel Cycle. *J. Am. Chem. Soc.* **138**, 7232–7235 (2016).

90. Mossini, E. *et al.* Optimization and Single-Stage Centrifugal Contactor Experiments with the Novel Hydrophilic Complexant PyTri-Diol for the i-SANEX Process. *Solvent Extr. Ion Exch.* **36**, 373–386 (2018).

91. Glatz, J.-P., Souček, P. & Malmbeck, R. 3 - Key challenges in advanced reprocessing of spent nuclear fuels A2 - Taylor, Robin BT - Reprocessing and Recycling of Spent Nuclear Fuel. in *Woodhead Publishing Series in Energy* 49–62 (Woodhead Publishing, 2015). doi:http://dx.doi.org/10.1016/B978-1-78242-212-9.00003-4.

92. Bucci, V. P. Process Intensification: Transforming Chemical Engineering. *Macromolecules* 22–34 (2000).

93. Orhan, R. & Dursun, G. Effects of surfactants on hydrodynamics and mass transfer in a co-current downflow contacting column. *Chem. Eng. Res. Des.* **109**, 477–485 (2016).

94. Vasudeva Rao, P. R. & Kolarik, Z. a Review of Third Phase Formation in Extraction of Actinides By Neutral Organophosphorus Extractants. *Solvent Extr. Ion Exch.* **14**, 955–993 (1996).

95. Vidyalakshmi, V., Subramanian, M. S., Rajeswari, S., Srinivasan, T. G. & Vasudeva Rao, P. R. Interfacial tension studies of N,N-dialkyl amides. *Solvent Extr. Ion Exch.* **21**, 399–412 (2003).

96. Mishra, S., Joshi, S., Mallika, C. & Pandey, N. K. Physicochemical properties of PUREX solvent on hydrolytic and chemical treatment. *J. Radioanal. Nucl. Chem.* **314**, 2301–2308 (2017).

97. Kanekar, A. S. *et al.* Hydrodynamic properties for N,N,N,N-tetraalkyl diglycolamides dissolved in n-dodecane system. *Can. J. Chem. Eng.* **90**, 682–689 (2012).

98. Ravi, J., Mishra, S., Pandey, N. K., Mallika, C. & Kamachi Mudali, U. Feasibility studies of using N,N-dihexyloctanamide (DHOA) for fast reactor fuel reprocessing applications. *Radiochim. Acta* **106**, 311–317 (2017).

99. Pal, K. K., Mishra, S., Mallika, C. & Kamachi Mudali, U. Evolution in the physiochemical properties of alternate PUREX solvent on hydrolytic and chemical treatment. *Sep. Sci. Technol.* **52**, 2715–2720 (2017).

100. Mishra, S., Mallika, C., Pandey, N. K., Kamachi Mudali, U. & Natarajan, R. Effect of Radiolysis in Altering the Physiochemical and Metal Retention Properties of Solvent-Diluent-Acid Systems. *Sep. Sci. Technol.* **50**, (2015).

101. Pathak, P. N., Kanekar, A. S., Prabhu, D. R. & Manchanda, V. K. Comparison of hydrometallurgical parameters of N,N-Dialkylamides and of Tri-n-Butylphosphate. *Solvent Extr. Ion Exch.* **27**, 683–694 (2009).

102. Bajoria, S. L., Rathod, V. K., Pandey, N. K., Mudali, U. K. & Natarajan, R. Effect of tri-n-butyl phosphate on physical properties of dodecane-nitric acid system. *J. Radioanal. Nucl. Chem.* **295**, 271–276 (2013).

103. Rajeswari, S., Antony, M. P. & Vasudeva Rao, P. R. Evaluation of hydrodynamic suitability of N,N-didodecyl N′,N′-di-octyl diglycolamide: a potential candidate for minor actinide partitioning. *J. Radioanal. Nucl. Chem.* **306**, 407–415 (2015).

104. Gujar, R. B. *et al.* Radiolytic Stability of N,N,N′,N′-Tetraoctyl Diglycolamide (TODGA) in the Presence of Phase Modifiers Dissolved in n-Dodecane. *Solvent Extr. Ion Exch.* **30**, 278–290 (2012).

105. Baker, A., Fells, A., Hanson, B. C. & Baker, A. Process intensification of element extraction

using centrifugal contactors in the nuclear fuel cycle †. *R. Soc. Chem.* 3964–3999 (2022) doi:10.1039/d2cs00192f.

106. Baron, P. *et al.* A review of separation processes proposed for advanced fuel cycles based on technology readiness level assessments. *Prog. Nucl. Energy* **117**, 103091 (2019).

107. Kumari, I., Kumar, B. V. R. & Khanna, A. A review on UREX processes for nuclear spent fuel reprocessing. *Nucl. Eng. Des.* **358**, 110410 (2020).

108. Regalbuto, M. C. *Alternative separation and extraction: UREX+ processes for actinide and targeted fission product recovery*. *Advanced Separation Techniques for Nuclear Fuel Reprocessing and Radioactive Waste Treatment* (Woodhead Publishing Limited, 2011). doi:10.1533/9780857092274.2.176.

109. Pereira, C. *et al.* LAB-SCALE DEMONSTRATION OF THE UREX+1a PROCESS USING SPENT FUEL. *wm'07 Symp.* 1–10 (2007).

110. Adnet, J. M. *et al.* Development of new hydrometallurgical processes for actinide recovery: {GANEX} concept. *Proc. {GLOBAL}* **I**, 17171 (2005).

111. Modolo, G., Geist, A. & Miguirditchian, M. 10 - Minor actinide separations in the reprocessing of spent nuclear fuels: recent advances in Europe. in *Reprocessing and Recycling of Spent Nuclear Fuel* (ed. Taylor, R. J.) 245–287 (Woodhead Publishing, 2015). doi:http://dx.doi.org/10.1016/B978-1-78242-212-9.00010-1.

112. Miguirditchian, M. *et al.* GANEX: Adaptation of the DIAMEX-SANEX Process for the Group Actinide Separation. *Glob. 2007* **I**, 30207 (2007).

113. Miguirditchian, M., Sorel, C., Cames, B., Bisel, I. & Baron, P. Extraction of uranium(VI) by N,N-di-(2-ethylhexyl)isobutyramide (DEHIBA): from the batch experimental data to the countercurrent process. in *International Solvent Extraction Conference - Solvent Extraction: Fundamentals to Industrial Applications* (2008).

114. Miguirditchian, M. *et al.* Development of the GANEX process for the reprocessing of Gen IV spent nuclear fuels. *Atalante 2008* 4 (2008).

115. Prabhu, D. R., Mahajan, G. R. & Nair, G. M. Di(2-ethyl hexyl) butyramide and di(2-ethyl hexyl)isobutyramide as extractants for uranium(VI) and plutonium(IV). *J. Radioanal. Nucl. Chem.* **224**, 113–117 (1997).

116. Pathak, P. N., Veeraraghavan, R., Prabhu, D. R., Mahajan, G. R. & Manchanda, V. K. Separation Studies of Uranium and Thorium Using Di-2-Ethylhexyl Isobutyramide (D2EHIBA). *Sep. Sci. Technol.* **34**, 2601–2614 (1999).

117. Pathak, P. N., Prabhu, D. R., Ruikar, P. B., Manchanda, V. K. & Division, R. Evaluation of di (2-ethylhexyl) isobutyramide (D2EHIBA) as a process extractant for the recovery of 233-U from irradiated Th. **20**, 293–311 (2002).

118. Pathak, P. N., Prabhu, D. R. & Manchanda, V. K. Distribution Behaviour of U(VI), Th(IV) and Pa(V) from Nitric Acid Medium using Linear and Branched Chain Extractants. *Solvent Extr. Ion Exch.* **18**, 821–840 (2000).

119. Condamines, N. & Musikas, C. *The extraction by n, n-dialk ylamides. II. extraction of actinide cations*. *Solvent Extraction and Ion Exchange* vol. 10 (1992).

120. Gasparini, G. M. & Grossi, G. Application of N,N-Dialkyl Aliphatic Amides in the Separation of some Actinides.pdf. *Sep. Sci. Technol.* **15**, 825–844 (1980).

121. Drader, J. A. *et al.* Radiolytic stability of N , N -dialkyl amide: effect on Pu(iv) complexes in solution. *Dalt. Trans.* **47**, 251–263 (2017).

122. Camès, B., Caniffi, B. & Rudloff, D. Radiolytic and hydrolytic stability of extractant molecules. in *Atalante 2008* 3–4 (2008).

123. Moyer, B., SenGupta, A., Morita, Y. & Tachimori, S. *Ion Exchange and Solvent Extraction*. (CRC Press, 2009).

124. Aneheim, E., Ekberg, C., Foreman, M. R. S., Löfström-Engdahl, E. & Mabile, N. Studies of a solvent for GANEX applications containing CyMe 4-BTBP and DEHBA in cyclohexanone. *Sep. Sci. Technol.* **47**, 663–669 (2012).

125. Pathak, P. N. N,N-Dialkyl amides as extractants for spent fuel reprocessing: An overview. *J. Radioanal. Nucl. Chem.* **300**, 7–15 (2014).

126. Pathak, P. N., Prabhu, D. R., Kanekar, A. S. & Manchanda, V. K. Evaluation of N,N - dialkylamides as promising process extractants . *IOP Conf. Ser. Mater. Sci. Eng.* **9**, 012082 (2010).

127. Malmbeck, R. *et al.* EURO-GANEX , a Process for the Co-separation of TRU. in *Sustainable Nuclear Energy Conference* 9–11 (2014).

128. ITU Hot Cells Facility, 2012.

129. Pleines, M., Hahn, M., Duhamet, J. & Zemb, T. A minimal predictive model for better formulations of solvent phases with low viscosity. *EPJ Nucl. Sci. Technol.* **6**, 3 (2020).

130. Chiarizia, R. *et al.* Third phase formation revisited: The U(VI), HNO3-TBP, n-dodecane system. *Solvent Extr. Ion Exch.* **21**, 1–27 (2003).

131. Brown, J. *et al.* Plutonium Loading of Prospective Grouped Actinide Extraction (GANEX) Solvent Systems based on Diglycolamide Extractants. *Solvent Extr. Ion Exch.* **30**, 127–141 (2012).

132. Brown, J. *et al.* Plutonium Loading of Prospective Grouped Actinide Extraction (GANEX) Solvent Systems based on Diglycolamide Extractants. *Solvent Extr. Ion Exch.* **30**, 127–141 (2012).

133. Berthon, L. *et al.* Diamex process for minor actinide partitioning: Hydrolytic and radiolytic degradations of malonamide extractants. *Sep. Sci. Technol.* **36**, 709–728 (2001).

134. Modolo, G., Asp, H., Schreinemachers, C. & Vijgen, H. Development of a TODGA based process for partitioning of actinides from a PUREX raffinate part I: Batch extraction optimization studies and stability tests. *Solvent Extr. Ion Exch.* **25**, 703–721 (2007).

135. Galán, H. *et al.* Radiolytic Stability of TODGA: Characterization of Degraded Samples under Different Experimental Conditions. *Procedia Chem.* **7**, 195–201 (2012).

136. Camès, B. *et al.* Diamex solvent behavior under continuous degradation and regeneration operations. *ACS Symp. Ser.* **1046**, 255–269 (2010).

137. Poinssot, C., Boullis, B. & Bourg, S. Role of recycling in advanced nuclear fuel cycles. in *Reprocessing and Recycling of Spent Nuclear Fuel* (ed. Taylor, R. J.) 52–53 (Woodhead Publishing, 2015).

138. Taylor, R. *et al.* The EURO-GANEX Process: Current Status of Flowsheet Development and Process Safety Studies. *Procedia Chem.* **21**, 524–529 (2016).

139. IAEA. Recycle and reuse of materials and components from waste streams of nuclear fuel cycle facilities. 56 (2000).

140. Authen, T. L., Tekikachew, B. E., Foreman, M. R. S. J., Wilden, A. & Ekberg, C. A comparison on the use of DEHBA or TBP as extracting agent for tetra- and hexavalent actinides in the CHALMEX Process. *J. Radioanal. Nucl. Chem.* (2022) doi:10.1007/s10967-022-08481-0.

141. Miguirditchian, M. *et al.* HA demonstration in the Atalante facility of the Ganex 1. cycle for the selective extraction of Uranium from HLW. in *GLOBAL 2009 congress - The Nuclear Fuel Cycle: Sustainable Options and Industrial Perspectives* 567 (2009).

142. Wilden, A. *et al.* Laboratory-Scale Counter-Current Centrifugal Contactor Demonstration of an

Innovative-SANEX Process Using a Water Soluble BTP. *Solvent Extr. Ion Exch.* **33**, 91–108 (2015).

143. Magnusson, D., Geist, A., Malmbeck, R., Modolo, G. & Wilden, A. Flow-Sheet Design for an Innovative SANEX Process Using TODGA and SO3-Ph-BTP. *Procedia Chem.* **7**, 245–250 (2012).

144. Malmbeck, R. *et al.* Partitioning of minor actinides from HLLW using the DIAMEX process. Part 2 – "Hot" continuous counter-current experiment. *Radiochim. Acta* **88**, 865 (2000).

145. Sorel, C. *et al.* Demonstration of a SANEX Process in Centrifugal Contactors using the CyMe 4 -BTBP Molecule on a Genuine Fuel Solution . *Solvent Extr. Ion Exch.* **27**, 97–106 (2009).

146. Wilden, A., Sypula, M., Modolo, G., Geist, A. & Magnusson, D. The Recovery of An(Iii) in an Innovative-Sanex Process using a Todga-based Solvent and Selective Stripping with a Hydrophilic BTP. *Procedia Chem.* **7**, 418–424 (2012).

147. Modolo, G. *et al. Development and demonstration of a new SANEX process for actinide(III)/lanthanide(III) separation using a mixture of CyMe4BTBP and TODGA as a selective extractant*. (Organisation for Economic Co-Operation and Development - Nuclear Energy Agency, 2010).

148. Romanovskiy, V. N., Smirnov, I. V, Babain, V. A. & Shadrin, A. Y. 9 - Combined processes for high level radioactive waste separations: {UNEX} and other extraction processes. in *Advanced Separation Techniques for Nuclear Fuel Reprocessing and Radioactive Waste Treatment* (eds. Nash, K. L. & Lumetta, G. J.) 229–265 (Woodhead Publishing, 2011). doi:https://doi.org/10.1533/9780857092274.2.229.

149. Endress+Hauser. Flow measuring technology For liquids, gases and steam Products and services at a glance. 1–63 (2018).

150. Bollesteros, M.-J. *et al.* Implementation of Americium Separation from a PUREX Raffinate. *Procedia Chem.* **7**, 178–183 (2012).

151. Bernier, G. *et al.* Hot Test in Mixer Settlers of Alpha Barrier with AHA in PUREX Process. *Procedia Chem.* **7**, 160–165 (2012).

152. Nancekievill, M. J. The Radiation Tolerance and Development of Robotic Platforms for Nuclear Decommissioning. 256 (2018).

153. Makowski, D. The Impact of Radiation on Electronic Devices with the Special Consideration of Neutron and Gamma Radiation Monitoring. *Tech. Univ. Lodz* 151 (2006).

154. Hua, F., Mon, K., Pasupathi, P., Gordon, G. & Shoesmith, D. A Review of Corrosion of Titanium Grade 7 and Other Titanium Alloys in Nuclear Waste Repository Environments. *Corrosion* **61**, 987–1003 (2005).

155. Canada, M. Specialized test procedure — Procedure for density determination. (2017).

156. Lee, J., Rowan, R., Susano, C. & Menis, O. *THE DENSITY OF URANYL SULFATE SOLUTIONS AND THE DETERMINATION OF URANIUM CONCENTRATION BY DENSITY MEASUREMENTS*. (1946).

157. Hedge, W. *LOCAL ATOMIC DISPLACEMENTS IN HIGH Tc OXIDES STUDIED BY PULSED NEUTRON SCATTERING*. (1989).

158. Kapustinsky, A. F. & Lipilina, I. I. The densities of aqueous uranyl nitrate solutions, and the apparent molar volumes of uranyl nitrate. *Bull. Acad. Sci. USSR Div. Chem. Sci.* **5**, 661–668 (1956).

159. Anton Paar. U-tube technology in digital laboratory density meters. (2021).

160. Saxena, M. C., Dubey, P. & Tripathi, A. Surface tension of binary liquid mixture. *Asian J. Chem.* **23**, 1411–1412 (2011).

161. Ouerfelli, N., Barhoumi, Z. & Iulian, O. Viscosity Arrhenius activation energy and derived partial molar properties in 1,4-dioxane + water binary mixtures from 293.15 to 323.15 K. *J. Solution Chem.* **41**, 458–474 (2012).

162. Azizian, S. & Bashavard, N. Surface tension of dilute solutions of alkanes in cyclohexanol at different temperatures (Journal of Chemical and Engineering Data (2008) 53 (2422-2425)). *J. Chem. Eng. Data* **53**, 2919 (2008).

163. Chen, Y. *et al.* Volumetric properties of binary mixtures of ionic liquid with tributyl phosphate and dimethyl carbonate. *J. Chem. Thermodyn.* **123**, 165–173 (2018).

164. Gunde, R., Kumar, A., Lehnert-Batar, S., Mäder, R. & Windhab, E. J. Measurement of the surface and interfacial tension from maximum volume of a pendant drop. *J. Colloid Interface Sci.* **244**, 113–122 (2001).

165. De Lorenzi, L., Fermeglia, M. & Torriano, G. Density, Refractive Index, and Kinematic Viscosity of Diesters and Triesters. *J. Chem. Eng. Data* **42**, 919–923 (1997).

166. Cases, A. M., Gómez Marigliano, A. C., Bonatti, C. M. & Sólimo, H. N. Density, viscosity, and refractive index of formamide, three carboxylic acids, and formamide + carboxylic acid binary mixtures. *J. Chem. Eng. Data* **46**, 712–715 (2001).

167. Marczak, W., Adamczyk, N. & Łężniak, M. Viscosity of associated mixtures approximated by the Grunberg-Nissan model. *Int. J. Thermophys.* **33**, 680–691 (2012).

168. Qadeer, R. Concentration and temperature dependence of viscosity of uranium solutions in H2O and 3 mol/L HNO3. *J. Zhejiang Univ. Sci.* **5**, 457–461 (2004).

169. Paquet, A., Diat, O., Berthon, L. & Guilbaud, P. Aggregation in organic phases after solvent extraction of uranyl nitrate: X-ray scattering and molecular dynamic simulations. *J. Mol. Liq.* (2019) doi:10.1016/j.molliq.2018.12.051.

170. Kumar, S. *et al.* Extraction of uranium from simulated highly active feed in a micromixer-settler with 30% TBP and 36% TiAP solvents. *J. Radioanal. Nucl. Chem.* **311**, 2111–2116 (2017).

171. Rodrigues, F., Boubals, N., Charbonnel, M.-C. & Morel-Desrosiers, N. Thermodynamic Approach of Uranium(VI) Extraction by N,N-(2–ethylhexyl)Isobutyramide. *Procedia Chem.* **7**, 59–65 (2012).

172. Applications, C. *et al.* & Low Sensors Are Used in Many Monitoring and Control Applications To Measure Both Ment Is a Useful Substitute That Is Generally Easier To Perform 4Here Are Numerous Reliable Technologies and Sensor Types Used for This Purpose 3Ome Technologies Have Been . doi:10.1016/B978-0-7506-7729-5.50050-1.

173. Gul, S., Shiriyev, J., Singhal, V., Erge, O. & Temizel, C. *Advanced materials and sensors in well logging, drilling, and completion operations*. *Sustainable Materials for Oil and Gas Applications: Volume 1 in Advanced Materials and Sensors for the Oil and Gas Industry* (INC, 2021). doi:10.1016/B978-0-12-824380-0.00004-9.

174. Kono, Y. Viscosity measurement. *Magmas Under Press. Adv. High-Pressure Exp. Struct. Prop. Melts* 261–280 (2018) doi:10.1016/B978-0-12-811301-1.00010-1.

175. RheoSense. VROC® TECHNOLOGY. https://www.rheosense.com/technology?hsLang=en.

176. Jantzen, C., Bibler, N., Beam, D., Crawford, C. & Pickett, M. *CHARACTERIZATION OF THE DEFENSE WASTE PROCESSING FACILITY (DWPF) ENVIRONMENTAL ASSESSMENT (EA) GLASS STANDARD REFERENCE MATERIAL (U)*. (1993).

177. Mukepoi, J. & Sanyal, A. S. Vitreous Matrices for the containment of High-Level PUREX waste. *Ann. Nucl. Energy.* **3**, 253–274 (1976).

178. Kondo, Y. & Kubota, M. Formation and filtration characteristics of solids generated in a High Level Liquid Waste treatment process: I. Solids formation behavior from simulated High Level Liquid Waste. *J. Radioanal. Nucl. Chem.* **221**, 45–52 (1997).

179. Rodrigues, F. *et al.* New insights into the extraction of uranium(VI) by an N,N-dialkylamide. *Mol. Phys.* **112**, 1362–1374 (2014).

180. Brambilla, L. *et al.* Physico chemical properties of irradiated i-SANEX diluents. *Nukleonika* **60**, 893–898 (2016).

181. Izumo, N. & Koiwai, A. Technological Background and Latest Market Requirements concerning " Static Viscosity " Measurement with a Tuning-fork Vibration Viscometer. *Proc. Asia-Pacific Symp. Meas. Mass, Force Torque* 51–57 (2009).

182. Brunner, D. *An applied investigation of viscosity – density fluid sensors based on torsional resonators*. (2020).

183. Cole-Parmer. Tuning Fork Vibration Viscometer. https://www.coleparmer.co.uk/p/tuning-fork-vibration-viscometer-43751/43751.

184. Carmack, J. Viscosity Measurement Technique for Metal Fuels.

185. Berger, C. *et al.* Extraction of Uranium(VI) and Plutonium(IV) by New Tri Alkylcarbamides. *Solvent Extr. Ion Exch.* **40**, 290–311 (2021).

186. Drelich, J. Measurement of Interfacial Tension in Fluid-Fluid Systems. 3152–3166 (2002).

187. Erbil, H. Y. *Surface Chemistry: Of Solid and Liquid Interfaces*. *Surface Chemistry: Of Solid and Liquid Interfaces* (2009). doi:10.1002/9781444305401.

188. Brahmmananda Rao, C. V. S., Srinivasan, T. G. & Vasudeva Rao, P. R. Studies on the Extraction of Actinides by Substituted Butyl Phosphonates. *Solvent Extr. Ion Exch.* **30**, 262–277 (2012).

189. McDowell, W. J. & Coleman, C. F. Interface mechanism for uranium extraction by amine sulphate. *J. Inorg. Nucl. Chem.* **29**, 1325–1343 (1967).

190. Shojaeian, A. Surface tension measurements of aqueous 1-alkyle-3-methylimidazolume tetrafluoroborate {[C n mim][BF 4] (n = 2, 4, 6)} solutions and modeling surface tension of ionic liquid binary mixtures using six various models. *Thermochim. Acta* **673**, 119–128 (2019).

191. Bąk, A. & Podgórska, W. Interfacial and surface tensions of toluene/water and air/water systems with nonionic surfactants Tween 20 and Tween 80. *Colloids Surfaces A Physicochem. Eng. Asp.* **504**, 414–425 (2016).

192. Li, Z. *et al.* Surface tension of binary mixtures of (ionic liquid + tributyl phosphate). *J. Chem. Thermodyn.* **132**, 214–221 (2019).

193. Halleröd, J., Ekberg, C., Kajan, I. & Aneheim, E. Solubility Thermodynamics of CyMe 4 -BTBP in Various Diluents Mixed with TBP. *J. Solution Chem.* **47**, 1021–1036 (2018).

194. Martin-Gassin, G. *et al.* Second harmonic generation monitoring of nitric acid extraction by a monoamide at the water-dodecane interface. *Phys. Chem. Chem. Phys.* **13**, 19580–19586 (2011).

195. Prochaska, K. Interfacial activity of metal ion extractant. *Adv. Colloid Interface Sci.* **95**, 51–72 (2002).

196. Wongsawa, T. *et al.* The experimental investigations on viscosity, surface tension, interfacial tension and solubility of the binary and ternary systems for tributyl phosphate (TBP) extractant in various organic solvents with water: Thermodynamic NRTL model and molecular inte. *J. Mol. Liq.* **251**, 229–237 (2018).

197. Nave, S., Modolo, G., Madic, C. & Testard, F. Aggregation properties of N,N,N1,N1 -Tetraoctyl-3-oxapentanediamide (TODGA) in n-dodecane. *Solvent Extr. Ion Exch.* **22**, 527–551 (2004).

198. Martin-Gassin, G. *et al.* Nitric acid extraction with monoamide and diamide monitored by second harmonic generation at the water/dodecane interface. *Colloids Surfaces A Physicochem. Eng. Asp.* **413**, 130–135 (2012).

199. Kay, T. *Changes in Interfacial Tension with Time in Two-Liquid-Phase Systems Issued :* (2018).

200. Zeppieri, S., Rodríguez, J. & López De Ramos, A. L. Interfacial tension of alkane + water systems. *J. Chem. Eng. Data* **46**, 1086–1088 (2001).

201. Goebel, A. & Lunkenheimer, K. Interfacial tension of the water/n-alkane interface. *Langmuir* **13**, 369–372 (1997).

202. Demond, A. H. & Lindner, A. S. Estimation of Interfacial Tension between Organic Liquids and Water. *Environ. Sci. Technol.* **27**, 2318–2331 (1993).

203. Daerr, A. & Mogne, A. Pendent_Drop: An ImageJ Plugin to Measure the Surface Tension from an Image of a Pendent Drop. *J. Open Res. Softw.* **4**, 2–6 (2016).

204. Jennings, J. W. & Pallas, N. R. An Efficient Method for the Determination of Interfacial Tensions from Drop Profiles. *Langmuir* **4**, 959–967 (1988).

205. Kayser, W. V. Temperature dependence of the surface tension of water in contact with its saturated vapor. *J. Colloid Interface Sci.* **56**, 622–627 (1976).

206. Nikitas, P. & Pappa-Louisi, A. Thermodynamic and modelistic study of surface solutions: Aqueous solutions containing 2-butanol. *J. Phys. Chem.* **94**, 361–370 (1990).

207. Ramanujam, A. Purex and Thorex Processes (Aqueous Reprocessing). *Encycl. Mater. Sci. Technol.* 7918–7924 (2001) doi:10.1016/b0-08-043152-6/01426-1.

208. OECD/NEA. Technology Roadmap Update for Generation IV Nuclear Energy Systems: Preparing Today for Tomorrow's Energy Needs. 7 (2014).

209. Mathur, J. N., Murali, M. S. & Nash, K. L. Actinide partitioning-A review. *Solvent Extr. Ion Exch.* **19**, 357–390 (2001).

210. Musikas, C. Solvent extraction for the chemical separations of the 5f elements. *Inorganica Chim. Acta* **140**, 197–206 (1987).

211. Pathak, P. N., Veeraraghavan, R., Ruikar, P. B. & Manchanda, V. K. Solvent Extraction Studies on Th(IV), Pa(V), and U(VI) from Nitric Acid Medium using D2EHiBA. *Radiochim. Acta* **86**, 129–134 (1999).

212. Musikas, C. Potentiality of Nonorganophosphorus Extractant in Chemical Separations of Actinides. *Sep. Sci. Technol.* **23**, 1211–1226 (1988).

213. Pathak, P. N., Kanekar, A. S., Prabhu, D. R. & Manchanda, V. K. Comparison of Hydrometallurgical Parameters of *N,N* -Dialkylamides and of Tri- *n* -Butylphosphate. *Solvent Extr. Ion Exch.* **27**, 683–694 (2009).

214. Aminabhavi, T. M. & Patil, V. B. Density, refractive index, viscosity, and speed of sound in binary mixtures of ethenylbenzene with hexane, heptane, octane, nonane, decane, and dodecane. *J. Chem. Eng. Data* **42**, 641–646 (1997).

215. De Guzman, J. Relation between fluidity and heat of fusion. *An. Soc. Espan. Fis. Y. Quim* **11**, 353–362 (1913).

216. Mehrotra, A. K., Monnery, W. D. & Svrcek, W. Y. A review of practical calculation methods for the viscosity of liquid hydrocarbons and their mixtures. *Fluid Phase Equilib.* **117**, 344–355 (1996).

217. Fort, R. J. & Moore, W. R. Viscosities of binary liquid mixtures. *Trans. Faraday Soc.* **62**, 1112–1119 (1966).

218. Kauzman, W. & Eyring, H. The Viscous Flow of Large Molecules. *J. Am. Chem. Soc.* **62**, 3113–3125 (1940).

219. Condamines, N. & Musikas, C. The Extraction By N, N-Dialkylamides.I. HNO3 and Other Inorganic Acids. *Solvent Extr. Ion Exch.* **6**, 1007–1034 (1988).

220. Drader, J. *et al.* Radiation chemistry of the branched-chain monoamide di-2-ethylhexyl-isobutyramide. *Solvent Extr. Ion Exch.* **35**, 480–495 (2017).

221. McCann, K., Mincher, B. J., Schmitt, N. C. & Braley, J. C. Hexavalent Actinide Extraction Using N,N-Dialkyl Amides. *Ind. Eng. Chem. Res.* **56**, (2017).

222. Pathak, P. N. *et al.* Distribution behavior of U (VI), Th (IV), and fission products with di (2-ethylhexyl) isobutyramide under process conditions. *Ind. Eng. Chem. Res.* **43**, 4369–4375 (2004).

223. Suzuki, S., Sasaki, Y., Yaita, T. & Kimura, T. Study on Selective Separation of Uranium by N,N-dialkylamide in ARTIST Process. *Proc. ATALANTA 2004* P1-63 (2004).

224. Miguirditchian, M., Sorel, C., Camès, B., Bisel, I. & Baron, P. HA demonstration in the Atalante facility of the Ganex 1 st cycle for the selective extraction of Uranium from HLW. *Structure* 1032–1035 (2009).

225. Kishbaugh, A. A. Development and Performance of Centrifugal Mixer-Settlers in the Reprocessing of Nuclear Fuel. 139–144 (2000).

226. Kishbaugh, A. A. *Performance of a Multi-Stage Centrifugal Contactor*. (1964).

227. Ban, Y., Hotoku, S. & Morita, Y. Application of N,N -di(2-ethylhexyl)butanamide for mutual separation of U(VI) and Pu(IV) by continuous counter-current extraction with mixer-settler extractors. *J. Nucl. Sci. Technol.* **49**, 588–594 (2012).

228. Condamines, N., Turq, P. & Musikas, C. The extraction by n, n-dialkylamides III, a thermodynamical approach of the multicomponent extraction organic media by a statistical mechanic theory. *Solvent Extr. Ion Exch.* **11**, 187–221 (1993).

229. Pathak, P. N., Kumbhare, L. B. & Manchanda, V. K. Structural effects in n n-dialkyl amides on their extraction behavior toward uranium and thorium. *Solvent Extr. Ion Exch.* **19**, 105–126 (2001).

230. Ferru, G. *et al.* Influence of Extracted Solute on the Organization of a Monoamide Organic Solution. *Procedia Chem.* **7**, 27–32 (2012).

231. Jha, R. K. *et al.* Third phase formation studies in the extraction of Th(IV) and U(VI) by N,N-dialkyl aliphatic amides. *Desalination* (2008) doi:10.1016/j.desal.2007.11.054.

232. Gupta, K. K. *et al.* Third Phase Formation in the Extraction of Uranyl Nitrate By N,N-Dialkyl Aliphatic Amides. *Solvent Extr. Ion Exch.* **18**, 421–439 (2000).

233. McCann, K., Drader, J. A. & Braley, J. C. Comparing Branched versus Straight-chained Monoamide Extractants for Actinide Recovery. *Sep. Purif. Rev.* **47**, 49–65 (2018).

234. Ruckenstein, E. & Nagarajan, R. Aggregation of Amphiphiles in Nonaqueous Media. *J. Phys. Chem.* **84**, 1349–1358 (1980).

235. Selker, A. H. & Sleicher, C. A. Factors affecting which phase will disperse when immiscible liquids are stirred together. *Can. J. Chem. Eng.* **43**, 298–301 (1965).

236. Joseph Donahue, D. & Bartell, F. E. The boundary tension at water-organic liquid interfaces. *J. Phys. Chem.* **56**, 480–484 (1952).

237. Stamatoudis, M. & Tavlarides, L. Effect of Continuous-Phase Viscosity on the Drop Sizes of Liquid-Liquid Dispersions in Agitated Vessels. *Ind. Eng. Chem. Process Des. Dev.* **24**, 1175–1181 (1985).

238. Mechanisms, T. & Drainage, F. Film Shapes for Deformable Drops at Liquid-Liquid Interfaces. *J. Colloid Interface Sci.* **42**, 15–34 (1973).

239. Charles, G. E. & Mason, S. G. The coalescence of liquid drops with flat liquid/liquid interfaces. *J. Colloid Sci.* **15**, 236–267 (1960).

240. Stone, H. A. Dynamics of drop deformation and breakup in viscous fluids. *Annu. Rev. Fluid Mech.* **26**, 65–102 (1994).

241. Desnoyer, C., Masbernat, O. & Gourdon, C. Experimental study of drop size distributions at high phase ratio in liquid-liquid dispersions. *Chem. Eng. Sci.* **58**, 1353–1363 (2003).

242. Hinze, J. O. Fundamentals of the hydrodynamic mechanism of splitting in dispersion processes. *AIChE J.* **1**, 289–295 (1955).

243. Tachimori, S. & Morita, Y. Overview of Solvent Extraction Chemistry and Reprocessing. in *Ion Exchange and Solvent Extraction* (eds. Moyer, B. A. & SenGupta, A.) (CRC Press, 2010).

244. Information, S. & Meeting, E. *Actinide and Fission Product Partitioning 14-16 October 2002 ORGANISATION FOR ECONOMIC CO-OPERATION AND DEVELOPMENT*. *Group* (2003).

245. Baron, P., Masson, M., Rostaing, C. & Boullis, B. Advanced Separation Processes for Sustainable Nuclear Systems. in (2007).

246. Ansari, S. A., Pathak, P., Mohapatra, P. K. & Manchanda, V. K. Chemistry of diglycolamides: Promising extractants for actinide partitioning. *Chem. Rev.* **112**, 1751–1772 (2012).

247. Bell, K. *et al.* Progress Towards the Development of a New GANEX Process. *Procedia Chem.* **7**, 392–397 (2012).

248. Geist, A. *et al.* Actinide(III)/Lanthanide(III) Separation Via Selective Aqueous Complexation of Actinides(III) using a Hydrophilic 2,6-Bis(1,2,4-Triazin-3-Yl)-Pyridine in Nitric Acid. *Solvent Extr. Ion Exch.* **30**, 433–444 (2012).

249. Carrott, M. *et al.* Distribution of plutonium, americium and interfering fission products between nitric acid and a mixed organic phase of TODGA and DMDOHEMA in kerosene, and implications for the design of the 'eURO-GANEX' process. *Hydrometallurgy* **152**, 139–148 (2015).

250. Carrott, M. *et al.* Development of a New Flowsheet for Co-Separating the Transuranic Actinides: The 'EURO-GANEX' Process. *Solvent Extr. Ion Exch.* **32**, 447–467 (2014).

251. Berthon, L. & Chabronnel, M. C. Radiolysis of Solvents Used in Nuclear Fuel Reprocessing In Ion Exchange and Solvent Extraction, A Series of Advances; Moyer, BA, Ed. (2010).

252. Pathak, P. N., Prabhu, D. R., Kanekar, A. S. & Manchanda, V. K. In Actinides 2009. in *In IOP Conference SeriesMaterials Science and Engineering* (eds. Rao, L., Taylor, R. J. & Shuh, D. K.) (2010).

253. Mincher, B. J., Modolo, G. & Mezyk, S. P. Review article: The effects of radiation chemistry on solvent extraction: 1. Conditions in acidic solution and a review of TBP radiolysis. *Solvent Extr. Ion Exch.* **27**, 1–25 (2009).

254. Sugo, B. Y. *et al.* Studies on hydrolysis and radiolysis of N,N,N′,N′-tetraoctyl-3-oxapentane-1,5-diamide. *Radiochim. Acta* **90**, 161–165 (2002).

255. Sánchez-García, I., Galán, H., Perlado, J. M. & Cobos, J. Stability studies of GANEX system under different irradiation conditions. *EPJ Nucl. Sci. Technol.* **5**, 19 (2019).

256. Berthon, L. & Cames, B. *Procédé DIAMEX : dégradatioi Textractant diamid*. (1999).

257. Jiang, P. Y., Nagaishi, R., Yotsuyanagi, T., Katsumura, Y. & Ishigure, K. γ-Radiolysis study of concentrated nitric acid solutions. *J. Chem. Soc. Faraday Trans.* **90**, 93–95 (1994).

258. Hern, T. O. Determination of Drop Size Distribution in a Centrifugal Contactor. (2011).

259. Tamhane, T. V., Joshi, J. B., Mudali, K., Natarajan, R. & Patil, R. N. Measurement of drop size characteristics in annular centrifugal extractors using phase Doppler particle analyzer (PDPA). *Chem. Eng. Res. Des.* **90**, 985–997 (2012).

Annexes

Annex A – Chapter 6 Regression Data

Table 40. Regression analysis data for Figure. 25

Density vs Temperature

Molar fraction TBP in *n*-dodecane	1.00	0.72	0.46	0.21	0.00
Intercept	0.99398	0.93355	0.87682	0.81834	0.76368
Slope	-8.57E-04	-8.27E-04	-8.05E-04	-7.68E-04	-7.27E-04
Pearson's r	-1	-0.99998	-0.99999	-0.99998	-0.99999
Adj. R-Square	0.99999	0.99995	0.99997	0.99996	0.99996

Table 41. Regression analysis data for Figure. 26

Density vs Temperature

y = ax + b							
Molar fraction DEHiBA in *n*-dodecane	1.00	0.78	0.66	0.50	0.38	0.18	0.00
Intercept	0.87912	0.86212	0.84979	0.83398	0.82058	0.7918	0.76367
Slope	-6.97E-04	-7.00E-04	-7.04E-04	-7.11E-04	-7.14E-04	-7.22E-04	-7.27E-04
Pearson's r	-1	-0.99999	-0.99999	-0.99999	-0.99998	-0.99998	-0.99999
Adj. R-Square	1	0.99998	0.99998	0.99999	0.99994	0.99996	0.99996

Table 42. Regression analysis data for Figure. 27 - 28

Density Prediction Fitting - a values

y = A + B*x + C*x^2	
A	0.7639 ± 4.17251E-4
B	0.16679 ± 0.00245
C	-0.05333 ± 0.00302
Reduced Chi-Sqr	2.05E-07
R-Square(COD)	0.99991
Adj. R-Square	0.99985

Density Prediction Fitting - b values

y = A + B*x + C*x^2 + D*x^3	
A	-7.27144E-4 ± 7.20002E-7
B	2.3749E-5 ± 6.96023E-6
C	3.77351E-5 ± 1.70892E-5
D	-3.12641E-5 ± 1.1113E-5
Reduced Chi-Sqr	5.55E-13
R-Square(COD)	0.99778
Adj. R-Square	0.99556

Table 43. Regression analysis data for Figure. 31

Viscosity vs Temperature

y = A1*exp(-x/t1) + y0						
Molar fraction DEHiBA in *n*-dodecane	1.00	0.78	0.66	0.50	0.38	0.18
y0	4.27707 ± 0.21635	2.9315 ± 0.33504	2.11977 ± 0.14875	1.66948 ± 0.08808	1.11304 ± 0.0647	0.75356 ± 0.04663
A1	3.70667E10 ± 2.6996E10	6.91834E8 ± 5.32092E8	6.75839E7 ± 2.53224E7	1.04922E7 ± 4.23453E6	515333.25417 ± 190937.05625	29584.03972 ± 8819.06223
t1	14.08351 ± 0.48686	16.49182 ± 0.73833	18.33825 ± 0.45543	20.31956 ± 0.5849	24.37201 ± 0.79205	29.77512 ± 0.99197
Reduced Chi-Sqr	63.05705	41.68899	8.36012	3.76706	1.92082	1.10974
R-Square(COD)	0.9994	0.99846	0.99971	0.99964	0.99959	0.99976
Adj. R-Square	0.9988	0.99692	0.99942	0.99928	0.99918	0.99951

Table 44. Regression analysis data for Figure. 32

Viscosity vs Temperature

y = A1*exp(-x/t1) + y0				
Molar fraction TBP in *n*-dodecane	1.00	0.72	0.46	0.21
y0	1.10915 ± 0.06081	0.80756 ± 0.05876	0.71992 ± 0.04894	0.57177 ± 0.03678
A1	73968.00076 ± 19340.75727	20049.25452 ± 6609.61058	14521.42284 ± 4947.49244	4647.59614 ± 1339.33979
t1	28.81905 ± 0.81685	32.05967 ± 1.25851	32.07664 ± 1.32037	35.7055 ± 1.38833
Reduced Chi-Sqr	1.15281	0.26247	0.2312	0.17308
R-Square(COD)	0.99996	0.99973	0.9998	0.9998
Adj. R-Square	0.99993	0.99945	0.9996	0.99961

Table 45. Regression analysis data for Figure. 33 - 34

Ln Visc vs 1/T

y = A + B*x							
Molar fraction DEHiBA in *n*-dodecane	1.00	0.78	0.66	0.50	0.38	0.18	0.00
A	-12.50679 ± 0.82171	-10.06218 ± 0.63339	-8.6423 ± 0.55698	-7.8581 ± 0.45653	-6.53848 ± 0.31462	-5.28815 ± 0.16903	-4.66208 ± 0.09228
B	4741.52807 ± 250.04002	3773.10422 ± 192.73478	3212.52532 ± 169.48464	2896.8614 ± 138.91833	2341.89644 ± 95.73813	1801.21427 ± 51.43371	1497.22846 ± 28.07967
Reduced Chi-Sqr	0.01261	0.00749	0.0058	0.00389	0.00185	5.34E-04	1.59E-04
R-Square(COD)	0.99173	0.99223	0.99172	0.99315	0.99501	0.99756	0.99895
Adj. R-Square	0.98897	0.98964	0.98896	0.99086	0.99335	0.99675	0.99859

Ln Visc vs 1/T

y = A + B*x					
Molar fraction TBP in *n*-dodecane	1.00	0.72	0.46	0.21	0.00
A	-5.65126 ± 0.09528	-5.29796 ± 0.13813	-5.14701 ± 0.14435	-4.82342 ± 0.10268	-4.66208 ± 0.09228
B	2063.5446 ± 27.90485	1872.17347 ± 41.78681	1754.01262 ± 42.73747	1593.5505 ± 31.18361	1497.22846 ± 28.07967
Reduced Chi-Sqr	13.86033	1.16019	1.53542	0.87223	1.59E-04
R-Square(COD)	0.99945	0.99851	0.99822	0.99885	0.99895
Adj. R-Square	0.99927	0.99801	0.99763	0.99847	0.99859

Table 46. Regression analysis data for Figure. 35 - 36

DEHiBA Viscosity change with dilution

x*(1-x)*(a0*(1-(2*x))^0+a1*(1-(2*x))^1+a2*(1-(2*x))^2)					
a0	-182.21083 ± 11.45612	-40.66909 ± 2.3192	-28.89622 ± 1.47646	-12.62657 ± 0.6756	-6.04194 ± 0.25732
a1	127.36544 ± 60.20622	23.63281 ± 12.18828	16.63596 ± 7.75937	6.41948 ± 3.55053	2.28857 ± 1.35231
a2	-62.42313 ± 63.53043	-9.16877 ± 12.86124	-6.00947 ± 8.18779	-1.63935 ± 3.74657	-1.24482 ± 1.42697
a3	47.10123 ± 185.27052	8.45401 ± 37.50657	4.52844 ± 23.87764	1.37324 ± 10.92592	1.83053 ± 4.1614
Reduced Chi-Sqr	16.64375	0.68211	0.27645	0.05788	0.0084
R-Square(COD)	0.99452	0.99513	0.99604	0.99547	0.99707
Adj. R-Square	0.96714	0.97079	0.97626	0.97281	0.98242

TBP Viscosity change with dilution

x*(1-x)*(a0*(1-(2*x))^0+a1*(1-(2*x))^1+a2*(1-(2*x))^2)					
a0	-2.45201	-1.36769	-0.9856 ± 7.89006E-17	-0.6935	-0.52528 ± 3.94503E-17
a1	0.39556	-0.04983	0.20027 ± 1.54159E-16	0.08969	0.03484 ± 7.70796E-17
a2	-0.39346	0.13186	-0.03299 ± 4.44383E-16	-0.01454	-0.25903 ± 2.22191E-16
Reduced Chi-Sqr	0	0	3.85E-34	0	9.63E-35
R-Square(COD)	1	1	1	1	1
Adj. R-Square	1	1	1	1	1

Annex B – Chapter 7 Regression Data

Table 47. Regression analysis data for Figure. 49

Density

2 M HNO_3 T = 293 K

y = a + b*x			
	2 M HNO_3 Post-contact	2 M HNO_3 Pre-contact	1 M DEHiBA
Intercept	1.06587	1.06699	0.79869
Slope	0.0015	0.00165	0.00131
Residual Sum of Squares	16.71227	52.67198	0.98339
Pearson's r	0.99993	0.99947	0.99991
R-Square(COD)	0.99986	0.99895	0.99983
Adj. R-Square	0.99979	0.99842	0.99974
y = a + b*x			
	2 M HNO_3 Post-contact	2 M HNO_3 Pre-contact	1 M DEHiBA
Intercept	1.05568	1.05807	0.78247
Slope	0.00148	0.00158	0.00149
Residual Sum of Squares	10.76888	89.54716	1271.279
Pearson's r	0.99995	0.99916	0.998
R-Square(COD)	0.9999	0.99832	0.996
Adj. R-Square	0.99985	0.99748	0.994
	2 M HNO_3 Post-contact	2 M HNO_3 Pre-contact	1 M DEHiBA
Intercept	1.04436	1.04466	0.76663
Slope	0.00145	0.0016	0.00144
Residual Sum of Squares	16.06512	19.4173	131.6461
Pearson's r	0.99993	0.99979	0.99349
R-Square(COD)	0.99985	0.99958	0.98702
Adj. R-Square	0.99978	0.99937	0.98053

Table 48. Regression analysis data for Figure. 50

4 M HNO_3 T = 293 K

y = a + b*x			
	4 M HNO_3 Post-contact	4 M HNO_3 Pre-contact	1 M DEHiBA
Intercept	1.11948	1.12095	0.80957
Slope	0.0014	1.70E-03	0.00122
Residual Sum of Squares	377.3536	166.3509	3.71433
Pearson's r	0.99827	0.99525	0.99989
R-Square(COD)	0.99654	0.99052	0.99978
Adj. R-Square	0.99481	0.98579	0.99966

y = a + b*x			
	4 M HNO_3 Post-contact	4 M HNO_3 Pre-contact	1 M DEHiBA
Intercept	1.10737	1.10759	0.79512
Slope	0.00138	1.63E-03	0.00115
Residual Sum of Squares	333.6501	169.559	3.52361
Pearson's r	0.99841	0.99826	0.99986
R-Square(COD)	0.99683	0.99653	0.99972
Adj. R-Square	0.99524	0.9948	0.99957

4 M HNO_3 T = 333 K

y = a + b*x			
	4 M HNO_3 Post-contact	4 M HNO_3 Pre-contact	1 M DEHiBA
Intercept	1.09377	1.09323	0.78036
Slope	0.00136	1.55E-03	0.00112
Residual Sum of Squares	292.871	138.3801	7.9107
Pearson's r	0.99856	0.99768	0.9996
R-Square(COD)	0.99712	0.99537	0.9992
Adj. R-Square	0.99568	0.99306	0.9988

Table 49. Regression analysis data for Figure. 51

6 M HNO_3 T = 293 K

y = a + b*x			
	6 M HNO_3 Post-contact	6 M HNO_3 Pre-contact	1 M DEHiBA
Intercept	1.18452	1.19056	0.81839
Slope	0.00136	1.62E-03	1.13E-03
Residual Sum of Squares	80.09846	4.09288	0.30013
Pearson's r	0.99959	0.99982	0.99998
R-Square(COD)	0.99919	0.99964	0.99997
Adj. R-Square	0.99878	0.99946	0.99994

6 M HNO_3 T = 313 K

y = a + b*x			
	6 M HNO_3 Post-contact	6 M HNO_3 Pre-contact	1 M DEHiBA
Intercept	1.1688	1.17385	0.80306
Slope	0.00133	1.51E-03	0.00112
Residual Sum of Squares	71.80149	10.65194	3.13253
Pearson's r	0.99962	0.99985	0.9998
R-Square(COD)	0.99924	0.99971	0.99959
Adj. R-Square	0.99886	0.99956	0.99939

6 M HNO_3 T = 333 K

y = a + b*x			
	6 M HNO_3 Post-contact	6 M HNO_3 Pre-contact	1 M DEHiBA
Intercept	1.15242	1.15756	0.78859
Slope	0.00131	1.41E-03	0.00112
Residual Sum of Squares	57.47992	12.41428	2.15195
Pearson's r	0.99969	0.99987	0.99987
R-Square(COD)	0.99937	0.99975	0.99974
Adj. R-Square	0.99906	0.99962	0.99961

Table 50. Regression analysis data for Figure. 52 - 54

Viscosity

1 M DEHiBA + *n*-dodecane + 2 M HNO_3

y = A1*exp(x/t1) + y0						
	293 K	Standard Error (±)	313 K	Standard Error (±)	333 K	Standard Error (±)
y0	2.3144	0.24085	1.26595	0.07817	0.71219	0.05071
A1	0.94422	0.191	0.7104	0.07065	0.57374	0.04842
t1	43.36913	4.08484	57.15998	3.26511	76.58331	4.36105
k	0.02306	0.00217	0.01749	9.99E-04	0.01306	7.44E-04
tau	30.06119	2.83139	39.62028	2.2632	53.0835	3.02285
Reduced Chi-Sqr	0.00513	-	1.39E-04	-	1.42E-05	-
Residual Sum of Squares	0.00513	-	1.39E-04	-	1.42E-05	-
R-Square(COD)	0.99956	-	0.99991	-	0.99995	-
Adj. R-Square	0.99867	-	0.99974	-	0.99986	-

1 M DEHiBA + *n*-dodecane + 4 M HNO_3

y = A1*exp(x/t1) + y0						
	293 K	Standard Error (±)	313 K	Standard Error (±)	333 K	Standard Error (±)
y0	1.90851	0.3216	0.92425	0.05042	-3.09125	4.23677
A1	1.54715	0.27307	1.12682	0.04697	4.43221	4.22953
t1	61.71263	5.6272	79.81298	2.0793	395.7922	345.9687
k	0.0162	0.00148	0.01253	3.26E-04	0.00253	0.00221
tau	42.77593	3.90048	55.32214	1.44126	274.3422	239.8072
Reduced Chi-Sqr	0.00522	-	3.15E-05	-	2.22E-04	-
Residual Sum of Squares	0.00522	-	3.15E-05	-	2.22E-04	-
R-Square(COD)	0.99966	-	0.99999	-	0.99948	-
Adj. R-Square	0.99897	-	0.99996	-	0.99844	-

1 M DEHiBA + *n*-dodecane + 6 M HNO_3

y = A1*exp(x/t1) + y0						
	293 K	Standard Error (±)	313 K	Standard Error (±)	333 K	Standard Error (±)
y0	2.32176	n/a - too few points	1.89112	0.1918	1.21401	0.35847
t1	51.13027	n/a - too few points	39.03615	6.72594	43.83486	26.44823
k	0.01956	n/a - too few points	0.02562	0.00441	0.02281	0.01376
tau	35.4408	n/a - too few points	27.0578	4.66207	30.38401	18.33252
Reduced Chi-Sqr	n/a - too few points		-	-	6.17E-03	-
Residual Sum of Squares	n/a - too few points		-	-	6.17E-03	-
R-Square(COD)	0.99996		-	-	0.98625	-
Adj. R-Square	n/a - too few points		-	-	0.95874	-

Annex C – Chapter 8 Regression Data

Table 51. Regression data for Figures. 67 - 72

	1 M DEHiBA	**1 M DEHiBA + 4 M HNO_3**	**0.2 M TODGA + 0.5 M DMDOHEMA**	**0.2 M TODGA + 0.5 M DMDOHEMA + 5.9 M HNO_3**
Density				
Equation	$y = A + Bx$	$y = A + Bx + Cx^2$	$y = A + Bx$	$y = A + Bx + Cx^2$
A	0.79066 ± 0.0001	0.80095 ± 0.0002	0.81569 ± 0.0002	0.8445 ± 0.0008
B	$8.4 \times 10^{-7} \pm 1.06 \times 10^{-7}$	$-0.00002 \pm 1.4 \times 10^{-6}$	$9.60 \times 10^{-7} \pm 4.42 \times 10^{-7}$	$-3.798 \times 10^{-5} \pm 5.46 \times 10^{-6}$
C	-	$1.68 \times 10^{-8} \pm 1.79 \times 10^{-9}$	-	$2.52 \times 10^{-8} \pm 6.97 \times 10^{-9}$
Residual Sum of Squares	0.01944	0.13889	0.33889	2.1125
Pearson's r	0.9845	-	0.83812	-
R^2	0.96923	0.99412	0.70244	0.99389
Adj. R-Square	0.95385	0.98237	0.55366	0.98167
Viscosity				
Equation	$y = A + Bx + Cx^2$	$y = A + Bx + Cx^2$	$y = A + Bx$	$y = A + Bx$
A	2.72 ± 0.09	3.09 ± 0.09	4.75 ± 0.10	7.79 ± 0.22
B	-0.0006 ± 0.0006	-0.0014 ± 0.0005	0.0005 ± 0.0002	-0.00262 ± 0.0005
C	$8.93 \times 10^{-7} \pm 7.811 \times 10^{-7}$	$1.64 \times 10^{-6} \pm 6.98 \times 10^{-7}$	-	-
Residual Sum of Squares	3.81356	3.042	10.668	55.208
Pearson's r	-	-	0.87	-0.969
R^2	0.61082	0.87146	0.757	0.939
Adj. R-Square	-0.16755	0.61438	0.636	0.909
Interfacial Tension				
Equation	$y = B*\exp(-x/C) + A$	$y = A + Bx$	$y = A + Bx$	$y = A + Bx$
A	14.42754 ± 0.02209	19.013 ± 0.23933	8.95781 ± 0.08747	4.85348 ± 0.06927
B	5.30863 ± 0.08317	-0.00993 ± 5.12539E-4	-0.00112 ± 0.0002	0.0007 ± 0.0001
C	214.15557 ± 7.23212	-	-	-
Residual Sum of Squares	-	11.9259	2.40991	0.38204
Pearson's r	-	-0.99735	-0.96845	0.988
R^2	0.99977	0.9947	0.93789	0.97615
Adj. R-Square	0.99931	0.99205	0.90683	0.95229